NISTIR 6242

ANNUAL CONFERENCE ON FIRE RESEARCH
Book of Abstracts
November 2-5, 1998

Kellie Ann Beall, Editor

Building and Fire Research Laboratory
Gaithersburg, Maryland 20899

United States Department of Commerce
logy Administration
l Institute of Standards and Technology

NISTIR 6242

ANNUAL CONFERENCE ON FIRE RESEARCH
Book of Abstracts
November 2-5, 1998

Kellie Ann Beall, Editor

October, 1998
Building and Fire Research Laboratory
National Institute of Standards and Technology
Gaithersburg, MD 20899

U.S. Department of Commerce
William M. Daley, *Secretary*
Technology Administration
Gary Bachula, *Acting Under Secretary for Technology*
National Institute of Standards and Technology
Raymond G. Kammer, *Director*

1998 Annual Conference on Fire Research
November 2 - 5, 1998

Green Auditorium
National Institute of Standards and Technology (NIST)
Gaithersburg, MD

TIME	MONDAY, NOVEMBER, 2 *FIRE SENSING*	PAGE
8:30 am	Open Session Welcoming Remarks by: Raymond G. Kammer, *Director, NIST* Jack E. Snell, *Manager, NIST Fire Research Program*	
8:55 am	1. A New Fire Detection System Using FT-IR Spectroscopy and Artificial Neural Networks: **Yonggang Chen, Sandeep Sathyamoorthy, Michael Serio**; *Advanced Fuel Research, Inc.*	1
9:20 am	2. Distinguishing Normal from Pre-Ignition Conditions to Prevent Cooking Fires on Kitchen Ranges: **Erik Johnsson**; *NIST*	3
9:45 am	3. Monte Carlo Simulations of Radiative Transfer in a House Including Specular and Diffuse Reflections for the Evaluation of Two Wavelength Optical Fire Detectors: **Jay Gore, Y.R. Sivathanu, Y.J. Zhu**; *Purdue University*	5
10:10 am	*BREAK*	
10:40 am	4. Development of Multi-signature Fire Detection Systems: **Daniel Gottuk**; *Hughes Associates, Inc.;* **Frederick Williams**; *Naval Research Laboratory*	7
11:05 am	5. Evaluation of Fire Detection Technology for Suitability in Aircraft Cargo Compartments: **Thomas Cleary, William Grosshander**; *NIST*	9
11:30 am	6. Particulate Entry Lag in Smoke Detectors: **Thomas Cleary, Artur Chernovsky, William Grosshandler, Melissa Anderson**; *NIST*	11
11:55 am	7. Matching Fires and Simulations: **Jonathan Barnett, Matthew Ward, Jayesh Govindarajan**; *Worcester Polytechnic Institute*	13
12:20 pm	*LUNCH*	

TUESDAY, NOVEMBER, 3 **PAGE**

POSTERS PRESENTED

10:35 am - 12:30 pm 1:30 pm - 2:15 pm

TUESDAY, NOVEMBER, 3 **PAGE**

POSTERS PRESENTED

10:35 am - 12:30 pm 1:30 pm - 2:15 pm

5:35 pm *ADJOURN*

6:00 pm *CASH BAR AT HOLIDAY INN*

7:00 pm *BANQUET AT HOLIDAY INN*

TIME	WEDNESDAY, NOVEMBER, 4 *FIRE SUPPRESSION*	PAGE
3:30 pm	65. Flammable Liquid Storeroom 1: Halon Alternatives Technology Testing Results: **Ronald Sheinson, James Cooke**; *Naval Research Laboratory*, **Alexander Maranghides**; GEO-CENTERS, Inc.	 129
3:55 pm	66. Flammable Liquid Storerooms: Halon 1301 Replacement Program: **Ronald Sheinson, Bryce Wentworth**; *Naval Research Laboratory;* **Alexander Maranghides;** *GEO-CENTERS, Inc*	 131
4:20 pm	67. Fire Tests of a Fixed Gaseous Fire Extinguishing System for Marine Application: **Soonil Nam**; *Factory Mutual Research Corporation*; **Richard Hansen**; *U. S. Coast Guard R & D Center*	 133
4:45 pm	DISCUSSION	
5:30 pm	*ADJOURN*	

INTRODUCTION

The NIST Annual Conference on Fire Research has long been the prime forum for the presentation and discussion of the latest advances in the science of fire and the engineering of fire safety. Hundreds of billions of dollars of products and services are involved in fire safety decisions each year. New technology is changing the way those products are developed, manufactured, evaluated, and used.

This conference enables all interested parties to hear of and discuss advances in fire science, with the intent of stimulating (a) new products that are more fire-safe and (b) new ways to capture that value in the ways products are tested and approved for use. The Conference scope includes all fire research performed within Federal laboratories or sponsored by Federal agencies, as well as work from laboratories around the world.

This booklet contains the abstracts of the 75 papers and posters focussing on the phenomenology of fire: fire sensing, fire measurement, fire-safe materials, fire suppression, flame structure, pool fires, fire-induced flows, fire plumes, combustion product generation and measurement, compartment fires, and outdoor fires. Discussion sessions will consider the status of our knowledge and the most important understanding yet to be developed. With this, we hope to continue cross-pollinating the elements of the fire research community while stimulating our members to new understanding that will lead to more fire-safe products and practices.

Richard G. Gann, Conference Chair
Chief, Fire Science Division
Building and Fire Research Laboratory
National Institute of Standards and Technology

For Presentation at the NIST Annual Conference on Fire Research
Gaithersburg, MD, November 2-5, 1998

A New Fire Detection System Using FT-IR Spectroscopy and Artificial Neural Networks

Yonggang Chen, Sandeep Sathyamoorthy, and Michael A. Serio
Advanced Fuel Research, Inc., 87 Church Street, East Hartford, CT 06108

Introduction

Future fire detection systems should have the ability of discriminating signatures between fire and non-fire sources as nuisance alarm problems have plagued existing smoke detectors. In high value installations, such as semiconductor clean rooms and telephone central offices, it is obvious that reliable fire detection systems are needed. In most cases, these detection systems are used to activate fixed fire suppression systems, and false discharges of the suppression agents are certainly undesirable. False alarms can cause unnecessary down time and undermine the operator's confidence in the detection system.

A new fire detection system using infrared diagnostics (FT-IR spectroscopy) together with advanced signal processing techniques (artificial neural networks) has been developed at Advanced Fuel Research, Inc. This new fire detection system promises to provide an early warning of hazardous conditions and has the ability to determine whether the hazardous conditions are from fire or nuisance/environmental sources.

Approach

It has been shown that multi-parameter fire detection systems are inherently more reliable than any single parameter measurement and can be made robust by the use of artificial intelligence methods (1-4). The objective of our research efforts is to use an advanced Fourier Transform Infrared gas analyzer to develop an intelligent fire detection system that can be used in high value facilities such as telephone central offices and semiconductor cleanrooms.

We have made extensive FT-IR gas measurements of flaming (2) and smoldering fires, as well as environmental/nuisance sources (5). The FT-IR measurements were made in open-path, cross duct, and extractive modes for flaming fires, while measurements of smoldering fires and environmental/nuisance sources were performed in the extractive mode. The extractive mode was selected in the latter case because most of the current fire detection technologies (e.g. VESDA and AnaLaser) for cleanrooms and telephone central offices are based on air sampling techniques in which the air samples from multiple locations of the rooms are drawn and delivered through an extensive piping network to a particle analyzer. The FT-IR system can be easily incorporated in this type of fire detection system, and comparison can be made with existing technologies.

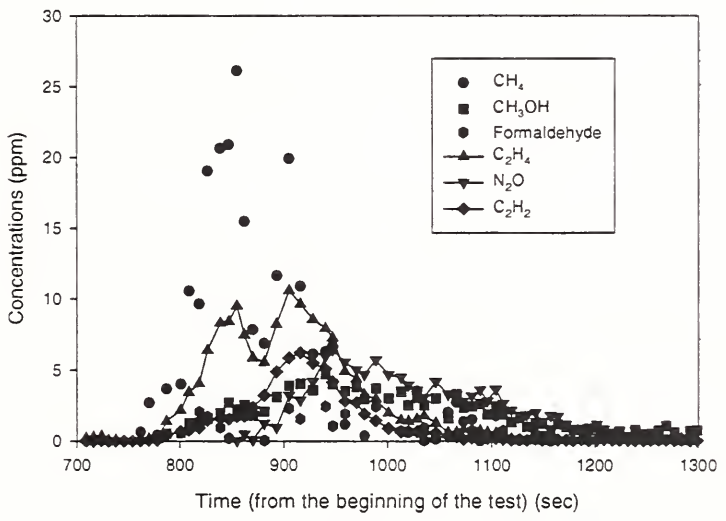

Figure 1 Gas concentrations of a Douglas fir fire test

Numerous materials were tested, including Polyurethane (PU), Polyvinylchloride (PVC), Polymethylmethacrylate (PMMA), Polypropylene (PP), Polystyrene (PS), Douglas Fir wood (DF), low density Polyethylene (LDPE), aqueous Ammonia (NH_3), Tetrafluoromethane (CF_4), Isopropyl alcohol (IPA), cables, etc

Figure 1 shows concentrations of some fuel specific species measured by an FT-IR spectrometer from a smoldering-flaming Douglas fir fire test. N_2O and formaldehyde were clearly observed in the figure. Similar observations can be made for other materials tested.

The species concentrations measured by a FT-IR, together with a neural network or fuzzy logic model, can be used to identify whether there is a fire or nonfire (environmental/nuisance) event, and to classify whether it is a flaming or smoldering fire if the event is indeed a fire. A commercially available neural network software package, NeuralWorks Professional II/Plus (6), was chosen to build the needed neural network. A so-called Learning Vector Quantization (LVQ) network has been built and tested (Figure 2). The inputs in the current version are concentrations of CO_2, CO, H_2O, CH_4,

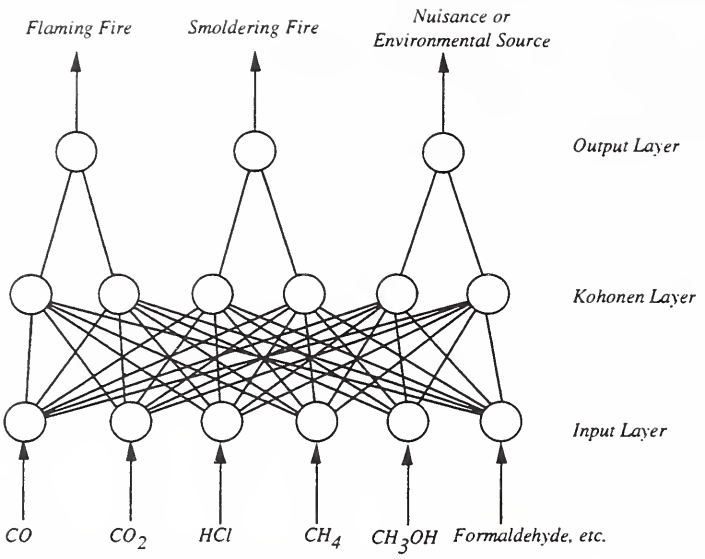

Figure 2 A Learning Vector Quantization (LVQ) network to characterize fire and non-fire events.

CH_3OH, Formaldehyde, HCl, C_2H_4, N_2O, NH_3, CF_4, NO, Methyl Methacrylate, Isopropyl alcohol, C_2H_6, C_3H_6, C_6H_{14}, C_2H_2, C_6H_6 (18 species from FT-IR measurements). The outputs of the network are classification of the input data as a flaming fire, smoldering fire, or nuisance/environmental source. The results of the above experiments look quite promising. From among the 248 cases tested, only 12 events were misclassified, most due to the difficulties in classifying the modes of combustion during a transition from smoldering to flaming fire.

We have incorporated the above-trained LVQ network into the data acquisition system for an On-Line 2010 Multi-Gas spectrometer. A real-time fire detection system has been constructed. Preliminary tests of this integrated software have been satisfactory using the test data described above.

Conclusions

FT-IR measurements of numerous fire (flaming and smoldering) and nonfire sources have been conducted. The combustion and fuel specific species have been identified and quantified. The species concentrations together with a neural network model were used to successfully distinguish fire and nonfire (environmental/nuisance) events as well as identify the modes of combustion (flaming or smoldering). The neural network model has been incorporated into the advanced FT-IR measurement system and a prototype fire detection system has been constructed.

Acknowledgement

The support by the National Institute of Standards and Technology under grant No. 50-DKNB-5-00174 with Dr. William Grosshandler as Technical Monitor is greatly appreciated.

REFERENCES

1 Milke, J.A. and McAvoy, T.J, Analysis of Signature Patterns for Discriminating Fire Detection with Multiple Sensors, Fire Technology, Second Quarter 1995.
2 Serio, M.A., Bonanno, A.S., Knight, K.S., Wójtowicz, M.A. and Solomon, P.R., Advanced Infrared Systems for Detection of Building Fires, Final Report to DOC under Contract No. 50-DKNA-4-000-96, February 1995.
3 Okayama, Y., Ito, T. and Sasaki, T., Design of Neural Net to Detect Early Stage of Fire and Evaluation by Using Real Sensors' Data, Fire Safety Science-Proc. of 4th Int'l Symposium, pp. 751-759, 1993.
4 Okayama, Y., A Primitive Study of a Fire Detection Method Controlled by Artificial Neural Net, Fire Safety Journal, pp. 535-553, 17, 1991.
5 Chen, Y, Sathyamoorthy, Y, And Michael A. Serio, An Intelligent Fire Detection System Using Advanced Infrared Diagnostics And Neural Network Techniques, The Eastern States Meeting of the Combustion Institute, October, 1997.
6 NeuralWare, Inc., NeuralWorks Professional II/Plus, Version 5.3, February 1997.

Distinguishing Normal from Pre-Ignition Conditions to Prevent Cooking Fires on Kitchen Ranges

Erik L. Johnsson
Building and Fire Research Laboratory
National Institute of Standards and Technology
Gaithersburg, Maryland 20899

A significant portion of residential fires stem from kitchen cooking fires.[1] Previous study has determined that strong indicators of impending ignition for several foods cooked on range surfaces are temperatures, smoke particulates, and hydrocarbon gases.[2] The purpose of this experimental investigation was to determine the physical feasibility of utilizing one or more of these common characteristics of the pre-ignition environment as input to sensors in a pre-fire detection device.

A total of 16 cooking procedures were examined. Simulations of unattended cooking leading to ignition as well as normal, or standard, cooking procedures that have the potential to mimic pre-ignition characteristics were included in the study. Each case was tested on a typical electric range with an inactive range hood. To determine the effects of range type and hood status on sensor performance, two cases were repeated with the range hood active and three cases were repeated on a gas range. The total number of variations was 21, and each test was repeated once for a total of 42 tests.

Both laboratory instrumentation and practical sensors were used to monitor the cooking-area environment. A sample probe carried gases to carbon monoxide, carbon dioxide, and hydrocarbon analyzers. Thermocouples provided temperature measurements near the food and around the range. Hydrocarbon-gas sensors were placed on and around the range. Photoelectric and ionization smoke detectors were placed around the room. Each sensor was evaluated for its ability to alarm before ignition and not generate false alarms.

For results, examples of a few sensors which performed well will be discussed. Figure 1 shows the time traces of 4 sensors located at site 9 which was the center of the front surface of the range hood. The sensors were variations of thin-film tin-oxide sensors tuned to particular families of hydrocarbon gases. The particular test shown was for french fries cooked in soybean oil. The procedure for that cooking case prescribed an initial period of normal cooking followed by an increase to the high heat setting to simulate unattended cooking. In the plot, all of the sensor outputs start to rise around 740 s which was about 30 s after the heat increase. For this particular cooking case and group of range-hood sensors, the levels of voltage produced for the normal and unattended cooking periods show a marked difference which would enable use of an alarm to warn of approaching ignition.

Figure 2 shows a different set of sensors for one test of another cooking case, blackened catfish. These sensors consisted of thermocouples located near the pan. The pan-bottom thermocouple was located between the pan and burner at the center. The drip-pan thermocouple was located beneath the center of the coiled heating element. The food thermocouple was located in/under the food at the center of the inside of the pan. The procedure called for heating butter, placing fish in the pan, turning the fish, and removing the pan from heat. The corresponding times in the plot are 60 s, 240 s, 390 s, and 480 s, respectively. This particular cooking case is a difficult one to accommodate within an alarm system design since the recipe procedure generates temperatures near the ignition point of the butter, and the gases and temperatures produced are similar to those found in unattended cooking cases.

Figures 3 and 4 portray a way to evaluate the magnitude of a window between normal and pre-ignition conditions for sensors at particular locations. Figure 3 shows the voltage output of the cooking-alcohols sensor at site 9 versus test number. The Xs represent maximum output reached during normal cooking periods. The circles represent minimum output experienced during the 30 s preceding ignitions. The dashed line is an alarm threshold chosen to most separate the two output types. Xs above the line represent normal cooking tests that would have caused false alarms with this alarm setting. Circles below the line would represent failures to alarm in situations leading to ignition. For this sensor and location

there were 5 tests exhibiting false alarms, and no failures to alarm. Figure 4 is a similar plot to Figure 3, but it is for the pan-bottom temperature. For the chosen alarm threshold, there were 4 tests with false alarms, and no failures to alarm. Better results were found for a simple multiplication of the two signals.

The experimental conclusions are based on measurements of combinations of specific ranges, pans, foods, and ventilation. The major conclusions of this research are: (1) Several sensors offered high levels of differentiation when used alone. Depending on the setting of the threshold, a majority of cooking cases would appropriately cause alarm or not alarm. (2) A limited effort at algebraically combining sets of two sensor signals generated even more robust differentiation. (3) Based on the findings of this investigation, pre-fire detection systems for range-top cooking are physically feasible and merit further consideration of economic viability and practicality.

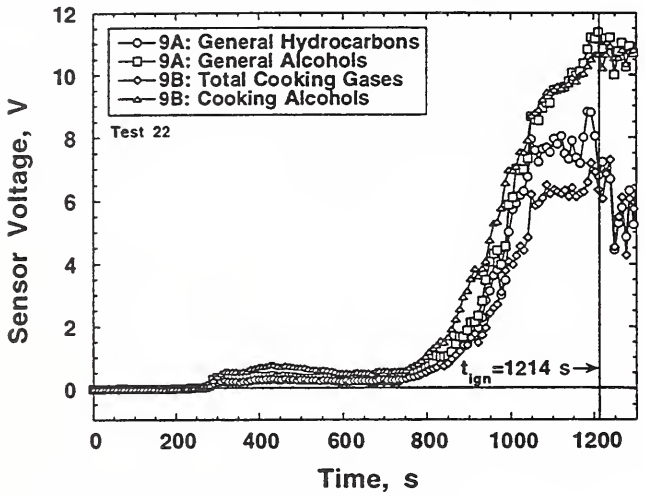

Figure 1. Site 9 Hydrocarbon Sensor Voltages vs Time for French Fries in Soybean Oil

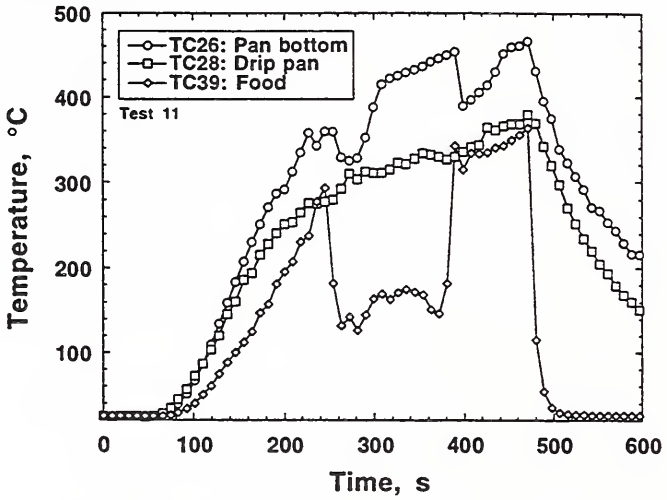

Figure 2: Temperatures vs Time for Blackened Catfish

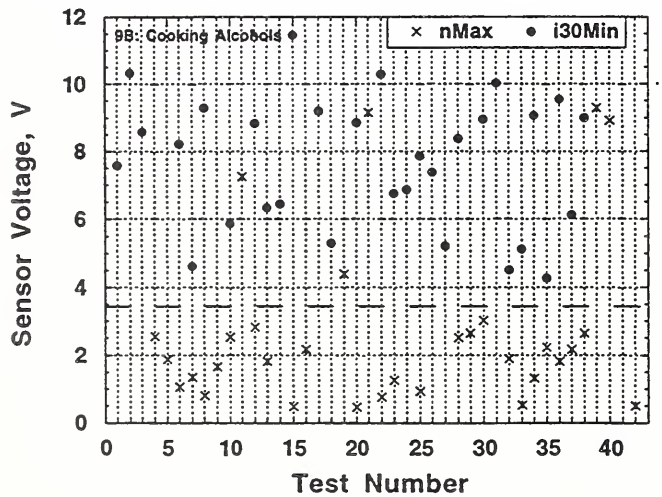

Figure 3. Site 9 Cooking Alcohol Sensor Voltage. Max Normal & Min 30 s Ignition vs Test No.

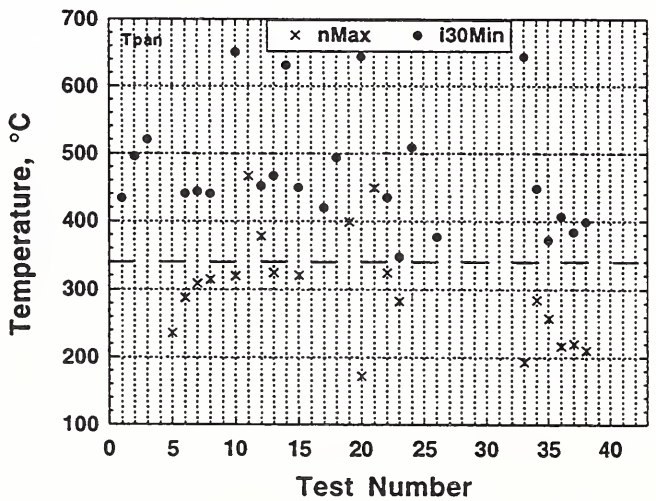

Figure 4: Pan-Bottom Temperature Max Normal & Min 30 s Ignition vs Test No.

References

1 Monticone, R., "Range Top and Oven Fires, Statistical Analysis of 1990-1994 Fire Incidents," U.S. Consumer Product Safety Commission, Bethesda, MD; 1997.

2 Johnsson, E. L. "Study of Technology for Detecting Pre-Ignition Conditions of Cooking-Related Fires Associated with Electric and Gas Ranges and Cooktops, Phase I Report," NIST IR 5729; National Institute of Standards and Technology, Gaithersburg, MD; 107 p., 1996.

Monte Carlo Simulations of Radiative Transfer in a House including Specular and Diffuse Reflections for the Evaluation of Two Wavelength Optical Fire Detectors

Y. R. Sivathanu, J. P. Gore and Y. J. Zhu
School of Mechanical Engineering, Purdue University
West Lafayette, IN 47907-1003

Fire detectors based on sensing thermal radiation from a starting fire have the potential to provide early warning and improve fire safety and reduce fire loss. However, these detectors must rely on sensing and discriminating radiation signals of a starting fire from those of common sources such as the sun, room lights and others. The radiation signal incident on a detector may have undergone multiple reflections at the walls with complex properties and configuration factors. Effective radiation temperature based on measurement of intensities at two wavelengths is one of the fire characteristics used in many flame sensors.

We have used Monte Carlo methods to simulate the radiative heat transfer in a simple house to examine the effects of spectral reflectivity of the walls on the radiation signal received by the detector. We also examined the effects of geometric parameters such as the sizes of the room with a fire and that of an adjacent room. The results show that the effective radiation temperature sensed by a two-wavelength fire detector depends on the spectral reflectivity of the walls and also on the number of reflections the photons have undergone. The later quantity depends on the angles of emission, configuration of the room, proportion of the specular and diffuse reflections. Therefore, the radiation temperature measured by a detector depends on all these properties in a non-trivial manner.

Figure 1 shows a sketch of a generic house considered in the present simulations. Only two rooms are considered for simplicity but additional rooms can be added in a modular fashion. We have constructed codes for rectangular and triangular enclosures of arbitrary aspect ratios and with the facility to place fires, detectors and openings at arbitrary locations. These modules can be combined to conform to the architectural plan of a house. In the present example, a fire occurs at the front wall of room 1, which has a triangular roof and a detector is placed on an inclined roof surface as shown in the sketch. The triangular enclosure of the roof is constructed using an imaginary surface separating it from the rectangular enclosure part of room 1. Room 2 is treated as a rectangular enclosure with a flat roof and is connected to room 1 with a full opening (marked as the second imaginary surface). The radiative transfer in the house can now be computed using interconnected program modules involving transfer in simpler enclosures. The fire, designated source in Fig. 1, is assumed to have an effective temperature of 1500 K. We track close to 18 million photons in the enclosure to arrive at converged statistics for radiative transfer between all parts if the enclosure including the detector and the fire. Fewer photons can certainly be used if computational economy is of essence.

Figure 2 shows the temperature measured by the detector as a function of the length of room 1. Longer the room, the larger is the number of reflections that the photons undergo prior to incidence on the detector. The reflectivity of building materials at shorter wavelengths is higher. The results of Fig. 1 are with a reflectivity of 0.66 at 900 nm and 0.6 at 1000 nm and a specular component of 0.4. The estimated temperature can be higher by up to 400 K compared to the fire temperature. Figure 3 shows the effect of reflectivity on the error in the temperature estimate. If the walls are perfectly absorbing, all of the photons incident on the detector are from the source. Therefore, the detector estimates the radiation temperature accurately. As the reflectivity of the wall increases the error in the temperature estimate increases, reaching almost 700 K error for a reflectivity of 0.8. Figure 4 shows the effects of the length and radiative properties of room 2 on the estimated temperature. The top panel shows that independent of the aspect ratio, if the reflective properties of room 2 are identical to those of room 1, the photons incident on the detector are primarily from room 1. Therefore the error in the temperature estimate is rather insensitive to the length of room 2. On the other hand, if room 2 is made more reflective than room 1, the number of photons that have undergone reflections in room 2 and are incident on the detector increases. Therefore, the error in the temperature estimate is sensitive to the length of room 2 as shown in the bottom panel.

Statistical simulations of the type described in this paper can be useful in the design and placement of optical fire detectors. These simulations also provide guidelines for material selection.

Acknowledgement: NIST Grant Number 60NANB8D0013 with Dr. Grosshandler serving as Program Officer supports this work.

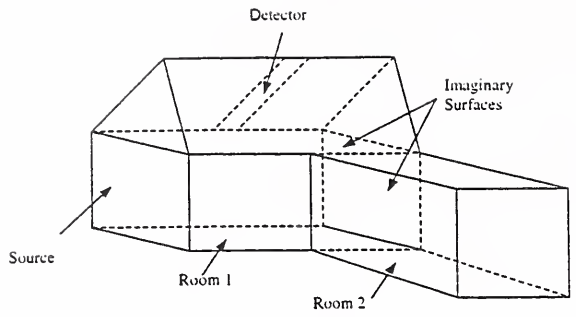

Figure 1: A sketch of a simple house for evaluation of radiative transfer.

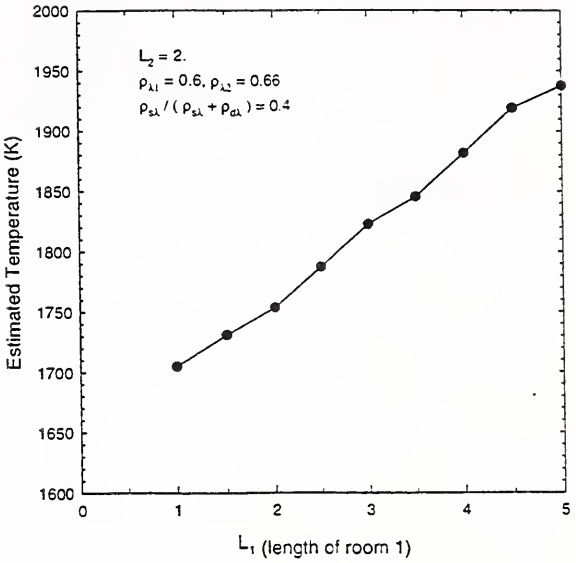

Figure 2: Estimated temperature as a function of length of room 1.

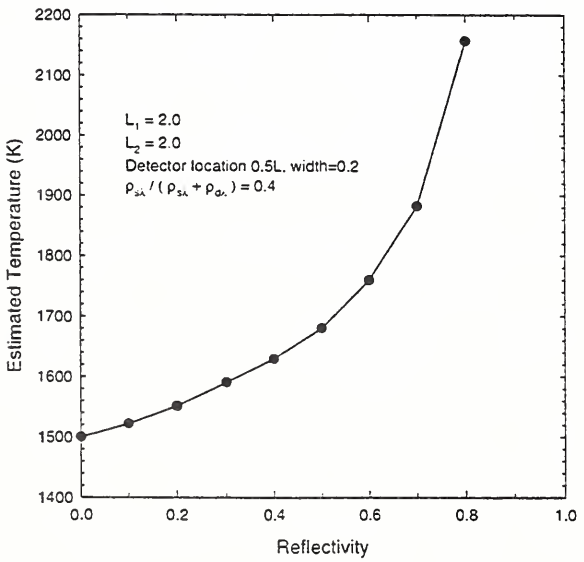

Figure 3: Estimated temperature as a function of reflectivity of the walls.

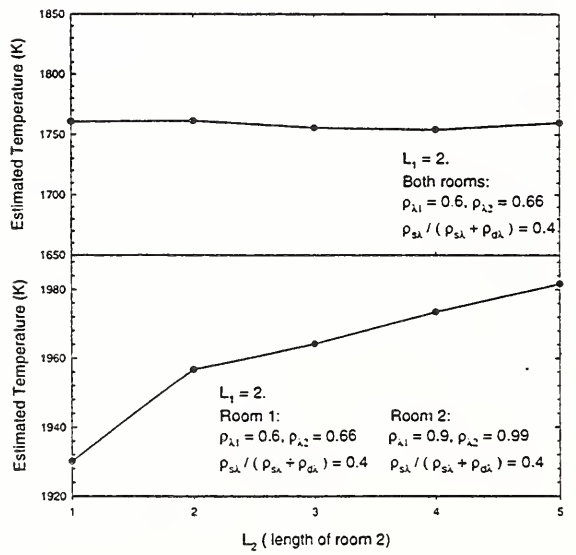

Figure 4: Effect if length and radiative properties of room 2 on the estimated temperature.

Development of Multi-signature Fire Detection Systems

Dr. Daniel T. Gottuk
Hughes Associates, Inc.
3610 Commerce Drive, Suite 817
Baltimore, MD 21227 USA

and

Dr. Frederick W. Williams
Naval Research Laboratory, Code 6180
4555 Overlook Avenue, SW
Washington, DC 20375 USA

The U.S. Navy is working toward enhanced automation of ship functions and damage control systems. A key element to this objective is the improvement of current fire detection systems. As in many applications, it is desired to increase detection sensitivity and, more importantly, increase the reliability of the detection system through improved nuisance alarm immunity. Improved reliability is needed such that fire detection systems can fully control fire suppression systems. The use of multi-sensor/multi-criteria based detection technology continues to offer the most promising means to achieve both improved sensitivity to real fires and reduced susceptibility to nuisance alarm sources. An early warning fire detection system can be developed by properly processing the output from sensors that measure multiple signatures of a developing fire.

Although work has been done in the area of multi-signature detection, in many cases few sensor types have been examined (e.g., standard photoelectric smoke detectors and temperature or CO and CO_2 for gas signatures), and only singular standard test sources have been used. The current Navy program is aimed at developing a broad database of signatures from real fire and nuisance alarm sources. Besides using standardized single component fire tests for comparison purposes, particular attention is given to evaluate composite fuels that are more realistic to actual fire sources. For example, furniture materials of cushion foam and upholstery, mattresses with bedding (i.e., sheets, blankets, etc.), or mixed trash (e.g., plastic, cardboard, paper, etc.) are combined as single fuel sources. Nuisance alarm sources include cooking events (e.g., deep fat frying, toasting, baking, burning popcorn in a microwave), cigarette smoking, welding, acetylene torch cutting, and combustion engine exhaust. Both flaming and smoldering combustion modes are investigated. Although this work is focussed on shipboard applications, the nature of ship operations make this work relevant to many industrial and commercial applications as well.

Tests are being conducted in a 6.5 m x 4.1 m x 3.6 m high compartment with no ventilation active. Fire and nuisance alarm sources are positioned 1.5 m below the ceiling and all sensors are positioned 4 m away from the source. A wide range of signatures are evaluated, including twelve gas species, temperature, light obscuration, light scattering, measuring ionization chamber, and multiple ionization and photoelectric detector signals. Detection criteria will be developed primarily in Phase 2 of the program during 1999. The results of this study will identify key signatures and preliminary signal processing methods based on an analysis of the state-of-the-art work presented in the literature.

Evaluation of Fire Detection Technology for Suitability in Aircraft Cargo Compartments[1]

Thomas Cleary and William Grosshandler

Building and Fire Research Laboratory
National Institute of Standards and Technology
Gaithersburg, Maryland 20899

ABSTRACT

NIST is assisting the FAA in its research to improve fire detection in Class C and D aircraft cargo compartments. Class C and D compartments are inaccessible in flight. Class C compartments are required to have detection and suppression systems installed. Almost universally, the fire detection systems consist of either ionization or photoelectric smoke detectors. Class D compartments are small in volume (28.5 m^3 or less) and are not required to have detection and suppression. However, a proposed rule change will require that these compartments also be protected within the near future. The number of aircraft affected by this proposed change is about 3000, and the attendant increase in the number of protected spaces will rise threefold. Adding such a large number of spaces to be protected will certainly impact the implications fire detection has on aircraft operation. Assuming application of current technology, this implies a tripling in the number of false positives (false alarms) without any growth in passenger traffic. For commercial aircraft, the rate of false alarm to fire is estimated to be as high as 500:1 . Historically, the impact of false alarms in cargo compartments has ranged from inconvenience, to unnecessary release of halon and potentially dangerous diversion and emergency evacuation of the aircraft. Thus, elements to improve fire detection include reducing false alarms in addition to assuring detection of all fire events.

A literature survey of existing and emerging fire detection technologies potentially suitable for aircraft cargo environments was conducted. An environment inside a cargo compartment typically experiences fluctuations in ambient temperature, pressure during a flight. Variations in moisture and aerosol concentration are produced by external ambient conditions, and in some cases the cargo itself. Detection based on gas sensing, radiation sensing, and multi-sensor detection schemes were identified as emerging technologies which may be suited to cargo environments.

One hurdle to implementing any technology other than particulate smoke detectors is the current certification and system evaluation methods used for U.S. commercial aircraft. Current regulations require a detection system to alarm within 60 seconds from the start of a test fire. Fire testing takes place on the ground at various testing locations around the country. The fire source used in the testing is ill-defined in terms the material burned. The FAA is currently working on improving the fire source used in certification. Airborne testing is usually performed with a glycol aerosol generator which produces a smoke of sufficient quantity to cause particulate detectors to alarm. This smoke generator does not replicate all characteristics of combustion processes and would be useless for in-flight testing for detectors sensing something other than particulates. Computational fluid dynamics could conceivably play a role in design and certification of aircraft cargo detection systems allowing for a wider range of fire conditions and configurations to be examined.

[1] Supported by FAA

There is no current standard for assessing a detector's immunity to false alarm. To confidently select a fire detection technology that will reduce false alarms in aircraft cargo compartments, a measure or estimate must be made of a detector's susceptibility to false alarm in the environment it will be exposed. A methodology for assessing the performance of existing and emerging fire detection systems under realistic and simulated cargo environments with and without the presence of a growing fire will be detailed. For example, moisture and condensation play a role in some cargo compartment false alarm scenarios. Temperature, moisture and flow conditions experienced in a cargo compartment could be simulated in a laboratory setting (such as in the NIST Fire Emulator/Detector Evaluator) and specific detector sensitivities to various levels of moisture, temperature and flow could be quantified.

Reference

Grosshandler W.L., "Nuisance Alarms in Aircraft Cargo Areas and Critical Telecommunications Systems: Proceedings of the Third NIST Fire Detector Workshop", National Institute of Standards and Technology, Gaithersburg, NISTIR 6146, March 1998.

Particulate Entry Lag in Smoke Detectors

Thomas Cleary, Artur Chernovsky, William Grosshandler, and Melissa Anderson

Building and Fire Research Laboratory
National Institute of Standards and Technology
Gaithersburg, Maryland 20899

ABSTRACT

It is well known that smoke detectors do not instantaneously respond to smoke concentration directly outside the detector. The smoke must be transported through the detector housing to a sensing location inside the detector. The sensing time lag is a function of the free stream velocity of the smoke laden air as it approaches the detector. Previous work correlated the detector time lag as a first-order response with a characteristic time defined as L/V, where L is a characteristic length and V is the characteristic velocity (ceiling jet velocity or free stream velocity).

The smart fire panel research program at NIST is evaluating the use of smoke detectors that provide continuous analog output as sensors. These "sensors" then could provide information on the fire to the smart panel. In support of that work, a number of tests were performed in the Fire Emulator/ Detector Evaluator (FE/DE) to characterize the sensing lag time over a range of flow velocities and smoke concentrations for fire ionization and photoelectric detectors that provide a continuous sensor output signal. A model was developed that uses two parameters to correlate the detector time response.

The FE/DE device is a flow tunnel with a cross section of 0.6 m by 0.3 m high at the test section. Air velocity and temperature can be controlled, and provisions to add CO, CO_2, hydrocarbon gases, water, smoke, and other aerosols to the flow are in place or in development. Temperature, velocity and species measurements are recorded at the test section. In the test described here, the temperature, velocity and smoke extinction values across the duct were recorded, in addition to the detector signal.

Smoke was generated by a co-flowing propene diffusion burner. By directing part of the burner smoke output into the flow tunnel, then shutting off the smoke flow to the tunnel, the smoke concentration in the duct steps up, then steps down some time later. Smoke is well mixed in the duct by the time it reaches the test section. Figure 1 and 2 show examples of the effect of flow velocity on the detector signal lag. The optical density curve was generated by a laser attenuation measurement across the duct at the height of the detector.

We chose a simple idealized mixing model consisting of a plug flow region followed by a perfectly stirred region (mathematically, the order of these regions can be reversed with no effect on the model output.) Two parameters are identified, a transport time (δt) associated with the plug flow region and a characteristic mixing time constant (τ) associated with the perfectly stirred region. This model is hydrodynamic only, thus a Reynolds number would correlate the effect of flow and mixing. Particle diffusion is not accounted for since it would only be significant at very low velocities (Reynolds numbers) and the associated detector time lag for a diffusion dominated process would be so long as to make the detector unsuitable as a smart panel sensor. A correlation in the form below is proposed.

$a_i = \alpha_i Re^{\beta i}$

where a_i is either δt or τ, Re is the Reynolds number, α_i and βi are the pre-exponent and exponent to be determined. The mixing model equation for constant velocity is:

$\kappa Y\ (t-\delta t) = \tau\ dx(t)/dt\ +\ x(t)$

where Y is the smoke optical density, k is a constant the changes optical density to detector output units, and x is the detector output. The model can be discretized, and for velocity changes, dt and t can be updated in a quasi-steady manner. Thus, one needs the velocity and temperature history at the detector location and the detector output to obtain the smoke optical density at an earlier time.

Figures 3 and 4 show the model results in the form of predicted optical density from the transformed detector signals in Figures 1 and 2 respectively.

Figure 1 - Ionization Detector

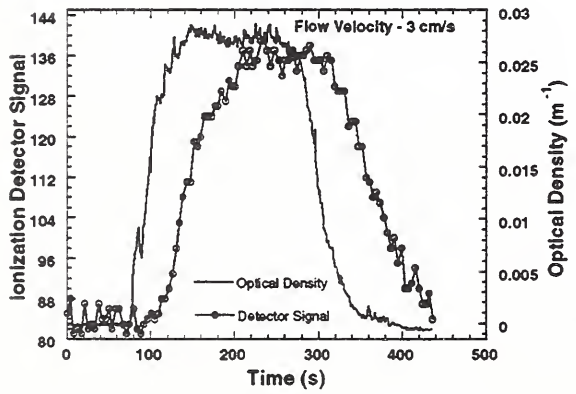

Figure 2 - Photoelectric Detector

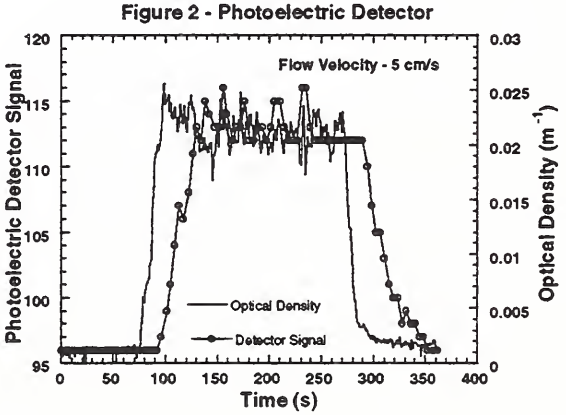

Figure 3 - Ionization Detector

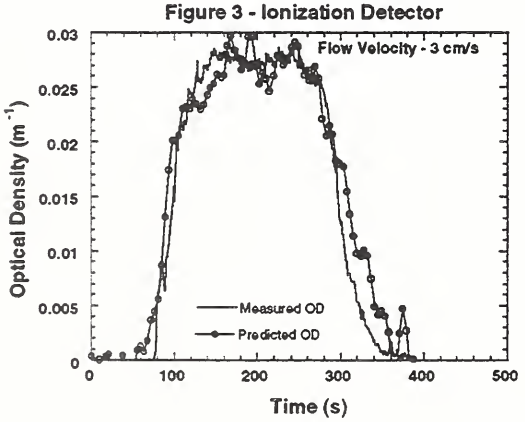

Figure 4 - Photoelectric Detector

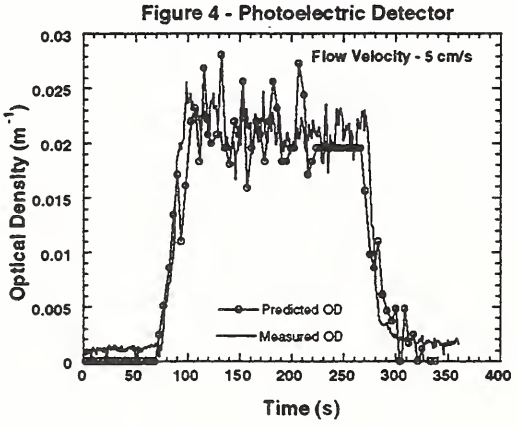

Matching Fires and Simulations

Prof. Jonathan R. Barnett, Prof. Matthew O. Ward and Jayesh Govindarajan
Worcester Polytechnic Institute, Worcester, MA, USA

Introduction

This paper describes a prototype system for matching a building-specific fire simulation database with information from real fire sensors situated within the building. One use of this would be as an aid to fire-fighting efforts. The system could be used to provide responding fire fighters with fire visualizations based on real time fire predictions from Computational Fluid Dynamics (CFD) fire models. This would be a major improvement over the current situation which depends on simplistic annunciator panels to illustrate the location of detectors that have operated, but which give little indication of the fire growth rate or future fire spread.

Others have discussed the use of computer fire models for real-time fire prediction [1]. However, it has been assumed that only zone models could be used for this purpose. Unfortunately, zone models do not give adequate spatial information to assist fire fighters in truly understanding a fire's spread and growth rate. The use of a CFD code can solve this problem. However there are two major problems using CFD codes for this purpose. The first is the significant amount of time and skill necessary to prepare a CFD simulation. This is something that is not available at a fire scene. Second are the lengthy run times of such models and the difficulty in interpreting model results. In the researcher's office, this problem is resolved through the use of fast computers, or "weekend" long runs. The results are then evaluated using sophisticated computer graphics software, sometimes running on dedicated hardware platforms.

This project investigates the use of previously generated and stored computer simulations in aiding manual fire suppression. Such simulations might be prepared months or even years in advance of a fire incident. The resulting data could then be stored in a simple to access database. During a fire, this database could be compared against real-time fire sensor information to determine which of the previously modeled fires best match the one occurring in real-time. The results could then be displayed in a simple format to aid arriving fire fighters in determining the fire's progression and future spread.

This paper discusses the problem of matching real-time sensor information with CFD results stored in a database.

Database Matching

Fire models based on CFD codes generate large volumes of data. This is because a continuum is divided into a grid of thousands of cells. Each cell is treated as an individual control volume where principles of conservation of mass, energy and momentum are applied. The result of such a simulation is cell property predictions of variables such as temperature and pressure and resulting flow fields.

For our purposes, cell properties needed to match real-time sensor measurements must be stored. In addition, one might also store pre-drawn computer visualizations of the simulated fires as animations or static images. In either case, one needs to store the information necessary to display the history and future for the simulated fire(s) which are sufficiently similar to the real-time sensor data. Obviously, these requirements place huge data storage demands on the problem. Concurrent with the storage issue is the retrieval and matching of the data with the active sensor information in the short time allowed (real time).

Matching actual sensor data, which is a continuously evolving sequence of locations and activation times (or location/time/temperature read-outs, depending on the sensor type), and CFD simulation output is complicated. It involves first the computation of a virtual sensor history for the simulation and then a calculation of a distance metric between the actual and simulated sequences. It is a difficult problem due to many factors:

1. There are only a finite number of simulated fires that can be stored for a particular building, and thus all possible scenarios will not be included.
2. Two very similar fires can have significant differences in the order in which sensors activate, due to building and sensor layout.
3. Sensors which have obstructions between them can have very distinct relationships from those with no obstructions (i.e., spatial position is not the only factor).
4. It is possible for sensors to fail.
5. Two fires can have identical ordering of sensor activation, but have different growth rates, leading to significant differences in timing.

In our matching algorithm, we first attempt to match on the order of sensor activation, and then by time between sensor activations. We compute a spatio-temporal distance between the real (incomplete) sensor sequence and all of the entries in the database [2]. The distance can consider all active sensors equally, or weigh later activations as more significant than earlier ones. As each new real sensor activation occurs, the metric must be recalculated. Simulations which match all active sensors of the real sequence but have additional active sensors (i.e., a larger fire than the actual one) have their scores penalized based on the number of and distance to these additional activated sensors.

If this procedure fails to identify a simulation of sufficient similarity to the real fire, we examine a number of different alternatives. In **substitution**, we identify sensors that are physically near those which have activated and swap one or more, followed by a recomputation of the metric. In **reordering**, we check to see if two activated sensors have approximately the same activation time and, if so, try swapping their order. Finally, in **elimination**, we assume one or more sensors have failed and remove them from consideration in computing the metric.

The result of this algorithm is an ordered set of simulations that approximately match the actual building fire to date. One or more of these simulations can then be visualized at the time fire fighters arrive to provide additional information in the development of a safe and effective suppression strategy. Visualization methods we have developed and evaluated are presented in another paper. As our ability to model fires becomes more and more accurate, we expect this approach to aiding fire suppression activities will become more effective.

References

[1] Plumb, O. A., and Richards, R. F., "Development of Economical Video Based Fire Detection and Location System," NIST Grantee presentation, Washington State University, 1994.

[2] Dyreson, C. E., and Snodgrass, R. T., "Valid-Time Indeterminacy," Proceedings of the International Conference on Data Engineering, pp. 335-343, 1993.

TEMPERATURE UNCERTAINTIES FOR BARE-BEAD AND ASPIRATED THERMOCOUPLE MEASUREMENTS IN FIRE ENVIRONMENTS

William M. Pitts, Emil Braun, Richard D. Peacock, Henri E. Mitler
Erik L. Johnsson, Paul A. Reneke, and Linda G. Blevins

Building and Fire Research Laboratory
National Institute of Standards and Technology
Gaithersburg, MD 20899

1. INTRODUCTION

Gas-phase temperature is the most ubiquitous measurement recorded in fire environments and plays a central role in understanding of fire behavior. Generally, either bare-bead or sheathed thermocouples are employed. While it is recognized that such thermocouples are subject to significant systematic errors when used in fire environments, e.g., see [1], in most fire studies uncertainties for temperature measurements are not estimated or reported.

The work summarized here has been undertaken to characterize the uncertainties in temperature measurements which can occur when bare-bead thermocouples are used in fire environments and to assess the potential of two approaches--aspirated thermocouples and the use of multiple thermocouples having different diameters--to reduce the uncertainties.

2. THERMOCOUPLE RESPONSE

Thermocouples are made from two dissimilar metal wires which are joined to form a junction. When a thermocouple junction is at a different temperature than the ends of the two wires, a potential voltage difference develops across the open ends which is related to the temperature of the junction. In general, the thermocouple junction temperature can be determined with a great deal of accuracy. The difficulty is that the junction temperature is not necessarily equal to the local surrounding gas temperature which is generally the quantity of interest.

For steady-state conditions, differences between the junction temperature and local surroundings can result from 1) radiative heating or cooling of the junction, 2) heat conduction along the wires connected to the junction, 3) catalytic heating of the junction due to radical recombination reactions at the surface, and 4) aerodynamic heating at high velocities. Radiative effects are particularly important in fire environments and are the focus of much of what follows.

3. EXPERIMENTAL

A practical approach for characterizing the errors associated with the use of thermocouples for gas measurements in fire environments has been adopted. Measurements using bare-bead thermocouples typical of those employed at NIST for fire tests, several types of aspirated thermocouples, and combinations of thermocouples having different diameters have been recorded at multiple locations in idealized enclosure fires, and the results are compared. Note that a drawback of this approach is that the actual temperatures being measured are not known with certainty.

Tests were performed in a 40%-reduced-scale model of a standard ASTM enclosure used for fire testing. Two fuels--natural gas and heptane--were employed. Temperature measurements for several types of thermocouples were compared at different locations in the upper and lower layers. Additional measurements included heat-release-rate measurements, upper- and lower-layer doorway velocities, and radiative heat flux in the center of the doorway at the floor.

4. RESULTS

Figure 1 compares temperature time records for 400 kW natural gas fires, recorded 22 cm above the floor

in the doorway, for two types of double-shield aspirated thermocouples and a NIST bare-bead thermocouple. The radiative flux measured by the floor-mounted radiometer is also shown. The actual temperature at the measurement point is unknown, but is expected to be on the order of room temperature or ≈ 25 °C. During the test, the bare-bead thermocouple recorded temperatures approaching a maximum of 250 °C and had a time dependence very similar to that for the radiant flux. For long times the error in the bare-bead temperature measurement due to radiation is on the order of 200 °C or roughly 70% in terms of absolute temperature. The two aspirated probes provide more accurate results than the bare-bead thermocouple, but are still subject to significant error.

Temperature measurements made in the upper layer were also subject to systematic uncertainties, but the errors were generally smaller in absolute terms than those made in the lower layer. Attempts to correct temperature measurements using several variable-diameter bare-bead thermocouples were unsuccessful due to their limited time response and the rapid temperature fluctuations present in the fire environment.

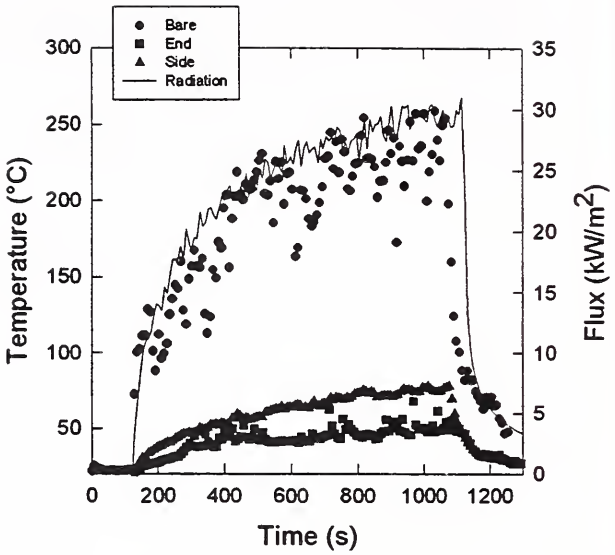

Figure 1. Temperatures measured in the lower layer of the enclosure doorway with end- and side-aspirated thermocouples and a 0.254 mm bare-bead thermocouple are shown for 400 kW natural-gas fires. Radiative flux was measured at the floor.

5. DISCUSSION

The findings of this investigation demonstrate that instantaneous and time-averaged temperature measurements recorded in fire environments using bare-bead thermocouples can have significant systematic errors due to both radiative heat transfer and finite time response. In principle, it should be possible to correct for such uncertainties when sufficient knowledge of thermocouple properties and the environment are available. However, such properties as the local radiation environment, the local gas velocity and composition, and the thermocouple surface emissivity are difficult to measure, and, in practice, such correction does not appear to be feasible. Perhaps the best approach is for a researcher to estimate the various properties along with their uncertainty ranges and use error propagation to calculate the resulting uncertainty range for the measurement. It is the responsibility of the researcher to assess whether or not the resulting uncertainty limits meet the requirements of the experimental design.

As part of this study, an idealized model of the relevant heat transfer processes for bare-bead and single- and double-shield thermocouples in typical fire environments has been developed. The calculated behaviors are qualitatively similar to those observed experimentally. The largest calculated relative errors occur for cool gases in highly radiative environments. The calculations show that for certain conditions aspirated-thermocouple measurements are subject to significant uncertainty and that double-shield aspirated thermocouples are predicted to perform significantly better than single-shield versions.

Based on the current results, it is concluded that extrapolation of temperature measurements to zero diameter for close groupings of bare-bead thermocouples having different diameters is not a viable approach for correcting thermocouple results in fire environments due to the strong temperature fluctuations present and the finite time response of the thermocouples.

The findings summarized briefly here are being prepared as a full internal report. [2]

6. REFERENCES

1. J. C. Jones, *J. Fire Sci.* **13** (1995) 261.
2. William M. Pitts, Emil Braun, Richard D. Peacock, Henri E. Mitler, Erik L. Johnsson, Paul A. Reneke, and Linda G. Blevins, *Thermocouple Measurement in a Fire Environment*, National Institute of Standards and Technology Internal Report, to appear.

Modeling of Thermocouple Behavior in Room Fires

Linda G. Blevins, Mechanical Engineer
Fire Science Division
Building and Fire Research Laboratory
National Institute of Standards and Technology

As part of a NIST effort to characterize the uncertainties of temperature measurements in fire environments, idealized models of bare-bead, single-shielded aspirated, and double-shielded aspirated thermocouples were developed and used to study the effects of varying gas and average effective surroundings temperatures on percent error in measured temperature of each type of thermocouple. Steady-state, non-linear, algebraic energy balance equations combined with appropriate convective heat transfer correlations were solved. Probe and bead sizes closely matched those used in recent NIST experiments [1]. Only one previous study has addressed aspirated thermocouples in fires [2].

Figure 1 depicts the predicted percent error in measured temperature for a 1-mm diameter, bare, spherical thermocouple, as a function of average effective surroundings temperature (T_∞), for a few gas temperatures (T_g) between 300 K and 1400 K. Percent error is defined as the difference between the thermocouple temperature and the true gas temperature expressed as a percentage of the latter, where all temperatures are absolute. The region where T_g is higher than T_∞ is termed the "upper layer," recognizing that the region includes but is not limited to the conditions generally found in the upper layer of a room fire. Similarly, the region where T_g is lower than T_∞ is termed the "lower layer." The ovals are printed on the figure to indicate that upper layer ($T_g > T_\infty$) conditions generally occur on the left side of the graph and lower layer ($T_g < T_\infty$) conditions generally occur on the right side. Figure 1 shows that a bare bead thermocouple behaves differently in the upper and lower layers of a room fire. In the upper layer, the percent error for a given T_g is relatively insensitive to T_∞, decreasing gradually to zero as T_∞ approaches T_g. In this region, percent error increases with increasing T_g. In contrast, in the lower layer, percent error is a strong function of both T_g and T_∞, increasing more and more rapidly with increasing T_∞ when the latter value is relatively high. In this region, percent error decreases with increasing T_g. The behavior in both regions is controlled by the fourth-order dependence of the radiation heat transfer rate on T_∞. The most extreme errors occur in the lower layer when T_g is at its lowest assumed value (300 K) and T_∞ is at its highest (1400 K), which would most likely be encountered during a fully-involved room fire.

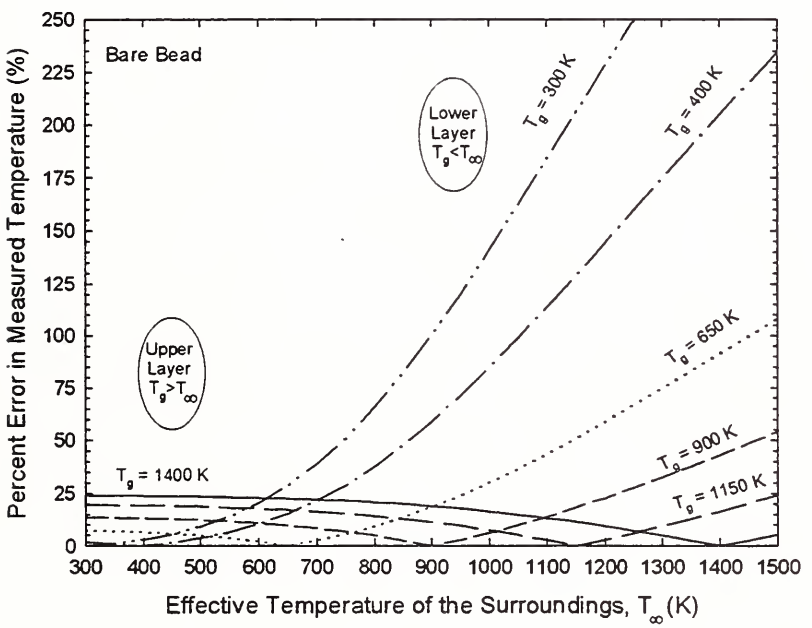

Fig. 1. Effect of surroundings temperature on percent error for a bare-bead thermocouple with diameter of 1 mm, emissivity of 0.8, and external flow velocity of 0.5 m/s.

Figure 2 depicts model results for percent error in measured temperature of a single-shielded aspirated thermocouple. The single-shielded probe behaves similarly to the bare bead, except errors in the upper and lower layers are reduced for a given T_g and T_∞, and the region of rapidly increasing error in the lower layer is shifted to higher T_∞. This shift is expected to decrease the likelihood that the region of high error will be experienced by the thermocouple in a fire test, based on the assumption that a lower-layer thermocouple is less likely to experience a given T_∞ as T_∞ increases to 1400 K and above. Although not shown here, the present modeling indicates that a double-shielded probe reduces errors further than a single-shielded one in both the upper and lower layers of a room fire.

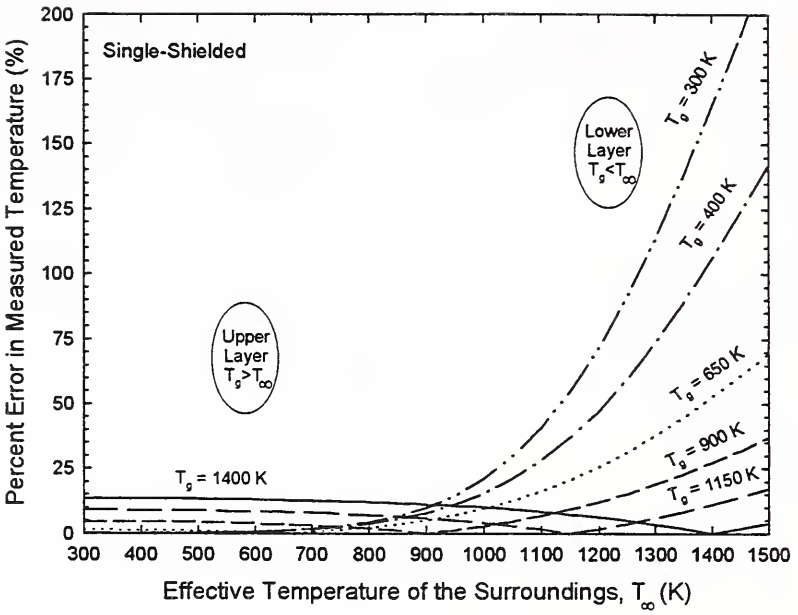

Fig. 2. Effect of surroundings temperature on percent error for an aspirated thermocouple with bead diameter of 1 mm, shield diameter of 8.6 mm, bead and shield emissivities of 0.8, external flow velocity of 0.5 m/s, and aspiration velocity of 5 m/s.

The use of an aspirated thermocouple reduces measurement error, but does not eliminate it. Figure 3 depicts model results for the temperature indicated by a single-shielded thermocouple (T_b) as a function of aspiration velocity (u) when T_g and T_∞ are 300 K and 1200 K, respectively. The predicted error is 60 % when using the ASTM-recommended 5-m/s aspiration velocity [3]. Hence, aspirated-thermocouple users are cautioned that, under certain conditions, the ASTM-recommended velocity is too slow to adequately reduce thermocouple error.

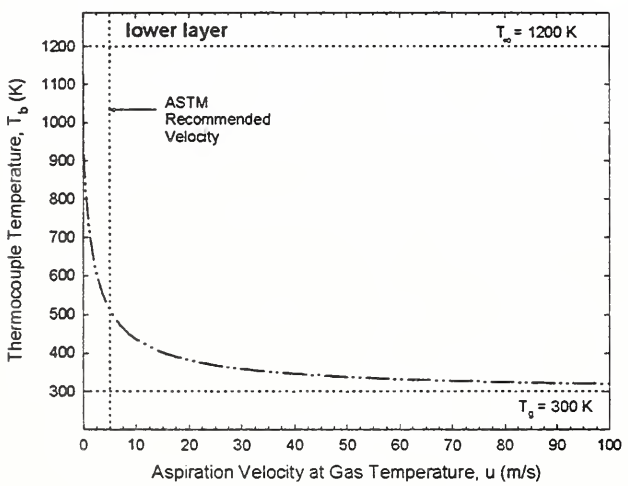

Fig. 3 Predicted aspirated-thermocouple response to variation in aspiration velocity in a lower layer. An ASTM-recommended 5 m/s exhibits 60% error.

In summary, thermocouples respond differently to changes in effective surroundings temperature in a hot upper layer than in a relatively cooler lower layer of a room fire. The most extreme errors occur in a lower layer when T_g is low and T_∞ is high. Finally, an ASTM-recommended aspiration velocity of 5 m/s may be too slow under certain conditions.

1. Pitts, W.M., Braun, E., Peacock, R.D., Mitler, H.E., Johnsson, E.L., Reneke, P.A., and Blevins, L.G., "Thermocouple Measurement in a Fire Environment." NIST Internal Report (to appear), 1998.
2. Newman, J.S., and Croce, P.A., *J. Fire Flammability* 10:327-336 (1979).
3. ASTM Standard E 603-95a, *1996 Annual Book of ASTM Standards.* ASTM Publication Code 01-040796-10, West Conshohocken, PA, 1995, p. 589.

Comparison of Near and Mid-Infrared Tunable Diode Laser Absorption Spectroscopy for the Analysis of Combustion Gases

J. Houston Miller
Department of Chemistry
The George Washington University
Washington DC 20052
houston@gwu.edu

The need for reliable, rapid, and accurate measurements of species concentrations in flames has been the motivation for the development of laser diagnostics for more than 20 years. A wide variety of techniques has been proposed including those which feature molecular absorption, fluorescence, and scattering. None of these techniques is universally applicable to all combustion species and all combustion environments. For instance, Raman scattering is relatively insensitive and is subject to interference by fluorescence by polynuclear aromatic hydrocarbons, which are found in many hydrocarbon flames. Laser-induced fluorescence is limited to molecules with accessible electronic transitions and is also subject to interference from other emitters. Therefore, the practical application of laser diagnostics requires compromises and a heavy dose of skepticism on the part of the researcher.

In our laboratory, we have had extensive experience in the development and application of mid-infrared (defined here as ≈3.5 to 16 μm) diode lasers in combustion systems. We have used these lasers to characterize the concentration of carbon monoxide and local flame temperature in methane/air and ethylene/air diffusion flames supported on laboratory scale burners (Miller et al. 1993, Skaggs and Miller, 1995). TDLAS has also been used for the detection of methane, carbon dioxide, and acetylene in a laboratory burner designed to model upset conditions in a hazardous waste incinerator (Skaggs et al., 1996, Tolocka and Miller, 1994).

A limitation of the mid infrared diode laser technology is the requirement for cryoscopic temperatures for the laser's operation and the high cost of both the devices and the detectors required at these wavelengths. In contrast, visible and near infrared lasers (and detectors) are relatively cheap. Further, low-loss and inexpensive optical fibers do not exist for the longer wavelength devices and application of the technology to systems with limited optical accessibility is hampered. For that reason, far more literature has appeared in the last several years exploring near infrared laser applications rather than mid infrared devices (Allen et al., 1995; Cassidy and Bonnell, 1988; Sonnenfroh and Allen, 1996). The former have found application in combustion systems for the detection of molecular oxygen, carbon dioxide, ammonia, methane, water, and carbon monoxide.

The Building and Fire Research Laboratory of NIST has followed these developments and has recently purchased a near infrared system for the analysis of combustion gases. In our laboratory, we have initiated a research program that will complement the NIST effort in two ways:

- We have continued the development of spectral simulation and fitting software which can be used in both the mid and near infrared.

- We have also acquired a near infrared system similar to that acquired by BFRL/NIST so that a side-by-side comparison of near and mid infrared technologies for the *in situ* analysis of combustion gases may be performed.

In this presentation, a progress report will be made on our efforts in the near infrared and implications for the detection of fire signatures will be discussed.

References

Allen, M.G., Carleton, K.L., Davis, S.J., Kessler, W.J., Otis, C.E., Palombo, D.A., and Sonnenfroh, D.M. (1995). Ultrasensitive dual-beam absorption and gain spectroscopy: applications for near-infrared and visible diode laser sensors. *Appl. Optics* 34 3240-3249.

Cassidy, D.T. and Bonnell, L.J. (1988). Trace Gas analysis with short-external cavity InGaAsP diode laser transmitter modules operating at 1.58 μm. *Appl. Optics* 27 2688-2693.

Miller, J.H., Elreedy, S., Ahvazi, B., Woldu, F., and Hassanzadeh, P.,(1993). Tunable Diode Laser Measurement of Carbon Monoxide Concentration and Temperature in a Laminar Methane/Air Diffusion Flame. *Appl. Optics* **32**, 6082-6089.

Skaggs, R.R. and Miller, J.H., (1995). A Study of Carbon Monoxide in a Series of Laminar Ethylene/Air Diffusion Flames Using Tunable Diode Laser Absorption Spectroscopy. *Combust. and Flame* **100**, 430.

Skaggs, R.R., Tolocka, M.P., and Miller, J.H. (1996) A Laboratory Evaluation of Surrogate Compounds for the Monitoring of Destruction and Removal Efficiencies. *Combustion Sci. and Tech.* in press.

Sonnenfroh, D.M. and Allen, M.G. (1996). Ultrasensitive, visible tunable diode laser detection of NO_2. *Appl. Optics* 35 4053-4064.

Tolocka, M.P. and Miller. J.H., (1994). Detection of Polyatomic Species in Non-Premixed Flames Using Tunable Diode Laser Absorption Spectroscopy. *Microchemical Journal* **50**,397

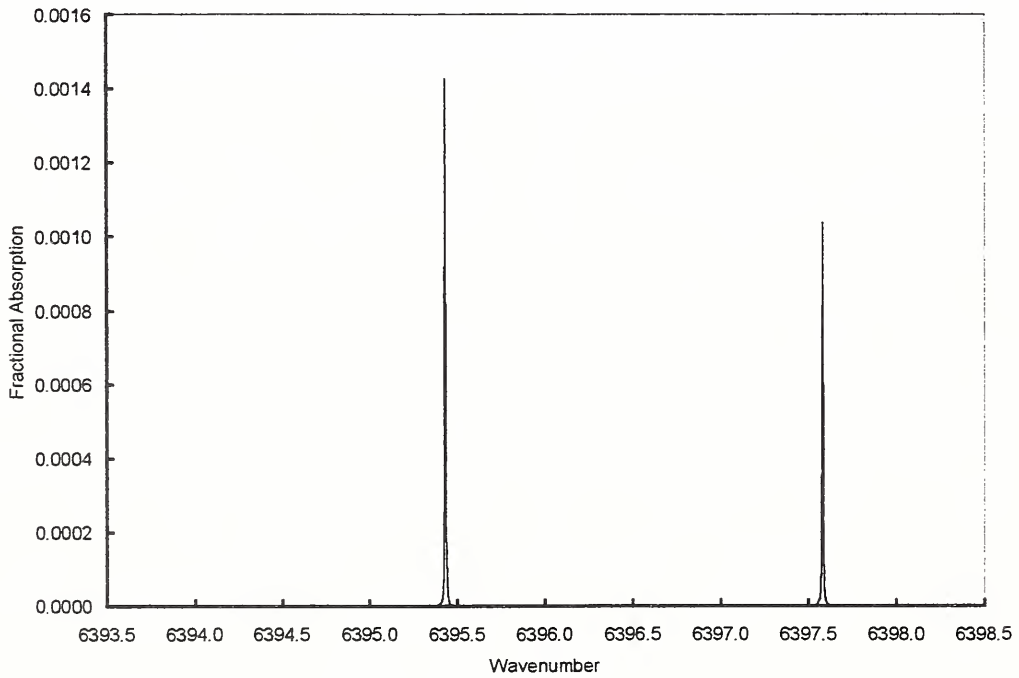

Figure 1: Simulation of expected spectrum in vicinity of 6395 cm^{-1} as observed on fuel rich side of flame front in Wolfhard-Parker slot burner supporting a methane/air diffusion flame. Both observable lines are attributable to carbon monoxide. Carbon dioxide and water, which both absorb in this spectral region, are much weaker in intensity.

Carbon Monoxide Measurement Using a Near-Infrared Tunable Diode Laser

Linda G. Blevins and William M. Pitts
Building and Fire Research Laboratory
National Institute of Standards and Technology

David S. Bomse, Southwest Sciences, Inc.

One important goal of fire research is to study the formation and consumption of chemical species in and around a fire. Instruments which possess rapid temporal response are required for resolving species concentration fluctuations and for studying rapid events such fire suppression. Presently-used probe sampling methods are slow, and system temporal response is difficult to determine because it is a complex function of sampling line length, sample flow rate, and gas analyzer response time. The limitations of probe sampling provide motivation to explore new techniques for rapidly measuring species concentrations in and around fires.

One technique that shows promise is tunable diode laser absorption spectroscopy (TDLAS), in part because market forces in the communications industry have recently made room-temperature, near-infrared semiconductor lasers, detectors, and fiber optics readily available. Tunable diode lasers are spectrally narrow and can be rapidly tuned over molecular absorption transitions. These low-cost, compact, easy-to-use lasers feature single-mode performance, long-term wavelength stability, fiber-optic compatibility, low power consumption, and suitability for implementation of rapid, sensitive detection schemes. Diode lasers have been used to measure CO, O_2, CO_2, H_2O, and CH_4 concentrations, along with temperature, in and around flames [see, e.g., 1-3].

The overall goal of the present work is to study the feasibility of combining diode lasers with rapidly advancing fiber optic technology to develop an absorption probe for use in or around fires. A prototype diode laser system is being designed to detect carbon monoxide at temperatures between 300 K and 1200 K in fire gases partially obscured by soot.

Initial efforts are underway at NIST to evaluate TDLAS technology for measurement of CO concentration in fire gases. Wavelength modulation spectroscopy (WMS) is presently being explored. A diode laser system has been assembled which consists of an Indium Gallium Arsenide Phosphide (InGaAsP) distributed feedback near-infrared laser with temperature and current controllers, fiber-optic collimators for delivering and retrieving laser light, an InGaAs photodiode detector, and a digital lock-in amplifier. A search is underway for a CO line which is relatively free from interference by species such as H_2O. This is a challenging task since H_2O strongly absorbs throughout the near-infrared spectral region, especially at high temperatures.

The amount of light absorbed by a molecule at its linecenter wavenumber ν_o (cm^{-1}) is quantified using the Lambert-Beer law, $I_\nu/I_{\nu o} = \exp\left[-S(T)g(\nu-\nu_0)NL\right]$, where $I_\nu/I_{\nu o}$ is the fractional laser light transmittance at ν_o, S(T) is the temperature-dependent line strength (cm^{-1}/molecule·cm^{-2}), $g(\nu-\nu_o)$ is the line shape function (normalized to unit area) evaluated at ν_o (cm), N is the number density of the absorber (molecule/cm^3), and L is the absorption path length (cm). Experimental determination of a species concentration involves measuring the fractional transmittance and the temperature. The number density of the absorber can then be computed from the known line strength, line shape function, and path length, and can be converted to concentration using the ideal gas law.

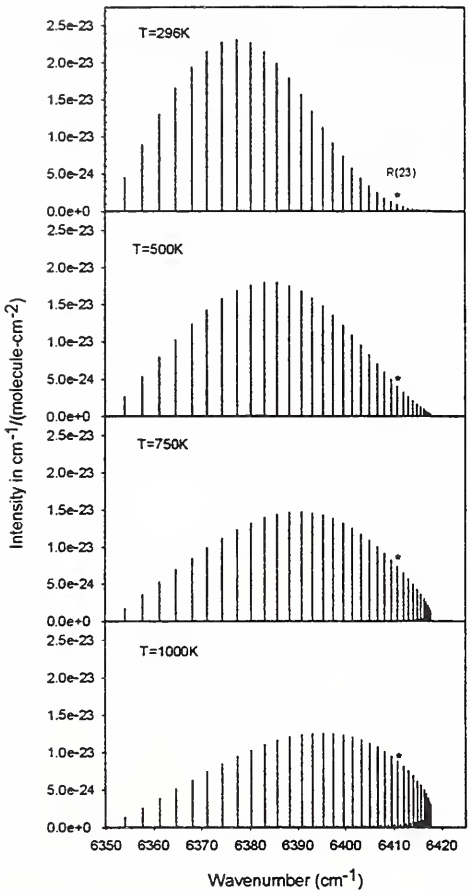

Fig. 1 Temperature-dependent line strengths for the R-branch of the second overtone of CO.

The temperature-dependent line strength for CO is obtained from the HITEMP database, which is a special version of HITRAN [4, 5]. Figure 1 depicts S(T) for the R-branch of the 3ν overtone band at temperatures of 296 K, 500 K, 750 K, and 1000 K. The rotational line marked with a star on the graph corresponds to the R(23) line, and the figure indicates that S(T) for this line increases from 8.3×10^{-25} cm^{-1}/molecule·cm^{-2} at 296 K to 8.8×10^{-24} cm^{-1}/molecule·cm^{-2} at 1000 K. Detection sensitivity depends on the product of S(T) and $g(\nu-\nu_o)$. A Voigt profile, which accounts for both collisional and thermal (Doppler) line broadening, is appropriate for computing $g(\nu-\nu_o)$ for most fire-gas applications [2].

Figure 2 shows preliminary data collected in flame gases for the R(23) CO line. Data were taken on the lateral centerline of a Wolfhard-Parker CH_4/air diffusion flame at a height of 9 mm from the burner. At this location, [CO] = 8700 ppm, $[H_2O]$ = 3.6 %, and T = 550 K along a 4.1-cm path [6,7]. The laser current was modulated at 20 kHz and detected at 80 kHz, so the signal is proportional to the fourth derivative of the lineshape (4f spectroscopy). Each scan is the difference between the demodulated detector signal and the 4f sloping background signal. Both are normalized by the d.c. component of the detector signal. The laser beam is delivered through a single-mode fiber-optic collimator and mirror-focused onto a detector. The spectrum is the average of 1000 sweeps, each of 26-ms duration. Increasing data point number on the abscissa represents decreasing wavenumber, and the resolved peak at point number 130 corresponds to the R(23) CO line at 6410.8 cm^{-1}. The figure demonstrates the potential for retrieving CO signals from hot fire gases with WMS.

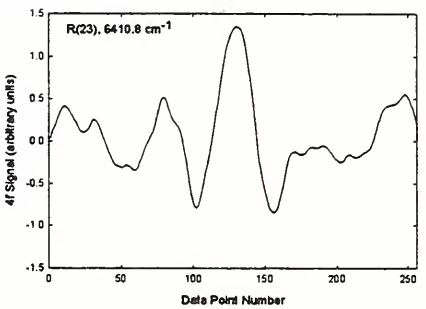

Fig. 2. 4f signal along lateral centerline at 9-mm height in WHP flame.

1. Silver, J.A., Kane, D. J., and Greenberg, P. S., *Applied Optics* 34:2787 (1995).
2. Allen, M.G., *Measurement Science and Technology* 9:545 (1998).
3. Mihalcea, R. M., Baer, D. S., and Hanson, R. K., *Measurement Science and Technology* 9:327 (1998).
4. Rothman, L.S., Gamache, R.R., Tipping, R.H., Rinsland, C.P., Smith, M.A.H., Benner, D. Chris, Devi, V. Malathy, Flaur, J.-M., Camy-Peyret, C., Perrin, A., Goldman, A., Massie, S.T., Brown, L.R., Toth, R.A., *Journal of Quantitative Spectroscopy and Radiative Transfer* 48:469 (1992).
5. Rothman, L.S., HITRAN home page, http://www.hitran.com/ (1998).
6. Miller, J.H., Elreedy, S., Ahvazi, B., Woldu, F., and Hassanzadeh, P., *Applied Optics* 32:6082 (1993).
7. Norton, T.S., Smyth, K.C., Miller, J.H., and Smooke, M.D., *Combustion Science and Technology* 90:1 (1993).

LARGE-SCALE PLANAR MEASUREMENTS AND SCALING OF SPRINKLER SPRAYS

David Everest and Arvind Atreya
Department of Mechanical Engineering and Applied Mechanics
University of Michigan; Ann Arbor, MI 48109-2125

INTRODUCTION

Water spray sprinklers are the most commonly used automatic fire protection systems in buildings ranging from small offices to large warehouses. For effective fire suppression, the sprinkler water must reach the burning surface. An optimum sprinkler system, for a given application, is one that providesthe maximum fraction of water delivered by the sprinkler (or sprinklers in a large warehouse) to the burning surfaces and suppresses the fire in the shortest time after its initiation. The design of such a sprinkler system depends on the geometrical relationship between the sprinkler(s) and the fire source and its heat release rate, the geometry of the room and its ventilation conditions and the sprinkler spray characteristics. Given the complexity of the problem, the optimization, as well as the evaluation, of various sprinkler systems ismost cost-effectively accomplished via fundamental mathematical models that can calculate the fire and sprinkler induced flows for different geometries. Such fundamental models are being developed at BFRL (NIST) by Drs. McGrattan and Baum. For experimental validation of these models, instantaneous field measurements are needed on the drop size distribution, drop velocity, sprinkler induced flows, fire induced flows and the actual delivered density resulting from the interaction of the sprinkler induced flows with the fire induced flows. This work attempts to provide some of these measurements. Measurements presented in this paper include planar optical measurements of: (a) Drop size distribution and droplet velocities produced by a scaled sprinkler head under various water flow rate conditions, and (b) The actual delivered water density at various heights from the sprinkler head (to provide an integral confirmation of the optical measurements). Sprinkler scaling relationships are also developed to relate the laboratory-scale & large-scale measurements.

EXPERIMENTS

Several axis-symmetric scaled pendent sprinkler heads were designed with different nozzle diameters [6, 8 & 10 mm] and different strike plate cone angles [90°, 120°, 140° & 180°]. These sprinklers were tested at different water flow rates [1 to 10 gpm]. A small nozzle diameter, high flow rate and a large strike plate angle is expected to create small droplets that will spread further from the center, whereas, a large nozzle diameter, low flow rate and a small strike plate angle will create large water droplets thatfall closer to the center. Thus, varying these parameters enables testing different sprinkler configurations. However, only some of these configurations could be contained within the 8'×8'×8' laboratory-scale experimental apparatus.

The flow rate and the pressure of the water to the sprinkler head is controlled by a valve and is continuously monitored. A red or yellow fluorescent dye (approx. 1 ppm concentration) is also introduced into the sprinkler water to enable filtering the scattered laser light and recording only the fluorescent emission from the droplets on to the photographs. This technique provides a more accurate drop size measurement by minimizing the "Gaussian ambiguity" and "ghost reflections". Furthermore, by appropriately choosing the fluorescent dye, two-color, double-exposed photographs are easily created. The dual Nd:Yag PIV laser is made to fire at the desired time intervals to measure the droplet velocity by the particle tracking technique. During these experiments, the water at the floor level is also collected tomeasure the actual delivered density.

High-resolution, large-scale planar [35cm×25cm] photographs taken during these experiments were digitized by a high resolution scanner. After digitization, the analysis was performed by the TSI INSIGHT software to determine the velocity vectors by the particle tracking technique The drop size distribution was determined by using the SCION IMAGE program. The measurements of drop size and velocity were made

near the sprinkler head to help define the initial conditions needed for developing a sprinkler scaling criteria. This criteria is to tested by the measured delivered density.

The results are presented in figs. 1, 2 & 3. The origin of the graphs in figs. 1 and 2 correspond to the sprinkler location. Figure 1 shows the instantaneous droplet locations, whereas, fig. 2 shows the velocity vectors. As expected, the angle of the strike plate has a dominant influence on the droplet spread and the magnitudes of the droplet velocities are affected by the flow rates. The instantaneous drop size distribution determined from the photographs is shown in fig. 3. These are for the 8mm diameter nozzle and different strike plate cone angles. Clearly, the drop size distribution is not significantly altered by changing the strike plate cone angle. The data seems to imply that the drop size distribution is controlled by the sheet breakup process, the droplet spread by the strike plate cone angle, and the droplet velocities by the water flow rate for the same orifice diameter.

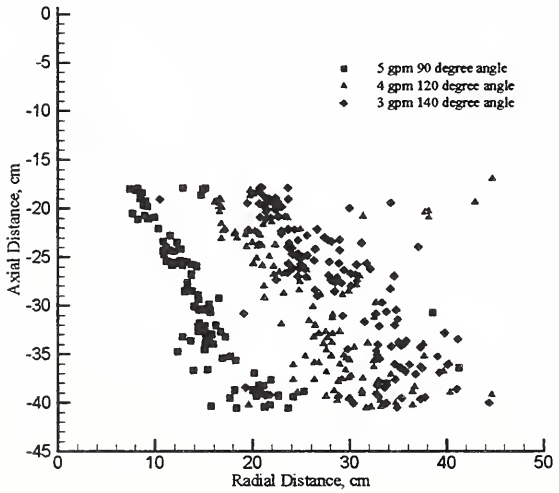

Figure 1. Drop Locations

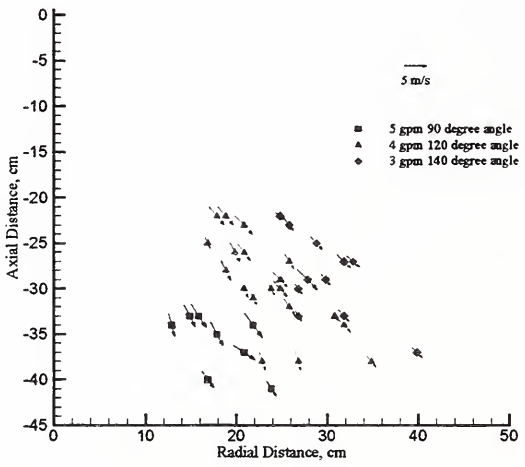

Figure 2. Drop Velocity Field

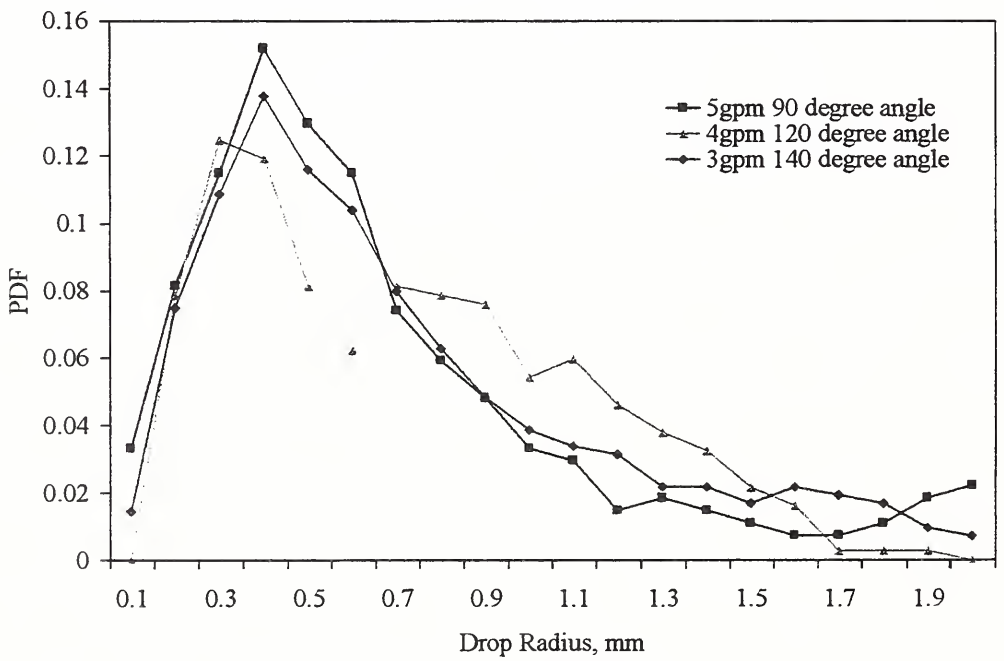

Figure 3. Drop Distributions Resulting from 8mm Nozzle

Drop Size Measurements in a Fire Sprinkler Using an Agricultural Testing Method

Linda G. Blevins, Building and Fire Research Laboratory
National Institute of Standards and Technology

Joe C. Oliphant, Center for Irrigation Technology
California State University, Fresno

The NIST Industrial Fire Simulation (IFS) computer model is being adapted to predict the interaction between sprinklers and fires at realistic scales [1]. The new formulation relies on a sprinkler submodel calibrated with experimentally measured water drop size distributions. Measuring drop sizes for large scale fire sprinklers is challenging because the range of diameters is large (~10 μm to ~5 mm) and instruments must be protected from flowing water (~200 L/min). Agricultural researchers experience similar challenges in studying crop-irrigation sprinklers. They are interested in measuring drop size to optimize the uniformity of a sprinkler's ground application rate, and have methods in place to perform the measurements [2]. Because many agricultural sprays are similar in drop size and flow rate to those from large fire sprinklers, NIST is exploring the possibility of applying agricultural measurement methods to fire sprinklers in support of the IFS effort. Initial findings of the investigation are reported here.

Measurements of drop size distribution in a fire sprinkler were made in a large agricultural sprinkler testing facility. An optical array probe consisting of a ribbon of laser light illuminating a photodiode detector array was used [3]. In this instrument, droplets pass between the laser and detectors, and a maximum horizontal drop width (diameter) is determined for each in-focus droplet from its shadowing pattern on the photodiodes. Corrections are made for drop overlap and partial drop shadowing [4]. The range of detectable drop widths is 0.2 mm (0.008 in) to 12.4 mm (0.49 in), and the probe is ruggedly designed with splash guards to withstand large flows. It should be noted that an optical array probe has also been used for fire sprinkler research, although for a smaller range of detectable drop sizes [5]. Rain-gauge style water collectors were used to determine water application rates [6]. The collectors are 10-cm in diameter and are placed at discrete intervals, providing less area coverage than that obtained by contiguously placed 30 cm x 30 cm x 30 cm collection pans used for fire sprinkler distribution tests [7]. The sprinkler tested was a 13.5-mm (17/32 in) diameter orifice, upright model with 130 kPa (19 psig) delivery pressure. Drop size spectra and application rates were measured at ground level with the sprinkler mounted at the end of a 4.5-m (14.8 ft) high, cantilevered pipe. Measurements were made at six equally spaced radii between 0.5 m (1.6 ft) and 3.0 m (9.8 ft) along a direction perpendicular to the sprinkler brace.

Median drop diameters based on volume and number, shown in Fig. 1, are defined in the following way: Half of the sprinkler's *total water flow* at each location exists as drops which are larger (or smaller) than the volume-based median, and half of the *number of droplets* at each location are larger (or smaller) than the number-based median. Volumetric median drop sizes are 2.2 mm at a radius of 0.5 m, and increase to 3.3 mm at a radius of 3.0 m. Number-based median drop sizes range from 0.5 mm to 1.0 mm. The increase in median drop size with radius is consistent with

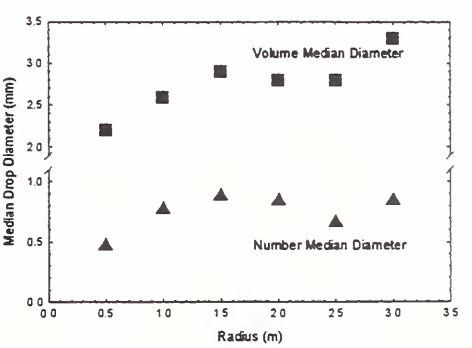

Fig. 1 Radial profiles of volume-based and number-based median drop diameter

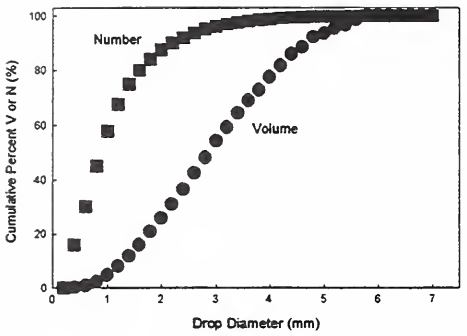

Fig. 2. Local volumetric and number-based size distributions for 1.5-m radial location.

other fire sprinkler results described in Ref. 5. Examples of local drop size distributions for the radial location of 1.5 m are shown in Fig. 2. A number distribution is shown because the IFS sprinkler submodel is based on the random selection of sizes from number-based distributions. These drop size data are presently being analyzed at NIST to determine their reliability.

Figure 3 depicts the application rate profile. The application rate is maximum at 43 cm/hr (0.18 gpm/ft^2) at a radius of 1.5 m. For agricultural testing, the application rate is used to combine local drop size distributions into an overall volumetric distribution for the sprinkler. This involves assuming that the application rate and drop sizes measured at a given radial location are constant throughout an annular ring bisected by the radius, computing individual volumetric flow rates for each ring, and then computing the overall distribution as a volume-weighted sum of the individual size distributions. This procedure was found to be inadequate for the present sprinkler because the individual annular volumetric flow rates sum to 114 L/min (30 gpm), which is just 55 % of the total water flow rate through the sprinkler. Hence, 45 % of the sprinkler flow is not accounted for when the constant-annular-ring assumption is made. This could be because the measurements were not spaced closely enough or because the distribution pattern is less uniform than that of a typical agricultural sprinkler. A procedure involving closely-spaced measurements over the entire two dimensional sprinkler distribution is more appropriate for fire sprinklers [e.g., as in Ref. 5].

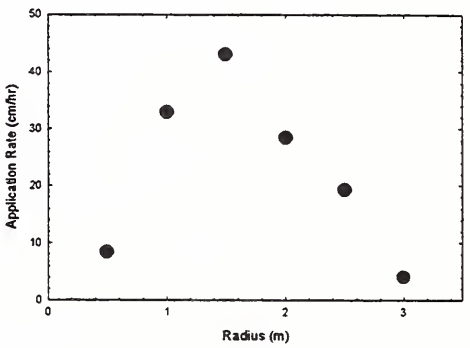

Fig. 3. Radial profile of application rate.

In summary, an agricultural sprinkler drop size measurement method was applied to a fire sprinkler. Local drop size data are presently being analyzed at NIST. The agricultural procedure must be modified to obtain useful overall size distributions for fire sprinklers with non-uniform distribution patterns.

---

1. McGrattan, K., and Stroup, D., "Large Eddy Simulations of Sprinkler, Vent and Draft Curtain Performance," Proceedings of the Fire Suppression and Detection Research Application Symposium, 1997, NFPA, p. 59.

2. Kincaid, D.C., Solomon, K.H., and Oliphant, J.C., "Drop Size Distributions for Irrigation Sprinklers," *Transactions of the American Society of Agricultural Engineers* 39:839 (1996).

3. Knollenberg, R.G., "The Optical Array Probe: An Alternative to Scattering or Extinction for Airborne Particle Size Determination," *Journal of Applied Meteorology* 9:86 (1970).

4. Solomon, K.H., Zoldoske, D.F., and Oliphant, J.C., "Laser Optical Measurement of Sprinkler Drop Sizes," California Agricultural Technology Institute Publication #961101, available online at http://www.atinet.org/cati/cit.

5. Chan, T.S., "Measurements of Water Density and Drop Size Distributions of Selected ESFR Sprinklers," *Journal of Fire Protection Engineering* 6:79 (1994).

6. Procedure for Sprinkler Distribution Testing for Research Purposes. ANSI/ASAE SS330.1, 1995.

7. Standard for Automatic Sprinklers for Fire-Protection Service. UL 199, 1997.

Design and Testing of a New Smoke Concentration Meter

George W. Mulholland, Erik L. Johnsson, David A. Shear, and Marco G. Fernandez
National Institute of Standards and Technology
Gaithersburg, MD 20899

An important parameter in assessing the fire safety of a new product is the smokiness of the material with regard to its effect on visibility. Materials with tendency to produce high levels of smoke make it more difficult for people to egress from the affected area. Minimizing smoke is especially important in transportation systems such as planes, trains, and subways. It is also important to avoid smoke deposition in high impact areas like communication systems and computer facilities. Smoke deposition is also a major concern in high cost production facilities where a clean environment is crucial such as for semiconductor fabrication and for pharmaceutical preparation.

One measure of the smokiness of a material is its smoke yield ε, which is defined as the mass of smoke produced/mass of material burned. This quantity varies from 0.005 for flaming combustion of wood cribs to as high as 0.15 for polystyrene. The rate of smoke production during a fire depends on both the value of ε and on the mass loss rate of the fuel. So it is possible for a material with a larger ε to produce less total smoke than a material with a higher burning rate.

The Cone Calorimeter and the NIST Furniture Calorimeter have been used to measure the specific-extinction area of a material σ_f, which is the light extinction coefficient normalized by the mass loss rate of the sample per volume flux through the collection hood. While this is a useful tool for relative comparison of materials, for modeling applications it is more convenient to use the mass concentration of smoke rather than an optical property.

Last year at this meeting we reported that the specific extinction coefficient of flame generated smoke, σ_s, has a value of 8.5 m^2/g with an "uncertainty" band of 2 m^2/g to include the effects of material chemistry and fire scale. With the knowledge of this constant, the mass concentration, m_s, can be determined from the transmission of light through the smoke in the duct via the following formula:

$$m_s = \frac{ln(I_0 / I)}{\sigma_s L} \qquad (1)$$

where L is the pathlength through the smoke and I_0 and I refer to the incident and transmitted light intensity for a monochromatic light source. The universality of σ_s is the impetus for the development of this new instrument.

The advantage of determining the mass concentration by an optical method is that it is much less labor intensive compared to filter collection and allows routine measurement at the same time one is performing a test to measure the heat release-rate.

In order to test practicality of this concept, we have developed a light-extinction system and incorporated in a Furniture Calorimeter at NIST. As with previous light-extinction meters used at NIST with the Cone Calorimeter and the Furniture Calorimeter, this system uses a He-Ne laser and a Si photodiode detector. One major design change was to use wherever possible commercially available components including the light source, detector assembly/optics, and mounting /positioning apparatus. The intention was to provide a design that could become a standard. A number of other changes were made to enable measurements at lower smoke concentrations and to reduce the overall measurement uncertainty:

- A stabilized light source to minimize the intensity drift.
- Measurement of pathlength in the presence of purge air quantified using a glass purge tube.

- A focusing lens and diffuser to minimize the effect of light-beam movement at high temperature.
- Commercial position equipment to simplify instrument alignment.

The initial system included a newly developed diode laser which included a high precision temperature controller to maintain constant laser intensity. This diode laser performed well for small fires, but as the ambient temperature in the building increased for the large fires, the temperature controller was not able to maintain a constant temperature and there was a drift in the laser intensity. The diode laser was replaced with a He-Ne laser together with a laser stabilizer to provide a constant output intensity with a drift of less than 0.1 % in intensity over a ten minute test.

The one component that was fabricated in house was the support assembly for the smoke concentration meter. This consisted of an approximately 1 meter-long section of 15 cm-wide U-channel attached to the 0.5 m-diameter duct with gussets. Both the light source assembly and detector assembly were attached to the U-channel assembly to minimize the effect of the thermal expansion of the duct. The effect of beam displacement was assessed by using "smokeless" natural-gas flames with heat release rates in the range 100 kW to 500 kW. Even for the 500 kW fire operated for 600 s, which is the maximum limit for the furniture calorimeter at NIST, the effect on the transmitted light intensity was minimal.

In addition to the mass concentration, the mass flux of smoke and the yield of smoke can be determined given the stack-flow rate and the mass-loss rate of the fuel. The temperature, velocity, and smoke-concentration profiles were measured to determine the relationship between the line-of-sight average smoke concentration and the cross-section averaged quantity needed for determining the total mass flux of smoke in the duct.

To assess the performance of the smoke meter, four repeat series of experiments with propane fuel at 50 kW, 100 kW, and 450 kW were carried out. A series of pool fire experiments were carried out to provide a more realistic test of the system. Heptane, toluene, and a mixture of heptane and toluene were burned in a 50 cm diameter pan. The mass-loss-rate of the fuel was measured with a load cell allowing the determination of the smoke yield. The heptane tests were performed to enable comparison with literature values of smoke yield and the light-extinction coefficient for the same size pan and same fuel. Toluene has one of the highest smoke yields of any material and was selected to provide test data at the upper limit of intended use.

We believe our design can be followed by other users for incorporation in their systems. In our case, the smoke concentration meter was mounted on an 0.6 m-long section of duct, which was then attached to the existing exhaust duct. The total cost of the components was approximately $8,000, and another $2,000 was necessary for shops to fabricate the support structure and optical ports.

OPTICAL PROPERTIES OF SOOT IN THE OVERFIRE REGION OF LARGE BUOYANT TURBULENT DIFFUSION FLAMES

by

S.S. Krishnan, K.-C. Lin and G.M. Faeth
Department of Aerospace Engineering
The University of Michigan
Ann Arbor, Michigan 48109-2140

Introduction. Information about the optical properties of soot is needed in order to develop optical measurements of soot properties and to compute soot radiation in flame environments. Unfortunately, current estimates of soot optical properties involve excessive uncertainties due to uncertainties about soot refractive indices [1]. Wu et al. [2] sought to correct this deficiency by measuring the refractive index properties of soot in the overfire region of large gaseous hydrocarbon fueled buoyant turbulent diffusion flames burning in still air where soot properties depend on the fuel but are independent of position and flame residence time [3,4] by exploiting the properties of Rayleigh-Debye-Gans scattering theory for polydisperse fractal aggregates (denoted RDG-PFA theory) which has been recently shown to be effective for soot optical properties [5,6]. Unfortunately, measurements of soot dimensionless extinction coefficients due to Wu et al. [2] were not in good agreement with contemporary measurements of Dobbins et al. [7] and Choi et al. [8] which raises questions about the corresponding accuracy of their refractive index measurements. Thus, the present study sought to resolve this issue by completing similar measurements of soot optical properties, again considering soot in the overfire region of large buoyant turbulent flames but for a broader range of both gas and liquid hydrocarbon fuels burning in still air.

Experimental Methods. The soot was produced by round burners exhausting into a large collection hood followed by a short exhaust duct. Soot properties were measured at the exit of the exhaust duct. Overfire soot physical properties were known for many of the fuels considered based on earlier work [2,4]. Soot volume fractions were measured by weighing soot collected on a filter while measuring the volume flow of gas over the collection period; this information combined with the known soot density yielded soot volume fractions at the test location.

Soot dimensionless extinction coefficients and other soot optical properties in the overfire region were found in the same way as before [2]. In particular, laser extinction and scattering properties were analyzed to indicate soot fractal dimensions, refractive index functions, refractive indices and dimensionless extinction coefficients based on RDG-PFA theory. Fuels considered included acetylene, ethylene, propylene, propane, benzene, toluene, cyclohexane, and n-heptane.

Results and Discussion. Similar to [2], present measurements confirmed that RDG-PFA theory was effective in the visible wavelength range (350-633 nm); notably, the evaluation included primary particle optical diameters as large as 0.46 which severely tests the approximations of this theory. Present scattering measurements in the visible established the fractal dimensions of the present soot at 1.8 with a standard deviation of 0.01 relatively independent of fuel type and properly independent of wavelength.

Present measurements of dimensionless extinction coefficients are plotted as a function of wavelength, in Fig. 1. Also shown on the figure are earlier measurements of this parameter for soot in the overfire region of crude-oil/air diffusion flames [7] and in the post-flame region of fuel-rich acetylene/air flames [8]. Present measurements exhibit little variation with wavelength and fuel type, except that results for acetylene soot are significantly lower than the other fuels. Thus, present results have been separated into two groups consisting of acetylene and the average for the rest of the fuels. Averaging the present results over all fuels and wavelengths yields a value of 8.6 with a standard deviation of 0.5. The results of Refs. 7 and 8 agree with this value within experimental uncertainties whereas in spite of extended efforts the somewhat smaller (by roughly 40%) values found by Wu et al. [2] could not be reproduced and it is recommended that they not be used in the future.

Present measurements of the refractive index functions E(m) and F(m), where m is the index of refraction of soot, are plotted in Fig. 2. Also plotted on the figure are earlier findings due to Dalzell and Sarofim [9], Batten [10], Lee and Tien [11], Chang and Charlampopoulos [12] and Vaglieco et al. [13]. Present results do not approach a resonance condition typical of graphite as uv is approached; instead, E(m) and F(m) decline continuously similar to recent observations for amorphous carbon and soot

[12,13]. Similar to the behavior of the dimensionless extinction coefficients, present measurements of E(m) and F(m) exhibit relatively little effect of fuel type except for acetylene soot which consistently yields smaller values of E(m) and F(m) than the rest. A number of earlier measurements [10-13] are not in good agreement with present measurements as the uv is approached because they involve questionable approximations when applying Drude-Lorence dispersion models or Kramers-Krönig causality relationship to close procedures to find soot refractive indices. These difficulties tend to disappear as the ir is approached where the various measurements are in better agreement, including the often criticized but widely used measurements of Dalzell and Sarofim [9].

Acknowledgments. This research was supported by NIST Grant No. 60NANB4D1696 with H. R. Baum of BFRL serving as Scientific Officer.

References

1. Faeth, G.M. and Köylü, Ü.Ö., Combust. Sci. Tech. 108:207 (1995).
2. Wu, J.-S., Krishnan, S.S. and Faeth, G.M., J. Heat Trans. 119:230 (1997).
3. Sivathanu, Y.R. and Faeth, G.M., Combust. Flame 81:133 (1990).
4. Köylü, Ü.Ö. and Faeth, G.M., Combust. Flame 89:140 (1992).
5. Köylü, Ü.Ö. and Faeth, G.M., J. Heat Trans. 116:152 (1994).
6. Farias, T.L., et al., J. Heat Trans. 117:152 (1995).
7. Dobbins, R.A. et al., Atmos. Environ. 28:889 (1994).
8. Choi, M.Y. et al., Combust. Flame 102:161 (1995).
9. Dalzell, W.H. and Sarofim, A.F., J. Heat Trans. 91:100 (1969).
10. Batten, C.E., Appl. Optics 24:1193 (1985).
11. Lee, S.C. and Tien, C.L., 18th Symp. (Intl.) on Combustion, The Combustion Institute, Pittsburgh, 1980, p. 1159.
12. Chang, H.Y. and Charolampopoulos, T.T., Proc. R. Soc. London A430:577 (1990).
13. Vaglieco, B.M. et al., Combust. Flame 79:259 (1990).

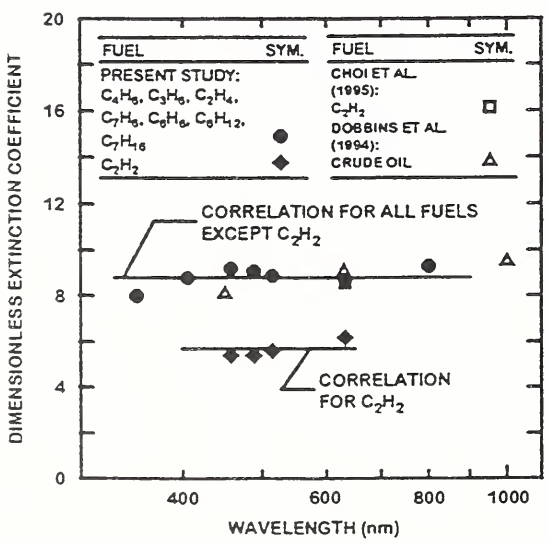

Fig. 1 Measured soot dimensionless extinction coefficients in the visible.

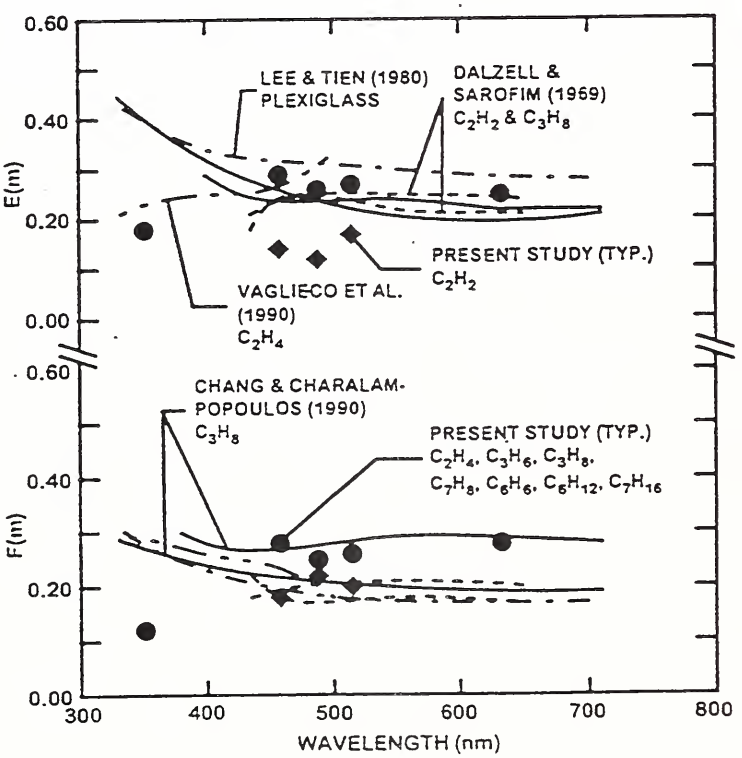

Fig. 2 Measured soot refractive index functions E(m) and F(m), in the visible.

A MIXED LAYER MODEL FOR PYROLYSIS OF BUBBLING THERMOPLASTIC MATERIALS

Kathryn M. Butler
Building and Fire Research Laboratory
National Institute of Standards and Technology
Gaithersburg, Maryland 20899

Introduction For many thermoplastic materials exposed to a strong heat flux from above, a layer of bubbles forms in the melted region near the upper surface. The action of these bubbles is observed to range from slow growth and bursting to vigorous boiling behavior. Although the bubbles appear to have a significant effect on the macroscopic thermal and mechanical properties of the material,[1] the mechanisms by which a bubbling layer affects heat and mass transfer are not well understood. Since the thermal conductivity of a gas is much lower than the thermal conductivity of a liquid, we might expect the transport of heat to be slowed considerably in the presence of bubbles. Alternatively, vigorous boiling behavior could be mixing the upper layer of melted thermoplastic material, resulting in a nearly uniform temperature throughout the bubbling layer. How would these seemingly contradictory mechanisms affect heat and mass transfer, and which dominates behavior during pyrolysis?

Several models have considered the effects of in-depth gasification on the temperature profiles and mass loss rate of pyrolyzing materials.[2,3] The physical effects of bubbles are generally neglected by assuming that gases escape on a timescale short compared to the phenomena of interest, although an effective thermal conductivity based on the local volume fraction of gas has been introduced as a simple way to investigate the insulating properties of trapped gas.[4] A literature on mixed layer effects on heat transfer may be found in oceanography, where such models have been used to understand diurnal and seasonal variations in the temperature profile of the upper ocean.[5] Although the driving forces in ocean models are very different, a similar approach can be used to study the limiting case of a perfectly mixed bubble layer. This is the model described in this abstract.

Model The geometry of this model is shown in Figure 1. At time $t = 0$, a solid slab of thermoplastic material of thickness L is exposed on its upper surface to a constant heat flux. The lower surface, located at $z = 0$, is perfectly insulated. The solid material heats up through conduction until the upper surface reaches the melt temperature, at which time a phase change takes place. The location $z = l_s(t)$ of the moving interface between solid and liquid layers, where the temperature is equal to the melt temperature, is one of the variables in this problem. The heat consumed during the phase change is included in the heat flux balance across this interface.

As the temperature in the melt continues to increase, gasification begins through a chemical reaction described by an Arrhenius expression. This causes turbulence that stirs the uppermost region of melt and forms a mixed layer of uniform temperature. The mixed layer thickness $h(t)$ increases through entrainment of the quiescent melt beneath the mixed layer. Over the thin entrainment layer (whose thickness goes to 0 in the analysis), the temperature varies linearly in space from the temperature at the top of the quiescent melt to the higher temperature of the mixed layer. Although gasification occurs over the entire sample according to temperature, turbulence is limited to the mixed (bubble) layer. The timescale of mass transport of the gases is assumed to be much smaller than the timescale over which the quantities of interest are evolving, so that gases escape instantly as they are generated. Mass transport is of interest in this problem only in that it results in thorough mixing of the uppermost layer of liquid.

To incorporate turbulent mixing into the model equations, Reynolds averaging is used. The existence of a timescale long enough to adequately average horizontal and vertical disturbances in the mixed layer but short enough to follow the evolution of the averaged quantities of interest is assumed. The problem is homogeneous horizontally, so that Reynolds-averaged quantities are functions of z and t only. Each field variable is then decomposed into the sum of a Reynolds averaged part and a deviation from the mean, and equations are derived for both mean and turbulent parts. At the upper surface, the incident heat flux transforms into a turbulent heat flux that is uniform within the mixed layer. The final model equations necessary to solve for temperatures and thicknesses in the solid, melt, and mixed layers are obtained by

relating the transport of turbulent heat flux and turbulent kinetic energy to gasification and the mixed layer thickness.

Results The mixed layer model can be compared to a model of a heated thermoplastic sample subject to melting and in-depth gasification but without a turbulent mixed layer. Figure 2 displays the temperature profiles near the upper surface from both models after the same time has elapsed. At this point mass losses have begun (the initial thickness of the sample was 2 cm) and the mixed layer has begun to grow. The mass loss rate is found to be slightly higher for the mixed layer model. At the upper surface, the temperature of the mixed layer exceeds the melt temperature of the in-depth model. However, the presence of the mixed layer actually decreases the temperature in the interior of the sample. This is an interesting result, since a reduction in interior temperature would also be expected for a model that takes the lower thermal conductivity of the bubbles into account.

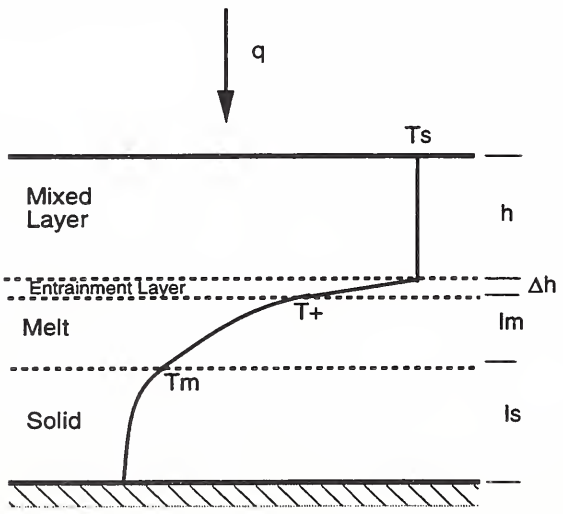

FIGURE 1: Mixed layer model

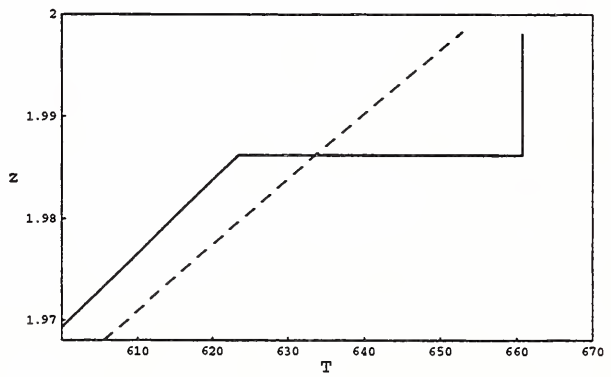

FIGURE 2: Comparison of temperature profiles near the upper surface for in-depth gasification model with (solid) and without (dashed) a turbulent mixed layer. Distance z is measured in centimeters and temperature T in degrees Kelvin.

Conclusions A model representing the bubbling behavior of a pyrolyzing thermoplastic material as a mixed layer of uniform temperature has been developed. Initial results indicate that the formation of a mixed layer tends to increase the mass loss rate and decrease the temperature in the quiescent melt and solid layers beneath.

References

[1] Kashiwagi, T. and Ohlemiller, T.J., "A Study of Oxygen Effects on Nonflaming Transient Gasification of PMMA and PE During Thermal Irradiation," *Nineteenth Symposium (International) on Combustion*, The Combustion Institute, pp. 815–823 (1982).

[2] Vovelle, C., Delfau, J.-L., Reuillon, M., Bransier, J., and Laraqui, N., "Experimental and Numerical Study of the Thermal Degradation of PMMA," *Comb. Sci. & Tech.* 53:187–201 (1987).

[3] Staggs, J.E.J., "A Theoretical Investigation into Modelling Thermal Degradation of Solids Incorporating Finite-Rate Kinetics," *Comb. Sci. & Tech.* 123:261–285 (1997).

[4] Anderson, Jr., C.E., Ketchum, D.E., and Mountain, W.P., "Thermal Conductivity of Intumescent Chars," *J. Fire Sci.* 6:390–410 (1988).

[5] Denman, K.L., "A Time-Dependent Model of the Upper Ocean," *J. Phys. Ocean.* 3:173–183 (1973).

HEAT RELEASE KINETICS

Richard E. Lyon
Fire Safety Section AAR-422
Federal Aviation Administration
W.J. Hughes Technical Center
Atlantic City International Airport, NJ 08405

A molecular basis for polymer burning is developed from thermal degradation kinetics and compared to experimental data for flaming heat release rate in fires. The solid-state fuel generation rate in fires has been derived [1] from the polymer thermal degradation scheme

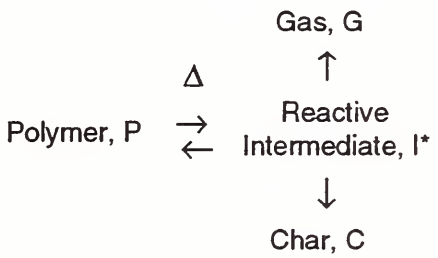

assuming that the majority of pyrolysis gases G and char C are produced anaerobically from the reactive intermediate I* in a single step via parallel reactions. The system of rate equations for the species at time, t, is

$$\frac{dP}{dt} = -k_p P + k_{-p} I^* \qquad (1)$$

$$\frac{dI^*}{dt} = k_p P - \left(k_{-p} + k_g + k_c\right) I^* \qquad (2)$$

$$\frac{dG}{dt} = k_g I^* \qquad (3)$$

$$\frac{dC}{dt} = k_c I^* \qquad (4)$$

The stationary-state assumption $dI^*/dt \approx 0$ eliminates I* from Equations 1-4. Defining an initial mass, $m_o = P + G + C + I^* \approx P + G + C$, and a sensible mass, $m = P + C + I^* \approx P + C$, the maximum fractional mass loss rate at a constant heating rate $\beta = dT/dt$ is

$$\frac{\dot{m}_{max}}{m_o} = \frac{-\beta(1-\mu)E_a}{eRT_p^2} \qquad (5)$$

where E_a is the molar activation energy for the rate limiting $P \rightarrow I^*$ decomposition step, $\mu = C(\infty)/m_o$ is the equilibrium char fraction at the peak mass loss rate temperature, T_p, R is the gas constant, and e is the natural number. Multiplying Equation 5 by the heat of complete combustion of the pyrolysis gases h_c° gives the *kinetic heat release rate*

$$\dot{Q}_c(W/kg) = h_c^\circ \frac{-\dot{m}_{max}}{m_o} = \frac{h_c^\circ \beta(1-\mu)E_a}{eRT_p^2} \qquad (6)$$

The pyrolysis zone thickness for steady burning of a polymer of thermal conductivity κ at net surface heat flux $\dot{q}_{net}$ is

$$\delta = \frac{e\kappa}{\dot{q}_{net}} \frac{RT_p^2}{E_a} \qquad (7)$$

The areal density of pyrolyzing polymer of bulk density ρ and surface area S is $m_o/S = \rho\delta$ so that the macroscopic heat release rate per unit area of burning surface is

$$\dot{q}_c(W/m^2) = \chi h_c^\circ \frac{\dot{m}}{S} = \chi\rho\delta\left[h_c^\circ \frac{\dot{m}}{m_o}\right] \qquad (8)$$

or with Equation 6

$$\dot{q}_c = \chi\rho\delta\,\dot{Q}_c \qquad (9)$$

Equation 9 states that the ratio of the steady-state macroscopic heat release rate to the peak kinetic heat release rate for comparable temperature histories is in the range

$$\frac{\dot{q}_c}{\dot{Q}_c} = \chi\rho\delta \approx 0.4 \pm 0.2\ kg/m^2 \qquad (10)$$

using typical values for the gas phase combustion efficiency in a fire, $\chi = 0.7 \pm 0.2$, the polymer density, $\rho = 1000 \pm 100$ kg/m^3, and the pyrolysis zone thickness, $\delta = 0.5 \pm 0.2$ mm at $\dot{q}_{net} = 50$ kW/m^2 from Equation 7.

The heating rate at the surface of a steadily burning polymer is

$$\beta = \left.\frac{dT}{dt}\right|_{x=0} = \frac{\dot{q}_{net}^2}{\kappa \rho c_p (T_p - T_o)} \qquad (11)$$

with $c_p = c(T_p)$ the polymer heat capacity at the peak pyrolysis temperature. Substituting Equation 11 along with Equations 6 and 7 into Equation 9 recovers the continuum result for thermal diffusion limited steady burning

$$\dot{q}_c(W/m^2) = \chi h_c^o \frac{\dot{m}}{S} = \chi \frac{h_c^o}{h_g} \dot{q}_{net} \qquad (12)$$

with the heat of gasification defined $h_g \equiv c_p(T_p - T_o)/(1-\mu) = \dot{q}_{net}/(\dot{m}/S)$.

In principle the macroscopic heat release rate at any net surface heat flux $\dot{q}_{net}$ is now calculable from the pyrolysis kinetic parameters and heat of combustion of the volatiles using Equations 6, 7, 9, and 11. However, these kinetic and combustion parameters are rarely known with any certainty, particularly at the surface heating rates in a fire.

Consequently, our approach [2] was to measure the kinetic heat release rate directly using pyrolysis-combustion flow calorimetry (PCFC). In the PCFC test a 1-3 milligram polymer sample is pyrolyzed by heating in an inert environment to a maximum temperature $T_{max} = 923$K at a linear heating rate $\beta \approx 8$ K/s (calculated from Equation 11) to approximate the rapid, anaerobic heating of a polymer surface in a fire or fire calorimeter at $\dot{q}_{net} = 50$ kW/m^2.

The pyrolysis gases are swept from the small volume pyrolysis chamber of the PCFC by flowing nitrogen and mixed with excess oxygen prior to entering a 900°C furnace to effect complete combustion. Combustion products are scrubbed from the gas stream prior to entering an oxygen analyzer. Heat release rate is calculated from oxygen consumption and the measured flow rate of the gas stream.

Results of these PCFC tests are compared to literature values for average macroscopic heat release rate at $\dot{q}_{net} = 50$ kW/m^2 in a cone calorimeter in the figure below.

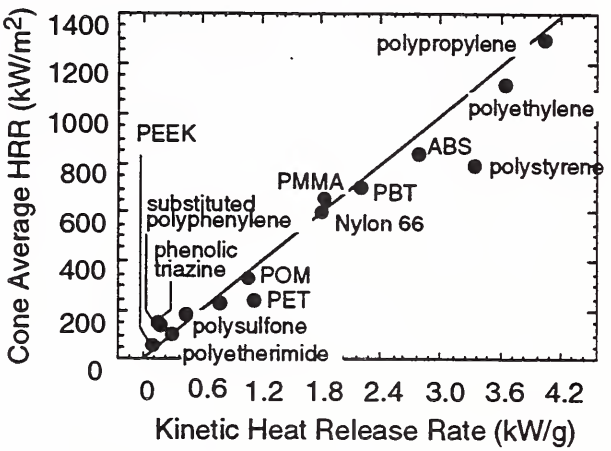

Macroscopic *versus* kinetic heat release rate for some polymers.

Proportionality is observed between the macroscopic and kinetic heat release rates with slope $\dot{q}_c/\dot{Q}_c = 0.33$ kg/m^2, which is within the range of predicted values using Equation 10.

We conclude that steady polymer burning is a thermal diffusion controlled kinetic process in which the rates of the solid-state reactions (pyrolysis) and gas phase reactions (combustion) are rapid in comparison to the rate of heat transfer at the flaming surface. The pyrolysis zone depth is determined by the coupling between thermal diffusion and pyrolysis kinetics and effectively correlates the molecular and macroscopic heat release rates.

REFERENCES

1. R.E. Lyon , Polym. Deg. Stabil. (in press).
2. R.N. Walters and R.E. Lyon, Proc. 42nd Int'l SAMPE Symp., 42(2), 1335-1344 (1997)

The Molecular Level Design of Flame Retardants and Fire Resistant Materials

Marc R. Nyden
Building and Fire Research Laboratory
National Institute of Standards and Technology
Gaithersburg, MD 20899
mnyden@nist.gov

Recent work conducted in this laboratory has demonstrated the application of molecular modeling techniques to the design of flame retardants and fire resistant materials [1-5]. This effort has culminated in the development of a novel computer program, hereafter called MD_REACT, that simulates the thermal degradation of polymers (see Figure 1). The basis of this model is molecular dynamics (MD), which consists of solving Newton's equations of motion for each of the 3N degrees of freedom associated with the model polymer. The feature that distinguishes MD_REACT from other MD codes is that it allows for the formation of new bonds from free radical fragments that are generated when bonds in the polymer break and, thereby, accounts for the chemical reactions that play a major role in the thermal degradation process [6].

Bond dissociation and formation are simulated in MD_REACT by the following algorithm. A list of the free radical sites, that are generated when bonds in the polymer break, is updated at every time step. These free radicals are eligible to react with each other to form new bonds. The specific criterion used in MD_REACT is that covalently bonded atoms become free radicals when their potential energy comes within a few k_BT of the bond dissociation energy. The program generates a new set of bonds, consisting of all possible covalent interactions between the available free radicals and retains those corresponding to the lowest energy subject to the constraints imposed by the rules of atomic valence.

The motivation behind the development of MD_REACT was to create a versatile model that could be used to study thermal degradation at a molecular level in a wide range of polymers. The strategy employed to accomplish this objective was to interface our program for performing reactive dynamics on simple vinyl polymers [2] with Discover 95 [7], a commercially available molecular dynamics code offered by Molecular Simulations (MSI). The interface between the programs is established using an inter-process communication protocol (IPC) to pass coordinates, forces and connectivity information between MD_REACT, which computes the reactive forcefield, and Discover 95, which updates the molecular structure on the basis of the solution to the equations of motion.

In order to extract meaningful information, the disparity between the time scales associated with laboratory measurements, such as the cone calorimeter (seconds) and those accessible to atomistic simulations (picoseconds) must be overcome. Our solution is to substitute the rate constants for random scission initiation (k_i), propagation (k_p), and termination (k_t) obtained from our computer simulations into a simple kinetic model [8]. The first step in this process is to generate a population of free radical polymer fragments. This is accomplished by performing simulations at very high temperatures (usually in excess of 2000 K). The resulting structures are then used to initiate the second stage of the computer experiment, the purpose of which is to simulate the propagation and termination reactions. These simulations can actually be performed at realistic thermal degradation temperatures (typically, 873 K) because the

activation energies for the β-scission reactions, corresponding to propagation (C-C scissions) and first order termination (C-H scissions), are comparatively low. The global rate of mass-loss is computed using the values of k_p and k_t, obtained directly from the results of the second stage simulations, and a value of k_i, which is extrapolated to thermal degradation temperatures using the kinetic parameters obtained by fitting the temperature dependence of the rates of random scission observed in a series of high temperature simulations. The global rates of mass-loss obtained in this way will be compared to the results of TGA and radiative gasification experiments performed on polypropylene and related polymers.

Figure 1. Frames from the simulated thermal degradations of polypropylene (left) and a polypropylene/graphite(right) nanocomposite.

References

1. M.R. Nyden and D.W. Noid, J. Phys. Chem. 95: 940-945, 1991.

2. M.R. Nyden, G.P. Forney and J.E. Brown, Macromolecules 25: 1658-1666, 1992.

3. M.R. Nyden, J.E. Brown and S.M. Lomakin, Mat. Res. Soc. Symp. Proc. 278: 47-53, 1992.

4. M.R. Nyden, T.R. Coley and S. Mumby, Polym. Eng. Sci. 37, No. 9:1496-1500, 1997.

5. M.R. Nyden and J.W. Gilman, Computational and Theoretical Polymer Science. in press, 1998.

6. C.F. Cullis and M.M Hirschler. The Combustion of Organic Polymers. Oxford, England: Clarendon Press, 1981, pp. 93-228.

7. Certain commercial equipment, instruments, materials or companies are identified in this paper in order to adequately specify the experimental procedure. This in no way implies endorsement or recommendation by NIST.

8. R.H. Boyd. The Relationship Between the Kinetics and Mechanism of Thermal Depolymerization. In: Thermal Stability of Polymers. New York: Marcel Dekker, 1970, pp. 47-89.

Flammability Studies of Polymer Layered Silicate (Clay) Nanocomposites

Jeffrey W. Gilman*[1], Takashi Kashiwagi[1], Marc Nyden[1], James E. T. Brown[1], Catheryn L. Jackson[2], Sergei Lomakin[†1]
[1] Fire Science Division, [2] Polymers Division, National Institute of Standards and Technology[ƒ] , Gaithersburg, MD USA 20899

Emmanuel P. Giannelis, Evangelos Manias
Cornell University
Ithaca, NY USA 14853

Background

In the pursuit of improved approaches to fire retarding polymers a wide variety of concerns must be addressed, in addition to the flammability issues. First, the low cost of commodity polymers requires that the fire retardant (FR) approach also be of low cost. This limits one primarily to additive type approaches. Second, these additives must be easily processed with the polymer. Finally, any additive must not excessively degrade the other performance properties of the polymer, and must not create environmental problems in terms of recycling or disposal of the end product. Polymer layered silicate (PLS) nanocomposites are materials that may partially fulfill the above requirements for high performance flame retardant products.

PLS nanocomposites are hybrid organic polymer - inorganic materials with unique properties when compared to conventional filled polymers (1). For example, the mechanical properties of a nylon-6 layered-silicate nanocomposite, with a silicate mass fraction of only 5 %, show excellent improvement over those for the pure nylon-6. The nanocomposite exhibits a 40 % higher tensile strength, 68 % greater tensile modulus, 60 % higher flexural strength, and a 126 % increased flexural modulus. The heat distortion temperature (HDT) is increased from 65° C to 152° C (2). Some PLS nanocomposites exhibit increased thermal stability: an important property for improving flammability performance, as well as decreased gas permeability, and increased solvent resistance, along with the improved physical properties.

Methods to prepare PLS nanocomposites have been developed by several groups over the last few decade (3, 4, 5, 6, 7, 8, 9). In general these methods achieve molecular level incorporation of layered silicate (e.g., montmorillonite) into the polymer by addition of a modified silicate; during the polymerization (*in situ),* or to a solvent swollen polymer, or to the polymer melt (1). Two terms (*intercalated* and *delaminated*) are used to describe the two general classes of nano-morphology that can be prepared. The *intercalated* structure results when the extended polymer chains are inserted into the gallery space between the individual silicate layers. These are well ordered multi-layered structures. The *delaminated* (or *exfoliated*) structures result when the individual silicate layers are more completely dispersed in the organic polymer. The interlayer spacing (5 nm -200 nm) is on the order of the radius of gyration of the polymer. The silicate layers in a *delaminated* structure may have the same well ordered multi-layer structure as the *intercalated* morphology, or they may be significantly less ordered (10).

We have reported previously on the flammability properties of *delaminated* nylon-6 layered silicate nanocomposites and *intercalated* polymer layered-silicate nanocomposites prepared from polystyrene

---

[†] NIST Guest Researcher from the Russian Academy of Sciences.

(PS) and polypropylene-graft-maleic anhydride (PP-g-MA) (11,12). Here, we will briefly review these results and report on our initial studies of the flame retardant mechanism.

We have characterized flammability properties of representative thermoplastic and thermoset polymer layered silicate nanocomposites. The peak and average heat release rates (HRR) are reduced by 40 % to 80% in *delaminated* and *intercalated* nanocomposites containing a silicate mass fraction of only 2 % to 6 %. This system does not increase the rate of carbon monoxide generation or the rate of soot produced during the combustion. Just as the nanocomposite structure of the PLS enhances the properties of the polymer, the nanocomposite structure in the char appears to enhance the performance of the char layer. This layer (TEM show in Figure 1) may act as an insulator and a mass transport barrier slowing the escape of the volatile products (mass loss rate) generated as the polymer decomposes.

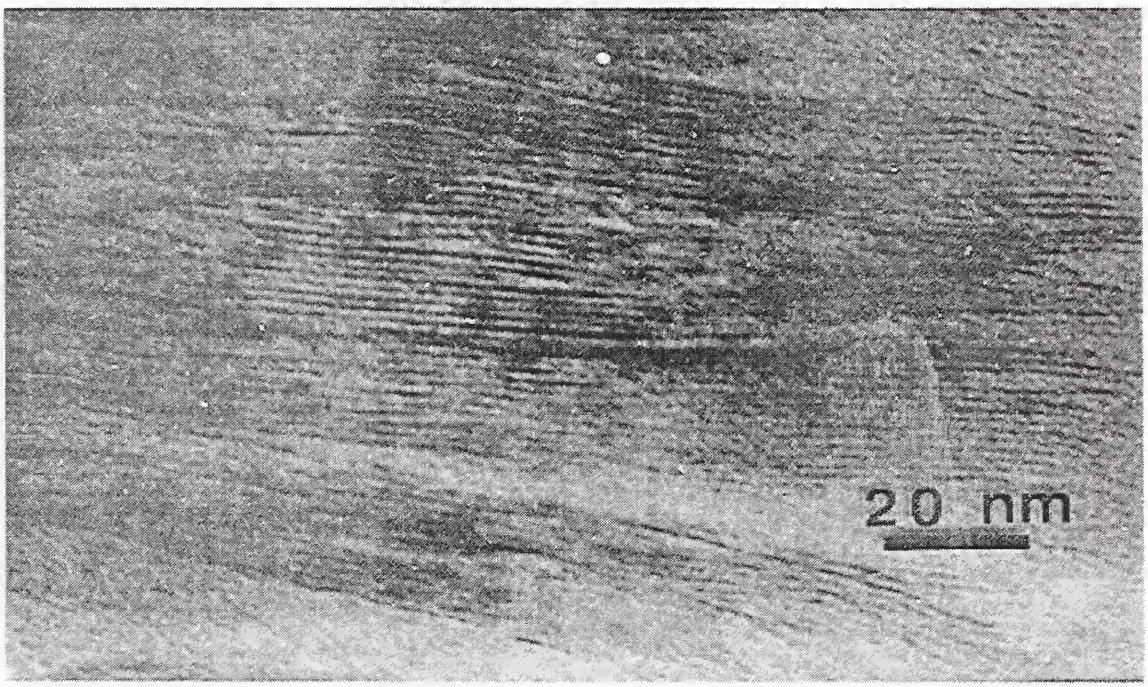

Figure 1.TEM of a section of the combustion char from the nylon-6 clay-nanocomposite (5 %) showing the carbonaceous-silicate (1 nm thick, dark bands) multilayered structure. This layer may act as an insulator and a mass transport barrier, slowing the escape of the volatile products generated as the nylon-6 decomposes.

---

1. E. P. Giannelis, *Advanced Materials*, 8, (1) 29 (1996).
2. Y. Kojima, A. Usuki, M. Kawasumi, A. Okada, Y. Fukushima, T. Kurauchi, and O. Kamigaito, J. Mater. Res. 8, 1185 (1993).
3. S. Fujiwara, T. Sakamoto, Japanese Patent Application no. SHO 51(1976)-109998.
4. M.S. Wang, T. J. Pinnavaia, Chem. Mater. 6, 468 (1994).
5. A. Usuki, A. Okada, T. Kurauchi, J. App. Poly. Sci. 63, 137 (1997).
6. A. Usuki, Y. Kojima, M. Kawasumi, A. Okada, Y. Fukushima, T. Kurauchi, and O. Kamigaito, *J. Mater. Res.* 8, 1179 (1993).
7. Y. Kojima, A. Usuki, M. Kawasumi, A. Okada, Y. Fukushima, T. Kurauchi, and O. Kamigaito, *J. Mater. Res.* 8, 1185 (1993).
8. J. Lee, T. Takekoshi and E. Gannelis, Mat. Res. Soc. Symp. Proc. vol 457, p. 513, (1997).
9. J. Lee and E. Giannelis, Polymer Preprints, vol. 38, p. 688, (1997).
10. T. Lan, and T. J. Pinnavaia, Mat. Res. Soc. Symp. Proc. Vol. 435. 79 (1996).
11. J. W. Gilman, T. Kashiwagi, J. D. Lichtenhan, SAMPE Journal, , 33, no. 4, 40 (1997).
12 . J. W. Gilman, T. Kashiwagi, S. Lomakin, E. P. Giannelis, E. Manias, J. D. Lichtenhan, P. Jones in Fire Retardancy of Polymers : the Use of Intumescence, G. Camino, M. Le Bras, S. Bourbigot & R. DeLobel eds., The Royal Society of Chemistry, Cambridge (1998) 203-221.

Flame Retardant Nanocomposite Materials

Emmanuel P. Giannelis
Department of Materials Science and Engineering
Cornell University

As use of synthetic polymers has grown dramatically over the past thirty years so have efforts to control polymer flammability. Developments to that end include intrinsically thermally stable polymers, fire retardant fillers and intumescent fire retardant systems. Brominated polymers that prevent flame spread have the significant disadvantages of producing dense smoke and corrosive combustion by-products. Furthermore, the effectiveness of fire retardant fillers tends to be limited since the large amounts of filler required make processing difficult and alter the mechanical properties. Therefore there exists a need for new, more effective, and environmentally benign approaches are needed that combine flame resistance and mechanical robustness with processability and low cost.

Solventless, melt intercalation of high molecular weight polymers is a powerful new approach to synthesize polymer-layered silicate (PLS) nanocomposites. This method is quite general and is broadly applicable to a range of commodity polymers from non-polar polystyrene to strongly polar nylon. PLS nanocomposites are thus processable using current technologies and easily scaled to manufacturing quantities. In general, two types of structures are possible: intercalated, in which a single, extended polymer chain is inserted between the silicate layers resulting in a well ordered multilayer with alternating polymer/inorganic layers, and disordered or delaminated, in which the silicate layers (1 nm thick) are uniformly dispersed, with random orientation throughout the polymer matrix.

Polymer nanocomposites, especially polymer-layered silicates nanocomposites, represent a radical alternative to conventionally filled polymers. Due to their nanometer size dispersion, the nanocomposites exhibit markedly improved properties when compared to the pure polymer or conventional composites. The improved properties include increased modulus, decreased gas permeability, increased solvent resistance, and decreased flammability. For example, a doubling of the tensile modulus and strength is achieved for nylon-layered silicate nanocomposites containing as little as 2 vol.% of inorganic. In addition, the heat distortion temperature of the nanocomposites increases by up to 100°C, extending the use of the composite to higher temperatures environments, such as automotive engine applications. Furthermore, the heat release rate in the nanocomposite is reduced by up to 63% at heat fluxes of 50kW/m^2 without an increase in the CO and soot produced during combustion (see Figure 1).

There are several proposed mechanisms as to how the layered silicate affects the flame retardant properties of polymers. The first is the increased char layer that forms when nanocomposites are exposed to flame. This layer is thought to inhibit oxygen transport to the flame front and therefore reduce the heat release rate of the burning polymer. Another possible mechanism is the catalytic ability of layered silicates. At higher temperatures, the inorganic has the ability to act as a radical sink due to adsorption to lewis acid sites. This interupts the burning cycle as radical species are needed to break polymer chains into oligamer fuel. The disordered nanocomposites also inhibit oxygen and combustible oligomer species transfer by increasing the path length of these species to

the flame front. The path length is dramatically increased due to the large surface area inherent in the silicates (approximately 760 $\frac{m^2}{g}$ for Na^+ Montmorillonite).

An excellent example of fire retardency in nanocomposites appears in the figure below. The heat release rate of pure Nylon 6.6 is compared to that of Nylon containing 5 wt% of the layered silicate, montmorillonite. It is clear from the plot, that with only a minute addition of silicate, it is possible to decrease the heat release rate by almost a factor of two. While the exact mechanism is still in question, a combination of the previously described causes is likely.

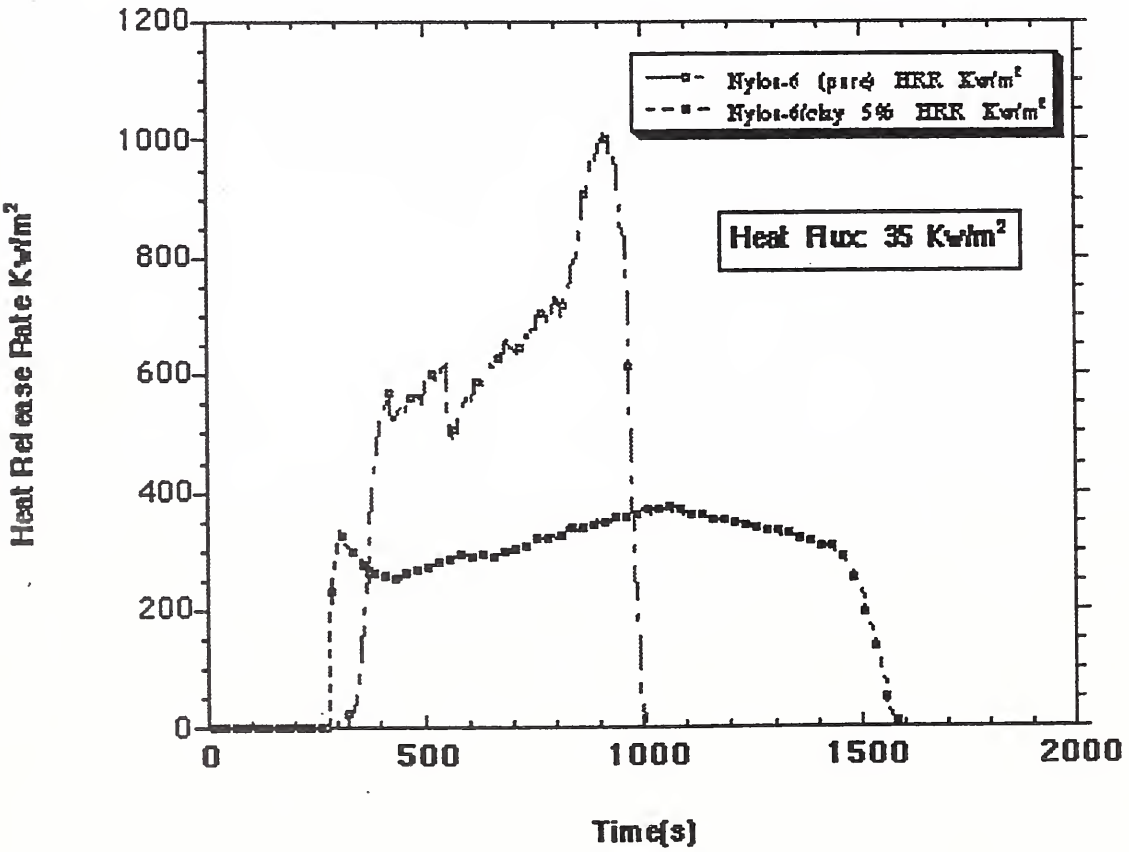

The Influence of Surface Silica on the Pyrolysis of Silicones

Robert Buch (Dow Corning), John Shields, Takashi Kashiwagi, Thomas Cleary, Kenneth Steckler (NIST)

ABSTRACT

Silicones encompass a wide variety of novel materials that find applications in virtually every major industry sector. The dominant polymer in the silicone industry is polydimethylsiloxane (PDMS). The combustion of long chain PDMS exhibits a low heat release rate and the unique characteristic that the heat release rate does not increase significantly with an increase in external applied thermal radiant flux [1] or pool size [2-5]. The depsition of amorphous silica ash (a major combustion product of silicones) on the fuel surface is believed to play a significant role in mediating the fuel formation rate of silicones in fire scenarios. The objective of this study was to document and quantify the influence of surface silica on the pyrolysis rates of PDMS.

For this study, the gasification apparatus developed at NIST-BFRL by Steckler and others was used. An earlier study on the gasification of silicones by Austin et. al., provides complete details on this unique apparatus [6]-both operational and data analysis. A range of silica types and fluids were studied.

The influence of silica on the pyrolysis rates of PDMS fluids was assessed by incrementally adding amorphous fumed silica in a uniform thin layer to the surface of the test fluid sample (100 g) and measuring their pyrolysis rates in the gasification apparatus. Pyrolysis rate data for incremental silica additions are given in Figure 1. The silica additions are estimated to be representative of the quantity of silica deposited on the surface of silicones during the earliest stages of burning. Note the continuous reduction in pyrolysis rate with silica additions. Average pyrolysis rates were obtained following Austin's pro- cedures [6]. These data are given in Figure 2 for external heat flux conditions of 50 and 70 kW/m^2. A pyrolysis rate of 0.04 g/s corresponds to a heat release rate of 125 kW/m^2 which is in good agreement with values measured for these polymers [1-4].

The use of silica based additives to mediate the burning rate of thermoplastics was demonstrated by Romenesko et.al. [7]. The potential utility of other inorganic fumed oxides was briefly assessed following the procedures used for silica. These data are summarized in Figure 3. Oxides of aluminum, zirconium and titanium were evaluated. The latter two oxides are effective in mediating the pyrolysis of PDMS similar to silica.

In the course of this investigation, a variety of PDMS polymers were pyrolyzed which resulted in new interesting insights into their high temperature behavior, i.e. the subtle influence of process chemistry and the influence of various additives used in formulating silicones. Data illustrating the influence of polymer molecular weight (I,H-intermediate or high molecular weight), residual catalysts (RCx = chemical form, UC = ultra clean, TCx = trace catalyst levels) and other polymer variables (V, M = polymer chain terminal endgroups) on the high temperature pyrolysis of PDMS are given in Figure 4. Note the profound influence of several of these parameters on the high temperature pyrolysis of PDMS under the thermal conditions in the gasification apparatus. The role and importance of these polymer parameters in the actual fire performance or fire test performance of formulated products have not been determined. However, an awareness and control of them in studies such as this is readily apparent. These findings and their implications regarding fire performance along with several unresolved observations will be discussed.

In summary, the NIST gasification apparatus provides a unique capability for both measuring fundamental fire parameters of materials and providing new insights into the high temperature behavior of polymers and formulations thereof.

REFERENCES:

1. Buch, R.R., *Fire Safety J.*, 17:1(1991).
2. Hemstreet, R.A., "Flammability Tests of Askarel Replacement Transformer Fluids," National Electrical Manufacturers Association, 2102 L Street N.W., Suite 300, Washington, D.C. 20037, FMRC Serial No. 1A7R3.RC, FMRC No. RC7T-43, August, 1978.
3. Kanakia, M., Characterization of transformer fluid pool fires by heat release rate calorimetry. Presented at the 4th Int. Conf. Fire Safety, Univ. of San Francisco, 1979.
4. Tewarson, A., Lee, J. L., and Pion, R. F., "Fire Behavior of Transformer Dielectric Insulating Fluids," prepared for US Department of Transportation, Kendall Square, Cambridge, MA 02142, Report # FRA/ORD-80/08, January, 1980.
5. Buch, R.R., Hamins, A., Konishi, K., Mattingly, D., and Kashiwagi, T., *Comb. Flame*, 108:118-126(1997).
6. Austin, P. J., Buch, R. R., and Kashiwagi, T., "Gasification of Silicone Fluids under External Thermal Radiation" NISTIR 6041, U.S. Department of Commerce, July 1997.
7. Romenesko, D., et.al., "Method for Imparting Fire Retardancy to Organic Resins", U.S. Patents 5,391,594 (Feb. 21, 1995) and 5,508,323 (April 16, 1996).

Figure 1. SURFACE SILICA-PYROLYSIS MEDIATION

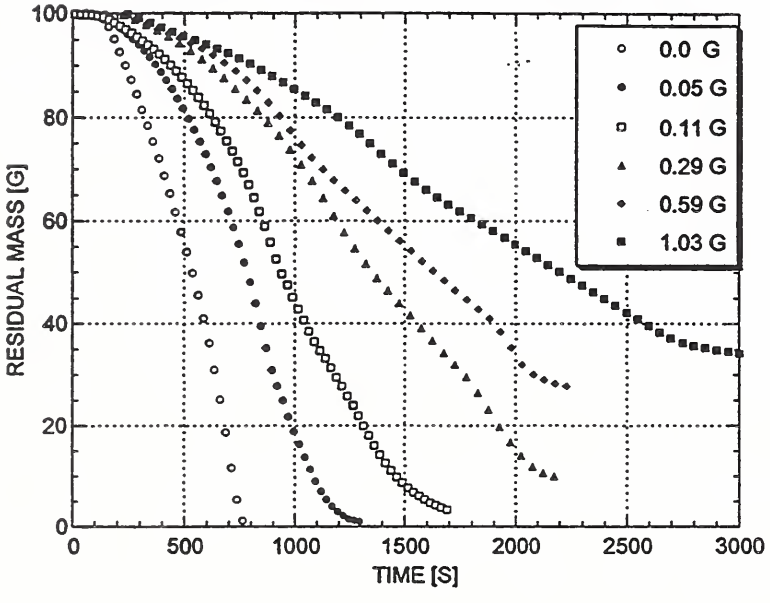

Figure 2. MASS PYROLYSIS RATE vs SURFACE SILICA

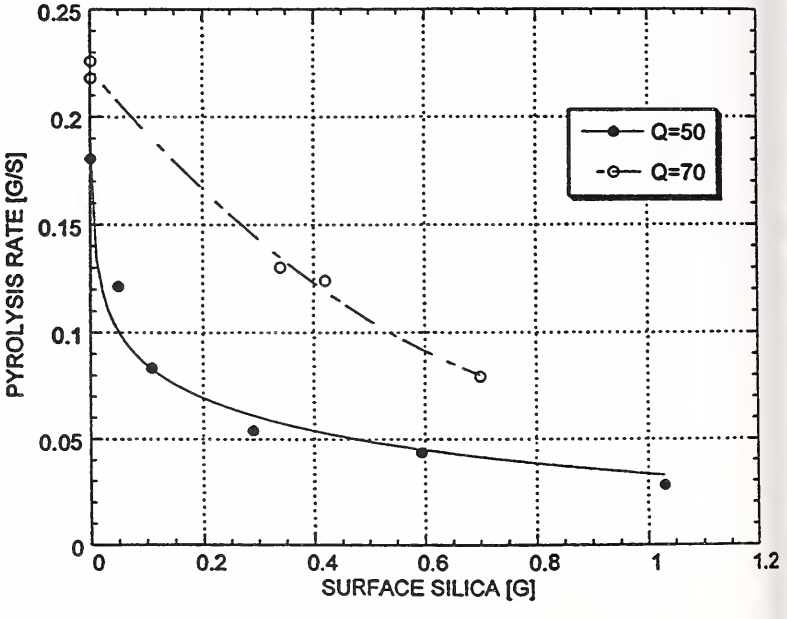

Figure 3. FUMED OXIDES-PYROLYSIS MEDIATORS

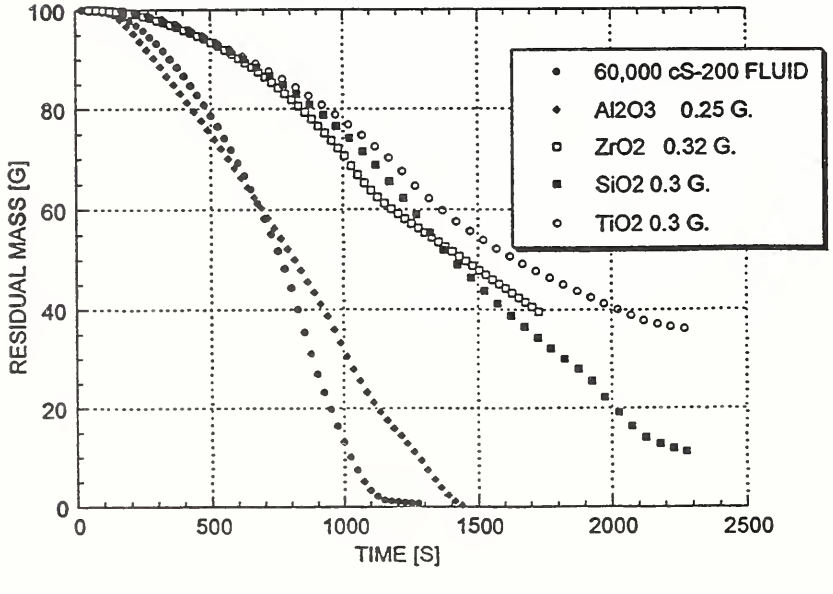

Figure 4. POLYMER VARIABLES

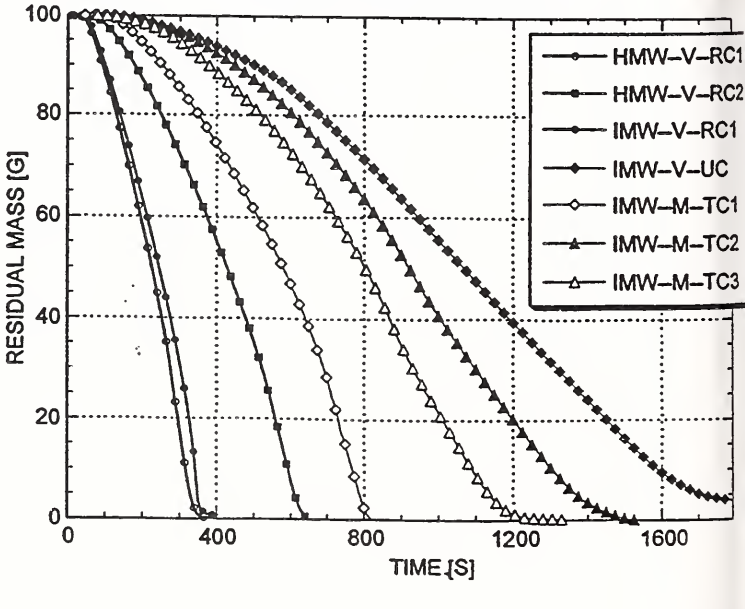

INTUMESCENCE AND POLYMER BLENDING : AN APPROACH FOR FLAME RETARDANCY ?

SERGE BOURBIGOT, MICHEL LE BRAS, MICHEL BUGAJNY and FRANÇOIS DABROWSKI
Laboratoire de Génie des Procédés d'Interactions Fluides Réactifs-Matériaux (GéPRIM), E.N.S.C.L., Université des Sciences et Technologies de Lille (USTL), BP 108, 59652 Villeneuve d'Ascq Cedex (France)
Phone : +33 (0)3 20 43 49 25 ; Fax : +33 (0)3 20 43 65 84 ; e-mail : serge.bourbigot@ensc-lille.fr

Fire protection of flammable materials by an intumescence process is known for several years. Fire retardant intumescent materials form on heating foamed cellular charred layers on the surface, which protects the underlying material from the action of the heat flux or of a flame. The proposed mechanism is based on the charred layer acting as a physical barrier which slows down heat and mass transfer between gas and condensed phase. Generally, intumescent formulations contain three active ingredients : an acid source, a carbonization compound, and a blowing agent. First, the acid source breaks down to yield a mineral acid then, it takes a part in the dehydration of the carbonific to yield the carbon char and finally, the blowing agent decomposes to yield gaseous products. These latter cause the char to swell and hence provide the insulating material which then decomposes under the action of the outer heat flux.

The carbonization agents (CA) commonly used in intumescent formulations for thermoplastics are polyols such as pentaerythritol, mannitol, sorbitol, ... One of the problem with this kind of compounds is the exudation and the water solubility of the additives. Moreover, there is not a good compatibility between the additives and the polymeric matrix and the mechanical properties of the polymer are then very poor. New carbonization agents have to be found. The Laboratory develops FR intumescent formulations using charring polymers as carbonization agent. The advantage of this concept is to obtain flame-retarded polymers with improved mechanical properties in comparison with polymers loaded with classical FR formulations and to avoid the problems of exudation and solubility of the additives (figure 1).

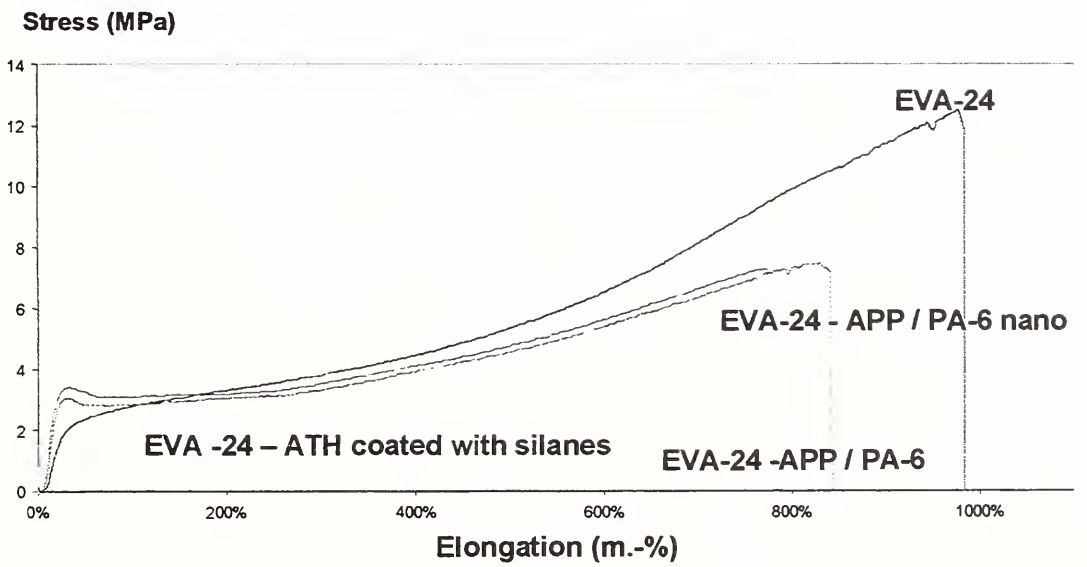

***Figure 1** : mechanical properties of the formulations EVA24-ATH, EVA24-APP/PA-6 and EVA24-APP/PA-6nano (PA-6nano=PA-6 clay hybrid from UBE Industries) in comparison with the virgin EVA24*

The aim of this work is to show the efficiency of charring polymers as carbonization agent in FR intumescent formulations using fire testing (LOI, UL-94 and cone calorimeter). In this study, we present some examples of formulations using polyurethane (PUR) and polyamide-6 (PA-6) as charring polymers respectively, in polypropylene (PP) and ethylene-vinyl acetate copolymers (EVA).

Figure 2 shows the RHR (Rate of Heat Release) values versus time in the conditions of the cone calorimeter of PP-APP(ammonium polyphosphate)/PUR formulations with different kinds of PUR (see the caption of the figure 2). The RHR values are improved when polyester-based PUR are used in comparison with polyether-based PUR. For the same polyol (S series), RHR values decreases when number of hard segments increases.

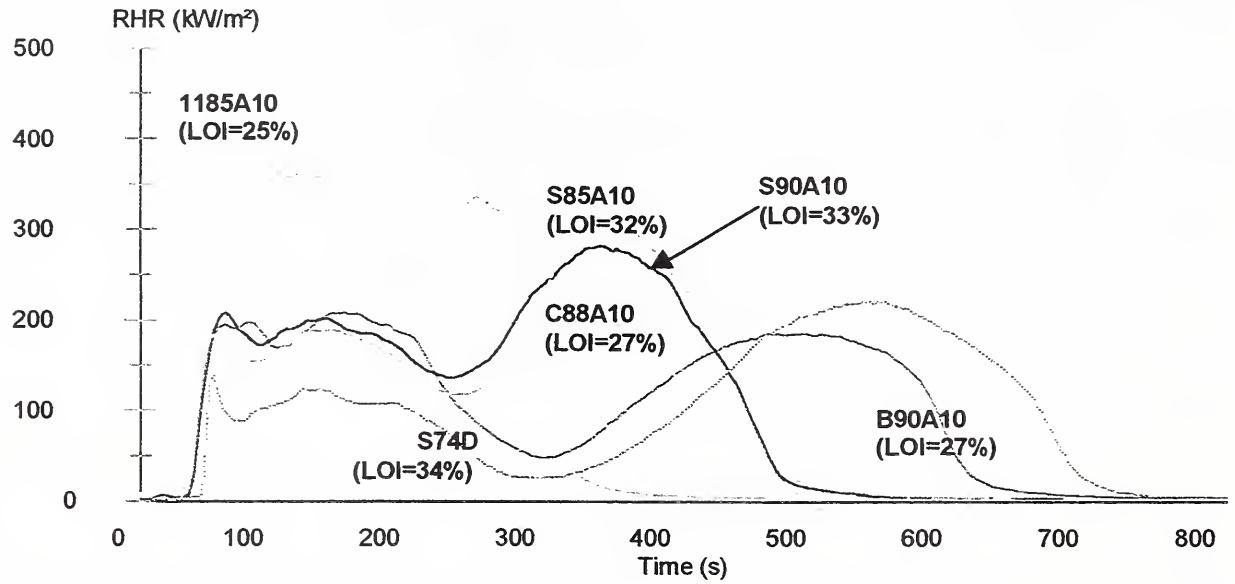

Figure 2 : RHR values versus time of PP-APP/PUR formulations in the conditions of the cone calorimeter under an external heat flux equaling 50 kW/m² (PUR from Elastrogran of the series Elastollan : 1185A10 polyether-based PUR and series S, C and B polyester-based PUR. In the series B, C and S the nature of polyol is changed. From S85 to S74 the number of hard segments is increased).

RHR values of the flame retarded EVA24 are strongly reduced in comparison with the virgin one (figure 3). As in the case of PP, it is demonstrated the efficiency of using charring polymers in FR intumescent formulations. It is also shown that the use of PA-6nano improves the FR performance of the system : RHR peak = 320 kW/m² without nanocomposite and RHR peak = 240 kW/m² with nanocomposite. Moreover, figure 4 shows an interesting result. The residual mass of EVA24-APP/PA-6nano is strongly increased in comparison with EVA24-APP/PA-6. This means that there are lower evolved gases during combustion which could feed the flame.

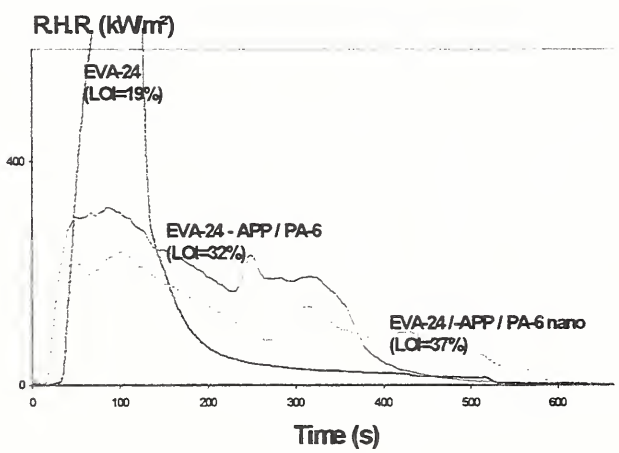

Figure 3 : RHR values versus time in the conditions of the cone calorimeter under an external heat flux equaling 50 kW/m²of the formulations EVA24-APP/PA-6 and EVA24-APP/PA-6nano in comparison with EVA24

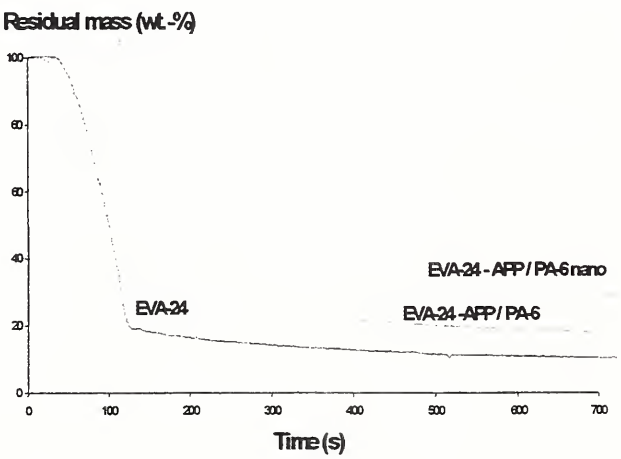

Figure 4 : Residual mass versus time in the conditions of the cone calorimeter under an external heat flux equaling 50 kW/m² of the formulations EVA24-APP/PA-6 and EVA24-APP/PA-6nano in comparison with EVA24

TELECHELIC ARYL CYANATE ESTER SILOXANES AS LOW FLAMMABILITY IMPACT MODIFIERS FOR CYANATE ESTER RESINS

Steven K. Pollack, Yemi Bullen and Zhidong Fu[1]

Department of Chemistry and the Polymer Science & Engineering Program
Howard University, Washington, DC 20059

Introduction

Cyanate ester resins (CERs) have found extensive use in applications where low-dielectric, high thermal stability materials are needed [2]. Polymerization occurs by the cyclotrimerization of aryl cyanate ester groups

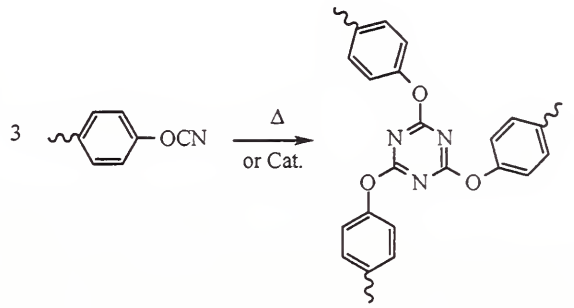

These applications include printed wire circuit boards (PCWBs), and radomes. Recently, these resins have been proposed as materials for use as the matrix in structural composites used in civilian air transport. In this application, the organic materials must exhibnit low flammibility as well as having the appropriate strength and toughness for this type of application. CERs, by themselves possess appropriate flammibility properties, but are too brittle for use alone as matrix materials for structure composites. However, their toughness can be greatly enhanced by the introduction of modifiers such as thermoplastics or elastomers. Siloxane based elastomers provide both the requisite improvement in toughness as well as having excellent flame retardency. To that end, there have been efforts to develop siloxane based impact modifiers for CERs. Previous workers have described approaches utilizing either amine or alcohol terminated siloxanes as impact modifiers[3]. There is also a patent issued for the development of allyl(2-phenylcyanate) terminated siloxanes[4]. In the former case, there is concern that the cross-linking reaction may introduce polar functionality into these materials causing excessive moisture absorbance. In the latter materials, the added hydrocarbon component of the allyl group is a potential problem in terms of combustability of the siloxane. We have focussed our attention on developing a family of telechelic siloxanes terminated with p-cyanatophenyl groups.

Results and Discussion

We were able to synthesize the a variety of cyanate-ester functional siloxanes in high yield[5].

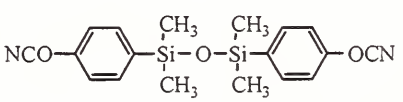

1

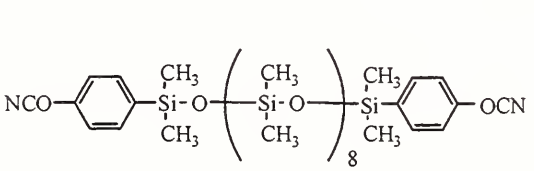

2

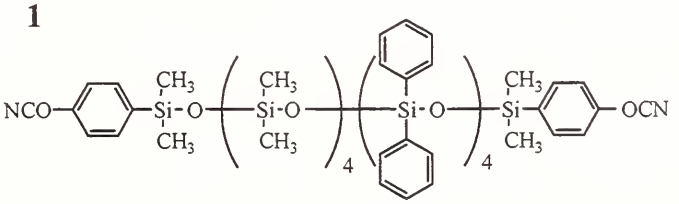

3

Hompolymerization of compound **1** by curing from 120-280°C leads to a glassy solid with T_g of 274°C. For compound **2**, the result is a rubber with a T_g of -110°C and for compound **3** a rubber with a T_g of 8°C. All three compounds exhibit a thermal decomposition at roughtly 500°C as observed via TGA. The longer chain siloxanes also exhibit a loss peak at 200°C. Commercial CERs show a loss only at 500°C. We interpret this to mean tha tthe 500°C loss is due to breakdown of the triazene and/or ether linkages.

When compound **1** was blended with the commercial CER Primaset PT-30 (a novolac-based CER from Lonza) at 10 phr, the resultant cured material exhibited a single phase. However, for blends with compounds **2** or **3**, a two-phase material

is formed. In both case the oligomer was not soluble and agitation during the initial stages of cure was required. For the blend with **2**, the morphology of the blend indicates that the siloxane forms the continuous phase, while for the blend with **3**, the PT-30 is the continous phase.For the blend with the diphenylsiloxane containing additive (**3**), the typical domain size of the rubbery phase is 20-30 μm (**Figure 1**).

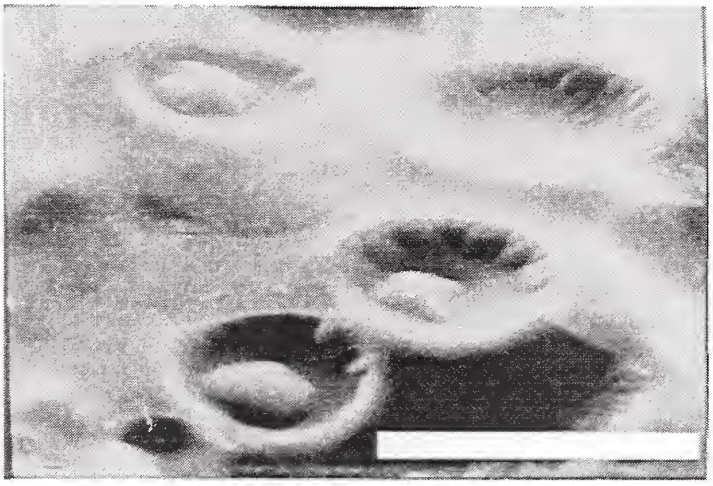

Figure 1. SEM photograph (100,000 x) of fracture surface of 10 phr telechelic siloxane **3** in PT-30 after curing. (inset bar is 50μm)

Conclusions

We have demonstrated the synthesis of a number of telechelic CERs which can be compounded with commercial CERs to form either single or two phase blends. In the case of the two-phase blends, the rubbery phase domain size is in the range necessary for improving the fracture toughness of the commerical resin. We are currently exploring the effect of oligomer composition and molecular weight on the the mechanical and flammability properties of these new materials. We are also examining the thermal and mechanical properties of cured blends of the disiloxane CERs with oligosiloxane CERs.

Acknowledgements

We thank the NIST Building and Fire Research Laboratory (Grant Number 60NANB6D0016) for support of this research. We also wish to thank Dr. Jeffrey Gilman of NIST BFRL for his help in this effort.

References

(1) Current Address: Colgate-Palmolive, 909 River Road, P.O. Box 1343, Piscataway, NJ 08855
(2) Hamerton, I., *Chemistry and Technology of Cyanate Ester Resins,* Chapman & Hall, 1994.
(3) Arnold, C.; Mackenzie, P.; Malhotra, V.; Pearson, D.; Chow, N.; Hearn, M.; Robinson, G, *37th Int. SAMPE Symp. Exhib.* 1992, **37**, 128.
(4) Liao, Z.K.; Wang, C.S. United States Patent, 5 260 398, 1993.
(5) S. K. Pollack and Z. Fu, ACS Polymer Preprints, 39(1), 452, 1998

FLAMMABILITY OF CYANATE ESTER RESINS

*R.N. Walters *, S. Gandhi * and R.E. Lyon*
Fire Safety Section AAR-422
Federal Aviation Administration
W.J. Hughes Technical Center
Atlantic City International Airport, NJ 08405

** Galaxy Scientific Corporation*
Egg Harbor Township, NJ 08234

Cyanate ester resins are being considered for composite applications in commercial and military aircraft because of their good thermal and mechanical properties and ease of processing. The cyanate ester resins are a one part system where several reactive -OCN functional groups undergo a cyclotrimerization reaction to form a six membered triazine linkage [1] as shown in figure 1. When multifunctional cyanate ester monomers react, the triazine ring formation serves as the polymerization reaction forming a highly crosslinked structure. There are no catalysts, curing agents or additives needed for the curing process and no by-products or voids are formed in the matrix [2]. Previous studies have show the glass transition temperature increases with increasing functionality of the monomer from about 200°C for difunctional monomers to above 400°C for trifunctional monomers [3]. The flammability of the series of polymers with varying crosslink densities due to their backbone structure and functionality will be presented.

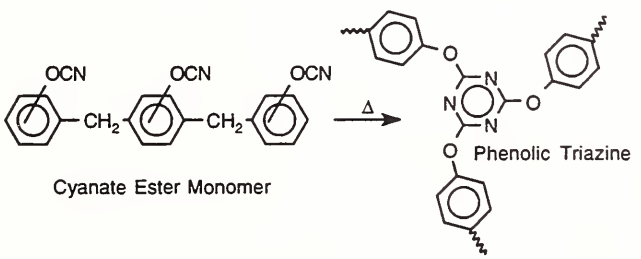

Figure 1: Cyclotrimerization reaction of the cyanate ester novolac to form the cyanurate network.

The resin samples for these experiments were used as received without any additives or purification. Cyanate esters B-10, F-10, L-10, M-10, XU-366 and XU-371 were from Ciba Specialty Chemicals and PT-30, PT-60 and PT-90 were from Allied-Signal Corporation. Table 1 shows the trade names and monomer structures of the materials. Samples were required for bomb calorimetry, thermogravimetric analysis (TGA), fire (cone) calorimetry, as well as for pyrolysis-combustion flow calorimetry (PCFC). All of the samples were cured by gradually heating the degassed resin in steps until the samples were solid then followed by a higher temperature post-cure.

Weight loss data was taken on a commercial thermal gravimetric analyzer (Perkin Elmer TGA 7). Samples weighing from 5 to 10 mg were heated from 50-1000°C at 10°C/min under nitrogen. From the experiments the onset of degradation, peak mass loss rate and char yield are determined.

Values for the gross heat of combustion were obtained with an oxygen bomb calorimeter (Parr Instrument Model 1341) using ASTM method D 2382-88 [4]. Samples of approximately 1 g each were run in triplicate to provide both the gross and net heats of combustion.

Trade Name	Structure
B-10	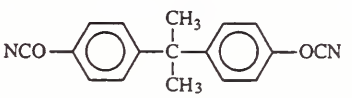
F-10	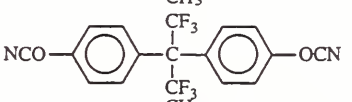
L-10	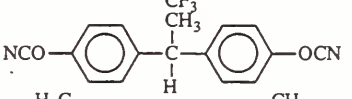
M-10	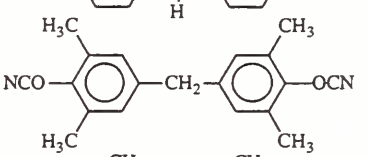
XU-366	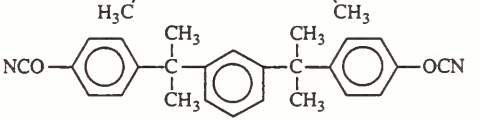
XU-371 (n=1) PT-30 (n=1) PT-60 (n=4) PT-90 (n=7)	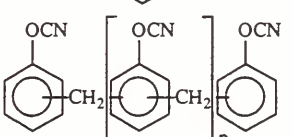
XU-717	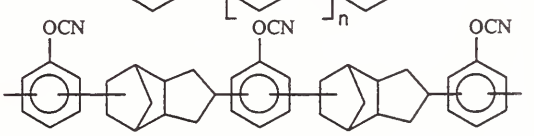

Table 1: Trade names and monomer structures of the cyanate ester resins.

Bench scale heat release rate data was obtained using a cone calorimeter (CONE2, Atlas Electric Devices) according to ASTM E-1354 [5] at radiant heat flux levels of 35, 50, 75 and 100 kW/m^2. Sample plaques for the test weigh around 75 g and measure 10 x 10 x 0.64 cm. Single samples of each cyanate ester were tested at each heat flux level in the horizontal configuration with an edge frame. Properties determined are the heat release rate from oxygen consumption, mass loss rate, smoke production, CO and CO_2 production, time to ignition and effective heat of combustion. From a series of tests at different heat flux

levels properties such as the heat of gasification and critical heat flux for ignition were also determined.

Microscale heat release data was obtained for the cyanate esters using a pyrolysis-combustion flow calorimeter developed by the FAA [6]. Approximately 1 mg of sample is pyrolyzed at 5°C/s in a nitrogen environment to simulate non-oxidative pyrolysis at the sample surface in a diffusion flame. The decomposition products are then completely oxidized in a high temperature combustion furnace. The combustion products are removed from the gas stream and the oxygen concentration measured over time. The heat release rates are obtained by using the oxygen consumption principle with Thornton's rule [7,8]. The properties that are determined are the peak heat release rate in W/g, heat release capacity in J/g-K, total heat released in kJ/g and the char yield in percent.

TGA shows the 5 % mass loss for all of the materials falls between 436 and 457°C which suggests a similar mechanism involving the triazine linkage which is independent of the backbone structure. The heat of complete combustion determined by bomb calorimetry is similar for all of the cyanate esters tested except for the fluorinated F-10 resin.

Fire calorimeter data show the shape of the heat release rate curves are highly dependent on the backbone structure of the cyanate ester. The burning behavior exhibited by the materials is related to the crosslink density, which is known to effect the fracture toughness and tear resistance of crosslinked materials in the leathery state. In general, the fire behavior can be described as ignition of the surface with rapid charring followed by surface cracking, the development of porosity and,/or swelling of the charring sample. Also, aromatic content, and gas permeability of the char appear to influence the fire response of thick specimens. A large crack which releases a burst of trapped volatiles gives rise to the high secondary heat release peak as for PT-30/60/90 and XU-371. The high crosslink density of phenolic triazines tends to cause the formation of thicker char. Large cracks which formed during burning of the series of cyanates indicate their brittle behavior. Distributed small cracks and porosity in the degrading and charring bisphenol cyanates L-10, B-10 and M-10 produce the diffuse secondary heat release peaks. The XU-366 and XU-717 exhibit very broad secondary heat release rate peaks which is associated with a large increase in the sample thickness due to the material intumescing. Figure 2 shows the trend in heat release rate at a 50 kW/m^2 heat flux for all of the cyanates tested. Data for 35, 75 and 100 kW/m^2 will also be presented.

Microscale PCFC data does not appear to correlate wholly with the bench scale fire calorimeter data. Surface effects and thermal diffusivity associated with the geometry and sample orientation are present in the bench scale test that are not in the microscale test.

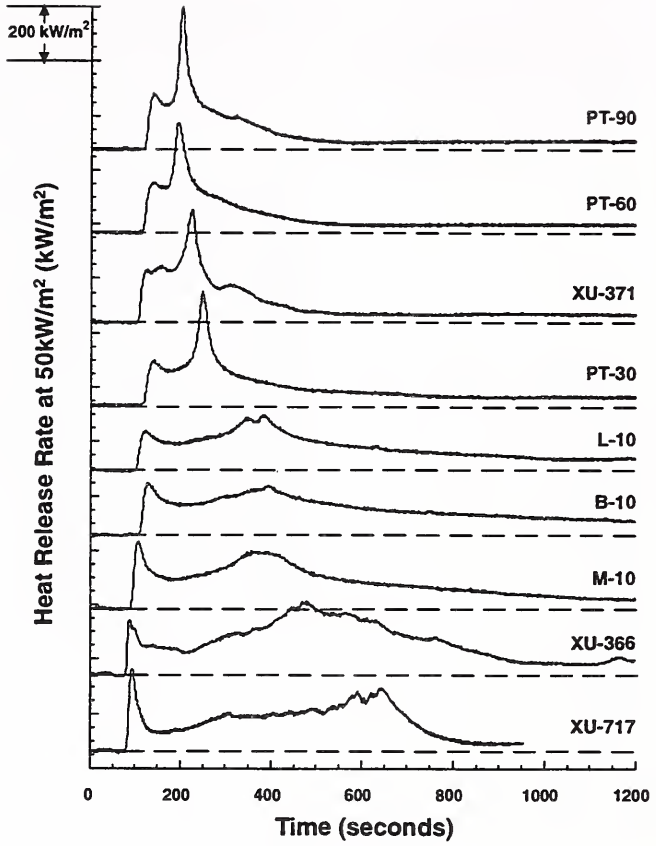

Figure 2: Heat release rate curves for the cyanate esters at 50 kW/m^2

All of the data mentioned will be presented and trends in the data relating to the structure will be discussed.

REFERENCES

1. Grigat, E.; Putter, R. *Angew. Chem. Internat. Edit.*, 6, 3, 207, **1967**.
2. Das, S.; Prevorsek, D. C.; DeBona, B. T., *Mod. Plast.*, Feb. **1990**.
3. I. Hamerton, Chemistry and Technology of Cyanate Ester Resins, Blackie Academic and Professional, London **1994**.
4. ASTM Fire Test Standards, 3rd Edition, D2382-88," Standard Test Method for Heat of Combustion of Hydrocarbon Fuels by Bomb Calorimeter (High Precision Method)," pp. 230-238, American Society for Testing of Materials, Philadelphia, PA, **1990**.
5. ASTM Fire Test Standards, 3rd Edition, E1354-90,"Standard Test Method for Heat and Visible Smoke Release Rates for Materials and Products Using an Oxygen Consumption Calorimeter," pp. 803-820, American Society for Testing of Materials, Philadelphia, PA, **1990**.
6. R.N. Walters and R.E. Lyon ,"A Microscale Combustion Calorimeter for Determining Flammability Parameters of Materials," Proc. 42nd Int'l SAMPE Symposium and Exhibition, 42(2), 1335-1344, **1997**.
7. W.M. Thornton, *Philos. Mag.* 33, 196, **1917**.
8. Clayton Hugget, Estimation of Rate of Heat Release by Means of Oxygen Consumption Measurements, Center for Fire Research, National Bureau of Standards, Washington, DC 20234, *Fire and Materials* Vol. 4 (2) **1980**.

CROSS-LINKING OF POLYSTYRENE BY FRIEDEL-CRAFTS CHEMISTRY OFFERS ENHANCED THERMAL PROTECTION

Charles A. Wilkie and Michael A. McKinney

Department of Chemistry, Marquette University, PO Box 1881, Milwaukee, WI 53201

Work from this laboratory has been focused on developing processes by which one may cross-link polystyrene, under fire conditions, in order to have enhanced thermal properties for this polymer. Friedel-Crafts chemistry is utilized in order to achieve cross-linking. The normal Friedel-Crafts reaction proceeds at room temperature and uses an alkyl chloride as the alkylating agent and aluminum chloride as the catalyst.

$$ArH + RX \xrightarrow{AlCl_3} ArR + HCl$$

This reaction is clearly unsuitable due to the evolution of hydrogen chloride and the presence of aluminum chloride as catalyst. An alcohol can also be used as the alkylating agent and materials such as zeolites may be effective catalysts for the reaction.

The system with which we have had the most success is a copolymer of styrene and *p*-vinylbenzyl alcohol. We have used a copolymer which contains at most 10% of the alcohol component and in many cases we have reduced the amount to a few per cent of alcohol. Below is shown a schematic of the cross-linking reaction.

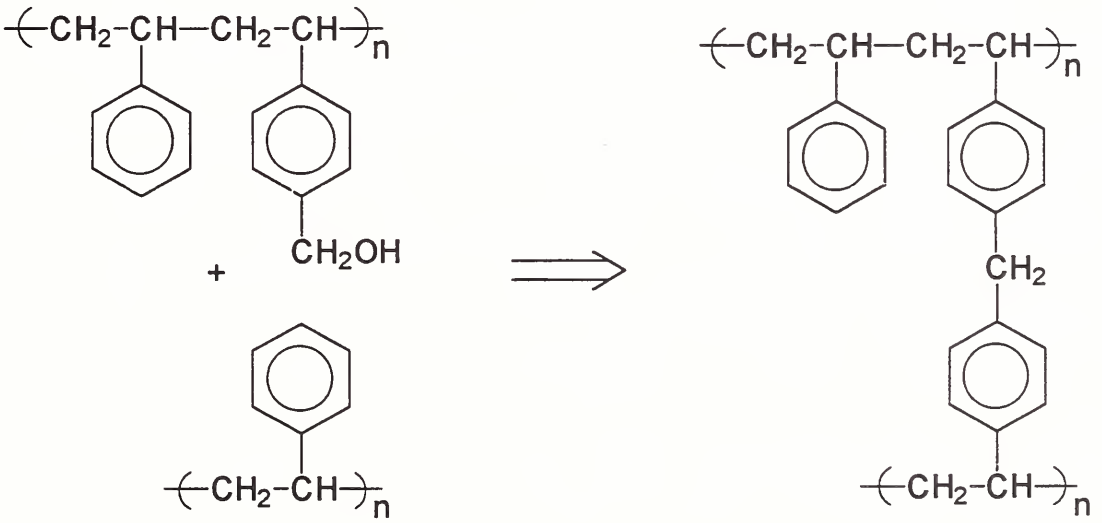

This copolymer undergoes spontaneous cross-linking at 200°C when the percentage of alcohol is about 15% but there is no cross-linking, in the absence of a catalyst, when the alcohol content is reduced to 5% or less. Somewhat traditional Friedel-Crafts catalysts, Lewis acids such as $CuCl_2$, $CoCl_2$, $ZnCl_2$, $MnCl_2$,

$SnCl_2$, and $NiCl_2$, effect the cross-linking reaction when the copolymer is heated with 1 to 3% of the catalyst at 250°C for 2 hours. When an intimate blend of the copolymer and additive is subjected to thermogravimetric analysis, the temperature at which 10% degradation occurs is increased by 40 to 90°C, depending on the catalyst, and the amount of residue which is non-volatile increases from 4 to 8%, depending on the catalyst. Of more interest is the fact that zeolites and phosphate esters will also catalyze the reaction. The phosphate ester, 2-ethylhexyl-diphenylphosphate, is of particular interest. Bronsted acids are also known to catalyze Friedel-Crafts chemistry and this phosphate ester is a protected substituted phosphoric acid. When 2-ethylhexyl-diphenylphosphate is heated to 250°C, it eliminates 2-ethylhexene with the formation of diphenylphosphoric acid. Thus one may control the temperature at which reaction occurs, since no reaction will occur until the catalyst has been formed by the thermal decomposition of the ester. The degradation of the copolymer begins 100°C higher in the presence of the phosphate ester than in its absence.

Cone calorimetry of polystyrene, the copolymer, blends of both of these with the phosphate ester have been studied and the results are shown below. It is clear that the rate of heat release is significantly decreased for the blend of the copolymer with the ester and that the presence of the ester has no effect on polystyrene.

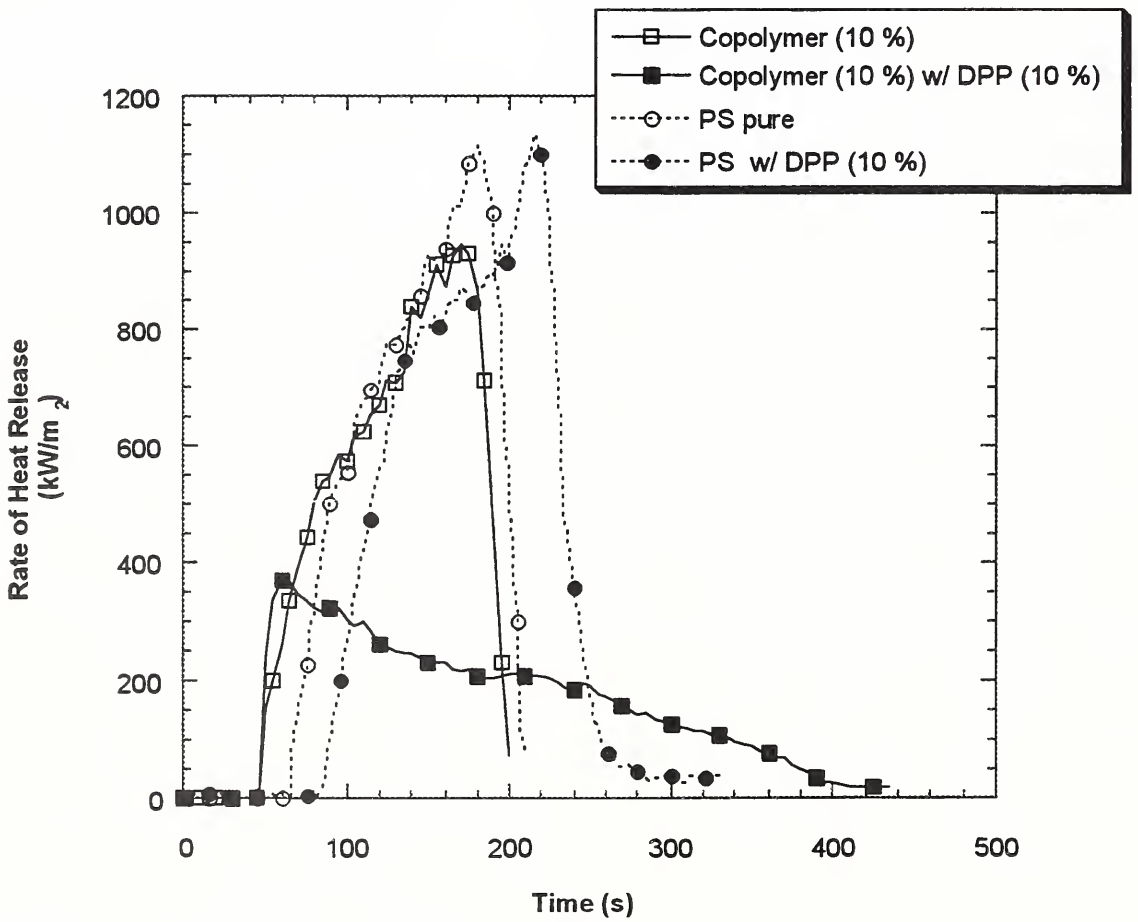

Figure 1. Cone calorimetry of polystyrene, the copolymer, and blends with the phosphate ester.

Condensed Phase Phenomena in Commodity Polymers Undergoing Degradation/Gasification

K. Steckler, T. Ohlemiller, and T. Kashiwagi
Building and Fire Research Laboratory
National Institute of Standards and Technology

ABSTRACT

A series of degradation/gasification experiments has been conducted to better understand the condensed phase processes during burning of commodity polymers such as polypropylene (PP), polyethylene (PE), and polystyrene (PS). Understanding the molten behavior of these thermoplastics is the first step. Although none of the polymers in this test series had flame retardants, future work will include flame-retardant materials. Indeed, understanding the action of these retardants in this molten polymer context is a goal of this study.

Most experiments were conducted in the gasification rig shown in Fig.1 using specimens in the form of 100 mm diameter disks. On the basis of direct observation, initial results for 25 mm-thick specimens of PP exposed to 40 kW/m^2 in nitrogen suggested that the bulk of the gasification layer might be rendered isothermal by the bubble motion, therefore, be simpler to model. To further investigate this, the gasification rig was equipped with a lamp to illuminate a portion of the specimen's surface with white light. This lighting, in combination with a new close-up lens, provided a very good camera view of the illuminated surface area. The bubbles, which at the beginning of the experiment were large and isolated (Fig. 2), eventually formed a froth of very small bubbles, very similar in appearance to that of a beer "head" (Fig. 3). The bulk of the gasification process (over time) was dominated by this behavior. Similar results were obtained for PE. In the case of PS, however, the melt viscosity appeared to be greater and the bubbles in the "froth" were somewhat larger than observed for PP and PE.

In subsequent experiments, sheathed thermocouples (0.25 mm dia.), supported by hypodermic stainless-steel sleeves were installed at positions 3, 6, and 9 mm below the original surface. The temperature traces for PP (Fig. 4) increased fairly steadily with time. Similar traces were obtained for PE and PS. Also, during this series of experiments, the thicknesses of the PP and PE froths were examined by blowing the froth aside with short bursts from a nitrogen nozzle. For both materials the thickness was judged to be one to a few bubble diameters. Consequently, these new results suggest that the idea of a deep, well-stirred (isothermal) vaporization layer is not likely to be appropriate for modeling.

Additional experiments on PE and PP specimens in the cone calorimeter (i.e. flaming conditions) revealed the same bubbling phenomena that were observed in the gasification (nitrogen) experiments.

The appearance of the froth suggests two points relevant to modeling the gasification rate: (1) the incoming radiation must be absorbed over a depth of at least a few bubble diameters; (2) the bubble breakage process which actually releases the polymer degradation vapors very near the surface is probably controlled in large measure by the surface tension of the polymer melt, coupled with thermal degradation of the bubble "windows".

A series of radiation-absorption experiments was conducted on PP specimens exposed to 40 kW/m^2 in the

gasification rig. The intent was to measure the attenuation by the bubbles. The center of the foamed-glass insulator, on which the specimen rests, was drilled-out to accommodate a 6.4 mm diameter heat flux gauge. The face of the gauge was recessed to provide an air gap of about 1.6 mm between the gauge and the lower surface of the specimen. Specimens approximately 12.7 mm, 6.4 mm, 3.2 mm, and 1.6 mm thick were tested. Unfortunately, a significant heat conduction flux developed across the air gap before bubbles were formed, and only the first few seconds of data, representing the non-degraded materials, were valid. Those data, corrected for reflections at the two air-specimen interfaces, show that over a distance of 1.6 mm, 80 percent of the radiant flux was absorbed, and over 12.7 mm, 98 percent was absorbed.

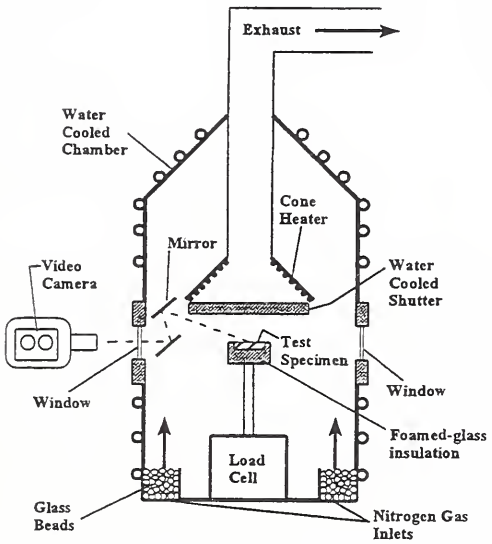

Fig. 1. Schematic of gasification rig.

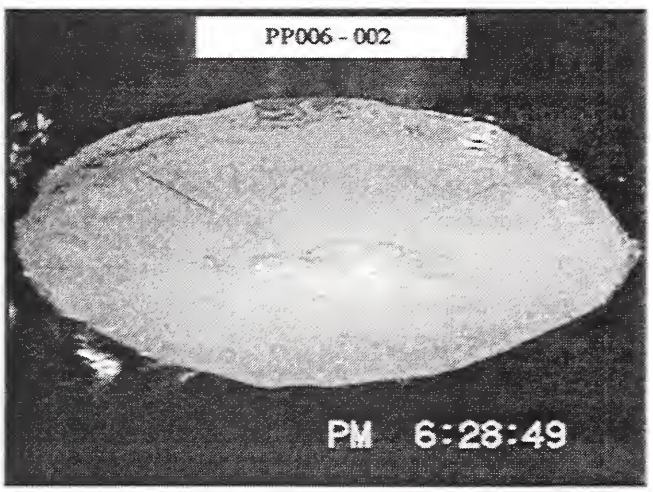

Fig. 2. PP specimen showing large isolated bubbles.

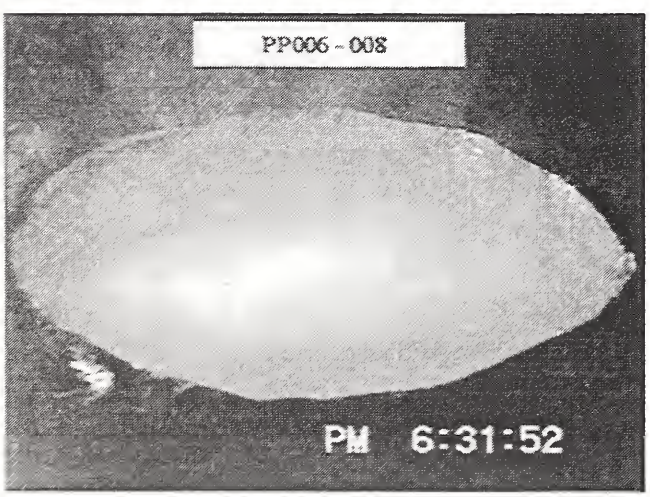

Fig. 3. PP specimen showing froth of very small bubbles.

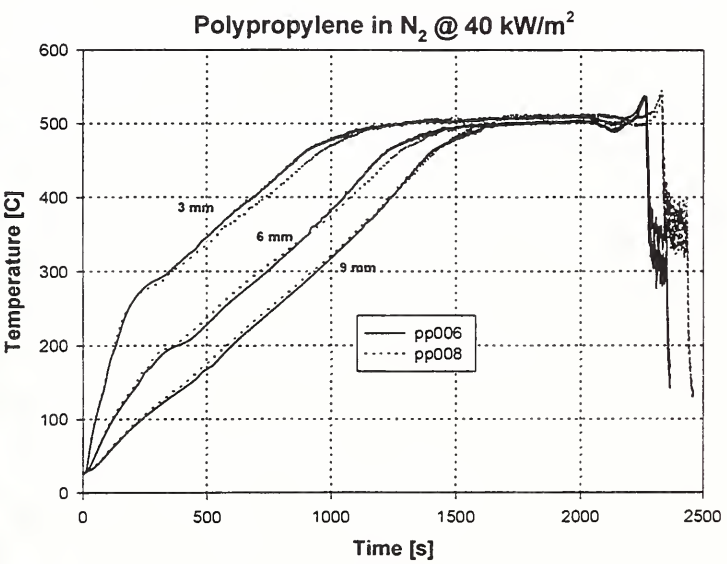

Fig. 4. Temperatures measured at various depths in PP specimens.

Near-Surface Vapor Bubble Layers in Low Stretch Burning of PMMA

S. L. Olson, NASA Lewis Research Center
J. S. T'ien, Case Western Reserve University

Abstract

Experiments on large-scale buoyant low stretch stagnation point diffusion flames over a solid fuel (PMMA) have been conducted over a range of stretch rates of 2-12 sec^{-1}, which are similar to low gravity flames [Olson, 1997]. During the experiments, an extensive layer of material above the glass transition temperature is observed, due to the low burning rates (low Peclet numbers). Unique phenomena associated with this extensive glass layer include substantial swelling of the burning surface, in-depth bubble formation and migration and/or elongation of the bubbles normal to the hot surface. Bubble layers can be a source of flow as the bubbles pop at the surface of the burning material (fuel vapor jetting and/or ejection of burning globules). This self-induced flow caused by the bubble layer enhances the burning of materials at low stretch .

Background

Materials which degrade in-depth to form bubbles as they burn have been shown [Kimzey, 1986; Olson and Sotos, 1987; Yang et al, 1997] to be a generate a flow (fuel vapor jetting or ejection of burning globules), which enhances burning in a quiescent microgravity environment through viscous entrainment of fresh oxidizer. Models which include in-depth degradation and bubble formation [Wichman, 1986; Butler, 1997] have been developed, but to date no quantitative model is available. The near-surface molten polymer and bubble layers in burning PMMA are very complicated. There are property variations with the glass transition. The in-depth degradation chemistry processes involved in bubble layer development are not fully understood.

Experiment

The experiments are conducted with a cylindrical flame configuration with different radii PMMA samples (2.4 cm thick) to vary the stretch rate. A large radius is required to establish low stretch rates [$a \propto (g/R)^{1/2}$ for buoyancy-induced stagnation point flow]. The range of stretch rates of interest is 2-12 sec^{-1}, which correspond to approximate radii of 5 - 200 cm. The oxidizer is simply room air.

Sample Swelling and Regression Transients

The position of the surface was measured from video of the experiment as a function of time for thick PMMA samples in a buoyant low stretch geometry, in order to measure the actual regression rate as a function of time. The regression rates were lower than previously obtained [Ohtani et al. 1981], due to the low stretch rate.

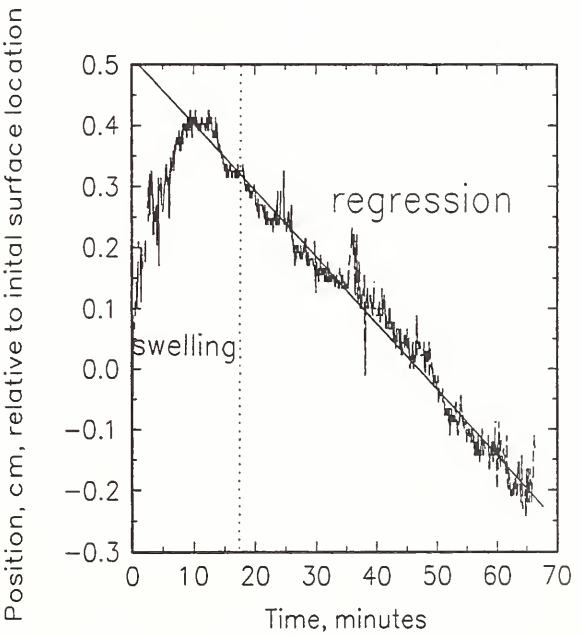

Figure 1: Swelling and regression data.

It was noted from these measurements that the sample surface swelled outward significantly during the early phase of the experiment. This was attributed to the development of the bubble layer during the ignition and solid-phase heatup of the sample. Swelling stopped as the bubble layer became fully-developed and regression began to dominate the surface motion. An example of this swelling and regression is shown in Figure 1. During the early phase, the surface swells outward (4 mm in this case) before regression is observable. Time scales of this period are of the same order as the solid-phase heatup timescales.

The initial swelling of the sample was unexpected in these experiments. Although other researchers have described a two-phase layer during combustion [Krishnamurthy and Williams, 1973; Seshadri and Williams, 1978; Ohtani et al, 1981], no one has mentioned this initial swelling. Thermal expansion of the PMMA as it is heated (estimated to be ~0.2 mm) is not sufficient to explain the swelling. Rather, the observed swelling appears to be linked to the bubble layer. The thickness of the bubble layer is measured after each experiment from the cooled, cut, and polished sample, and plotted in Figure 2. Maximum swelling is normalized with the measured bubble layer thickness and plotted in Figure 2 (swelling ratio) as a function of stretch rate. Also in Figure 2, the regression during the swelling phase is estimated from the steady regression rate (see Fig.1), and can be considered as unrealized swelling.

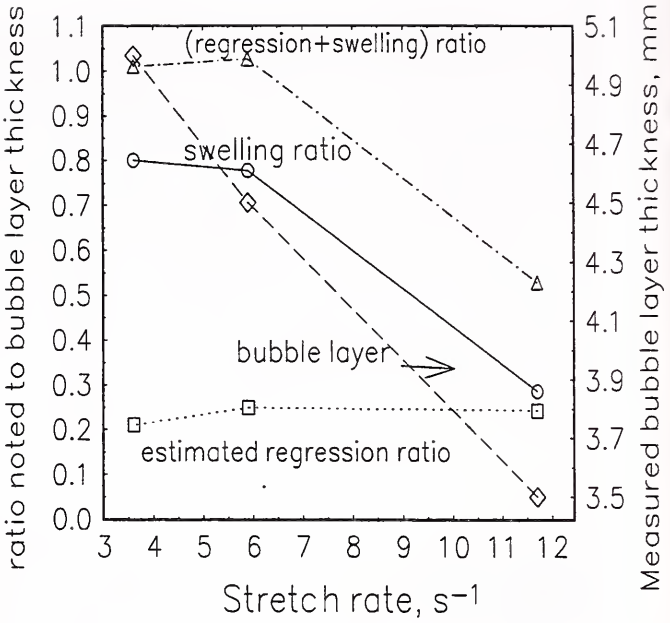

Figure 2: Ratio of swelling to measured bubble layer thickness as a function of the stretch rate.

For larger stretch rates ($a>12\ s^{-1}$), which would be typical of normal gravity experiments, the trend in the data indicates that swelling would be masked by the surface regression, due to the high burning rates. At high burning rates, where the solid-phase Peclet number is large (Pe>3.6), the heated layer is thin. This explains why the swelling due to the bubble layer has not been observed in previous investigations. The combined swelling and regression normalized by the bubble layer thickness approaches unity as stretch rate is reduced, until unstable flame coverage occurs below stretch rates of 3 sec^{-1}. The initial total swelling (swelling+regression) is thus commensurate with the in-depth bubble layer which develops during the low stretch (Pe<1) burning of these samples.

Conclusions

Low stretch buoyant stagnation point combustion of cylindrical PMMA samples have been conducted with the lowest burning rate data obtained for this geometry. The very low regression rate experimental results showed for the first time the sample swelling during the heatup phase of PMMA combustion, and linked that swelling directly to the development of the bubble layer. This swelling is only easily observable when solid-phase Peclet numbers are low (Pe<1). A much more detailed model is needed to describe these processes in the solid phase.

References

Butler, K.M., "Numerical Modeling for Combustion of Thermoplastic Materials in Microgravity", *Fourth International Micorgravity Combustion Workshop*, NASA Conference Publication 10194, pp.249-254, 1997.

Kimzey,J.H., 1986; "Skylab Expeirment M-479, Zero Gravity Flammability, NASA JSC-22293.

Krishnamurthy, L, and Williams, F.A.; 1973; "On the Temperatures of Regressiong PMMA Surfaces", *Combustion and Flame*, Vol. 20, pp. 163-169.

Ohtani, H., Hirano, T., and Akita, K., 1981; "Experimental Study of Bottom Surface Combustion of Polymethylmethacrylate", *Eighteenth Symposium (International) on Combustion*, The Combustion Institute, pp. 591-599.

Olson, S.L., "Buoyant Low Stretch Stagnation Point Diffusion Flames over a Solid Fuel", Ph.D. Dissertation, CWRU, May, 1997.

Olson, S.L., and Sotos, R.G.,"Combustion of Velcro in Low Gravity", NASA TM 88970, 1987.

Seshadri, K. and Williams, F.A., 1978; "Structure and Extinction of Counterflow Diffusion Flames above Condensed Fuels: Comparison Between Poly (methyl Methacrylate) and its Liquid Monomer, both Burning in Nitrogen-Air Mixtures", *Journal of Polymer Science: Polymer Chemistry Edition*, Vol. 16, pp. 1755-1778.

Wichman, I.S., "A Model Describing the Steady-State Gasification of Bubble-Forming Thermoplastics in Response to an Incident heat Flux", *Combustion and Flame*, 63: 217-229 (1986).

Yang, J.C., Hamins, A., Glover, M., and King, M.D., "Experimental Observations of PMMA Shperes Burning at Reduced Gravity", *Fourth International Micorgravity Combustion Workshop*, NASA Conference Publication 10194, pp.243-248, 1997.

Diode Laser Measurements of HF concentrations from Heptane/Air Pan Fires Extinguished by FE-36 and FE-36 plus Ammonium Polyphosphate

R.G. DANIEL, R.R. SKAGGS, A.W. MIZIOLEK, AND K.L. McNESBY

U.S. Army Research Laboratory, Aberdeen Proving Ground, MD 21005

CRAIG HERUD, WILLIAM R. BOLT, AND DONALD HORTON

Aberdeen Test Center, Aberdeen Proving Ground, MD 21005

The mandatory phasing out of halons 1301 (CF_3Br) and 1211 (CF_2ClBr) for use as the primary fire extinguishing agent aboard U.S. Army combat vehicles has led to the development of replacement agents such as FE-36 ($C_3F_6H_2$) and FM-200 (C_3F_7H). These chemicals though effective at extinguishing fires, typically are deficient in terms of increased weight and volume requirements needed for fighting the most difficult military fires. The increased amounts of replacement agent required for extinguishment poses a concern with the levels of hydrogen fluoride formed as the primary decomposition product [1]. This concern has limited the acceptance of these agents for deployment in occupied spaces.

The two mechanisms by which HF concentrations can be decreased in real fire situations extinguished by FE-36 or FM-200 are 1) reduce the time required to extinguish the fire, or 2) release a scavenging agent in conjunction with the fire suppressant chemical to remove HF from the affected space. These mechanisms are investigated here with tunable diode laser absorption spectroscopy (TDLAS) measurements of HF concentrations produced from a series of enclosed heptane/air pan fires extinguished by FE-36 or FE-36 plus ammonium polyphosphate (APP). A potential chemical scavenging agent of HF is APP which is a commercially available chemical with fire retardant properties where the agent is typically suspended in an extinguisher as a gel and released as a white powder. A series of extinguishment tests were conducted with FE-36 and FE-36 plus APP. By measuring how much the HF concentrations are reduced in fires extinguished with FE-36 plus APP compared to fires extinguished by FE-36 alone, the effectiveness of APP as a HF scavenging agent will be demonstrated and evaluated.

---

1. McNesby, K.L., Daniel, R.G., Widder, J.M., and Miziolek, A.W., *Applied Spectroscopy* 50: 126-130 (1996).

EXTINCTION OF HYDROFLUOROCARBON FLAMES WITH F/H RATIOS OF UNITY AND GREATER[1]

W. Grosshandler, M. Donnelly, and C. Womeldorf

National Institute of Standards and Technology
Gaithersburg, Maryland 20899 U.S.A.

Hydrofluorocarbons (HFCs) are being considered as replacements for chlorofluorocarbon (CFC) refrigerants because HFCs do not deplete stratospheric ozone when released to the atmosphere. In general, the exchange of a halogen atom in a molecule with hydrogen decreases the atmospheric lifetime of the compound. It may also increase the efficiency of the refrigeration machine. Both of these effects are highly desirable from environmental considerations since they act to mitigate global warming; however, more hydrogen on an HFC is usually associated with an increase in flammability. An accepted method for determining the flammability limits of gaseous fuels is ASTM Standard E 681. The minimum and maximum concentrations of the fuel in air for flame propagation are based upon the observed ignition and growth of a flame in a vessel filled with a quiescent fuel/air mixture. A clear distinction is sought between a non-propagating flicker and a flame which has enough horizontal propagation to be hazardous. When applied to hydrocarbons, these tests give well-defined results. Fuels with fluorine-to-carbon ratios approaching unity have a great sensitivity to the test conditions and provide ambiguous limits due to vagaries in the ignition source, to vessel geometry complexities, and to operator subjectivity.

Many of the difficulties associated with the ASTM apparatus are not present in a premixed, counter-flow burner. With this apparatus, steady flames first are established under favorable conditions, and then the fraction of fuel is diminished in small increments until the flame is extinguished. The tests are repeated at progressively lower flow rates, which are inherently more capable of sustaining combustion. By plotting the fraction of fuel at extinction versus the flow rate and extrapolating to an experimentally unattainable zero-flow condition, an unambiguous limit of flammability can be attained. Unlike the ASTM apparatus, the counter-flow burner method entirely avoids issues surrounding the design of an ignition mechanism, it minimizes heat loss and wall effects, and also it is amenable to computational analysis.

HFC flame studies are typically carried out in mixtures with hydrocarbons, in which the overall H-atom concentration is considerably greater than the F-atom. As the F/H ratio approaches unity, the flame speed decreases substantially, making it difficult to stabilize even lightly stretched stoichiometric flames. The HFCs investigated in this study [CH_2F_2 (R-32), C_2HF_5 (R-125) and $CHF_2CF_2CH_2F$ (R-245ca)] have F/H ratios equal to or greater than one. The pure CH_2F_2/air flame can be established over a range of equivalence ratios and stretch rates. Figure 1 shows the limiting mole fraction of CH_2F_2 in air for which a flame can be sustained for a given global stretch rate (defined as the mean burner nozzle velocity divided by the distance from the outlet to the stagnation plane). The open diamonds and circles represent dry initial conditions, and the filled symbols are data taken with the air humidified to a dew point of about 12 °C. The solid line is the best fit through the humid data for an initial mixture temperature of 100 °C. The dotted line corresponds to a fit of dry conditions for a nominal initial temperature between 25 °C and 35 °C. Extrapolating the straight lines to the vertical axis yields a mole fraction that is equivalent to a lower flammability limit for CH_2F_2/air mixtures. Increasing the temperature decreases the limiting mole fraction of CH_2F_2 from 0.14 ± 0.004 at 30 °C to 0.13 ± 0.004 at 100 °C; changing the relative humidity has no statistical significance.

A flame of C_2HF_5 and air can not be stabilized under any condition. Hence, R-125 is properly classified as non-flammable. By mixing the C_2HF_5 with CH_2F_2, a critical mole fraction of R-125 in the refrigerant mixture can be reached which just renders it non-flammable. Figure 2 shows how increasing the fraction of R-125 decreases the stretch rate necessary to extinguish the flame, as a function of equivalence ratio. The equivalence ratio that leads to the highest extinguishing stretch rate lies between 1.15 and 1.25, with higher mole fractions of C_2HF_5 pushing the peak closer the stoichiometric condition. Note that both

[1] Research supported by the Air-conditioning and Refrigeration Technology Institute, the Department of Energy, and the NIST Advanced Technology Program

refrigerants are treated as fuels when computing the equivalence ratio since equilibrium calculations indicate that, at flame temperatures, the main products are HF, COF_2, CF_4, and CO_2. The critical flammability ratio (CFR), defined as the minimum mole fraction of R-125 in the refrigerant mixture required to prevent flame propagation under any conditions, can be estimated by extrapolating the peak extinction stretch rate versus R-125 mole fraction curve to a zero-stretch condition. Using this technique, a CFR of 0.18 ± 0.004 is found for dry air initially at 30 °C ± 5°C. For experiments performed at 100 °C and humidified to a dew point of 12 °C, a greater mole fraction of R-125 was required to extinguish the flame at each stretch rate, increasing the CFR to 0.22 ± 0.004 for these conditions.

Pure $CHF_2CF_2CH_2F$ with air does not produce a stable flame under the conditions examined in the counter flow burner. It does burn easily when supplemented with CH_2F_2, and it is possible to decrease the amount of CH_2F_2 needed for a flame as the stretch rate is decreased. Extrapolating to a zero mole fraction of CH_2F_2 suggests that a flame might exist if the initial temperature is 100 °C and dew point is 12 °C for a narrow range of equivalence ratios around 1.3, as long as the stretch rate is below 6 s^{-1}. Flames with such low stretch rates can not be maintained in the presence of normal buoyant forces. If the water vapor is removed from the air, or if the temperature is reduced to 50 °C, no flammable range can be obtained for a finite value of stretch rate.

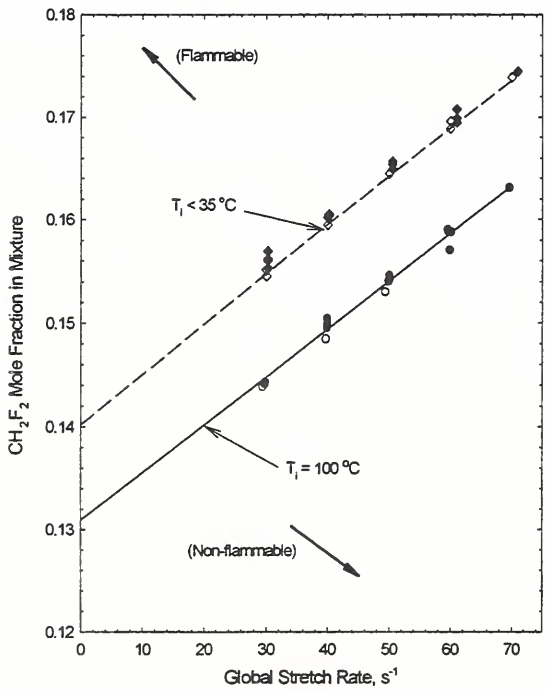

Figure 1. Extinction mole fraction of CH_2F_2/air mixtures as a function of flame stretch, showing impact of initial temperature and humidity. Solid symbols: $T_{dew\ pt}$=12 °C; open symbols: dry air.

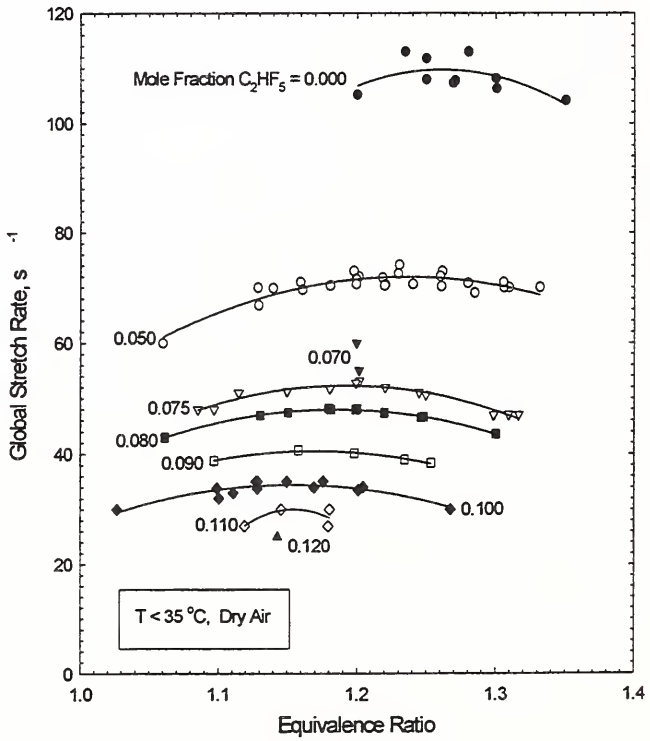

Figure 2. Extinction stretch rates for fixed values of C_2HF_5 mole fraction in fuel mixture, as a function of total equivalence ratio.

Comparison of the Behavior of Foams and Gels Exposed to Fire

A.M. Tafreshi & M. di Marzo

Mechanical Engineering Department
University of Maryland
College Park, MD 20742

Introduction: Water is the principal component of both foams and gels used as fire protection agents. The foam is expanded to several times its original liquid volume with air. Data from a previous study show that, when the foam is subjected to a radiant heat input of 18 kW/m^2, the peak of the radiant heat absorption is at about 30 mm in the depth of the foam layer while radiant heat penetrates to depths up to 60 mm [1]. The reason for this behavior is the decreasing density of the foam near its exposed surface as the water is evaporated away from the foam matrix. As the density decrease, so does the extinction coefficient leading to lower absorption of the incoming radiation. In the depth of the foam layer, as the thickness and the density both increase, the radiant heat is absorbed causing the water to vaporize in-situ since the contribution of thermal diffusion is small. In contrast with this phenomenology, the behavior of the gel, in a similar situation, is dominated by thermal diffusion [2]. The radiant heat input is absorbed in the immediate proximity of the gel surface and the exposed surface approaches saturation conditions for the duration of the transient. These differences result in significantly different fire protection behaviors. These observations complemented with other, more qualitative considerations will identify a rationale for recommending the proper agent for the specific fire protection scenario.

Apparatus: A series of experiments are conducted with the Radiant Exposure Apparatus (REA), developed in the Building and Fire Laboratory of the National Institute of Standards and Technology. In the REA, two vertical gas-fired panels, 0.38 m wide and 0.83 m high, are used to supply the radiant heat input. The flame is obtained from a regulated mixture of natural gas and air fed to the two panels which are oriented at a 120° angle from each other. They are capable of generating uniform heat fluxes at the sample surface of up to 18 kW/m^2. The sample is square in shape (0.3 m each side). Thermocouples are placed on its surface at various locations. Two flux gages are mounted on the sides of the sample to monitor the heat flux level during the test.

Results: Figure 1 illustrates the behavior of the foam in comparison with the gel. Both curves are for the average surface temperature of Plywood samples (T1-11) with a radiant heat flux of 18 kW/m^2. The wood is kept at controlled temperature (23°C) and relative humidity (40%) prior to the test. The gelling agent concentration used is

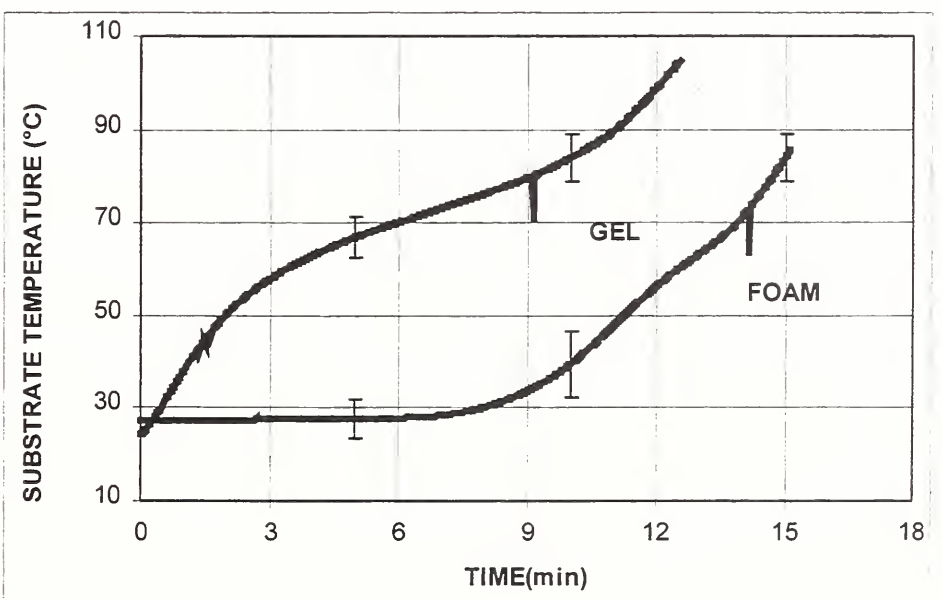

Figure 1 - Comparison of gel and foam on wood substrate.

6% and the thickness of the applied layer is 5 mm. The foam is obtained from a 3% liquid solution expanded twenty times with air that results in an initial foam density of 50 kg/m^3. The foam layer thickness is of 0.1 m. In both cases, the amount of water applied per unit surface area of the sample is 5 kg/m^2. Therefore, the comparison of the performance of the foam and gel is based on the same amount of water content for sample unit surface. The temperature at the sample surface exhibits a completely different behavior for these two agents. For several minutes, there is no indication that the sample coated with foam is exposed to radiant heat input. This is due to the strong insulating effect of the foam which exhibits very low thermal diffusion transport. Recall that the radiant energy is absorbed in the depth of the foam layer and that it propagates up to 60 mm into it. Considering that the foam layer is evaporated at about 0.1 mm/s, it follows that the forefront of the radiant heat wave reaches the sample as 40 mm of foam are evaporated from the original 0.1 m layer. This would take place in about 7 minutes. This coarse prediction is consistent with the measurements shown in the figure. Thereafter, the heat-up transient is steeper than for the sample coated with gel. The foam is completely evaporated in about 14 minutes. The vertical lines at 9 and 14 minutes indicate the failure of the protective layer and represent the end of the protective time. Note that the foam provides about 5 minutes of additional protective time. Consider that the longer duration of the foam protection layer (compared with the gel) must be carefully weighted against the wind effect present in the field which will reduce the foam protection time by disrupting the foam layer as its density decreases. This effect may result in a comparable overall performance of the two agents.

Conclusions: The gel is best suited for urban applications because:

a) extensive smooth surfaces (such as windows) are easily coated and the structural characteristics of the gel layer insure reliable protection;

b) the higher temperatures of the substrate are well within the limit of typical building exterior materials;

c) the gel is not greatly affect by wind;

d) the relatively simpler geometrical characteristics of the urban setting do not require the filling action of the foam.

The foam is best suited for forestry applications or for urban-wild-life settings because:

a) it keeps the substrate (which in this case is living vegetation) at ambient temperature completely shielding it from the fire radiation;

b) exhibits excellent coating and gap-filling properties for applications where the surfaces are irregular (such as trees and bushes);

c) its drawbacks are due to the limited adhesion to smooth surfaces and to the effect of wind (the wind may easily shear the low-density foam on the outer portion of the layer).

Acknowledgement: This work was supported by the BFRL NIST under grant No. 60NANB6D0073. The advise and encouragement of Drs. Baum and Evans are greatly appreciated.

References:

1. Boyd, C. & diMarzo, M., The behavior of a fire-protection foam exposed to radiant heating, *Int. J. Heat Mass Transfer*, **41** (1998) 1719-1728
2. Staggs, J.E.J., A discussion of modeling idealized ablative materials with particular reference to fire testing, *Fire Safety Journal*, **28** (1997) 47-66
3. Tafreshi, A., M., di Marzo, R. Floyd, S. Wang, Characterization and Evaluation of Fire Protection Foams, *NIST-GCR-98-742* (1998)

Measurements of Heat Release Rate and Vorticity Distributions in a Buoyant Diffusion Flame for the Calculation of Fire Induced Flows

J. P. Gore and X. C. Zhou
School of Mechanical Engineering,
Purdue University
West Lafayette, IN 47907-1003

Fire induced flows are of importance in a variety of fire phenomena including entrainment, pollutant formation, fire size and fire spread. A recipe pioneered by Baum and McCaffrey[1] at NIST utilizes the distributions of heat release rates and vorticity in the fire in the evaluation of the fire induced flow field. In this work, we utilize mean mixture fraction measurements and mean velocity measurements in the fire to deduce these distributions. Using these distributions in conjunction with the methodology of Ref. [1], we have calculated the flow field of a 7.1 cm natural gas fueled buoyant flame. The results are in excellent agreement with experimental data.

The methodology of Baum and McCaffrey involves separating the velocity field into irrotational and solenoidal components. The irrotational component is described by a velocity potential Φ, which is governed by $\nabla^2\Phi = Q$ and the solenoidal velocity component V is governed by $\nabla x V = \omega_p$. The source Q for the velocity potential consists of normalized heat conduction and heat release rate contributions and that for the solenoidal velocity component is the vorticity ω_p in the fire. Using conservation of energy and conservation of mixture fraction the source Q is related to the diffusion rate of mixture fraction (defined as the fraction of local mass that originates in the fuel stream) and the rate of change of specific volume with respect to mixture fraction. The vorticity in the fire is by definition the curl of the velocity field. We used measurements of mean mixture fraction obtained using sampling and gas chromatography to estimate the source term Q. We also used measurements of the velocity field obtained with particle imaging velocimetry to obtain the vorticity in the fire.

Figure 1 shows sample measurements of the velocity potential source term at three axial stations above a 7.1 cm natural gas fire. The measurements show that the source term is nonzero in an annular region where the flame sheet resides. The small negative values at intermediate radial location result from the dominance of thermal conduction away from the flame sheet in this region. The large positive values result from heat release in the flame sheet. Figure 2 shows measurements of vorticity at four axial stations above the fire. The two components of vorticity and their summation are shown. At lower elevations the derivative of radial velocity contributes to the vorticity but at higher elevations the radial derivative of the axial velocity dominates. The correlations from Ref. 1 overestimate the source at larger radii but underestimate it at shorter radii. This caused discrepancies in measurements and predictions of entrainment velocity as discussed in Ref. 2. The modified source terms based on visible flame radius used in Ref. 2 are also shown in Fig. 2 and approximate the data better except for the 1 cm location.

Figure 3 shows measurements and predictions of the two dimensional velocity field in the fire obtained using the source term distributions at many stations similar to those shown in Figs. 1 and 2. The qualitative and quantitative agreement between the measurements and predictions observed in Fig. 3 suggests that given an appropriate estimate of the source terms, the velocity field can be calculated using the NIST methodology. The flow field shows low velocities near the fuel surface and strong acceleration close to it.

References:
[1] Baum H. R. and McCaffrey B. J., *Fire Safety Science – Proceedings of the Second International Symposium*, Tokyo, Japan, 1988.
[2] Zhou, X. C., Gore J. P., and Baum H. R., *Twenty Sixth Symposium (International) on Combustion*, The Combustion Institute, Pittsburgh, pp. 1453-1459 (1996).
Acknowledgement: NIST Grant number NANB6D0118 with Dr. Baum serving as Program Officer supports this work.

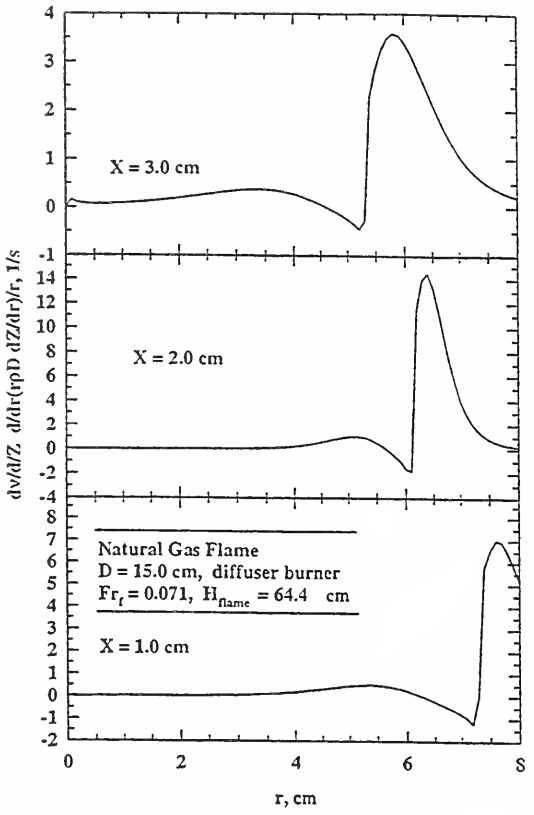

Figure 1: Source term for velocity potential deduced from mixture fraction measurements.

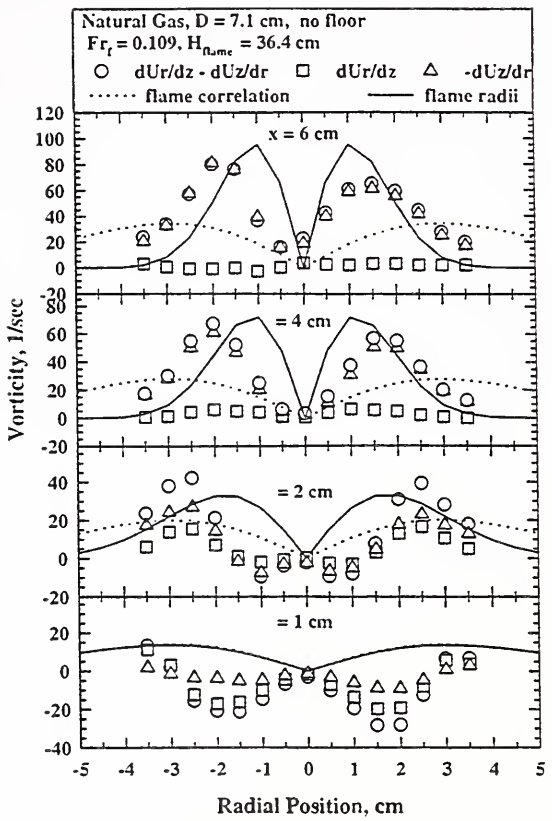

Figure 2: Vorticity deduced from velocity measurements and past correlations.

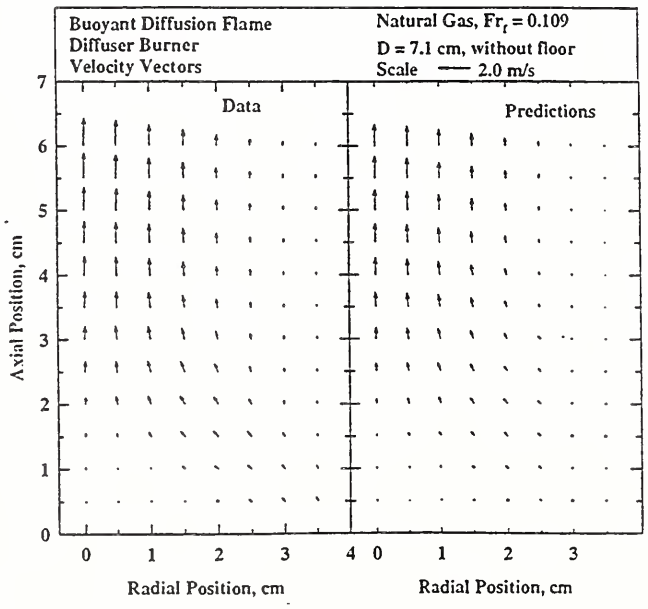

Figure 3: Measurements and predictions of two dimensional mean velocity vectors in a 7.1 cm fire.

DETECTION IN DIFFICULT ENVIRONMENTS

Fred Conforti

Pittway Systems Technology Group
4225 Naperville Road, Suite 155
Lisle, IL 60532
Tel 630-577-3700
Fax 630-577-0808
fred_conforti@pittway.com

ABSTRACT

Although the majority of early warning fire detection applications can be covered by photoelectric and ion detectors, these technologies are too sensitive for very dirty, dusty or wet areas. Use of these standard types of fire detectors in harsh environments would result in a high occurrence of nuisance alarms. A "harsh environment detector" needs to provide early detection while eliminating nuisance alarms and the need for frequent maintenance. To do this, these detectors need to be provided with protection from airborne particles such as dust, water mist and insects.

A new, intelligent early warning detector is designed for dusty, dirty, or wet locations such as paper mills, textile plants, subways, or wash-down areas. The detector uses micro-pore filters to remove airborne matter before it reaches the smoke sensor. The air intake flow and aspiration fan are both supervised. By filtering particles such as dust and water mist, this intelligent detector can now be provided as early warning protection in harsh environments where slower responding thermal detectors have typically been used.

Actual "dirty" environment installations will be described and system performances will be documented.

REFERENCES

1. Dubivsky, P. M. & Bukowski, R. W., False Alarm Study of Smoke Detectors in Department of Veterans Affairs Medical Centers (VAMCS). Technical Report 4077, National Institute of Standards and Technology, Gaithersburg, MD, 1989.

FEWER UNWANTED ALARMS:
Technology and education are helping to reduce the occurrence of unwanted fire alarms.

Fred Conforti

Pittway Systems Technology Group
4225 Naperville Road, Suite 155
Lisle, IL 60532
Tel 630-577-3700
Fax 630-577-0808
fred_conforti@pittway.com

ABSTRACT

Although our real world perception indicates that we are getting more unwanted alarms, research and data supporting this perception have been non-existent. Our belief was that this perception was wrong.

In search for real data, Pittway Systems Technology Group joined with the Naperville, Illinois Fire Department and Buddingh & Associates (an independent research firm) to study the history, causes and frequency of unwanted alarms across all types and ages of fire protection equipment installed in commercial environments. The hypothesis that the study was designed to test was: Commercial buildings with the latest technologies in fire detection will experience fewer unwanted alarms than buildings using older technologies.

To test the hypothesis, Naperville, a suburb of Chicago, was chosen because it was a growing community with a variety of commercial establishments whose fire department logged pertinent data continuously. The Naperville Fire Department had extensive information on false alarms since 1985 and specific information on commercial type systems installed since 1990. The original goal of the study was to identify 200 reporting sites having unwanted alarms. The eventual research yielded a database of 821 sites of 3,510 systems installed.

Unwanted alarms consist of false alarms and nuisance alarms. Too often, the two terms are used interchangeably. False alarms are a result of non-smoke stimuli, including system malfunction, electrical problems and lightning strikes. Nuisance alarms are those caused by non-threatening smoke or smoke-like stimuli, including kitchen and bathroom steam, cigarette smoke, burnt toast, etc. In the Naperville study, false and nuisance incidents were logged separately and were analyzed across the commercial base.

The study clearly showed that the original hypothesis was valid: newer systems experience fewer false alarms. The ratio of false alarms per system in 1985 was 1.15 per system per year on a base of 578 installed systems. In 1997, the ratio was 0.56 per system per year on an installed base of 3,510 systems. This is a 2-to-1 reduction in false alarms per system per year during a period when the number of installed systems grew sevenfold. The reduction in false alarms took place steadily as newer, improved systems were installed.

While the study showed the rate of false alarms has clearly declined, it also showed that the rate of nuisance alarms per system has remained relatively constant, indicating areas for future improvements in technology, testing, and education.

The data also showed that new installations are the worst offenders in generating unwanted alarms. This phenomena is well known to installers and fire professionals who have come to expect a "shakedown period" during which a new system is tested with real occupants, their usage patterns, and the environment. New system problems are typically nuisance alarms due to poor location. The study indicated that in 1996, new systems (those installed within the previous twelve months) were responsible for 30% of all unwanted alarms. In checking to determine if this was an isolated or unusual year for unwanted alarms, it was compared to 1988, where data indicated that 32% of the unwanted alarms were from installations less than twelve months old. Not much difference. This data provides us with areas to concentrate on to further reduce unwanted alarm phenomena, and a benchmark by which to measure our progress.

Since 1986, manufacturers have focused on improving detection technologies and alarm systems with significant advances in bug screens, humidity and dust immunity, development of alarm verification, the introduction of intelligent systems and multi-sensing, multi-criteria detectors to name some. All of these have combined to help reduce the rate of false alarms.

While the Naperville study clearly supports the fact that false alarms are coming down and the notion that the newer systems, once "settled in", are responsible for fewer false alarms than older systems, the study does not differentiate the impact that improved test standards versus improved designs have played in helping to improve system reliability and reducing nuisance alarms. Many significant refinements to agency test programs have been made over the years to verify a product's probable satisfactory performance in the real world.

Organizations like the National Fire Protection Association (NFPA) and the Automatic Fire Alarm Association (AFAA) have worked tirelessly to help increase the fire industry's access to training and resources. The U.S. Department of Commerce, through its National Institute of Standards and Testing, has added considerably to the body of knowledge concerning fire phenomena. Manufacturers, engineers, distributors, and installers continue to offer, develop, and seek out educational opportunities, like NICET certification, to improve the performance and delivery of fire protection products and services.

Together, technology, testing and education work hand-in-hand to improve fire protection reliability. While we will never be able to completely eliminate the human factor by design, construction and usage, it is obvious that the tools and tests necessary to continue to reduce unwanted alarms are within our reach. The Naperville study provides us with our first measurable indicator that we are making progress. It also gives us a benchmark to monitor our progress and reminds us that this is a complex issue requiring active involvement of the entire fire community.

REFERENCES

1. Dubivsky, P. M. & Bukowski, R. W., False Alarm Study of Smoke Detectors in Department of Veterans Affairs Medical Centers (VAMCS). Technical Report 4077, National Institute of Standards and Technology, Gaithersburg, MD, 1989.
2. Donohue, P. A., False alarms from automatic fire detection systems. Fire Research Station Information Paper 13/92. Borehamwood, BRE, 1992.

Three Dimensional Radiative Ignition and Flame Spread over Thin Cellulose Fuels

S.L. Olson, NASA Lewis Research Center
T. Kashiwagi, National Institute of Standards and Technology

Abstract

Radiative ignition and transition to flame spread over thin cellulose fuel samples was studied aboard the USMP-3 STS-75 Space Shuttle mission in February and March of 1996, using the RITSI hardware. A focused beam from a tungsten/halogen lamp was used to ignite the center of the fuel sample while fan-drawn air flow was varied from 0 to 6.5 cm/s. Non-piloted radiative ignition of the paper in air was found to occur more easily in microgravity than in normal gravity. Ignition of the sample was achieved under all conditions studied, with transition to flame spread occurring for all but the quiescent flow condition. After ignition, the flame spread only upstream, in a fan-shaped pattern. The fan angle increased with increasing external flow from zero angle (tunneling flame spread) at the limiting 0.5 cm/s external air flow, to 90 degrees (semicircular flame spread) for external flows at and above 5 cm/s. The downstream flame is inhibited due to the 'oxygen shadow' of the upstream flame, despite the convective heating from the upstream flame. Only after the upstream flame spread was complete could downstream flame spread occur.

Ignition

Radiative ignition was achieved easily in microgravity, unlike normal gravity where the irradiation alone was insufficiently energetic to ignite the quickly-convected hot degradation products over a vertical sample surface. Ignition delay times varied linearly with inverse iflow, as shown in Figure 1. The slower the flow, the longer the ignition delay time. This dependence is believed to be due to gas-phase mixing times, which are also inversely proportional to the imposed flow. Ignition is quite energetic; a thermal expansion wave from the ignition event easily exceeds the imposed flow and is quickly sensed by the thermocouples both upstream and downstream of the ignition spot. The crew, monitoring the experiment visually, commented "There was a great burst of flame perpendicular to the surface." and "I can peak inside and I can tell you that it's incredible: they're really 3-D."

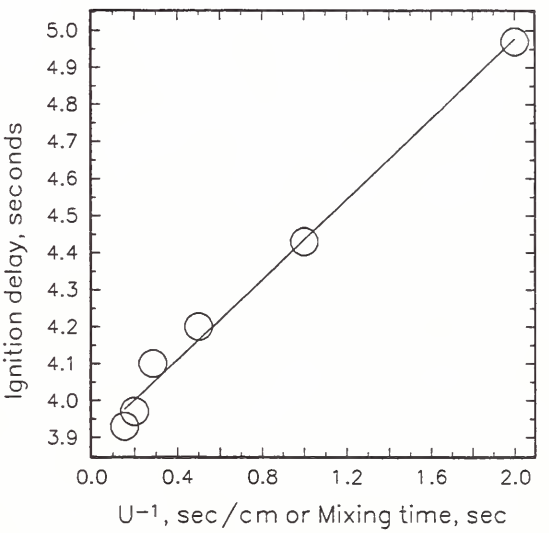

Figure 1: Ignition delay varies with the inverse flow

Flame Spread

Flame spread from a central ignition spot is unique in that the flame in this situation can go in whatever direction(s) it finds conducive to spread. The resultant direction(s) are revealing about the important controlling mechanisms for flame spread in this weakly ventilated microgravity environment. Ignition in a quiescent environment occurred, but transition failed and the flame extinguished. With flow, transition to spread only occurred in the upstream direction as shown in Fig 2. Despite convective heating, the downstream region was not flammable due to the 'oxygen shadow' cast by the upstream flame. The incoming oxidizer was consumed by the upstream flame, and the combustion products from that flame were swept downstream. The downstream flame, unable to obtain sufficient oxygen in the vitiated flow, was not viable. The flame spread only upstream until the edge of the sample was reached. At that point, once the upstream flame was gone, the flame wrapped around along the unburned edges of the sample and a concurrent flame (Fig.2d), now able to obtain unvitiated oxidizer flow, began to spread. These preliminay downstream flame spread rates are more difficult to measure because of this non-ideal geometry.

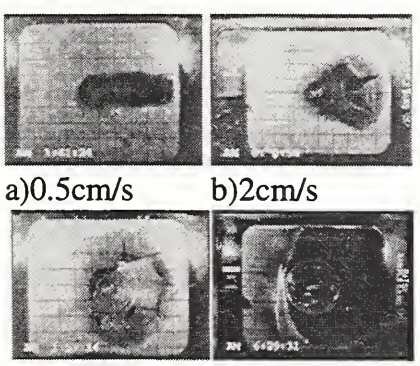

a)0.5cm/s b)2cm/s

c)6.5cm/s d)5cm/s

Figure 2

Flame spread rates were measured in each test for both the upstream and later for downstream flame spread. At the lowest flows tested (0.5 and 1 cm/s), viable flame spread occurred only in the upstream direction. The measured flame spread rates are plotted in Figure 3, where upstream flame spread flows are positive and downstream spread flows are negative. Symbols are sized to represent the scatter in the data from the least squares regression line through the data. The quench region is indicated in Fig 3, generally centered around quiescence but skewed to the downstream side. Simultaneous upstream and downstream flame spread was not observed over the flow range studied. Upstream (opposed-flow) flame spread is faster than downstream (concurrent) flame spread at a given flow over the range of flows studied due to this skewing. These results agree qualitatively with model predictions [1]. Faster upstream flame spread is the exact opposite of normal gravity flame spread where not only is simultaneous upward (downstream) and downward (upstream) flame spread possible, but the downstream flame spread is much faster.

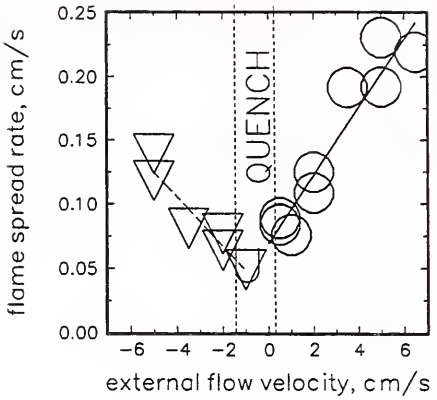

Figure 3: upstream and downstream flame spread

3D Limiting Flame Angles

The upstream flame spread propagated radially from the ignition region. However, there appears to be a maximum angle of flame spread for a given flow. This maximum fan angle of the propagating flame front can be seen in the char patterns in Fig 2. The experimental angles, defined as the angle from direct upstream motion to the edge of the char region, were measured from the video images. The measured values are shown in Fig 4 as a function of flow. At sufficiently high flows (>3.5 cm/s), the flame angle is nearly 90 degrees, indicating semicircular flame propagation in the upstream direction. Below that flow, however, the flame angle reduces with flow until a limit of zero angle is reached at 0.5 cm/s flow. The flame at 0.5 cm/s propagated directly upstream without any lateral growth. A quiescent flow case extinguished shortly after ignition, so the 0.5 cm/s flow case is very near the extinction limit. A simple analysis estimates the flow normal to the flame front to determine the limiting flame angles at which the normal flow (with diffusional flow, U_D, superimposed) becomes the limiting value of 0.5 cm/s, to be $\alpha_{lim} = \cos^{-1}[(U_{n,lim} + U_D)/(U + U_D)]$. Curves of this equation are shown in Figure 4 for values of U_D of 0, 1, and 2 cm/s. Good qualitative agreement is obtained at the higher flow rates (convective regime) when diffusion is neglected (U_D=0), but the importance of diffusion is pronounced for the flows at and less than 2 cm/s (diffusive regime), where qualitative agreement is good only when a U_D=2 cm/s is used. Simply estimating the oxidizer flow normal to the flame front is sufficient to reasonably predict the limiting spread angle.

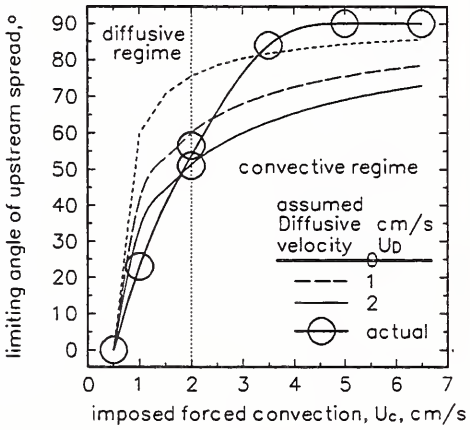

Figure 4: flame angle increases with flow

Conclusions

Radiative ignition occurred more readily in microgravity than in normal gravity. The ignition delay time is linearly dependant on the gas-phase mixing time. After ignition, flame spread occurred only in the upstream direction, indicating a strong need for fresh oxidizer. The angle of the flame as it spreads upstream is shown to be directly related to the limiting flow velocity normal to the flame front. A downstream flame is not simultaneously viable due to an 'oxygen shadow' of the upstream flame. Once the upstream spread is complete, a downstream flame becomes viable and concurrent flame spread occurs.

References

[1] McGrattan, K.B., Kashiwagi, T., Baum, H.R, and Olson, S.L., Comb. Flame 106, pp. 377-391 (1996).

Numerical Modeling of Methanol Liquid Pool Fires for Fire Suppression

Kuldeep Prasad[1], Chiping Li, K. Kailasanath
Laboratory for Computational Physics and Fluid Dynamics
Naval Research Laboratory, Washington DC.

Chuka Ndubizu[2], Ramagopal Ananth and P. A. Tatem
Navy Technology Center for Safety and Survivability, Chemistry Division
Naval Research Laboratory, Washington DC.

This study is part of a larger program on numerical modeling of fire suppression using water-mist. Water-mist fire suppression has been studied for at least 50 years. Recent research in water-mist technology has been motivated by 1) the phase out of Halons and search for alternative technologies and 2) the need for low weight sprinkler systems on commercial ships as required by IMO regulations. Fine water-mist relies on relatively small (less than 200 μm) droplet sprays to extinguish fires. In Reference 1, we reported on the numerical modeling of water-mist suppression of gaseous methane-air diffusion flames. A two-continuum formulation was used in which the gas phase and the water-mist are both described by equations of the Eulerian form. The model was used to obtain a detail understanding of the physical processes involved during the interaction of water-mist and flames. The relative contribution of various mist suppression mechanisms was studied. The effects of droplet diameter, spray injection density and velocity on water-mist entrainment into the flames and flame suppression were quantified. Droplet trajectories were used to identify the regions of the flame where droplets evaporate and absorb energy. The model was used to determine the water-mist required for extinction, and this was reported in terms of the ratio of mist supply rate to the fuel flow rate. In Reference 2, a numerical study on optimizing various water-mist injection characteristics for maximum flame suppression were reported. The effects of droplet diameter, mist injection angle (throw angle), mist density and velocity on water-mist entrainment into the flame and flame suppression were quantified. Numerical results were presented for symmetric and asymmetric spray pattern geometries resulting from base injection and side injection nozzle orientation. Results indicate that smaller droplet diameters produce optimum suppression under base injection configuration, while larger droplets diameters are needed for optimum suppression for the side injection configuration.

We are currently extending the previous work on fire suppression to liquid pool fires. As a first step, we focus on the development of a numerical model to simulate the evaporation and burning of liquid methanol. The complete set of unsteady, compressible Navier-Stokes equations are solved in the gas phase to describe the advection of the fuel gases and the diffusion of these gases into the surrounding air. Heat transfer into the liquid pool and the metal container through conduction, convection and radiation are modeled by solving a modified form of the energy equation. The local burning rate of a two-dimensional pool is obtained by assuming that the gas phase and the liquid phase are in equilibrium with each other. The governing equations along with appropriate boundary and interface conditions are solved using the Flux Corrected Transport (FCT) model. Numerical results exhibit a flame structure that compares well with thermocouple experimental data. The overall burning rate was also found to compare well with experiments in single compartment and three compartment laboratory burners.

Figure 1 shows vorticity contours for a pulsating fire stabilized above a methanol liquid pool. These contours clearly show the presence of coherent vortical structures which are shed periodically by the fire. This phenomena has been documented for a wide range of burner diameters, heat release rates and fuel types. The pulsing nature of the flow field propagates downstream leading to a time varying flame length. The puffing frequency obtained from our simulations compares favorably with data compiled by various researchers. The local burning rate (or the rate of evaporation) as a function of distance along the pool surface has been shown in Figure 2 for an air co-flow velocity of 40 cm/s. We observe that the burning rate is very high at the pool edges and is smallest at the pool center. An energy equation is solved to obtain the temperature distribution (Figure 2) in the methanol liquid pool. It is observed that pool surface temperature is very close but lower than the boiling point temperature of pure liquid methanol ($T_{boil} = 337.5K$). The pool surface temperature is highest in the center of the pool and falls down to 332.5 K at the pool edge. This reduction in pool temperature is due to heat losses to the surrounding air and the metal container, as well as due to the high burning velocities at the pool edges.

1. Prasad, K., Li, C., Kailasanath, K., Ndubizu, C., Gopal, R. and Tatem, P. A., *Numerical Modeling of Water-Mist Suppression of Methane-Air Diffusion Flame,* Comb. Sci. & Tech., V. 132, 1-6, p. 325 (1998).

2. Prasad K., Li, C. and Kailasanath, K., *Optimizing Water-mist Injection Characteristics on Jet Diffusion Flames,* 27^{th} Symposium (Int.) on Combustion, (1998).

[1] Science Application International Corporation, VA.
[2] Geo-Centers Inc., MD

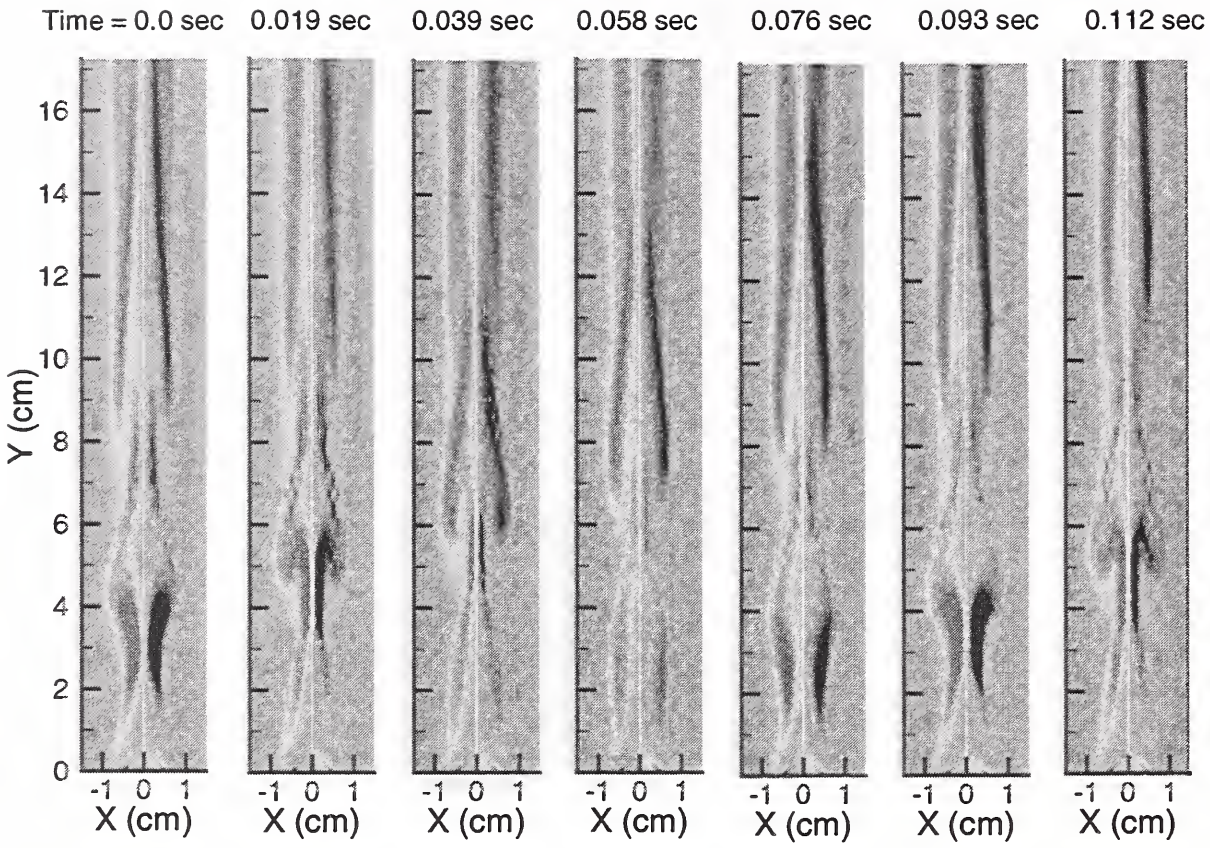

Figure 1: Vorticity contours at different time levels, above a pulsating methanol liquid pool fire illustrating the puffing nature of the diffusion flame for an air co-flow velocity of 10 cm/s.

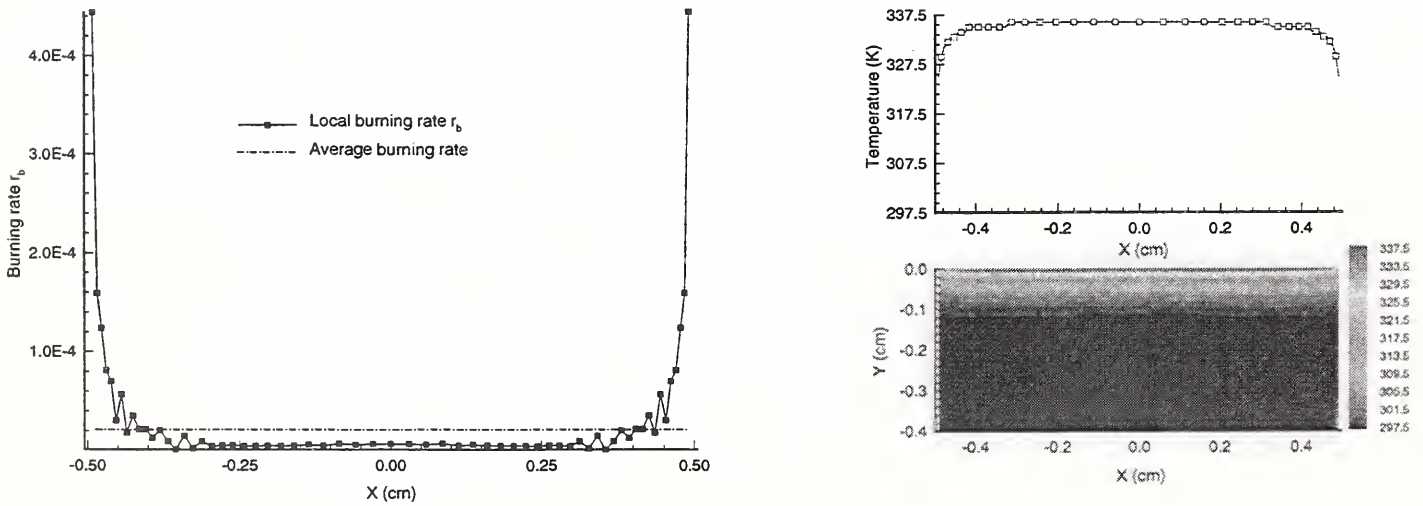

Figure 2: Variation of burning rate as a function of time for air co-flow velocities of 40 cm/sec. On the right are temperature contours in the liquid pool showing the structure of the thermal wave and pool surface temperature profile.

Effects of Freeboard and Lip Thickness on the Properties of Flames Burning in Open Metal Containers

Mark L. Robin, Ph.D.
Great Lakes Chemical Corporation
1801 Highway 52 NW
West Lafayette, IN 47906

ABSTRACT

We report here the effects of freeboard and wall thickness on the properties of n-heptane and diesel fuel flames burning in open metal containers. Lip temperatures, flame temperatures and heat release rates were measured for flames of n-heptane and diesel fuel in both round and square metal containers ranging in size from 0.05 to 5.00 ft^2 of fuel surface area and for wall thicknesses ranging from 0.03 to 0.25 inches. The effects of varying freeboard on the measured quantities was also examined. Concentration requirements for the extinguishment of n-heptane and diesel fuel flames with halocarbon and inert gas type agents was also examined under varying conditions of freeboard and container wall thickness.

Aircraft Hangar Fire Protection System Evaluation
Full Scale Fire Test Report

by

G. G. Back, A. J. Parker, and J. L. Scheffey
Hughes Associates, Inc.
Baltimore, MD

F. W. Williams
Navy Technology for Safety and Survivability
Chemistry Division

J. E. Gott and R. J. Tabet
Naval Facilities Engineering Command

Current Navy design standards for protecting large aircraft hangars include both overhead and low level aqueous film forming foam (AFFF) extinguishing systems [1]. The overhead AFFF system typically consists of standard closed head sprinklers that are zoned within areas defined by draft curtains. In some existing installations, the overhead systems are open head deluge systems. The low level system typically consists of multiple high flow monitors (e.g., 1893 Lpm (500 gpm)). The low level AFFF and overhead deluge sprinkler systems are activated by separate detection systems (heat detection or UV/IR).

Due to high costs incurred from damage of aircraft and electronics resulting from accidental discharges of the overhead AFFF system, the Navy is exploring alternate suppression techniques. The proposed approach would replace the overhead foam suppression system with a closed-head water sprinkler system. The ground level AFFF delivery system would become the primary means of fire suppression, and the overhead sprinklers would be used to cool adjacent aircraft and protect the structural integrity of the hangar. The time delay in activating the overhead system would also be minimized through the use of quick response sprinklers. This time delay has already been quantified in previous studies [2].

The Navy initiated this investigation to evaluate the capabilities of an aircraft hangar fire suppression system consisting of a low level AFFF extinguishing system and an overhead water sprinkler system. A future investigation will determine the capabilities of a proposed low level AFFF system that would eliminate high flow foam monitors, using instead, numerous lower flow nozzles mounted very close to the hangar floor.

Twenty three full-scale fire tests were conducted in the large burn building at Underwriters' Laboratories, Inc. (UL) to evaluate the effects of overhead water sprinklers on AFFF foam blankets. One AFFF application rate (4.0 Lpm/m^2 (0.1 gpm/ft^2)) and two sprinkler application rates were included in this evaluation (6.5 and 10.2 Lpm/m^2 (0.16 and 0.25 gpm/ft^2)). The tests were conducted against a range of spill fire scenarios. The spill fires were produced using either JP-5 or JP-8 aviation fuels and were evaluated on a concrete pad with similar drainage characteristics of typical Navy hangars.

The results show that the use of water sprinklers (with application rates up to 10.2 Lpm/m^2 (0.25 gpm/ft^2)) in conjunction with a low level AFFF fire suppression system (with an application rate of 4.0

Lpm/m^2 (0.1 gpm/ft^2)) had minimal effects on the ability of the system to suppress the fire and resist burnback. In all tests, the low level AFFF system was capable of quickly extinguishing the test fire (control ~ 30 sec and extinguishment ~ 1:00) independent of the sprinkler application rate. The time required for the fire to burnback across the fuel surface was apparently a function of the drainage characteristics of the hangar and was only slightly affected by the application of water through the overhead sprinklers. The tests also show that the flashpoint of the fuel has minimal effect on the control and extinguishment capabilities of the system but had a greater effect on the burnback capabilities of the system. Although the burnback times for the lower flashpoint fuels were faster than the higher flashpoint fuels, the duration of protection was not significantly altered. In summary, these tests show that overhead water sprinklers (with application rates up to 10.2 Lpm/m^2 (0.25 gpm/ft^2)) have minimal effect on AFFF foam blankets, independent of the test fuel, fire scenario, and sprinkler application rate. The tests show that a combined low level AFFF extinguishing system operating in conjunction with an overhead water sprinkler system will provide adequate protection for the hangar during AFFF discharge but the protection in terms of burnback resistance, may be lost shortly (a few minutes) after the end of AFFF discharge.

In conclusion, the data show that a low level AFFF system alone can achieve rapid fire control and extinguishment without the use of overhead sprinklers. This is consistent with data in the literature [3]. In these tests, with the nozzles adjusted/positioned in a less-than-optimum configuration, control times ranged from 20-40 sec, and total extinguishment of the spill fire was generally achieved in 60 seconds. This is consistent with the requirements of NFPA 409 design objectives of 30 sec for control and 60 sec for extinguishment after system activation [4]. It has been demonstrated that the operation of overhead water sprinklers does not degrade the performance of the low level system during AFFF discharge. Design criteria for Navy hangar protection can be revised to incorporate AFFF application from only the low level system, combined with overhead closed head quick response water sprinklers.

REFERENCES

1. Military Handbook 1008C, "Fire Protection for Facilities Engineering, Design, and Construction," Headquarters, Naval Facilities Engineering Command, Alexandria, VA., June 1997.

2. Gott, J.E., Lowe, D.L., Natarianni, K.A., Davis, W., "Analysis of High Bay Hangar Facilities for Fire Detection Sensitivity and Placement," NIST Technical Note 1423, National Institute of Standards and Technology, 1997.

3. Scheffey, J.L., "Foam Agents and AFFF System Design Considerations," *The SFPE Handbook of Fire Protection*, National Fire Protection, Quincy, MA, 1995.

4. NFPA 409, "Standard on Aircraft Hangars," National Fire Protection Association, Quincy, MA, 1995.

Toxic Gas Analysis and Fire Detection in the Crew Compartment of Ground Combat Vehicles

John F. McFassel
Fire Protection Team
U.S. Army Aberdeen Test Center
Aberdeen Proving Ground, MD 21005-5059
jmcfasse@atc.army.mil

William R. Davis
Fire Protection Team
U.S. Army Aberdeen Test Center
Aberdeen Proving Ground, MD 21005-5059
wdavis@atc.army.mil

Background

The Halon 1301 replacement program for ground combat vehicles is organized into three different components. These components focus on the engine compartment; crew compartment and hand held fire extinguishers HHFE). The engine compartment program received the most attention initially because the engine compartment had the earliest retrofit requirement. Test criteria such as time of suppression, maximum temperature and toxic fumes for the engine compartment were much less stringent than for the crew compartment. Major Army system Program Managers (PM's) have identified Halon 1301 replacements for the engine compartment only. Retrofit will begin in fiscal year 99.

The crew program is now receiving the most emphasis and will build on the experience gained during the engine compartment phase. The HHFE program is continuing concurrent with the engine and crew compartment programs.

Test Objective and Description

The main threat to the crew compartment is ballistic penetration of a fuel cell. The crew compartment test program is a three-phase program. The first two phases are being sponsored by the U.S. Army Tank-Automotive and Armaments Research, Development and Engineering Center (TARDEC). Phase III will be sponsored by the individual vehicle program managers. This technical approach is an adaptation of engine compartment test methodology.

Phase I is on track for completion in September 1998. This first phase involved seven different vendors. Phase II will include a more stringent scenario and will involve only those vendors who performed well in Phase I. Phase III will be sponsored by individual program managers and will customize fire suppression systems for specific vehicles.

Test Fixture Description

Testing is being conducted in modified Bradley Fighting Vehicle, which was used previously for ballistic testing. This vehicle looks like an operational vehicle from the outside, but there are almost none of the working components on the inside.

Vendors systems are brought to the range individually for three-four weeks to demonstrate system performance against a "standard test sequence". Initially the system is fine tuned against an ATC developed Fireball Generator . After achieving successful results at this stage, the system is then used against a fire initiated by a shaped charge penetrating a fuel cell.

Vendors are provided considerable latitude with regard to the number, size and location of fire bottles. Fire suppression agents under test have been either water-based or fluorinated hydrocarbons. While water-based systems present less toxicity issues, they are not as effective at suppressing fires.

Instrumentation

Typical test measurements used in the evaluation of each system include temperature, heat flux, toxic fumes and fire intensity as seen by video and infrared-sensors. Approximate instrumentation locations are shown in the following diagram.

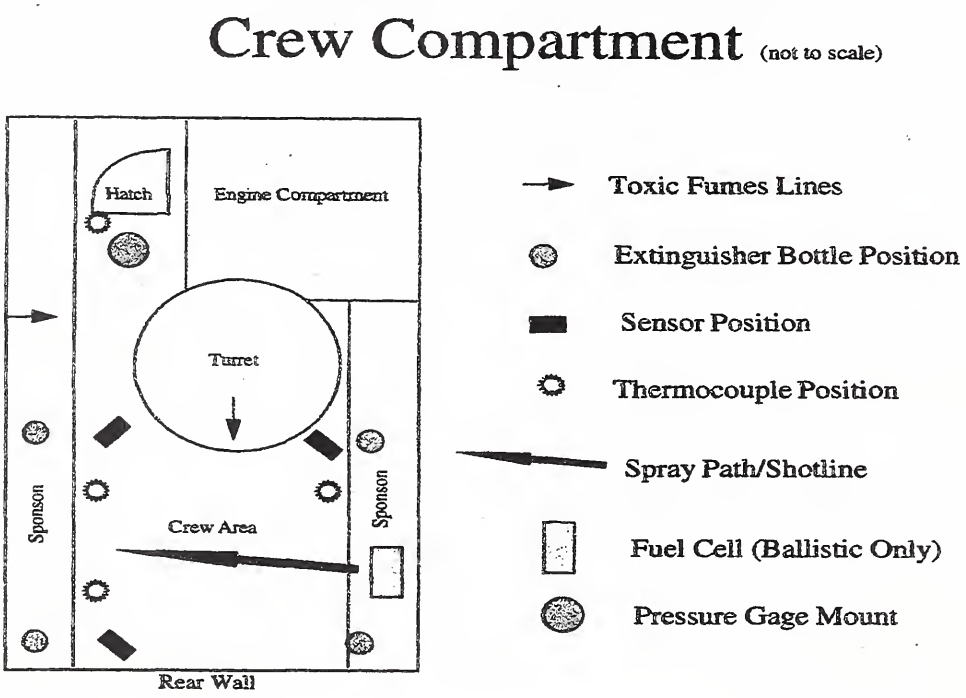

Toxic gases including CO, Co_2, HF and COF_2 are measured at 1.6-second intervals using a Fourier Transform InfraRed Spectrometer (FTIR). The reactivity of hydrofluoric acid gas dictates the very near proximity of the FTIR to the test vehicle. The use of shaped-charges to initiate the fires subjects the FTIR to shock and blast overpressure and creates a difficult operating environment. Acid Gas Analyzers, developed by the U.S. Army Center for Health Promotion and Preventive Medicine (CHPPM) are used to measure the total fluoride ion. Oxygen levels are also measured to assess crew survivability.

Three solid state infrared detectors in testing. For the Fireball generator tests, the detectors are used to initiate the suppression activation when the fire reaches a specified intensity. For the ballistic tests the detectors are used to measure the fire duration. The sensors also have to operate in an extremely hostile environment with high temperatures, shock waves and highly reactive chemicals.

Future Plans

Phase II crew compartment testing will be conducted in FY 99. This phase will be conducted in the same fixture, but will include clutter representing the vehicle crew and equipment stowage. This will greatly complicate the distribution of fire suppressant.

Subsequent testing will occur in the Fire Safety Test Enclosure (FSTE). This new facility, which will become operational in the fall of 1998, will allow testing of full-scale test items while containing all liquid and gaseous test effluents.

Smoke Detection by Ultrasound

[Two-Page Abstract]

By David K. Churches, Dr. Ed da-Silva (Open University - UK), David Holifield (UWIC - UK)

The paper discusses a smoke detection device that uses Ultrasound as a detection principle. The heart of the device is a double layer perforated matrix board which facilitates a unique perturbated flow pattern in a smoke plume at laminar velocities, that enables the Ultrasound medium to readily detect the presence of smoke particulates.

---

1. Introduction

Ultrasound has long been used as a detection medium in industrial and medical applications, but has not proved to be practical in the detection of post combustion particulates such as smoke for every day use. Although laboratory experimentation for many years has used Ultrasound as smoke detection medium, its adaptation into practical device for post combustion detection at a range of ambient conditions has proved to be problematic.

This research work has attempted to overcome many of the difficulties and demonstrates a method that may be further developed into a practical Ultrasound smoke detector device for every day use.

In order to more fully understand the difficulties of smoke detection by Ultrasound its worthwhile generalising on ambient conditions in the post combustion zone.

At a short distance from the combustion zone, the airflow in flaming fires is usually observed to be turbulent in nature, while in smouldering fires the airflow is usually seen to be laminar.

At a larger distance from the combustion zone smoke plumes from many fire types may develop an isotropic laminar pattern where the fluid flow may be described as semi-viscous. Here the friction forces seem to predominate, and the plume adopts the typical homogeneous structure of a typical fully developed smoke plume.

At an even greater distance from the combustion zone the plume may adopt a semi-inviscid flow pattern where the inertial forces are predominant. Here the flow of the homogeneous plume usually becomes polytropic and appears to break up as the smoke particulates are dispersed in the ambient air mass.

Analysis of smoke plume fluid flow dynamics over the last few years has shown that the plume travel appears initially to be dependent on the thermal entropy of the combustion processes. While later in the plume travel the fluid flow dynamics are more dependant ambient effects such as temperature, local air velocity, relative humidity, and the ergonomic flow of the combustion products.

In conclusion, it may be correct to say that there is no typical position for a practical smoke detection device. Therefore, a practical smoke detection device should detect the presence of smoke particulates under a variety of conditions. This may be when the plume fluid flow is turbulent or laminar, and when the flow pattern is isotropic and semi-viscous, or when it is semi-inviscid and polytropic.

The myriad of fire types, fluid flow patterns, and ambient conditions, has made practical smoke detection by Ultrasound very difficult. This is especially true at low smoke densities and when the flow is laminar at low relative air velocities. This research work developed a method that demonstrates that smoke particulates can be detected in this flow region.

2. Double Layer Matrix Board

The Double Matrix Board is heart of the smoke particulate detection method used in this research work. In many ways it is a unique and original approach to detecting the presence of fine particulates in air suspension at low plume velocities (typically 0.05 m/sec).

The Double layer Matrix as its name implies, is two separate layers of compressed fibreboard perforated with a regular array of apertures of capillary diameter (1 mm ϕ). The double layer board is mounted directly in a moving smoke plume perpendicular to the direction of the flow.

The conventional method of detecting the difference between two dissimilar media sequentially passing through an Ultrasound wave is to measure the Doppler shift frequency. However, the sensitivity of the detector system relies heavily on a rapid frequency shift to be effective. When the Doppler shift is lowered it becomes increasingly more difficult to differentiate between a genuine media density change and that created by ambient noise and atmospheric effects.

This is the case when smoke particulates are introduced into an air volume at a slow rate (such as the inchoate fire stage) when the relative air velocity is low. The problem is further compounded when the density change with time continues at a slow rate, when very high densities may eventually be present with only a small or insignificant change in the Doppler shift frequency.

The Double Matrix Board System has two main properties that enable the detection apparatus to be sensitive to smoke plumes at low relative air velocities. And when the two properties combine in tandem, their synergy increases the sensitivity of the detection system by several factors when compared to either property operating alone. Broadly two particular properties are as follows:

- Induces a disassociated flow pattern (pseudo-turbulence) in the smoke plume as it enters the double matrix layer (strainer effect) at laminar velocities when the detector system has a low Reynolds Number. And when the smoke plume exits the double matrix layer, a rapid reassociation is induced within the plume and a cohesive and structured laminar flow pattern is reformed.

- A spatial resonance is formed when the combination of the critical dimensions of the double layer matrix array are similar to a function of the half-wave (½ λ) of a time varying Ultrasonic wave emanating through the detector equipment.

During this research work, the smoke from several differing fire types at varying optical densities was passed through the detector equipment. It was noted that the rate of the onset of pseudo-turbulence (disassociated flow pattern) and the speed of the subsequent reassociation of the cohesive laminar flow, differed for dissimilar smoke types and varying optical smoke densities.

It was also observed that the differing perturbated flow patterns of a variety of dissimilar smoke types had another affect within the Double Layer Matrix Board. The frequency of the incident Ultrasound wave within the apparatus was tuned to the spatial and cavitational resonant frequency of the Double Layer Matrix Board. This meant that the system was particularly sensitive to a media density change within the Double Matrix interstitial cavity, such as the introduction of smoke particulates into the slow moving air column passing through the apparatus.

Since the apparatus uses a single point piezo detector mounted just after the Double Layer Matrix Board, it receives the Ultrasound signal from each aperture across the whole area of the matrix board at different time intervals. Therefore, the composite signal received at the single point piezo detector is the algebraic sum of all the Ultrasound signals from each aperture. When a density change occurs in the media within the apparatus such as the introduction of smoke particulates, it was observed that the frequency bandwidth (phase delay) and the amplitude (group delay) correspondingly changed in the composite signal.

3. Discussion

It was observed during the research work, that the Double Layer Matrix Board System could adequately detect a density change in a Two-Phase Fluid Flow such as smoke particulates in air suspension. The observations also demonstrated that the Double Layer Matrix Board System could form the basis of a practical smoke detector with further development work. The Author(s) also speculate that other research into the measurement of slow moving Two-Phase fluids might also find the method useful.

EXPERIMENTS ON BUOYANT DIFFUSION FLAME DYNAMICS UNDER CONDITIONS SIMULATING PARTIAL GRAVITY

Y. Dong and B. M. Cetegen
Mechanical Engineering Department
University of Connecticut, Storrs, CT 06269-3139
[cetegen@eng2.uconn.edu]

Introduction:

Study of buoyant diffusion flame dynamics under different gravity levels is of interest for several reasons. First, the scaling of flame dynamic behavior such as the quasi-periodic flame oscillations is expected to be different at partial low gravity environments. Second, the entrainment characteristics of buoyant diffusion flames at partial gravity conditions are not available to date and this information is needed for fire safety considerations at extraterrestrial settlements currently planned by NASA. So far, small diffusion flame experiments have been performed at microgravity conditions at NASA facilities. These experiments typically have very short durations which preclude experimentation requiring long periods such as those required for steady state fire entrainment measurements. Given these constraints and the need for such experiments, we are conducting laboratory experiments where the buoyant driving force is reduced by tailoring the bulk density differences in earth gravity. This can be accomplished by hydrocarbon flames burning in synthesized oxidizing environments other than air. Helium/oxygen/nitrogen /carbon dioxide mixtures provide conditions of reduced and augmented gravity environments for propane flames as will be shown by the preliminary results obtained so far.

The global buoyancy force per unit volume can be expressed as $(\rho_\infty - \rho_f) * \mathbf{g} / \rho_\infty$ where ρ_∞ is the ambient density, ρ_f is the density in the flamelet regions and $\mathbf{g}$ is the gravitational acceleration. Upon rearranging, the buoyancy force can be written as $\rho_\infty * \mathbf{g} * (1- \rho_f/\rho_\infty)$. The ambient density can be altered by synthesizing ambient atmospheres of different densities. Table 1 shows calculated oxidizing medium densities and the density factor, $\rho_\infty (1- \rho_f/\rho_\infty)$ for air, He/O_2 and CO_2/O_2 mixtures. It is seen that the latter factor can be altered up and down by about 50 % with respect to the air case. While, it has some differences in details from the partial gravity flames burning in air, the global effects such as the large scale flame dynamics and entrainment can be studied at simulated partial gravity conditions by affecting changes in the ambient density instead of the gravitational acceleration. In the following, we present results demonstrating the feasibility of this experiment.

Experimental Set-up:

The set-up for these experiments was similar to those employed in our earlier studies [1]. The experimental facility consists of a concentric nozzle configuration with an inner 2.5 cm dia. fuel nozzle surrounded by a 30 cm dia. coflow nozzle, all being situated under a 1.0 m. dia. hood. The fuel nozzle exit was 3.0 cm further downstream from the exit plane of the coflow nozzle. The fuel nozzle contained a retainer screen above which a bed of glass beads (2.0 mm in dia.) provided the flow resistance for flow uniformity. The coflow nozzle had a honeycomb flow straightener followed by a 20 mesh screen and a bed of glass beads for flow uniformity. Wrapped around the coflow nozzle was a 20 mesh screen to guide the coflow stream upward and prevent the ambient disturbances to adversely affect the flame. The experimental diagnostics included (1) video recordings of the visible flame and (2) detection of small dynamic pressure fluctuations along the flame centerline to determine the oscillation frequencies.

Experimental Results:

A series of visualization experiments were performed to determine the oscillatory behavior of propane diffusion flames. Figure 1 shows the sequence of flame images for a 0.8 kW propane flame burning in air (upper row) as well as the same flame burning in a mixture of helium and oxygen (lower row). The flame burning in air exhibited periodic oscillations characteristic of buoyant diffusion flames

with an oscillation frequency of about 10 Hz. This frequency agrees well with the value of 9.5 Hz from the correlation reported in [2]. In the second row of images shown in Fig. 1, the flame oscillations were found to be completely suppressed in a flame burning in a mixture of 75 % helium and 25 % oxygen by volume. The complete elimination of the flame pulsations is attributed to the decrease of buoyancy and resulting changes in the flame dynamics. Figure 2 shows the frequency spectrum of oscillations for the 0.8 kW flames burning in air and helium-oxygen media. While the flames in air exhibit a clear oscillation frequency peak at the fundamental frequency of 10 Hz, the flame burning in helium-oxygen mixture shows no such distinct frequency peaks beyond the background noise level. Similar to our earlier experiments with non-reacting buoyant plumes, there appears to be a threshold of density ratio or buoyancy parameter beyond which the oscillations are completely eliminated. Currently, this transition between steady laminar flames and unsteady, more buoyant oscillatory flames is being studied in our laboratory. Additionally, we are simulating the effects of elevated buoyancy by studying flames burning in CO_2-O_2 mixtures as indicated in Table 1. The presentation will include the results from these ongoing experiments.

References:

1. B. M. Cetegen and K. D. Kasper , Experiments on the Oscillatory Behavior of Buoyant Plumes of Helium and Helium-Air Mixtures, *Physics of Fluids*, **8**(11),pp. 2974-2984 (1996)

2. Cetegen, B. M. and Ahmed, T., "Experiments on the periodic instability of buoyant plumes and pool fires", *Combustion & Flame,* Vol.93, pp.157-184 (1993)

3. Cetegen, B. M., "Behavior of naturally oscillating and periodically forced axisymmetric buoyant plumes of helium and helium-air mixtures", *Physics of Fluids*, Vol. 9. No. 12, p. 3742-3752 (1997)

Table 1: Calculated Densities

Oxidizing Medium	ρ_∞	$\rho_\infty(1-\rho_{fl}/\rho_\infty)$*
Air	1.1601	1.0160
He: 70%, O_2: 30%	0.5038	0.4589
He: 50%, O_2: 50%	0.7313	0.6810
CO_2 : 70%, O_2: 30%	1.6414	1.4442

* Fuel: Propane, ρ_{fl} is the flame zone density for adiabatic combustion, density is in kg/m^3

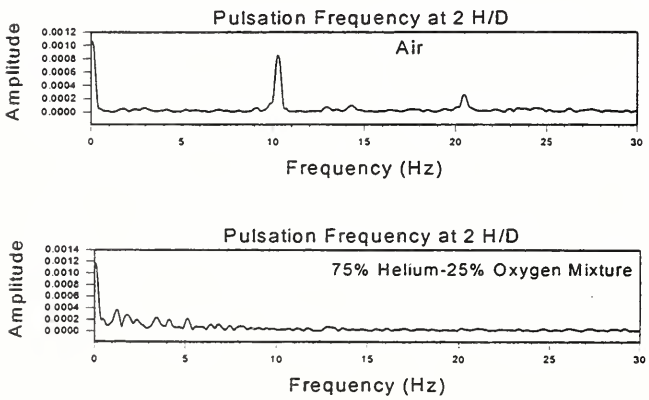

Fig. 2: Frequency spectra of flame oscillations kW propane flame burning in air (top) and in a mixture of helium-oxygen (bottom)

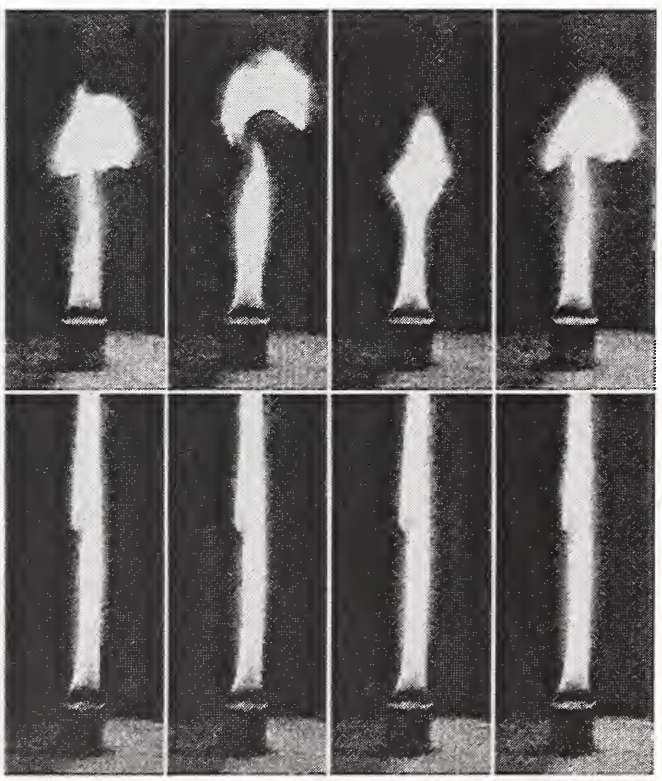

Fig.1: Upper image sequence for 0.8 kW for a 0.8 propane flame in air. Lower sequence for 0.8 kW flame burning in 75 % He-25 % O2 mixture

Numerical Study Of The Near-Field Unsteady Dynamics Of Planar Plumes

Marios C. Soteriou, Yan Dong and Baki Cetegen
Department of Mechanical Engineering
University of Connecticut, Storrs, CT 06269-3139

Introduction: Non-reacting buoyant plumes occur frequently in nature and in engineering practice, e.g. release of effluents from smokestacks, thermal plumes in the atmosphere, etc. Their dynamics are also known to exhibit similarities to those of pool fires [1-3]: In both cases the flow in the near-field of the source is characterized by large-scale coherent vortical structures that trace their origin to the buoyancy driven mechanism of vorticity generation. In the past, the study of buoyant plumes has, for the most part, been focused on the circular source case [e.g. 1-4]. Furthermore, the few studies dealing with the planar case have focused on the far-field dynamics [e.g. 5,6]. In this work we concentrate on the unsteady, near-field dynamics of planar plumes. The focus of the research lies in identifying the nature of the instabilities manifested in these flows. To this end, numerical simulations of the time-depended and un-averaged flow are performed. Numerical results are compared extensively with experimental evidence.

The numerical model: The unsteady two-dimensional buoyant motion of helium or of a helium-air mixture that flows from a nozzle into a stagnant atmosphere consisting of air at S.T.P. is considered. Isothermal conditions prevail. Two geometrical configurations are investigated. In both, the gravity vector is normal to the nozzle exit plane. In one of them, however, the nozzle is surrounded by a flat plate at the nozzle exit, while in the other the plate is removed and the nozzle is free-standing. These geometrical arrangements are assumed to distinguish plumes emanating from free-standing slots and from slots on the ground, respectively. Both helium and air are assumed to exhibit Newtonian-fluid and ideal-gas behavior, and to be essentially incompressible. The viscosity, μ, is assumed to be constant and the mass diffussivity, D, to vary according to $\rho D = \text{constant}$ where ρ is the mixture density. The governing equations (mass, momentum and species conservation equations coupled with the equation of state) are solved in non-primitive variable form. This involves the introduction of the vorticity, the streamfunction and of the gradients of the species mass-fractions.

The numerical solution is obtained using the Transport Element Method [7]. This *Lagrangian* methodology has its origins in the Vortex Element Method (VEM) [8] and is able to efficiently resolve the unsteady vortical flow and the coupled scalar fields. The numerical solution is initiated by discretizing the vorticity and the gradient of the scalar over a field of Lagrangian elements each of which is associated with a finite strength and a local distribution function. The velocity and scalar fields are obtained via convolutions over the elements. The time evolution of the flow and scalar fields, is accomplished via two-step local integration of the transport equations for each element.

Results: Comparison of the numerical results with experimental evidence indicates that the computational model is very effective in capturing the unsteady flow behavior. This can be witnessed qualitatively in Fig.1 where instantaneous experimental (left) and numerical (right) visualizations of the flow at similar parameters is shown. The figure makes evident that this flow is asymmetric about the nozzle centerline. Quantitative comparison between experiments and simulations is offered in Fig.2 where the frequencies of pulsation of the buoyant flow, i.e. the frequencies of the shedding of the vortical structures, are presented as a function of the Richardson number. The figure displays results for the nozzle-with-wall case. Results further indicate that the presence of the wall does not significantly affect the pulsation frequency. Transition from steady to pulsating behavior is also captured reasonably well by the simulations. Plumes emanating from a free-standing nozzle are more stable than those from a nozzle attached to horizontal wall. Despite the fact that the pulsation frequency varies weakly with the Richardson number, the instantaneous flow structure changes substantially as this parameter is varied. At relatively low Richardson number (weak buoyancy) the formation of the vortical structures occurs downstream, away from the nozzle, in a rather ordered, repeatable manner. Counter-rotating vortices form in a sequence resembling a Von-Karman street. At high Richardson number (strong buoyancy) the formation of the vortices occurs close to the nozzle exit forming the traditional mushroom structure characteristic of buoyant flows. Further downstream the flow becomes quite chaotic. In the experiments three-dimensionality ensues in this region. For intermediate values of the Richardson number the flow appears to alternate between the two extreme behaviors described above.

Future work: The mechanism of the instability will be probed in more detail assessing its origin and determining whether it may be characterized as absolute or convective. In addition, theoretical arguments will be developed to support the numerical-experimental findings described above.

REFERENCES

1. Cetegen, B.M. and Ahmed, T.A., *Combust. Flame*, **93**, 157 (1993).
2. Hammins, A., Yang, J.C., Kashiwagi, *Proceedings of the 24th International Symposium on Combustion*, The Combustion Institute, p.1695 (1992).
3. Ghoniem, A.F., Lakkis, I. and Soteriou, M.C., *Proceedings of the 26th International Symposium on Combustion*, The Combustion Institute, p.1531 (1996).
4. McGrattan, K.B., Baum, H.R and Rehm, R.G., *Atmospheric Environment*, **30**, p.4125 (1996).
5. Sangras, R., Dai, A. and Faeth, G.M., "Mixing Structure of Plane Self-Preserving Buoyant Turbulent Plumes," 1998 Joint AIAA/ASME Thermophysics and Heat Transfer Conference.
6. Lee, S., and Emmons, H., *J. Fluid Mech.*, **11**, p.353 (1961)
7. Soteriou, M.C. and Ghoniem, A.F., *ESAIM Proceedings*, **1**, p.429 (1996).
8. Chorin, A.J., *J. Fluid Mech.*, **57**, p.785 (1973).

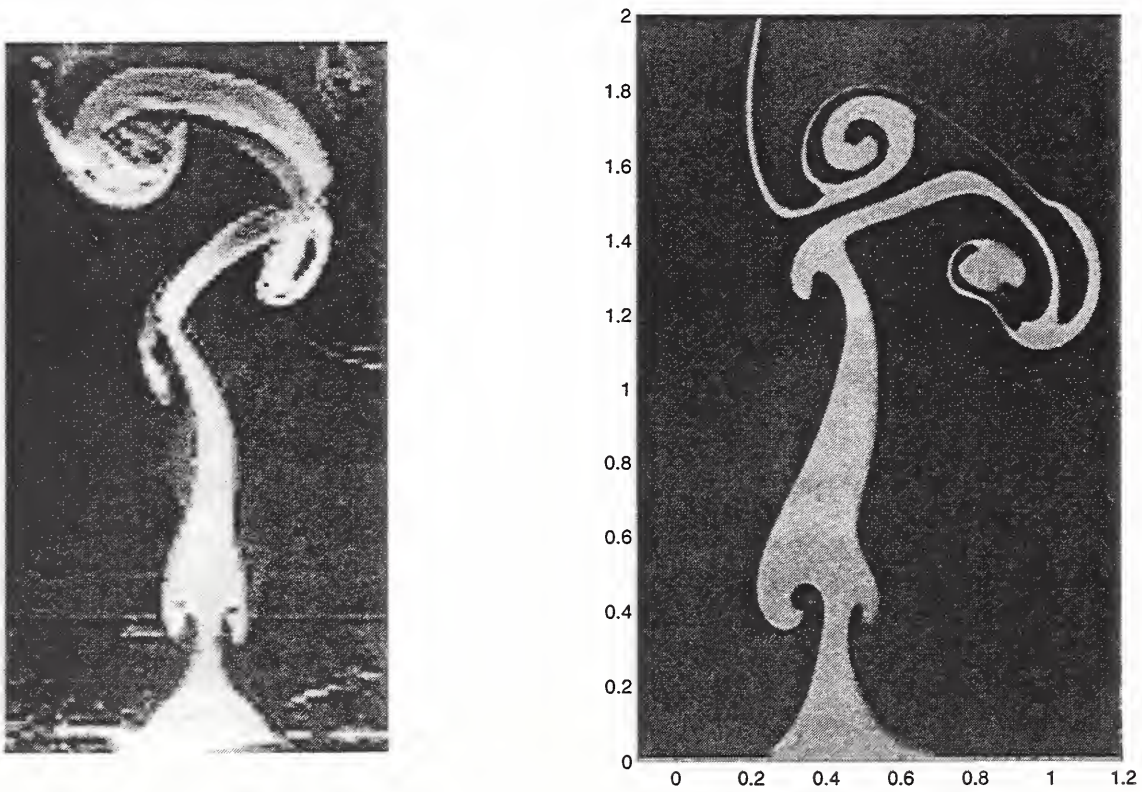

Figure 1. Experimental (left) and computational (right) instantaneous visualizations of the buoyant flow. Smoke seeded to the flow is displayed in gray-scale shades

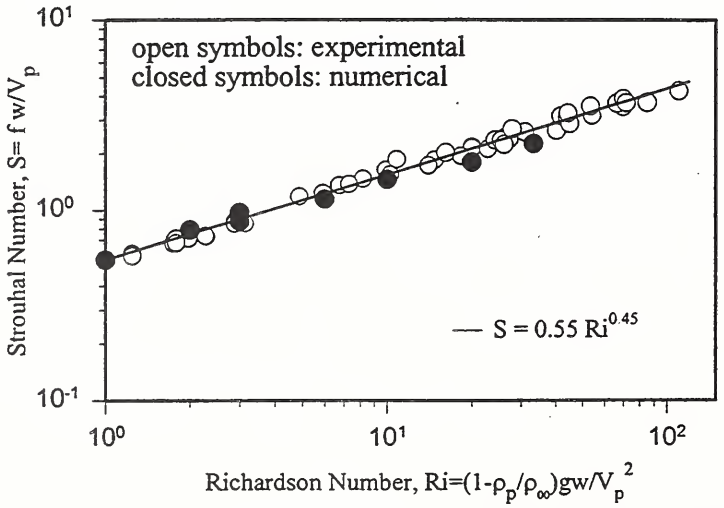

Figure 2. Correlation of the plume pulsation frequency in terms of the Strouhal and Richardson numbers. Comparison of experimental and numerical findings.

THE DISCRETE-SOURCE APPROXIMATION OF RADIATIVE TRANSPORT IN FIRE PLUMES

Issam Lakkis and Ahmed F. Ghoniem
Massachusetts Institute of Technology

A novel approach for incorporating radiative transport processes in the simulation of fire plumes, or any other fluid dynamic/combustion process in which gaseous radiation plays an important role in determining the temperature field, has been developed. The approach is particularly suited for cases in which the radiating gas is confined within a relatively small subset of the overall flow domain, and when conditions deviate form those consistent with conventional thin, thick, or differential approximations of the radiative transport equations. Contrary to the methods of spherical harmonics and discrete ordinates, which results in a systems of PDEs that should be integrated, the proposed discrete source method is based on expressing the integrals in the radiative flux and the irradiation as sums of integrals over small volumes within which the radiating gas (source) temperature and properties can be assumed to be nearly uniform. The resulting integrals over these "discrete sources," each representing the radiation field of a single source, are then evaluated for target points which are close (near field) and distant (far field) from the source. In the case of almost constant absorption coefficient between the source and target, an equivalent to a radiative Biot-Savart law is obtained. The formulation can also be extended to the case of variable absorption coefficient by treating the exponent in the radiation kernels as a polynomial in the optical distance. The method has been validating by comparing its results for a number of cases to those obtained using direct solutions.

The formulation of the method starts with the following expression for the divergence of the radiative flux, which is the source terms in the energy equation, in terms of the black body radiation I_b and the incident radiation, or irradiation, G:

$$\nabla \cdot \vec{q} = \kappa(4\pi I_b - G) \tag{1}$$

where the κ is the linear absorption coefficient, $I_b = \frac{\sigma T^4}{\pi}$, σ being the Stefan-Boltzmann constant, and the irradiation, is;

$$G = \int_{4\pi} I \, d\Omega = \iiint_V \kappa(\vec{r}\,') \, I_b(\vec{r}\,') \frac{e^{-(\tau-\tau')}}{|\vec{r}-\vec{r}\,'|^2} dV(\vec{r}\,') + \iint_\Sigma I(\vec{r}_\Sigma') \frac{e^{-\tau_\Sigma}}{|\vec{r}-\vec{r}_\Sigma'|^2} cos(\vec{r}-\vec{r}_\Sigma', \vec{n}_\Sigma) \, d\Sigma(\vec{r}_\Sigma') \tag{2}$$

where $\tau = \int_0^s \kappa \, ds$ is the optical path length, V is the volume of radiating gas and Σ is the surface surrounding this volume. A similar form can be written for the radiative flux. A similar expression can be written for the radiative flux.

Writing $T(\vec{x}) = \sum T_i f_\delta(\vec{x} - \vec{x}_i)$ where f is a symmetric function which is non zero only within a distance δ around x_i, the volume integrals in equations (2) for each single source can be evaluated as a generic source-target interaction (similar to the Biot-Savart law in hydrodynamics). The total irradiation is hence evaluated as the sum over all the elements' contributions. In the case of spatially uniform absorption coefficients, the integrals of the radiation kernel over the area of an individual source are evaluated via near field and far field expansions of the exponential term, e.g., for the near field:

$e^{-\kappa\sqrt{x}} \approx (1-\kappa\sqrt{x}) + \sum_{k=0}^{n} C_k \kappa^{2k} x^k$. It is possible then to obtain analytical solutions for the integrals, which can also be tabulated for computational efficiency. For instance, in the case of axisymmetric flow, the irradiation from a single element (ring) is given by: $G_i(\vec{r}) = \kappa(\vec{r}_i)\, I_b(\vec{r}_i)\ \Xi(\frac{R}{\delta}, \frac{\zeta}{\delta}, \frac{r}{\delta}, \kappa\delta)$ where R and r are the source and target radii, and ζ is the axial separation between them. The function Ξ pre-tabulated for the expected range of interest of all its arguments.

We have applied this approach to compute the irradiance and radiative flux from a square ring within which the temperature varies exponentially away from its center. The ring radius is taken to be unity, its width and height are 0.4. The direct solution was obtained by carrying out the triple integrals in equation (2) using a very fine mesh within and around the square ring to guarantee convergence. The discrete source solution was obtained by dividing up the square into 16 – 400 (4x4 – 20x20) elements. The comparison between the direct solution and the discrete source solution at different levels of refinement, for the normalized irradiation and flux are shown in figures 1 and 2, respectively. As shown in the figure, the method provides good accuracy even at relatively crude discretization of the body of radiating gas (since the near field of the sources is evaluated almost exactly). Extensions to: (1) the case of variable absorption coefficients, (2) the evaluation of radiative fluxes from a fire plume, and (3) the simulation of a fire plume with "internal" radiative transfer will be presented at the meeting.

REFERENCES:

1. Modest, M.F, *Radiative Heat Transfer*, McGraw Hill, 1993.
2. Ghoniem, A.F., Lakkis, I., and Soteriou, M, *Twenty Six (Int) Symposium on Combustion*, The Combustion Institute, Pittsburg, 1996, pp. 1531-1539.
3. Lakkis, I and Ghoniem, A.F. "Lagrangian Simulation of Fire Plumes," *7th AIAA/ASME Joint Thermophysics and Heat Transfer Conf.*, Albuquerque, NM, June 1998.

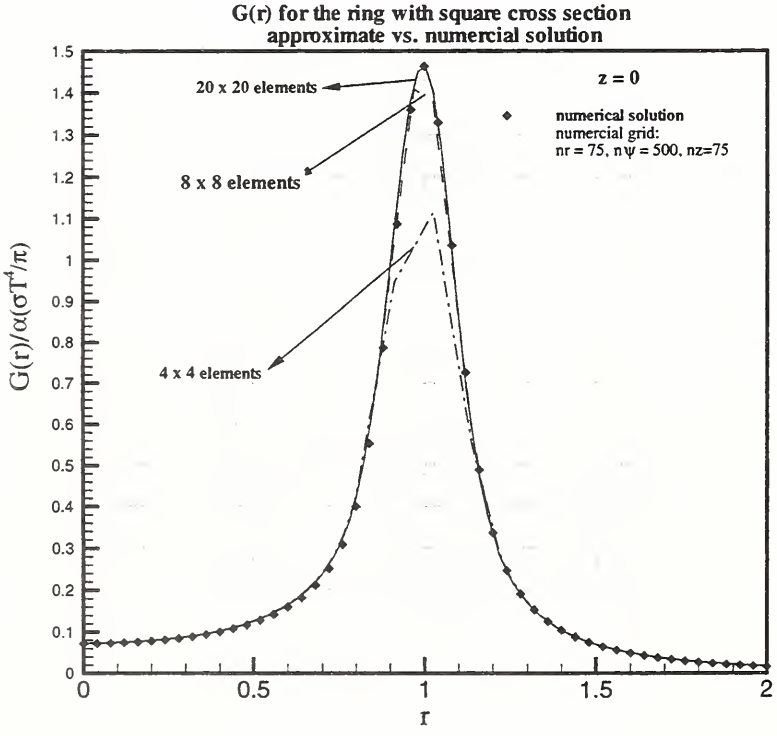

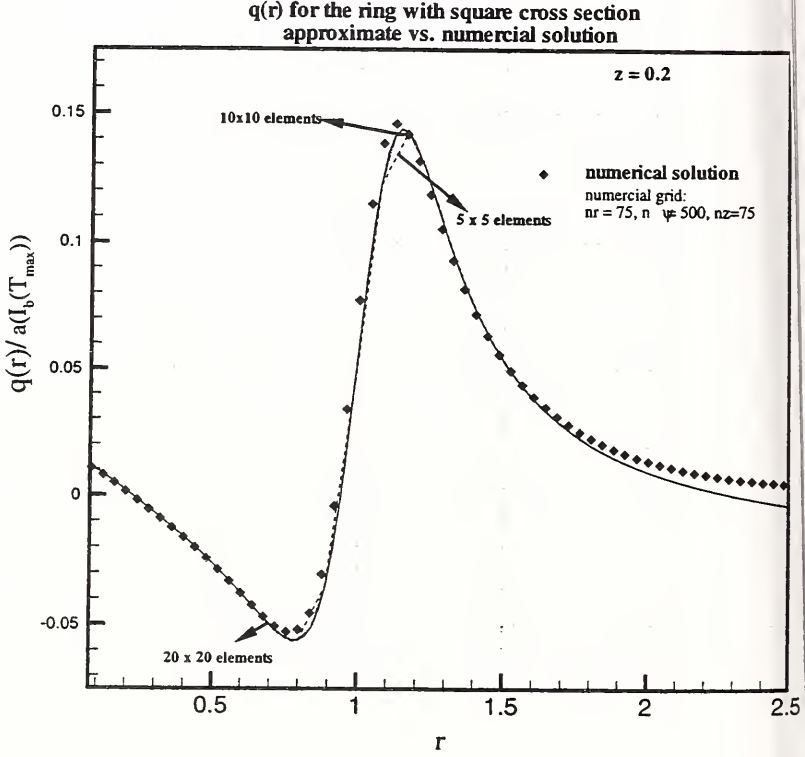

In-situ Burning of Water-in-Oil Emulsions : Model Results and Comparison with Data

Ajey Walavalkar and Anil K. Kulkarni
The Pennsylvania State University
University Park, PA 16802, USA

Introduction

In-situ burning of oil or water-in-oil (w/o) emulsion supported on top of a water-base, such as the ocean, is a complex process, and it involves several interdependent and complex physicochemical processes which are not yet fully understood. The technique of in-situ oil spill combustion has been tried in practice and investigated by researchers sporadically over the past thirty years. The focus of this report is on the burning of water-in-oil emulsions with an emphasis on computation of timeline for the important events in the process, such as the ignition delay, complete consumption of the emulsion layer, burnout period, residue left, and efficiency of removal.

The Model

The combustion process starts with heat transfer from a source, such as an igniter or adjacent fire, to the emulsion layer. For the modeling purpose, the overall burning process is divided into three regimes as follows.

1. *Initial Regime* ($t = 0$ to t_1) : The emulsion layer is heated with a constant heat flux source and the top surface reaches the emulsion-breaking temperature.

2. *Intermediate Regime*: ($t = t_1$ to t_2): Continued input of heat provides the energy required for emulsion breaking which causes the first appearance of oil on top of the emulsion. Thus, there are three layers in this regime, oil, emulsion and water. Figure 1 shows a schematic at this stage. The temperature of the oil layer increases while the oil-emulsion interface temperature remains constant at the emulsion breaking temperature. When the oil surface temperature reaches vaporization temperature, the intermediate regime ends.

3. *Final Regime*: ($t = t_2$ to t_3): The vaporized oil burns because of the presence of the fire, energy is released by oil combustion, and a part of it is fed back to the oil. The burning process continues until the emulsion layer completely depletes, oil layer continues to burn, and finally extinction occurs because the loss of heat to the water becomes greater than the heat feedback to the oil surface.

The mathematical model is one-dimensional. Full set of governing equations and additional details may be found in a paper by Walavalkar and Kulkarni, 1997.

Results and Comparisons

All numerical results were obtained assuming emulsions were prepared from SAE30 motor oil because of availability of properties for that oil. Figure 2 shows comparison of ignition delay values with those obtained by Putorti et al., (1994). The average burning rate is compared with the data of Buist et al. (1995) in Fig 3. A comparison of data by Buist et al. (1995) for ANS crude oil emulsions and by Guennette et al.(1994) for the burn efficiency is shown in Fig. 4. Though most of these experiments were conducted with emulsions of other oils the experimental values and model results compare very well. The present model illustrates the parametric effects of external heat flux, emulsion layer thickness and emulsion composition on such important quantities as the ignition delay, total burnout period, efficiency of removal, residual layer thickness, and transient and steady burning rates (not all results are presented here). There is a strong need for a systematic experimental study to verify applicability of the model. Also, accurate property data for crude oils and their emulsions, along with a realistic assessment of weathering and other conditions, are needed for applying the model to practical

situations. Once validated, the present model can give reasonable idea as to whether an emulsion layer under given conditions can burn, and if so, how long will it take and what will be its effectiveness.

Part of this research and a major experimental program to study burning of w/o emulsions is currently funded at Penn State under a recent NIST grant no. NANB0036.

References

1. Buist, I. A., N. Glover, B. McKenzie, and R. Ranger, "In-situ Burning of Alaska North Slope Emulsions," *Proceedings of the 1995 International Oil Spill Conference*, 139-146, 1995.

2. Guenette, C., P. Sveum, I. Buist, T. Aunaas, and L. Godal, *In-Situ Burning of Water-In-Oil Emulsions*, SINTEF Report STF21 A94053, MSRC Technical Report Series 94-001, 139, 1994.

3. Putorti, A. D., Jr. and D. Evans, "Ignition of Weathered and Emulsified Oils," Proceedings of *the Seventeenth Arctic and Marine Oil Spill Program (AMOP) Technical Seminar*, 1:657-667, 1994.

4. Walavalkar, A. and Kulkarni, A. K., 1997. A Mathematical Model for In-Situ Burning of Water-in-Oil Emulsions, Proceedings of the *Twentieth Arctic and Marine Oilspill Program Technical Seminar*, pp 809-821, Vancouver, Canada.

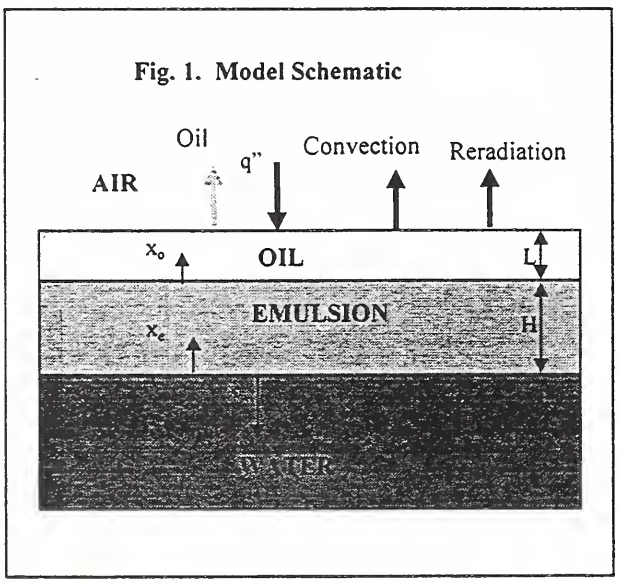

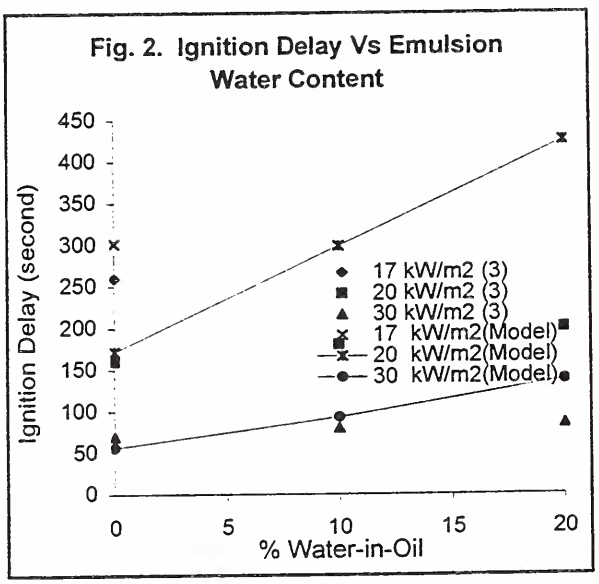

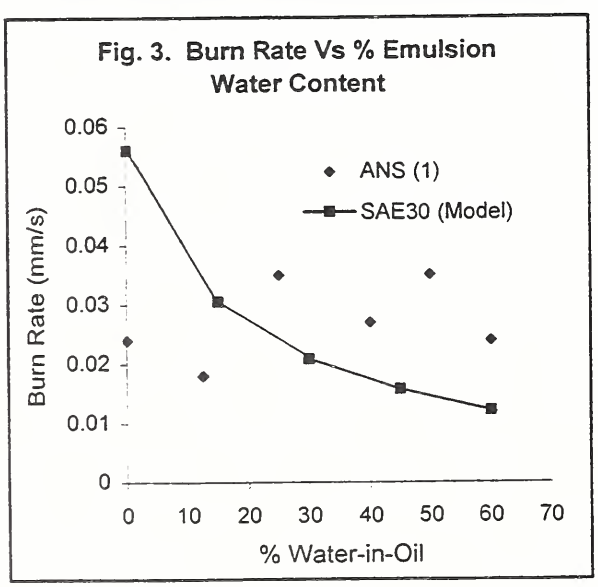

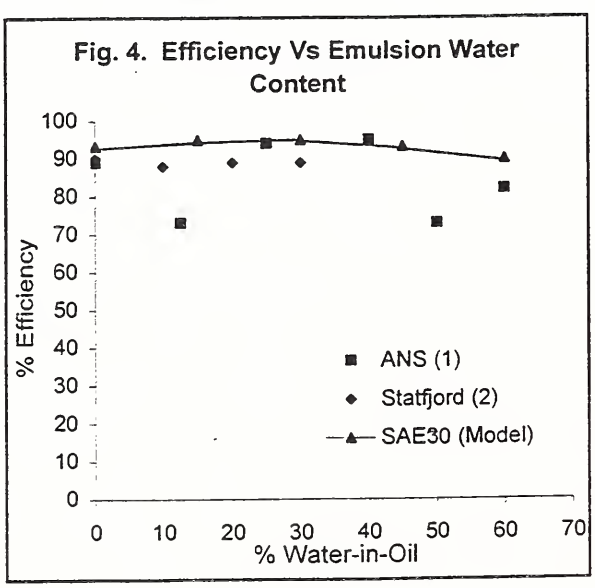

(Reference numbers in figures correspond to the citations above.)

SIMULATION OF LARGE INDUSTRIAL OUTDOOR FIRES

Howard R. Baum and Kevin B. McGrattan
National Institute of Standards and Technology
Building and Fire Research Laboratory
Gaithersburg, MD 20899

Large outdoor fires can be conveniently divided into two categories based on the fuel source. Wildland fires are characterized by a relatively low heat release rate per unit area of ground covered by fuel, but a very large area over which the fire can spread. Indeed, the description of the fire spread process is an essential part of any successful simulation of such an event. Industrial fires, in contrast, are usually more highly localized but intense emitters of heat, smoke, and other combustion products. This is particularly true if the fuel is a petroleum based substance, with a high energy density and sooting potential. This latter type of fire is the object of study in the present paper.

The hazards associated with such fires occur on two widely separated length scales. Near the fire, over distances comparable to the flame length, the radiant energy flux can be sufficiently high to threaten both the structural integrity of neighboring buildings, and the physical safety of firefighters and plant personnel. At much greater distances, typically several times the plume stabilization height in the atmosphere, the smoke and gaseous products generated by the fire can reach the ground in concentrations that may be unacceptable for environmental reasons. The far field hazard has been studied previously by the present authors [1], [2]. This work has led to the development of a computer code ALOFT, which is available from NIST. A comprehensive description of ALOFT and its generalizations to complex terrain can be found in [3].

In this paper the near field hazard associated with the flame radiation is studied. The scenario chosen is a fire on top of an oil storage tank adjacent to several neighboring tanks. This scenario is chosen both for its intrinsic importance and because it illustrates the ingredients needed to generate a realistic simulation of such an event. The heat release generated by a fire on this scale can reach several gigawatts if the entire pool surface is exposed and burning. Such fires interact strongly with the local topography (both natural and man made) and the vertical distribution of wind and temperature in the atmosphere. Moreover, the phenomena are inherently time dependent and involve a wide temperature range. Thus, the simplifications employed in ALOFT and its generalizations can not be used in the present analysis.

A mathematical model is presented that contains the basic components needed to address this problem. The model consists of a version of the authors three dimensional enclosure fire model [4], [5] modified to account for a stratified atmosphere. This is supplemented by a simple radiative tranport model that ignores the absorption by the smoke generated in the fire. The effect of the absorption is accounted for by lowering the radiant energy emission from the flames. The wind in the atmospheric boundary layer is represented by a power law velocity profile and the ambient temperature fields are taken to be isothermal. The storage tank farm is represented by a 3x3 array of identical tanks 84 meters in diameter and 27 meters high. Each tank sits in a 9 meter deep trench arranged so that the spacing between tank centers is two tank diameters. The surrounding terrain is flat. The computational domain is a cube 3/4 kilometer on a side. This geometry is an idealization of a portion of an oil storage facility in Tomakomai, Japan.

Two simulations will be discussed, showing an upwind and a centrally located tank top fire. The plume dynamics, velocity, and radiant heat flux incident on the tank surfaces will be shown. The implications of these results for both storage tank safety and the utility of this methodology in general will be considered. The examples illustrate the complex interaction between the topography, the ambient atmosphere, and the fire scenario. Even for the relatively simple configuration chosen for study here, there are many factors that strongly affect the resulting fire dynamics. The ambient wind and temperature fields play at least as significant a role as they do in the downwind smoke dispersion described by the ALOFT code. The presence of natural topographical features in the vicinity of the storage tanks would further modify the flow patterns, and hence the radiation fields. Finally, the absorption of thermal radiation by the smoke and gaseous combustion products will alter the plume structure by creating distributed energy sources in the flow field.

Rather than arbitrarily choosing topograpical, structural, and meteorological features to simulate, it would seem to make more sense to couple this emerging simulation capability to databases that describe the actual built environment and associated topography. Similarly, arbitrary prescriptions of the ambient atmosphere could be replaced with local meteorology simulations based on databases and computer models in use by the weather prediction community. The result would be a simulation capability that could be used routinely to predict the fire hazards resulting from natural or man made disasters in the real world.

References

[1] Baum, H.R., McGrattan, K.B., and Rehm, R.G., "Simulation of Smoke Plumes from Large Pool Fires", *Twenty Fifth Symposium (International) on Combustion*, The Combustion Institute, Pittsburgh, pp. 1463-1469, (1994).

[2] McGrattan, K.B., Baum, H.R., and Rehm, R.G., "Numerical Simulation of Smoke Plumes from Large Oil Fires", *Atmospheric Environment*, Vol. 30, pp. 4125-4136, (1996).

[3] McGrattan, K.B., Baum, H.R., Walton, W.D., and Trelles, J., "Smoke Plume Trajectory from In Situ Burning of Crude Oil in Alaska — Field Experiments and Modeling of Complex Terrain", NISTIR 5958, National Institute of Standards and Technology, Gaithersburg, (1997).

[4] Baum, H.R., McGrattan, K.B., and Rehm, R.G., "Three Dimensional Simulation of Fire Plume Dynamics", *Jour. Heat Trans. Soc. Japan*, Vol. 35, pp. 45-52, (1996).

[5] Baum, H.R., McGrattan, K.B., and Rehm, R.G., "Three Dimensional Simulation of Fire Plume Dynamics", *Fire Safety Science - Proceedings of the Fifth International Symposium*, Y. Hasemi, Ed., International Association for Fire Safety Science, pp. 511-522, (1997).

Brand Propagation of Post-Earthquake Fires

John P. Woycheese and Patrick J. Pagni

Mechanical Engineering Department, University of California, Berkeley, CA 94710-1740

Fires following earthquakes are a serious problem due to multiple simultaneous ignitions. The difficulties are exacerbated by brand propagation, where burning particles are deposited downwind from large, post-earthquake fires. Calm winds after the 1989 Loma Prieta, 1994 Northridge, and 1995 Kobe earthquakes reduced the effect of fire spread by brand propagation; it is unlikely that future earthquakes will be so conveniently correlated with the weather. This research is intended to optimize limited resources by quantifying the effects of wind speed and particle shape on the maximum brand propagation distance from large, post-earthquake fires.

Post-earthquake fire growth by remote spotting can be decomposed into three sequential events[1]: lofting, propagation, and downwind burnout or deposition with possible fire initiation. The dimensionless equations for spherical, cylindrical, or disk-shaped brands during the first two phases [2][3] are

$$\frac{dV_x^*}{dt^*} = \frac{\|W^*\|W_x^*}{L^*} - \frac{V_x^*}{m^*}\left(\frac{dm^*}{dt^*}\right)$$
$$\frac{dV_z^*}{dt^*} = \frac{\|W^*\|W_z^*}{L^*} - \frac{V_z^*}{m^*}\left(\frac{dm^*}{dt^*}\right) - 1 \qquad (1)$$

where the symbols are defined in the notation and the average ambient wind is assumed to be aligned with the x-axis. Note that the non-dimensional length scale, L^*, absorbs the shape-dependent aspects of the acceleration due to drag. The drag coefficient is assumed to be constant, with $C_d = 0.45$, 1.2, and 1.17 for $100 < Re < 2 \times 10^5$ for the three shapes. Eqs. (1) are coupled with the position equations, $dx^*/dt^* = V_x^*$ and $dz^*/dt^* = V_z^*$, and with an equation for the temporal mass change that is shape- and orientation-dependent to provide a closed set of equations for the brand lofting and propagation. Combustion rates for constant-density brands have been determined for spheres and for disks -- oriented perpendicular to the relative velocity -- as follows

$$\frac{1}{m^*}\left(\frac{dm^*}{dt^*}\right) = -\frac{3}{\Phi L^*} \qquad \text{sphere}$$
$$\frac{1}{m^*}\left(\frac{dm^*}{dt^*}\right) = -\Psi\left(\frac{W^*}{L_o^*}\right)^{1/2} \qquad \text{disk} \qquad (2)$$

with $\Phi = \left(\frac{9}{64}\right)\left(\frac{\rho_a}{\rho_s}\right)\left(\frac{C_d^2}{\alpha \ln(1+B)}\right)\left(\frac{\dot{Q}_o{}^3\sqrt{g}}{\rho_a c_p T_o}\right)^{3/5}$, $L_{c,\,sphere} = (3/4)(z_c C_d)(\rho_a/\rho_s)$,

$L_{c,\,disk} = (3/4)(z_c C_d)(\rho_a/\rho_s)$, and $\Psi = \left(\frac{32}{3}\right)\left(\frac{\nu g \varepsilon \rho_s}{\rho_a C_d^3 V_c^3}\right)^{1/2}(0.353 r^{-0.02} B^{0.611 - 0.0651 \ln(B)})$, so that

$L_{c,\,sphere} = (3/2)\, L_{c,\,disk}$. The combustion rate for spheres is based on the burning droplet model, while that for disks is derived from stagnation-point burning.

The flow field is divided into a Baum and McCaffrey plume [4] ($V_c = ((\dot{Q}_o g^2)/(\rho_a c_p T_o))^{1/5}$ and $z_c = (\dot{Q}_o/((\rho_a c_p T_o)\sqrt{g}))^{2/5}$), lofting the brand, and a constant horizontal wind, pushing the particle downstream. The ALOFT large eddy simulation will replace these approximations during the current grant period. Brands are removed from the plume and propagated such that the maximum downwind distance is realized; a brand with higher loft will burn out above the ground, while one that is removed ear-

lier will not propagate the maximum distance.

Disk brands that are tilted about an axis of symmetry at an angle of attack γ, which is positive CCW, have a lift force acting perpendicular to that of drag. The acceleration due to drag in Eqs. (1), $\|\mathbf{W}^*\|W^*_{x,z}/L^*$, is modified to include lift,

$$\frac{dV_x^*}{dt^*} = \frac{\|\mathbf{W}^*\|}{L^*}(W_x^*\cos(\gamma) - W_z^*\sin(\gamma)) - \frac{V_x^*}{m^*}\left(\frac{dm^*}{dt^*}\right)$$
$$\frac{dV_z^*}{dt^*} = \frac{\|\mathbf{W}^*\|}{L^*}(W_z^*\cos(\gamma) + W_x^*\sin(\gamma)) - \frac{V_z^*}{m^*}\left(\frac{dm^*}{dt^*}\right) - 1 \qquad (3)$$

where $\cos(\gamma)$ and $\sin(\gamma)$ resolve the drag and lift forces from the force normal to the brand's surface. This normal force is constant for a given Reynold number for $-54^\circ < \gamma < 54^\circ$ [5], the range over which Eqs. (3) are valid. The normal coefficient, $C_n = 1.17$, is used in lieu of C_d in the equations for L_c and mass loss. Equations (3) collapse to Eqs. (1) for $\gamma=0$, and are coupled with position and mass change equations to determine the lofting and propagation path of disk brands with an angle of attack. Note that Eqs. (3) do not require that γ remains constant during the brand's lifetime, allowing the calculation of the flight paths of fluttering disk brands. Mass loss models for disks with $\gamma \neq 0$ and experimental measurements of drag and lift coefficients are the subject of current research.

References

1. Woycheese, J.P., Pagni, P.J., and Liepmann, D., "Brand Lofting Above Large-Scale Fires," *2nd ICFCE Proceedings*, pp. 137-150, SFPE, 1998.

2. Woycheese, J.P., Pagni, P.J., and Liepmann, D., "Brand Propagation from Large-Scale Fires," *J. Fire Protection Engineering*, in review, 1998.

3. Pagni, P.J., and Woycheese, J.P., "A Modular Model for Post-Earthquake Fire Growth," *Proceedings of the Fourteenth Joint Meeting, United States-Japan Panel on Fire Research and Safety*, Building Research Institute, Tsukuba, Japan, 1998, in press.

4. Baum, H.R., and McCaffrey, B.J., "Fire-Induced Flow Field - Theory and Experiment," *Fire Safety Science - Proceedings of the Second International Symposium*, pp. 129-148, New York, Hemisphere, 1989.

5. Hoerner, S.F., *Fluid Dynamic Drag*, 1st ed., published by the author, Midland Park, N.J., 1958.

Notation

B	Mass transfer number [ ]
C_d	Coefficient of drag [ ]
c_p	Specific heat of air (J/kg K)
g	Acceleration due to gravity [m/s^2]
L	Length [m]
m	particle mass [kg]
$\dot{Q}_o$	Rate of heat release for the fire [kW]
r	Mass consumption number [ ]
t	Time [s]
T_o	Ambient temperature [K]
V	Scalar particle velocity relative to ground [m/s]
W	Vector-valued relative velocity of brand to its surroundings [m/s]
W	Scalar relative velocity of brand to its surroundings [m/s]
x	Propagation distance [m]
z	Vertical height of particle [m]

Greek

α	Thermal diffusivity of air [m^2/s]
γ	Angle of attack from relative velocity vector [ ]
e	Length-to-diameter ratio for disk [ ]
ν	Kinematic viscosity of air [m^2/s]
ρ	Density [kg/m^3]
Φ	Droplet parameter [ ]
Ψ	Disk parameter [ ]

Superscript

*	Dimensionless variable

Subscripts

a	Air
c	Characteristic constant
n	Normal
o	Initial
s	Sphere
x, z	Cartesian coordinate direction

Crude Oil Full Scale Pool Fire Experiment in Tomakomai in 1998

Toru Takahashi*, Hiroshi Koseki**, Yusaku Iwata**

* Japan National Oil Cooperation

** National Research Institute of Fire and Disaster

Tokyo, Japan

Introduction

Japan National Oil Corporation (JNOC), National Research Institute of Fire and Disaster and the University of Tokyo conducted a large crude oil burning experiment at Tomakomai city in January 20-21, 1998. The experiment field was located 5 km south of JNOC's Tomakomai Oil Storage site, on the outskirts of Tomakomai City. We burned from 1 to 20 kl crude oil in pans which were 5 m, 10 m and 20 m in diameter. The ingredients was the same as these in Arabian Light.

The biggest problem in this experiment was the smoke. ALOFT, which was developed by NIST, was a very strong tool for persuading the parties concerned.

The purpose of the experiment is to predict accurate data of crude oil fires for fire- fighting. JNOC needs data involving tanks ranging in size from 82 to 97 m in diameter. However, due to budget constraints, environmental concern and limited techniques, we were able to conduct experiments using 20-m tanks. JNOC will estimate large-diameter tank fires using the data from 5, 10 and 20 m pans.

We could conduct the experiment only when the north wind was blowing because there small residential areas to the north and the experiment field faced the sea to the south. The wind blows constantly from the north only in winter. We selected late January.

Measurements

We measured

a) Burning Rate (Fuel level)
b) External Radiation (See Fig.1 and Fig. 2)
c) IR-Image of flame
d) Image of flame by video camera and high speed video camera
e) Temperatures inside the flame by thermocouple
f) Gas composition inside flame
g) Image inside the flame by video camera
h) Smoke dispersion observation on the ground level and on the air using helicopter
i) Smoke particle size
j) Temperature of side shell
k) Temperature of side shell of small tank at the side of burning pan by thermocouple and IR-Image
l) Ionic current inside flame

m) Flammable gas dispersion observation before burning

n) Smell observation before burning

o) Temperature, humidity, wind direction and wind velocity

We conducted burning two or more times on each size and conducted a total of 10 tests. Most of them could be done in calm weather conditions, especially those involving the 20 m pan.

Result

Any violent boil-over was not observed. But mild water boiling might have occurred because noise and flame changed in the latter half.

Irradiation of down wind side was much larger than that of upwind side. There were much smoke at downwind side and it was seemed that smoke blocked radiation. But still irradiation was higher at down wind side.

Radioactive fraction decreased with an increase in pan diameter. It was about 16% in a 20 m pan fire.

There was clear flame pulsation only when the wind blew very calmly. Intervals of pulsation of 20 m pan were from 3.2 to 3.5 second.

Smoke dissipated quickly. About 60 minutes after ignition(40 minutes after burning was finished) in 20 m pan, we could not detect most of the smoke. Smoke dissipating times were consisted with ALOFT's predictions.

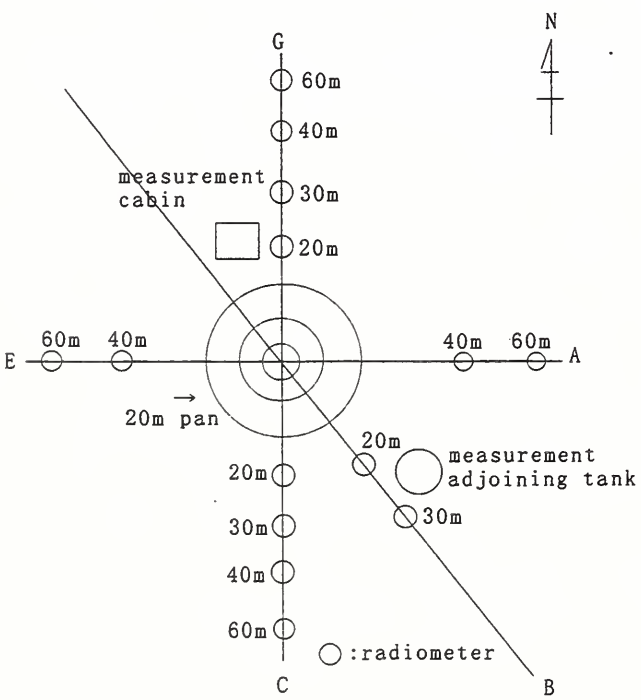

Fig.1 Layout of burning pan and radiometers

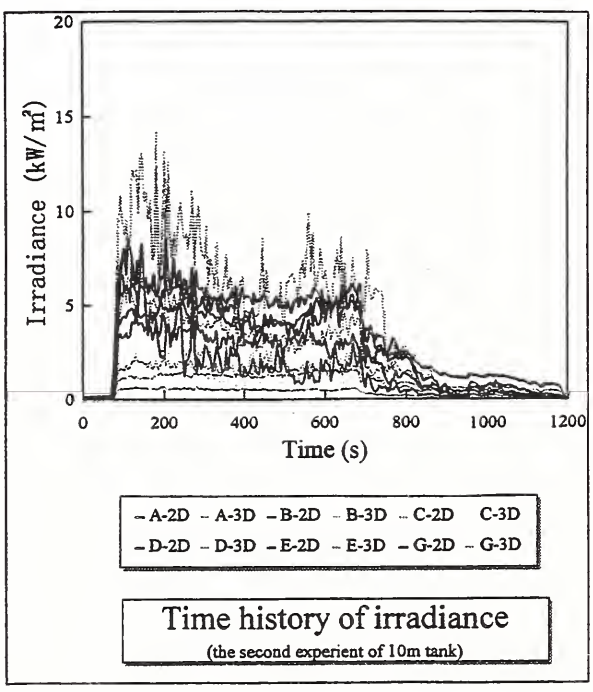

Fig.2 An Example of irradiance time history from 10 m fire

RADIATION CHARACTERISTICS AND FLAME TEMPERATURE OF LARGE SCALE CRUDE OIL POOL FIRES

Yusaku Iwata*, Hiroshi Koseki* and Toru Takahashi**
* National Research Institute of Fire and Disaster
Tokyo, Japan
** Japan National Oil Cooperation
Tokyo, Japan

ABSTRACT

Large oil fire experiments were conducted in Japan in 1998, where Arabianlight crude oil was burned in pans which were 5 m, 10 m and 20 m in diameter. The experiments were done in very good condition. Huge data were obtained in terms of radiation, flame temperature, gas concentration inside flame and other burning characteristics. In this report, results relating radiation and flame temperature were discussed.

INTRODUCTION

It is important to investigate protection of fire brigades and surrounding facilities against radiation heat from a fire in advance. However, it is difficult to do large scale fire tests due to budget constraint, environmental problems and limited techniques for measurement. There were a few large pool fire experiments[1,2] in Japan, for example, the experiment[1] which was done in Gotemba, Shizuoka, in 1981, in which kerosene was burned.

Large scale pool fire tests using Arabianlight crude oil were conducted through the collaboration of the National Research Institute of Fire and Disaster, Japan National Oil Corporation and the University of Tokyo in Tomakomai, Japan in January 1998.

It is useful to predict the burning characteristics of large scale fire on basis of result of small scale fire tests. Three different steel pans, 5 m, 10 m and 20 m in diameter were used as burning tank to investigate the scale dependency. The experiments were conducted for the purpose of preparing basic data for making fire fighting system of the petroleum storage facilities.

MEASUREMENTS

Irradiance was measured by twelve radiometers[3] which were set around the burning pan. Distance between pan center and each radiometer was set at L/D = 2 or 3. Here L was the horizontal distance from pan center, and D was the pan diameter. The radiometers faced to the fire center to obtain the maximum irradiance at each place. They were set about 1.2 m height. They had wide angle view, 120 ° and their time constant was 0.3 second. Outputs of radiometers were stored in a personal computer through a data acquisition system every 5 seconds.

Temperature inside flame were measured by four K-type thermocouples at pan center. Diameter of thermocouples was 0.3 mm. All data of temperature inside flame were stored in a personal computer every second.

RESULTS AND DISCUSSION

Tests were run twice in all tanks. Most tests were done in calm weather conditions. There was little wind in the second test of 20 m tank. Average wind speed was about 0.05 m/sec during the test. Relationship between irradiance and dimensionless distance from tank center (L/D) was examined for all tests. The ratio of decrease of irradiance between the point at L/D=2 and the point at L/D=3 was almost the same values in terms of all tests.

Relationship between irradiance at L/D = 2 and 3 and pan diameter was shown in Fig. 1. The data of circle points (○ and ●) were measured in this work. The data of triangle points (△ and ▲) were from the reference[1] of kerosene test and converted into the values at L/D=2 and L/D=3 following to the square law. The data of square points (□ and ■) were from the reference[2] of crude oil test and converted by the same way. Irradiance at the points of L/D = 2 became low with increasing of D. The results at the points of L/D = 3 had the similar tendency with the results at the points of L/D = 2. Angle factor was 0.10 at L/D=2 and 0.05 at L/D=3, which was calculated with assuming that configuration of flame was cylinder. Flame height was about 30 m (Hf /D=1.5, Hf: flame height). The ratio of decrease of angle factor between the point at L/D=2 and the point at L/D=3 was 0.5. Irradiance of 20 m pan tests decreased greater than the result of this calculation.

Radiative fraction, ratio of total radiation loss and total heat release rate was about 29 % in 10 m, 16 % in 20 m pan fires, smaller than that of small scale tests[3]. Here total heat release rate was calculated with assuming complete combustion, and radiation outputs were calculated with averaged irradiance data at L/D = 3. These results mean most flame surface might be covered with huge amount of smoke produced from fire.

Relationship between the maximum temperature of the flame axis and dimensionless height (H/D) from the liquid surface was shown in Fig. 2. At height of H =4.4 m (H/D=0.22) in 20 m pan test, the maximum temperature became about 1350 ℃. K-type thermocouple may not give exact value in such high temperature. Flame core, which means the zone in the flame has the maximum temperature along with the flame axis, should be at H/D=0.22 or higher. In 5 m and 10 m pan tests, temperature decreased where height was beyond H/D=0.1.

REFERENCES

1)The Japan Society for Safety Engineering, 1981, Report of Petroleum Burning Tests

2)The Japan Society for Safety Engineering, 1979, Report of Tank Fire Tests

3)H.Koseki and T.Yumoto, 1988, Fire Technology, 24(1) p.33

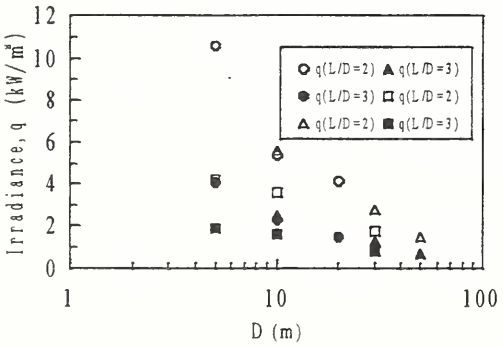

Fig.1 Relationship between irradiance and pan diameter

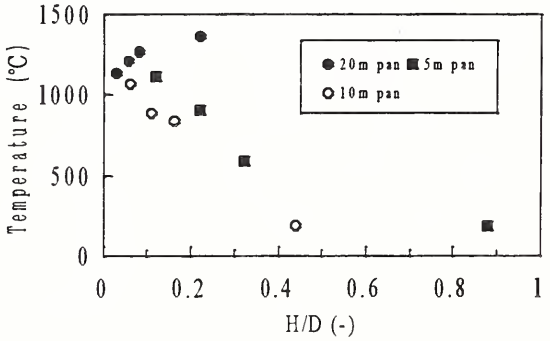

Fig2. Relationship between maximum temperature of flame and dimensionless height from the liquid surface

Smoke Plume Trajectory from In-Situ Burning of Crude Oil in Tomakomai
----- Field Experiments and Prediction with ALOFT-PC ----

Tokiyoshi YAMADA
National Research Institute of Fire and Disaster
14-1,Nakahara 3 chome Mitaka,
TOKYO,181-8633 JAPAN
TEL:+81(422) 44-8331, FAX:+81(422) 42-7719

Background

A series of large scale crude oil tank burning test were conducted at Tomakomai, Hokkaido in Japan Jan.'98, for obtaining basic knowledge necessary for developing "Information and Command Support System for Oil Stockpiling Base " in a case of emergency such as tank fire and oil spill. Prediction of smoke plume trajectory from *in-situ* burning is one of the key issues for the system, because hazardous combustion products can be transported by a windblown smoke plume and delivered over a wide area. For assessing and establishing emergency corresponding plan, even a coarse prediction of smoke spread will be very helpful. NIST/BFRL have been developing prediction models for such a large scale fire smoke dispersion and some of the validation have been done[1,2]. For utilizing a simple prediction model named ALOFT-PC as one of the tools for the system, validity of the model is examined by comparing between the prediction and the experiment.

Experiment and Prediction

Experiment : Total 7 test runs were conducted with 5, 10 and 20 m diameter tank of 0.3, 0.5 and 0.7 m depth respectively. As a test fuel, equivalent of Arabian Light crude oil with the API gravity of 32.8 was used. The oil was supplied into the water filled tank with 5cm depth, which enables about 20 min. burning. For ALOFT-PC model validation, two runs of 10 meter tank tests were targeted, because both of wind condition were relatively constant and stable smoke trajectory were observed. Smoke trajectory of each test was recorded with VCR and still camera at sea berth platform about 2. km away from fire source in downwind side. Also observation up in the air was made by helicopter, and main direction of smoke flow was determined by the observation. To estimate the height and downwind distance of the plume, a power plant chimney of 200 m height was referred as a landmark. Figure 1 shows the location of observatory, fire source and landmark.

Input data for prediction : Each of two runs, wind condition seemed to be relatively constant for about 6 minutes after ignition. As an input data for prediction, temperature data at the landmark of ground and 185 m height level are adopted as shown in Figure 1. Also average of wind velocity at 185m height is adopted as background velocity. For a category of Pasquill Stability, "unstable (strong)" is selected, i.e.,"C" for both runs. In this experiment, the equivalent of Arabian-Light crude oil is used as a fuel, however the effective heat release rate and emission factors were not analyzed yet. The burning rate was about 0.06kg/s/m^2 estimated from pool level decrease. Then relatively high heat release rate of Louisanna crude oil data base in ALOFT-PC(ver.3.04) was used for convenience: i.e., burning rate per unit area is 0.056 (kg/s/m^2), heat release rate per unit area 2.14 (MW/m^2) and emission factor of PM10(*particulate combustion product with diameter less than 10 micrometer)* is 130(g/kg).etc.

Summery of the Results

Rough comparisons were made between PM10 concentration prediction and view of smoke plume trajectory. Figure 2 is an example of prediction of PM10 conc. shaded contour of plume on center vertical plane. Crosswind section of the simulated plume shows two large counter-rotating vortices characterizing the structure of the rising smoke plume, and its center reaches to about 350 m height at 1.0 km downwind distance from fire. Within the 500 m distance, the prediction contour seems to be relatively primitive due to coarse calculation cells' effect. Figure 3 shows comparison of picture view of transient smoke trajectory and PM10 conc. prediction on a specific

section plane. In spite of coarse estimation, both prediction of downwind and crosswind side agree well with transient smoke plume transport in the region beyond 500m downwind from fire source. Whereas in closer region to fire source, coarse calculation cells cause less accuracy of the prediction as indicated[1,2]. In this experiment, distinct two counter rotating vortices were not well observed, however similar pattern of smoke spread shape can been seen. On the whole, the ALOFT-PC can be expected as simple but powerful tool for practical purpose.

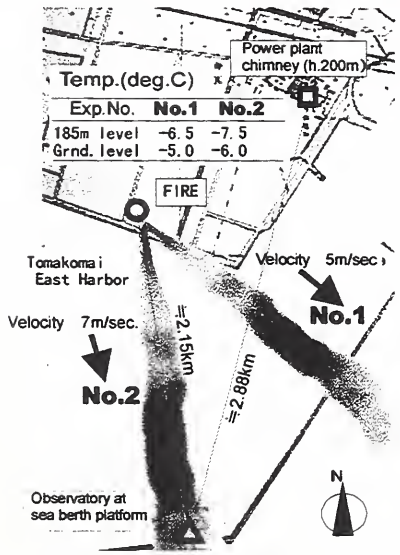

References

[1] W.D.Walton, K.B. McGrattan *et al.*, "ALOF-PC Smoke Plume Trajectory Model for Personal Computer", *Artic and Marine Oil spill Program Technical Seminar*, Calgary, Alberta, Canada 19th, Vol.2 (1996)

[2] K.B.McGrattan,H.R.Baum *et al.*,"Smoke Plume Trajectory from In Situ Burning of Crude Oil in Alaska --Field Experiments and Modeling of Complex Terrain", *NISTIR* 5958 (1997)

Acknowledgements

This experiment was successfully carried out by the National Research Inst. of Fire and Disaster, the Japan National Oil Corp., and Univ. of Tokyo in collaboration with Japan Ground Self Defense Force, Fire Departments concerned, and other organizations. And the prediction could be done with NIST/BFRL collaboration, especially special thanks to Drs. H.Baum and R.Rehm for giving useful advice.

Figure 1: Location of fire source , observatory and land mark, and input weather conditions

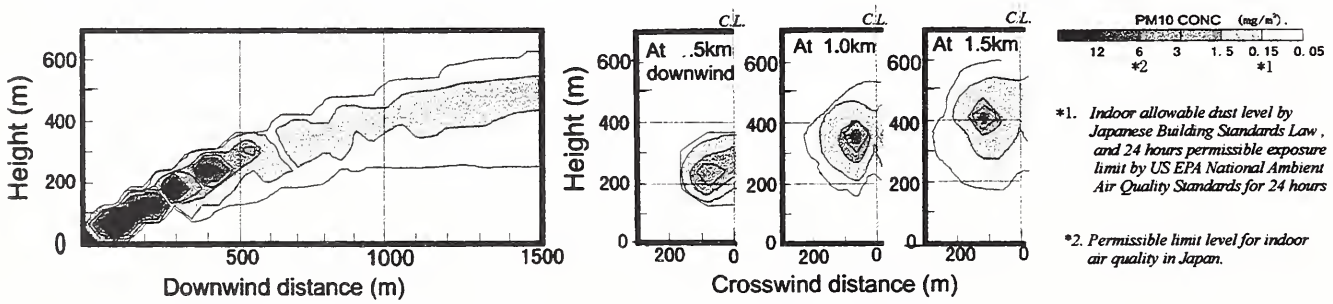

(a) Downwind vertical section **(b) Crosswind section**

Figure 2 :Example of PM10 concentration prediction contour : Exp.No.1 (wind velocity =5m/s, Fire=10m Diameter tank of Arabian Light crude oil, Pasquil Giiffor Categ.= "C", smoke plume travels over "water")

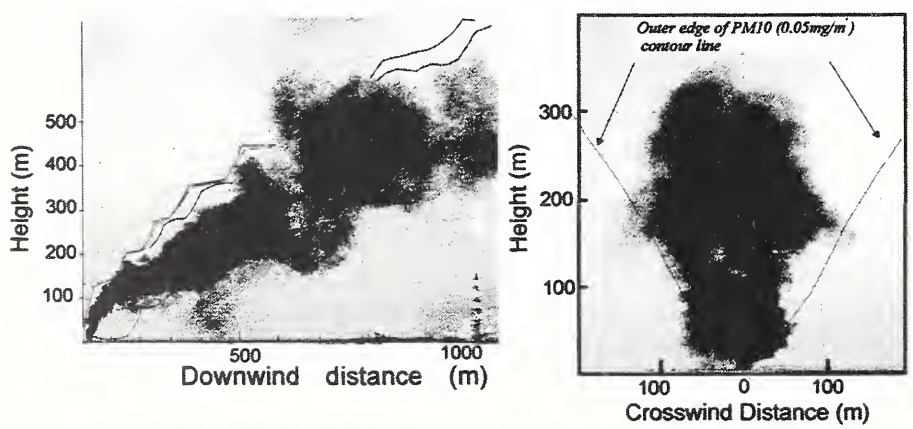

(a) Downwind side view **(b) Crosswind side view**

Figure 3
Comparison with view of transient smoke transport and PM10 conc. prediction: :
(a)Exp.No.1 at 5min30sc after Ignition, contour is of downwind vertical section.
(b)Exp.No.2, at 2min.,contour is of 500m downwind cross-section.Outer contour line indicats 0.15mg/m^3 of PM10

FIRE WHIRL SIMULATIONS

Francine Battaglia, Kevin B. McGrattan, Ronald G. Rehm and Howard R. Baum
National Institute of Standards and Technology
Building and Fire Research Laboratory
Gaithersburg, MD 20899

Abstract

Fire whirls are a rare but potentially catastrophic form of fire. In order for one to exist, there must be an external source of organized angular momentum that produces large swirl velocity components as air is entrained into the fire plume [1]. The vertical acceleration induced by the buoyancy generates strain fields which stretch out the flames as they wrap around the nominal plume centerline. Fire whirls are known to increase substantially the danger of naturally occurring or post-disaster fires [2].

A numerical investigation of swirling fire plumes has been undertaken to understand how swirl alters the plume dynamics and combustion. In a buoyant plume, heated gases rise and entrain ambient fluid from the environment. If vorticity is present in the ambient fluid, it is entrained and concentrated by the plume. This concentration changes the dynamics of the buoyant plume including the entrainment and mixing which control the combustion.

The equations are those that govern three-dimensional, transient, buoyant flow of a thermally expandable ideal gas [3]. The fire is prescribed as a heat source consistent with a mixture-fraction approach to combustion [4]. As in the experiments of Emmons, a circulation is imposed on the fire plume at a prescribed radial distance from the nominal centerline. Three dimensionless parameters govern the flow generated by this model: 1.) the heat-release rate made dimensionless using the thermal characteristics of the ideal gas, 2.) the circulation made dimensionless using the length scale and buoyant velocity based on the heat-release rate [5], and 3.) a Reynolds number for the flow. The experiments of Emmons and Ying measured fire-whirl temperature, radius and height for different imposed values of circulation. The second of these dimensionless parameters is analogous to the reciprocal of the Rossby Number defined in the model of Emmons and Ying to interpret their experimental results.

Large eddy simulation (LES) methodology developed earlier by the authors has been applied [6]. A Poisson equation for pressure is solved using fast direct methods, and a second order explicit Runge-Kutta scheme is used to advance the velocity and temperature fields. This model and computational methodology, using the dimensionless scaling noted above, have been found to reproduce very well mean temperature and buoyant velocity correlations for large fire plumes in the absence of circulation [5,6]

Numerical results show that the structure of the fire plume is significantly altered when swirl is imparted to the ambient fluid. The whirling fire is found to constrict radially and stretch the plume vertically which, in turn, reduces the entrainment of ambient fluid. Consequently, the plume is at higher temperatures over a larger volume and the heat release rate increases throughout the plume. Figures 1a–1b show instantaneous views of the temperature field in a non-swirling fire plume and a whirling fire plume, respectively. The plume temperatures decrease both axially and radially away from the nominal centerline. In Fig. 1b, the

height of the visible flame marked by the dark gray region from the base to about $z = 0.06$ m, increases for the swirling fire and the plume is found to have higher temperatures over a larger region. The overall plume structure of the fire whirl tends to stretch upward and constrict radially, i.e., at $z = 0.20$ m, and appears conical in shape as seen Fig. 1b. In contrast, the fire plume of Fig. 1a does not appear to constrict radially with height and the centerline temperatures are lower near the base. Additional numerical simulations are underway to understand and quantify the dynamics of the swirling fire plume. Results of these simulations will be reported and interpreted in terms of angular momentum conservation under stretching by the buoyant flow induced by the fire. The effects of the circulation on the entrainment and combustion are of particular interest.

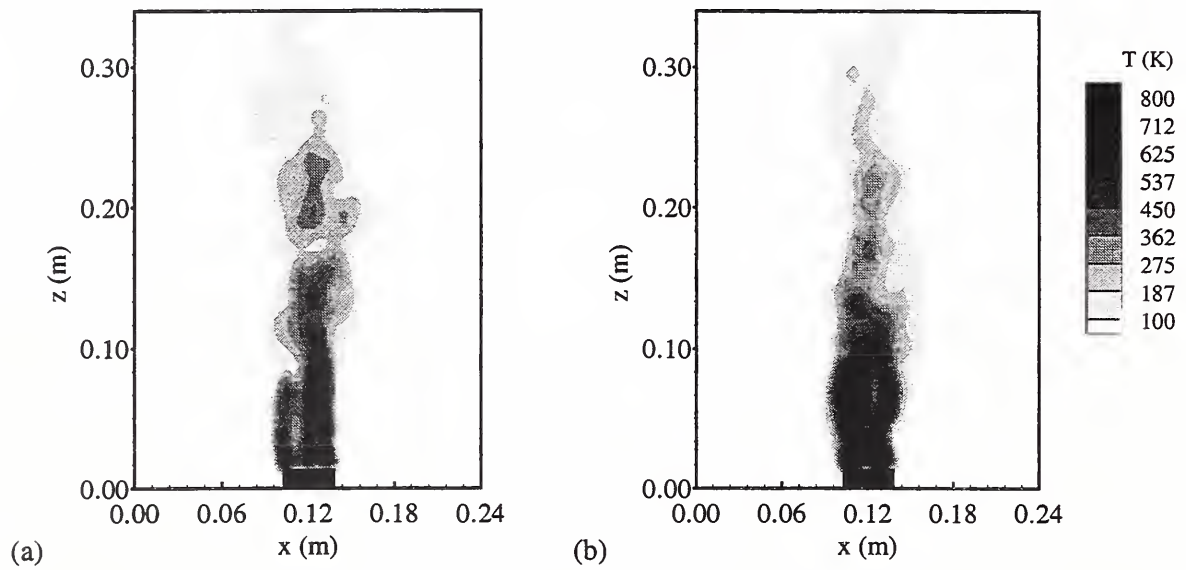

Figure 1: Temperature field in the plume centerplane for a.) a non-swirling fire, and b.) a whirling fire.

References

[1] Emmons, H.W. and Ying, S.-J., *Eleventh Symp. (Int'l.) on Comb.*, 1966, pp. 475-488.

[2] Soma, S. and Saito, K. *Comb. and Flame* **86** 1991, pp. 269-284.

[3] Rehm, R.G. and Baum, H.R., *Journal of Research of the Nat. Bur. of Standards* **83**, 1978, pp. 297-308.

[4] Baum, H.R., McGrattan, K.B. and Rehm, R.G., *Int'l Symp. on Fire Safety Science*, 1997, pp. 511-522.

[5] Baum, H.R., McCaffrey, B.J., *Int'l Symp. on Fire Safety Science*, 1989, pp. 129-148.

[6] McGrattan, K.B., Baum, H.R. and Rehm, R.G., *Fire Safety Journal* **30**, 1998 pp. 161-178.

Thermal Sensors for Evaluating Firefighter Protective Clothing

H. Hamouda, R.L. Barker, J.W. Johnson, and M. Bender
Center for Research on Textile Protection & Comfort
College of Textiles
North Carolina State University
Raleigh, NC

Abstract

The Center for Research on Textile Protection and Comfort (T-PACC) at North Carolina State University (NCSU) has conducted research which had, as its primary objective, the selection and evaluation of sensors that can be used to measure heat transferred through firefighter protective clothing materials. This paper will describe the comparative performance of these sensors in exposures to intense sources.

A review of state-of-the-art thermal sensor technologies led to the identification and selection of sensors that are currently used for evaluating materials for firefighting applications. Each of the candidate sensors was tested and comparatively evaluated based on a set of performance requirements for thermal sensors used for materials testing, or for thermal measurements in firefighting environments. Laboratory experiments were conducted to characterize sensor response to different levels of heat exposure and to evaluate the accuracy of the thermal measurements. Also, a burn model was developed to determine tolerance times for each exposure condition.

Instrument studies successfully identify critical differences in sensor performance that provides a useful basis for selecting the optimum sensor for this application.

The NCSU insulated copper sensor is demonstrated to be a reliable and versatile thermal sensor for applications related to evaluating the thermal protective performance of firefighter's protective clothing. Laboratory tests indicate that the insulated copper sensor provides a consistent and stable reading over the wide range thermal exposures of interest in this application. They show that the insulated copper sensor registers heat flux much like the TPP calorimeter, a device with a long history of use in bench scale testing of thermally protective materials. At the same time, the insulated copper sensor is packaged in a smaller and far less bulky housing than is required to insulate the TPP calorimeter against heat loss. The insulated copper sensor has the additional advantage of possessing a small mass in comparison to the TPP calorimeter (1.3 grams vs. 17.9 grams). This is an important consideration, since the small mass of the insulated copper sensor should significantly reduce heat sink effects associated with the use of the TPP calorimeter. This should contribute to improve the accuracy of the bench top TPP tests when used in sample mounting configurations that require intimate contact between the thermal sensor and the test fabric.

Although the sensors that utilize relatively insulative materials with surface mounted thermocouples and embedded thermocouples, perform comparatively well in thermal tests, they lack the durability in use that can be expected from the insulated copper device. Most significantly, the insulated copper sensor overcomes a significant drawback associated with this type of sensor: it does not require an inverse heat transfer calculation to estimate heat flux. This avoids errors associated with thermocouple location, and the mathematics of the heat transfer calculations. Direct heat flux measurements, using the insulated copper sensor, circumvent these errors and provide a more accurate direct reading.

Center for the Simulation of Accidental Fires & Explosions at University of Utah: An Overview

David W. Pershing and Philip J. Smith
Department of Chemical and Fuels Engineering
University of Utah, Salt Lake City, UT 84112

The University of Utah in an alliance with the DOE Accelerated Strategic Computing Initiative (ASCI) created the Center for the Simulation of Accidental Fires and Explosions (C-SAFE) to focus specifically on providing state-of-the-art, science-based tools for the numerical simulation of accidental fires and explosions, especially within the context of handling and storage of highly flammable materials. The objective of the C-SAFE is to provide a system comprising a problem-solving environment in which fundamental chemistry and engineering physics are fully coupled with non-linear solvers, optimization, computational steering, visualization and experimental data verification. The availability of simulations using this system will help to better evaluate the risks and safety issues associated with fires and explosions. Our team will integrate and deliver a system that will be validated and documented for practical application to accidents involving both hydrocarbon and energetic materials.

Although the ultimate C-SAFE goal is to simulate fires involving a diverse range of accident scenarios including multiple high-energy devices, complex building/surroundings geometries and many fuel sources, the initial efforts will focus on the computation of a scenario of slow and rapid heating of a container with conventional explosives in a pool fire (e.g., a container of high explosives involved in an intense jet-fuel fire after an airplane crash).

These large-scale problems require consideration of fundamental gas and condensed phase chemistry, structural mechanics, turbulent reacting flows, convective and radiative heat transfer, and mass transfer, in a time-accurate, full-physics simulation of accidental fires. This simulation will be expansive enough to include the physical and chemical changes in containment vessels and structures, the mechanical stress and rupture of the container, and the chemistry and physics of organic, metallic and energetic material inside the vessel. We will include deflagration-to-detonation transitions (DDT) of any energetic material in the fire, but the simulation will end when/if detonation occurs. C-SAFE will provide coupling of the micro-scale and meso-scale contributions to the macroscopic application in order to provide full-physics across the breadth of supporting mechanistic disciplines, and to achieve efficient utilization of ASCI program supercomputers.

We will utilize a simulation development roadmap (SDRM) consisting of distinct, sequential steps, which parallel the events in our physical problem: Fire Spread Following a Prescribed Ignition, Container Dynamics and High Energy Transformations. A fire or explosion is initiated by an ignition; depending on the magnitude of heat generation and dissipative terms, a perturbation by an ignition source either decays or grows into a flame, followed by a spreading fire and possibly explosion. The fire or explosion can cause the container of HE material to undergo changes, perhaps rupture and, simultaneously or sequentially, the HE material itself can undergo transformations which lead to an explosion. The overall mission is to integrate these

computational steps into a coupled fire and explosion system. To fulfill this mission we will draw on three core disciplines available at the University: molecular fundamentals, computational engineering, and computer science.

The thrust of the molecular fundamentals team will be to perform micro-scale analyses of physical and chemical processes. To this end, they will be concerned with aspects of molecular dynamics, electronic structure, and statistical mechanics in an integrated fashion to dynamically obtain properties for all materials (condensed phases, vaporized phases, and structures) in the fire and explosion. The thrust of the computational engineering team will be to develop meso-scale models that bridge the ranges of length and time scales between microscopic and macroscopic properties. They will also develop large-scale Eulerian and Lagrangian models to describe structural and transport processes with geometric and mechanistic fidelity. The computer science effort will focus on a system development framework which combines target architecture performance analysis tools at the lowest level with an integrated, higher level scientific problem solving environment to provide interactive computational steering, visualization and large data set analysis capabilities.

University of Utah faculty have joined with strategically selected faculty from nearby Brigham Young University and Utah State University and experimental scientists from Cordant Technologies (formerly Thiokol Corporation) to create C- SAFE. A tightly integrated structure has been set up to simultaneously ensure that (1) the common objective of developing a verified, fire and explosive simulation system is attained and (2) modern scientific/computational techniques are used throughout. Decisions regarding selection of key components to integrate into each step will be based on nonlinear sensitivity analysis and numerical optimization of our overall accidental fire simulation. The C-SAFE system requires a computational infrastructure that can support multi-physics modeling of large- scale, complex phenomena. C-SAFE models the physical complexities from the molecular level of HE materials, through millimeter-sized representations of the container, to the meter-sized representations of the fire spread. At each of these levels, the simulations will involve up to 109 discrete mesh points. Due to the multiple scales, the spatial requirements may exceed the terabyte range for the full simulation. The computation will also require 1010 time-steps to compute the physical time scales ranging from microseconds to minutes or hours. Thus the storage requirements far exceed the capacities of most computing facilities. Not only are the memory and storage requirements at the terascale, the computational demands are also on the order of tens to hundreds of teraflops. When these requisites are compounded with the visualization needs, successful realization of the C-SAFE system involves dataset management, model building, simulation, and visualization at the Terascale level.

The C-SAFE system will be validated by comparison with experimental data for a variety of conditions at four different levels: fundamental rates and submodels; individual and coupled SDRM steps; well-defined, integrated multistep experiments; actual, full-scale fires and explosions. Initially, the primary focus will be on utilizing existing data, especially from the National Labs, fire research laboratories, and Cordant. Additional, detailed data to validate the C-SAFE computations will be carried out at the University supplemental tests with high energy materials at Cordant.

Species Formation using Liquid *n*-hexane Fires in a Scaled ISO Compartment

Christopher J. Wieczorek, Christopher McKay, Uri Vandsburger and Brian Lattimer*
Department of Mechanical Engineering, Virginia Polytechnic Institute and State University
Blacksburg, Virginia, 24061-0238

Fires occurring in occupancies such as hospitals, dormitories, and nursing homes pose a serious treat to occupants. Poisoning due to carbon monoxide inhalation affects not only the occupants in the room of origin but also those located at remote locations from the fire.[1] The objectives of the present study is the development of correlations for CO formation and transport in compartment-hallway assemblies. The first step, present here, addresses the compartment.

Initial studies[2,3,4] of CO formation were conducted in the open under a collection hood. Data from these studies indicated that the CO yields could be correlated to the equivalence ratio, however the studies also indicated that the CO levels were dependent on the upper layer gas temperatures. Studies to determine if similar correlations between the CO levels and the global equivalence ratio (GER) could be made within a compartment were conducted by Tewarson[5] and Gottuk[6]. Tewarson assumed that the mass flow rate of air into the compartment through the widow openings was ventilation limit. Gottuk performed his studies with an experimental apparatus which allowed the direct measurement and calculation of the mass flow rates of air and fuel and therefore the direct calculation of the GER. Gottuk showed that the CO levels within the experimental apparatus could be well correlated to the GER.

More recently, studies have been conducted within scaled ISO compartments. Bryner et al.[7] conducted tests using natural gas, supplied from a burner placed in the center of the compartment. Bryner et al. stipulated that the concentrations within the compartment could not be correlated to a single GER, instead local GER's would be required, since the measured species concentrations were non-uniform between the front and the rear of the compartment. Bryner et al. attributed the non-uniformity of the concentrations within the compartment to the presence of a door, which was not present in the previous studies of Tewarson and Gottuk. Also, the compartment clearly presented a different reactor geometry than in the hood experiments.

Tests were conducted in a ½-scaled ISO compartment using *n*-hexane pool fires placed at the center of the compartment, Figure 1. Fully and partially opened door fire scenarios were simulated by varying the door width between 0.165m and 0.33m. A gas sampling probe was located 0.10m down from the compartment ceiling and 0.10m back from the front of the compartment. The concentrations of produced species, CO, CO_2, and UHC, measured as equivalent ethylene (C_2H_4), were measured along with the concentration of O_2.

The mass flow rates through the door were calculated using the temperature profile method discussed by Janssen and Tran.[8] The temperature profiles were determined by using two aspirated type K thermocouple rakes, each containing 8 thermocouples evenly spaced 0.10m apart. The rakes were located in the doorway and front left corner of the compartment as shown in Figure 1.

The experimental parameters examined in this investigation were the fire size and door width, while the analyzed parameters were the species concentrations, species yields and the GER. The GER for the compartment was varied by using different size hexane pools and by changing the door width. In addition to having an effect on the GER, the narrow door increases the residence time of the gases within the compartment.

The following results represent a total of 24 tests of which 11 were performed with the baseline door width (0.33m) and 13 were performed with the narrow door width (0.165m). The GER varied between 0.2 and 3.7. The concentrations and species yields shown represent an average over the quasi-steady-state periods of the developed fire. The criterion for quasi-steady burning was a constant GER.

The GER is a function of the mass flow rates into and out of the compartment. Since there is no direct method for measuring the flow rates with the compartment, it is necessary to determine if the calculated GER's were accurate. In previous studies[2,6,7] it was shown that at a GER of 1.0 the oxygen concentration was approximately zero. The oxygen concentration shown in Figure 2 does in fact decrease to approximately zero at an equivalence ratio of 1.0. This indicates that the calculated GER is valid, therefore the method of Janssen and Tran[8] for determining the mass flow rates into and out of the compartment is also valid for this configuration.

The CO yields are shown in Figure 3 compared to those of Beyler and Gottuk. A larger degree of scatter is seen in the current data for equivalence ratios between 1.0 and 2.0, however the data tends to plateau to a level

* Hughes Associates Inc., Baltimore, Maryland.

slightly less than that of Gottuk, for GER's greater than 1.5. The yields of other species, CO_2, O_2, and UHC also compare well with previous data and can be correlated to the GER (not shown here).

The data combines results for both door geometries, no measurable impact on the species levels was seen between the results. The difference between the two geometries is in the rate of air entrainment resulting in different global residence times within the compartment. The residence time within the compartment for the baseline door was calculated to be on average 9.3 seconds, while for the narrow door the residence time of the gases was on average 19.5 seconds. For both instances the compartment fires are oxygen limited at equivalence ratios greater than 1.0. With the narrow door no further impact on the species levels is observed because there is no additional oxygen present in the system to react with either the unburned hydrocarbons or the carbon monoxide, hence the longer residence time has no additional effect.

The objective of this study was to determine if the species levels within a compartment with a doorway could be correlated to the global equivalence ratio. The current findings have shown that the combustion products and reactants correlated well over a wide range of equivalence ratios, 0.21 to 3.7. The data included two door scenarios, fully and partially open, simulated by varying the door width. The correlations applied equally for both cases, implying that in both the reactions progress is limited by the available oxygen and not the residence time. The species yields reported here are those exiting the compartment. The development of correlations for the evolution of these fire product gases in adjacent spaces, e.g. a hallway, is the subject of the continuation of the study reported herein.

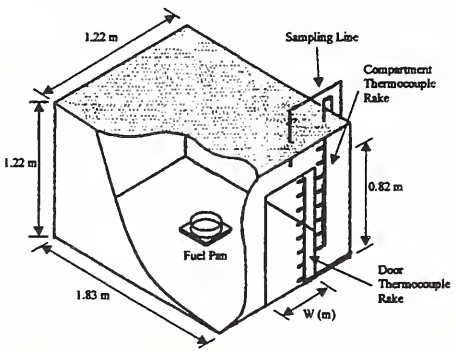

Figure 1: ½-scaled ISO 9705 compartment with instrumentation.

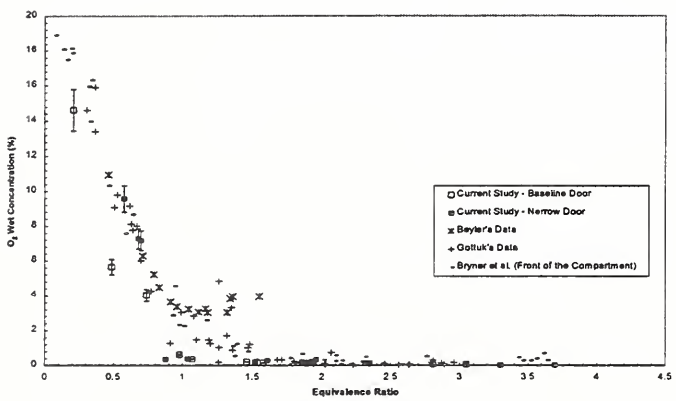

Figure 2: Wet concentration of O_2 within the compartment exhaust plume compared with Beyler, Gottuk and Bryner.

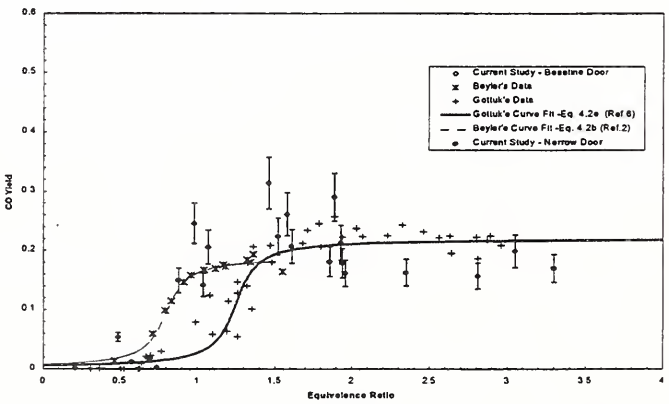

Figure 3: Yields of CO as a function of the global equivalence ratio compared with data from Beyler and Gottuk and the curve fits to the data.

---

[1] Gann, R.J., Babrauskas, V., and Peacock, R.D., *Fire and Materials*, **18**, (May/June), pp. 193-199, 1994.
[2] Beyler, C.L., Fire Safety Science - Proceedings of the First International Symposium, Hemisphere, Washington, D.C., 1986.
[3] Toner, S. J. , E. E. Zukoski, and T. Kubota, NBS, Center for Fire Research, Report NBS-GCR-87-528, 1987.
[4] Morehart, J. H., E. E. Zukoski, and T. Kubota, NBS, Center for Fire Research, Report NBS-GCR-90-585, 1990.
[5] Tewarson, A., *Combsution and Flame*, Vol. 19, pp. 101-111, 1972.
[6] Gottuk, D., Roby, R., Peatross, M., Beyler, C., *Journal of Fire Protection Engineering*, Vol. 4, 4, pp. 133-150, 1992.
[7] Bryner, N., Johnsson, R. J., Pitts, W. M., NIST, NISTIR 5568.
[8] Janssen, M. and Tran, H.C., *Journal of Fires Sciences*, Vol. 10, Nov./Dec., pp. 529-555, 1992.

MITIGATION OF COMPARTMENT JET FIRE USING WATER SPRAY

K Alageel, BCR Ewan, J Swithenbank
Department of Chemical and Process Engineering, University of Sheffield, Mappin Street, Sheffield, S1 3JD, UK

INTRODUCTION

The main objective of the study is to investigate the interaction of the water sprays with a jet fire in an underventilated (confined) space, using CFD. In order to achieve the above objective, it is necessary to produce a workable CFD model of a confined jet which is representative of conditions which might exist offshore.
For this purpose a compartment has been chosen since this represents a geometry which has been the subject of a number of experimental and analytical studies.

COMPARTMENT GEOMETRY AND OPERATING CONDITIONS

The compartment dimensions were those of a standard container being 6m in length by 2.4m high and 2.4m in width. In order to extend the computation space beyond the actual compartment, in the manner recommended for example by Markatos (1), the compartment was situated within a larger chamber, allowing the cells at the compartment opening to be live. This outer environment provided the source for combustion air and an outlet for all the gases to exit, without imposing restrictions to the flow into and out of the compartment.
Propane gas is injected into the compartment through a 1.5 cm diameter nozzle of length 25 cm situated on the floor of the compartment and at its centre. Air is provided from the outer environment chamber into the region of the compartment opening and at low velocity to enable the compartment to entrain as much as is required for combustion.
The propane gas jet entrains air into the compartment, and so the flow rate of air into the domain defined by the outer chamber needed to be several times the stoichiometric quantity needed for combustion. This outer air supply flow velocity was around 0.3m/s and the propane velocity at the jet nozzle was equal to 250 m/s.

TWO-PHASE MODELLING

In order to combat fire it is necessary to understand the nature of the interaction between the hot combustion products and the liquid water. Factors which need to be considered include water flow rate, spray pattern, droplet size and the number and location of spray heads.
It is important also to find out the maximum amount of water that can be discharged from an appropriate spray head in order not to flood the compartment and cause water damage.
The simulation started by studying the effects of a single spray located at different positions in the roof of the compartment. This will give a chance to better understand the fire-spray interaction and evaluate the best spray(s) location to be used to carry out a more detailed investigation. The total water flow rate for each of these arrangements was varied from 0.1 to 3.3 kg/s and the velocities of the droplets used varied between 5 and 25 m/s. The mean droplet diameters could be chosen within the range from 100 to 600 μm. Finally the spray angle used for each of the spray heads is represented by 5 injection directions with each direction having the possibility of an independently defined size and velocity range.
Three spray locations were examined. In the first, a single spray is located above the propane nozzle. The remaining two placed on the front/rear axis and 2.0m on each side of the centre.

RESULT AND DISCUSSION

Initially, the steady state behaviour of the compartment fire was evaluated and used as the starting condition for the subsequent two phase calculation. Prior to the spray activation, the fire plume was able to rise straight upwards and spread outwards along the ceiling. For the case of a single spray located above the propane jet and at a low flow rate less than 1 kg/s, two major flows were apparent after the solution fully developed. The first, generated by the water spray, was downwards whilst the second, generated by the fire, was along the ceiling. These two currents met towards the centre of the compartment, aiding the mixing and cooling process.
The value for temperature used in the calculations throughout this paper, is the average temperature from the upper two-third of the compartment. Because of the configuration of the inlet to the compartment, realistic values of temperature are only obtained above this cooler inlet region.
From the modelling of different spray locations, the results show that less water is needed to extinguish the flame in the case of a single spray located centrally above the jet nozzle. For most flow rate, this location also gave lowest temperatures as shown in Figure 4. Subsequent modelling therefore used a single spray located in the centre of the compartment above the jet nozzle.
Figure 1 shows the average temperature in the compartment as function of mean droplet diameter of 100, 200, 300, 400, 500 and 600 μm. The curve is nearly parabolic and the lowest temperature was found with mean droplet diameters of 300 μm. Subsequent modelling was therefore carried out using mean diameters of 300 μm. It is likely that the minimum arises from

the competing effects of droplet penetration which increases with droplet diameter and total droplet surface area for evaporation.
Modelling different spray angles of 30, 60, 75, 90, 100, 120, 135 and 150° indicated that using spray angle of 60° and 75°

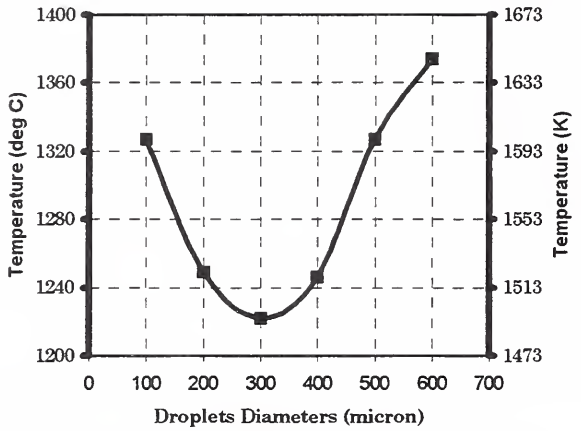

Figure 1. Comparison of different droplets diameters.

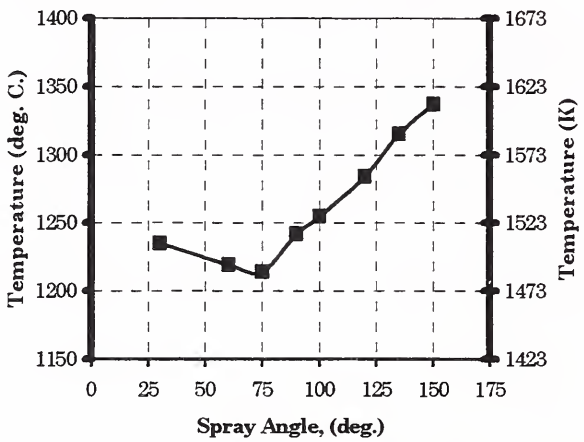

Figure 2. Comparison of different spray angles.

was most effective in reducing the overall temperature as can be seen in Figure 2. Subsequent examination of the effect of spray droplet velocity has therefore used this optimised 60° spray angle. The effect on average temperature of varying this velocity from 5-25m/s is shown in Figure 3. This shows the limiting behaviour due to the effectiveness in penetrating the flame and indicates that for this geometry, velocities in excess of 18 m/s should be used.
For those cases where the water flow rate produced large reduction in average temperature, it was considered that the assumption of steady state was invalid since extinguishment was the likely outcome. For these cases, a time dependent calculation was performed which has the capability of predicting the change in combustion variables with time during this process.
The time dependent simulation was performed with a 1 second time step and during each of these steps, iterations across the domain were carried out until convergence criteria of the variables solved were satisfied. Further details of these results can be found in reference (2).

CONCLUSION

The water discharge rate, the median drop size of the water spray, the spray angle of injections, the droplets velocity, and the heat release rate of the fire source were recognised as important parameters in the cooling of compartment fires by water spray. Time dependent calculations provide a valuable insight into the changes taking place during the extinguishment process. It is clear that present CFD codes with combustion are now able to provide us with details of the factors which control the steady state behaviour of confined fires and emphasise the importance of a mechanistic approach to the study of the dynamics of extinguishment.

REFERENCE

1. Markatos N.C., Malin M.R. and Cox G., Int. Journal of Heat Mass Transfer; Vol. 25 (1); pp.63-75. 1982
2. Alageel, K., Ewan, BCR and Swithenbank, J., IChemE Research Event, Newcastle Upon Tyne, UK, 7-8 April 1998.

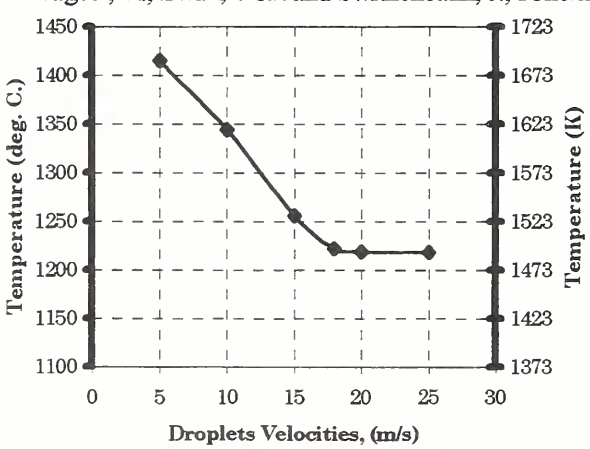

Figure 3. Comparison of different droplets velocities.

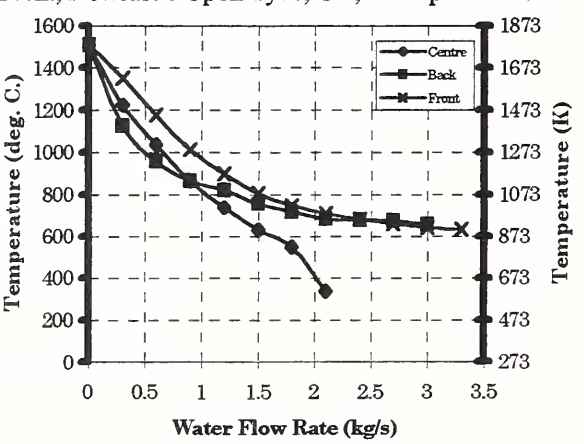

Figure 4. Comparison of different flow rate for different locations.

An Integrated Modeling of Water Mist Penetration Through Obstructions

S. C. Yao and L. S. Hung[1]
Department of Mechanical Engineering
Carnegie Mellon University
Pittsburgh, Pennsylvania 15213

The use of fine water mist as a possible Halon 1301 replacement for certain fire suppression applications has been discussed by Jones and Nolan [1] and by Ramsden [2]. One current research effort is to apply the water mist sprays to suppress the fire occurring in hidden location behind obstructions or inside the equipment compartments. This study presents an integrated approach to model the penetration of water mist through the obstructions for fire suppression applications. The objective is to reveal the transport mechanisms, impacting dynamics, and penetration of mist droplets through the obstructions during fire situations.

Since the mist usually contains a spectrum of drop sizes, the smaller mist droplets may follow the gas streams closely and penetrate directly through the slots of the obstructions while the larger droplets may be intercepted or impacted by the obstructions. Figure 1 displays the schematic of the mist flow in the vicinity of an obstruction. When the mist droplets are approaching the structures, the overall penetrating process of the mist flow through the obstruction depends strongly on the transport of the mist droplets in the gas streams, the ability of the droplets flowing through the obstruction, and the behavior of droplets subsequent to the impaction.

Numerical simulations of a two-phase gas droplet flow based on Navier-Stokes equations are performed to study the transport of mist droplets around a rectangular strip obstruction. The penetration of fine mist droplets is not straight forward because their trajectories approaching the obstruction might be deviated due to the aerodynamic effects. In general, the amount of mist penetrating would depend upon the incoming drop size and the speed of approach. Therefore, a non-dimensional impaction parameter (K) is used to determine the amount of mist arriving the obstruction. The collection efficiency (η) is correlated with this K parameter to determine the amount of droplets to be captured by the obstruction. Then, the by-passing droplets through the adjacent slots of the obstruction can be accounted for by the penetration efficiency (α) which is formulated based on the collection efficiency and the geometric fraction of the obstruction to the flow domain configuration. In addition, the flow wake in the form of vortex shedding at the downstream of the obstruction would affect the motions of the droplets which have already penetrated. Based on the above numerical analysis, it seems that fine water mists may be preferred in suppressing certain hidden fire situations because they have a better ability to follow air streams closely with higher penetration efficiency. A general methodology has been reported by Hung and Yao [3].

Experimental investigations are also accomplished to study the actual droplet impacting phenomena on the obstruction. Typical obstruction objects such as the single wires [4,5] and complex wire screens [6] are considered in details in the impaction experiments. A portion of the mist intercepted by the obstruction may build up liquid films and subsequently penetrate in a different form. Images of the impacting phenomena based on digital image processing demonstrate that the impacting phenomena generally include dripping and disintegration. The results have been correlated in non-dimensional forms with the incoming droplet Weber number, wire Bond number, drop to wire diameter ratio, and

[1] Currently with the Delphi Automotive Systems, Rochester, New York

screen number. Non-dimensional regime maps and the correlations of the impaction outcome are also developed. The conclusions from both the numerical and experimental investigations are integrated to provide an overall understanding to the mist penetration phenomena and to establish a procedure for predicting the outcome of this process.

Acknowledgment

Financial support by the Department of Commerce, NIST, Building and Fire Research Laboratory, under Grant No. 60NANB5D0093, is greatly appreciated.

Reference

[1] Jones, A., and Nolan, P.F., 1995, "Discussions on the use of fine water sprays or mists for fire suppression," *J. Loss. Prev. Process Ind.*, Vol. 8, No. 1, pp. 17-22.

[2] Ramsen, N., 1996, "Water Mist - a Status Update," *J. Fire Prev.*, Vol. 287, pp.16-20

[3] Hung, L.S., and Yao, S.C., 1997, "Numerical Studies on the Transportation of Water Mist for Fire Suppression Applications," ASME HTD-352, Vol. 2, pp. 73-80.

[4] Hung, L.S., and Yao, S.C., 1997, "Study of Droplet Impaction on Wires for Fire Suppression Applications," ASME HTD-341, Vol.3, pp.13-18.

[5] Hung, L.S., and Yao, S.C., 1997, "Investigations on the Phenomena of Water Droplets Impacting on Cylindrical Objects," Submitted, *International Journal of Multiphase Flow.*

[6] Hung, L.S., and Yao, S.C., 1998, "An Experimental Study of Droplets Impacting on Screens," To be presented at the 1998 *ASME International Mechanical Engineering Congress and Exhibition*, Anaheim, CA.

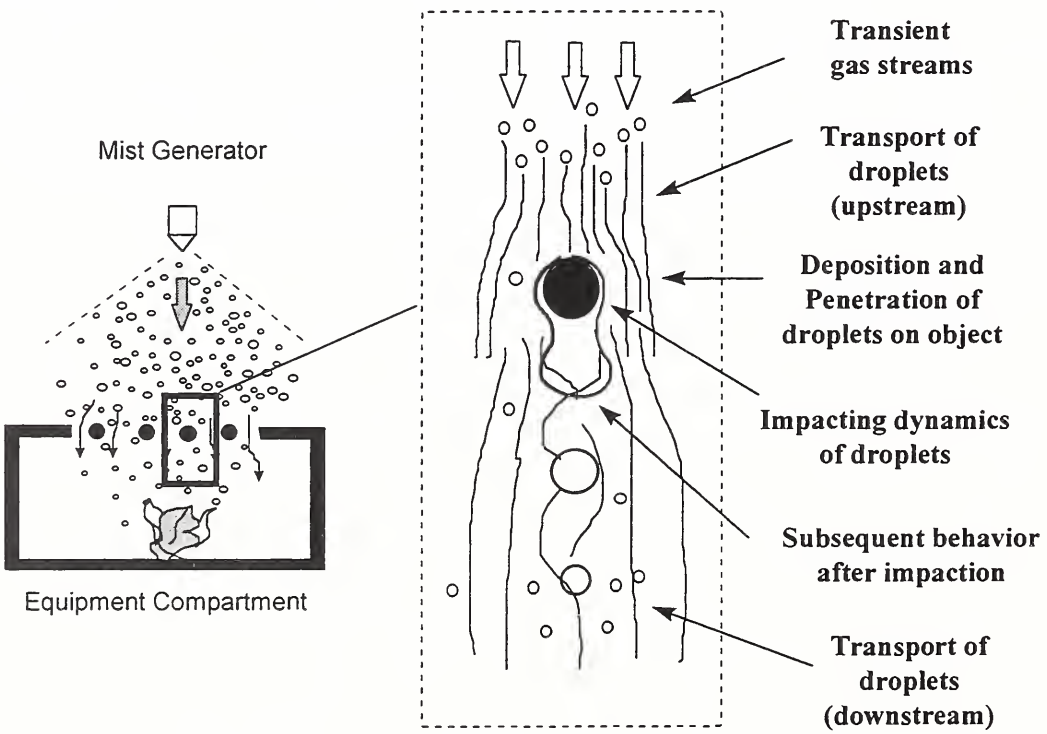

Figure 1 A schematic of water mist penetrating through the opening slots of the obstruction

Water Mist Suppression of Small Methanol Pool Flame

Chuka C. Ndubizu, Ramagopal Ananth and Patricia A. Tatem
Navy Technology Center for Safety and Survivability
Navy Research Laboratory
Washington D.C

Experimental observations have shown that small (less turbulent) flames are more difficult to extinguish with water mist than large turbulent flames[1]. This difficulty has highlighted the need to understand the mechanisms of interaction of water mist with small flames. Water mist suppresses fire through four key mechanisms, namely; gas phase cooling, oxygen dilution, fuel surface cooling and radiation attenuation. The purpose of this study is to examine the contributions of thermal cooling and oxygen dilution effects in the suppression of the flame sheet temperature of a small methanol pool flame.

The key component of the experimental setup is a modified Wolfhard - Parker burner where the fuel slot is 75mm long, 10mm wide and 150mm deep [2]. The methanol level in the fuel slot is kept constant using the Navy Research Laboratory's self-leveling mechanism described in [3].The burner has two identical oxidizer channels 82mm long, 35mm wide and 150mm deep on each side. Beside each oxidizer channel is the mist generation chamber, where mist is generated with commercial low flow Delavan ® nozzles. A fraction of the mist generated in this chamber is entrained into the air stream through a slot on the air channel. The characteristics of the droplets are measured as they exit from the burner. The flame temperature is mapped with a 50μm diameter fine platinum/platinum - 13%- rhodium thermocouple which can be moved around in the flame domain with a computer controlled Newport 3D positioning instrument. Thermal images of the flames were also obtained using Agema Thermovision ® 870.

A simple analysis was performed to provide estimates of the upper bound on the suppression in flame sheet temperature when small quantities of suppressants (far from extinction) are used. The results of both theory and experiments are summarized in figure 1 in terms of degree of suppression in flame sheet temperature. Experiments were conducted with nitrogen and with water mist as suppressants. Water mist absorbs latent heat from the flame as it evaporates to form steam. Steam dilutes oxygen concentration as well as absorbs sensible heat since its heat capacity is about twice that of air. Nitrogen, on the other hand, has only oxygen dilution effect since its heat capacity is about equal to that of air.

In Figure 1, the mist curve reveals the effects of latent heat, sensible heat and oxygen dilution while the nitrogen curve reveals the effects of oxygen dilution only. By considering the mist curve and the nitrogen curve in Figure 1, one can deduce (based on the suppression in flame sheet temperatures) that thermal cooling effects of water mist on small liquid pool flames are very significant. The results presented above are for small size water mist (sauter mean diameters between 30μm and 70μm).

References

1 Hanauska, C.P and Back, G.G, "Halon alternative Fire protection systems, An overview of water mist fire suppression system technology", Hughes Associate Inc. Columbia , MD. 1993.

2. Ndubizu, C.C; Ananth R.; Tatem, P.A and Motevalli, V "On Water Mist Suppression Mechanisms in a gaseous Diffusion Flame"; *Fire Safety Journal* (In press)

3. Tatem, P.A; Williams, F.W; Ndubizu, C.C and Ramaker D. *Comb. Sci. and Tech.* 45 pp185 (1986)

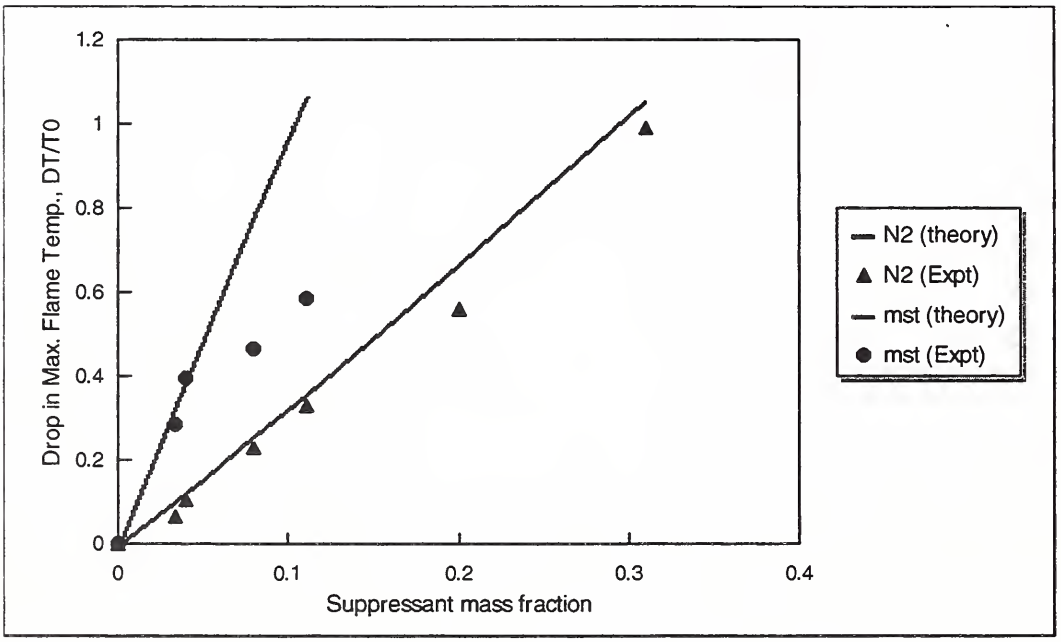

Figure 1: Degree of suppression in Maximum Flame temperature versus suppressant mass fraction, T_0 = 338 K

Water Mist Suppression of Fires in Underground Diesel Fuel Storage Areas

by

Alex C. Smith and Charles P. Lazzara
National Institute for Occupational Safety and Health
Pittsburgh Research Laboratory

Introduction

A fire risk associated with mobile diesel-powered equipment in underground mines is the storage and transfer of large quantities of diesel fuel in underground storage areas. Research by the Pittsburgh Research Laboratory (PRL) and others has shown that water mist technology, developed as a replacement for above ground halon extinguishing systems, may be applicable for fighting diesel fuel fires. The National Institute for Occupational Safety and Health/PRL is investigating the application of this technology for controlling and extinguishing fires in underground diesel fuel storage areas in order to develop design criteria for the use of these systems in underground mines. A large-scale fire suppression test facility was constructed to simulate an underground fuel storage area. Experiments were conducted to determine the relationship between the extinguishing effectiveness of water mist and the drop size and distribution and the location, geometry, and size of the fire for restricted diesel fuel fires.

Large-Scale Fire Suppression Facility

A large-scale fire suppression facility (FSF) was constructed to simulate an underground diesel fuel storage area. The Code of Federal Regulations, Part 75.1903 requires that permanent underground diesel fuel storage facilities be constructed of noncombustible materials and ventilated with intake air. The areas must be provided with self-closing doors and an automatic fire suppression system that initiates the means for closing of the doors. Typically, these areas are located off a main mine entry in a crosscut that is isolated from the adjacent entries by a permanent-type mine stopping. The main entry of the FSF is 153-ft long and the crosscut is 40-ft-long. Each entry is 18-ft-wide and 7-ft-high. Self-closing doors are located in the main entry, 30 ft from the crosscut. The storage area is fire-proofed and instrumented with thermocouples, gas monitoring instrumentation, and video equipment to monitor the fire tests in progress. The FSF is equipped with a closed water system in which the water is collected, filtered, and reused. The system has a 2,000 gal capacity with a pump that can provide a flow of 100 gal/min at 175 psi.

Experimental Procedure

To conduct the extinguishment experiments, the water mist nozzles were installed in the crosscut area in accordance with manufacturers specifications to ensure total water spray coverage of the area. The fires were contained in either 3-ft by 3-ft by 0.5-ft or 5-ft by 7-ft by 0.5-ft metal trays producing fire sizes of about 0.5 or 2.0 MW, respectively. Five gallons of low sulfur diesel fuel were used in each experiment. The fires were ignited and allowed to burn for 1 minute before the water mist suppression system was turned on. Depending on the parameter under study, the tray fires were located either directly under a nozzle in the center of the entry, geometrically centered between nozzles in the center of the entry, against the wall between two nozzles, or in the corner of the crosscut against the permanent stopping. The tray fires were monitored using 5 Type K thermocouples mounted just above the fuel and were considered extinguished when all 5 thermocouples showed temperatures below 30° C and the fire did not

reignite when the water mist was turned off. Temperatures were also recorded at each nozzle, along the center-line of the roof, in the cross-sectional area of the crosscut, and on the permanent stopping.

Experimental Results

Droplet size: To determine the relationship between droplet size and extinguishing effectiveness, experiments were conducted with 0.5 and 2.0 MW fires at 4 different locations; in the center of the crosscut, either directly under a nozzle or between nozzles, against the wall, or in the corner. Similar type nozzles were used that produced droplet sizes ranging from 200 to 800 μm. Droplet size or droplet diameter refer to the $Dv_{0.9}$ of the nozzle, defined as 90 pct of the droplets being less than the droplet diameter specified. The results indicated that the extinguishing effectiveness of the water mist decreased with increasing droplet diameter, independent of fire location. At droplet diameters above 500 μm, there appeared to be a change in the effectiveness of the water mist resulting in longer times to extinguishment.

Pressure and flow rate: Experiments were conducted at different water system pressures and flow rates, using the same nozzle, fire size, and fire location, to determine if water pressure or flow rate had an effect on extinguishment. In tests with droplet diameters less than 500 μm, no effect of pressure was observed. However, in tests with droplet diameters greater than 500 μm, the mist was more effective at higher water pressures. This is probably due to the generation of a larger number of smaller droplets at higher pressures, even though the $Dv_{0.9}$ is greater than 500 μm. The results of the flow rate experiments showed a slight increase in the time to extinguish the fires a flow rate increased.

Nozzle type: Two different types of water mist nozzles, spiral and impingement, were evaluated. Spiral nozzles produce a conical shaped water distribution pattern, with the larger droplets forming the outer edge of the cone, while the impingement nozzles produce a more even droplet size distribution pattern. In experiments with droplet diameters less than 300 μm, no difference was observed in the extinguishing effectiveness of the two types of nozzles. Impingement-type nozzles producing droplet diameters greater than 300 μm were not available.

Fire location: To evaluate the effect of fire location on extinguishment effectiveness, tests were conducted with the same nozzles, flow rate, and pressure conditions on fires located directly under a nozzle, geometrically between the nozzles, against a rib, and in the corner of the crosscut against the rib and permanent stopping. For droplet sizes less than 400 μm, no effect was seen. As the droplet sizes increased from 400 to 800 μm, the water mist was less effective in extinguishing the wall and corner fires.

Fire size: Experiments were conducted on 0.5 and 2.0 MW fires using droplet sizes ranging from 200 to 800 μm to evaluate the effect of fire size on extinguishing effectiveness over a wide range of droplet sizes. In tests with water mists less than 500 μm, no effect was observed. In the tests with the larger droplet sizes, the smaller fires were more difficult to extinguish.

Conclusions

A large-scale fire suppression facility was constructed to simulate an underground diesel fuel storage area. Experiments were conducted to determine the relationship between the extinguishing effectiveness of water mist and the droplet size and distribution and the location, geometry, and size of the fire for restricted diesel fuel fires. The results indicated that the extinguishing effectiveness of the water mist decreased with increasing droplet diameter. The optimum droplet size was between 200 and 400 μm, independent of pressure, flow rate, nozzle type, fire location, and fire size.

Submitted to the Annual Conference on Fire Research, NIST, November 2-5, 1998

A DISPERSED LIQUID AGENT FIRE SUPPRESSION SCREENING METHOD[1]

Jiann C. Yang, Michelle K. Donnelly, Nikki C. Privé, and William L. Grosshandler

Building and Fire Research Laboratory
National Institute of Standards and Technology
Gaithersburg, Maryland 20899

ABSTRACT

The recent ban on halon 1301 (CF_3Br) production (as a result of its ozone depleting potential) has resulted in an extensive search for replacements and alternatives. The applications of fire suppression efficiency screening methods constitute an important aspect of this search process because good screening methods can facilitate the identification, comparison, and selection of potential candidates for halon replacement. Most of the current methods for fire suppression efficiency screening (e.g., cup burners) are designed for evaluating fire suppressant agents that can be delivered in the form of vapor. Potential uses of liquid agents as replacements have been recently proposed in several applications (*e.g.*, shipboard machinery spaces, engine compartments in armored vehicles). Therefore, there is a need for the development of a reliable screening method for liquid agents that can be delivered in droplet form. The objective of our work is to design, construct, and demonstrate a laboratory-scale apparatus to screen liquid agents in a well-controlled experimental setting.

There are two major elements in the apparatus: (1) a burner and (2) a droplet generator. Several design parameters for these two elements have been carefully considered. The burner should be versatile enough to accommodate the screening of liquid and gaseous agents as well as solid particulates (with the addition of a powder delivery system), if possible. A counterflow cylindrical burner is selected. This type of burner has been extensively used in the past to characterize flame extinction and suppression using inert gases, halons, and powders (sodium bicarbonate and Purple K) due to the ease of maintaining a stable flame over a wide range of fuel and oxidizer flows and the ease of introducing condensed phase materials in the carrier (oxidizer) stream. The burner, which is replaceable and is made of sintered stainless steel and water-cooled, is located across the test section of a vertical wind tunnel. Air is supplied to the tunnel via a frequency-controlled blower and a series of flow straighteners. Propane is used as fuel.

Since some potential new liquid agents may only be synthesized and available in minute quantity, the application of a commercial spray may not be ideal or feasible to perform a test. In addition, the fan-out of a spray due to its angle could cause collision of droplets with the wind tunnel wall. Therefore, a droplet generator is specifically designed and used in the proposed screening in lieu of a spray because all the droplets can be directed to the flame zone, thus minimizing droplet loss to the wall of the wind tunnel. A piezoelectric droplet generator is used to create liquid droplets (< 150 μm) from controlled breakup of jets emerging from a sapphire orifice. The droplet generator consists of a liquid chamber which is connected to a reservoir, a bleed port (for eliminating any air bubbles trapped inside the chamber during priming), a 25 μm sapphire orifice mounted on a set screw, and a piezoelectric transducer. The droplet generator is located in the settling chamber and is approximately 42 cm upstream of the burner. The presence of the droplet generator in the wind tunnel does not create any significant perturbation or blockage effect on the oxidizer flow field near the burner. The air stream in the wind tunnel facilitates the dispersion of the single droplet stream into a small droplet cloud. By adjusting the location of the droplet generator with respect to the burner, droplet loss to the wind tunnel walls can be eliminated or minimized because the resulting dispersed droplet cloud is confined to a very narrow region near the burner.

[1] Supported by DoD/SERDP/NGP

The stability limits, which delineate the operating modes (enveloped and wake flames) of the burner, were constructed using various fuel and oxidizer flows. The stability envelopes compared favorably with those reported in the literature. The screening apparatus was first characterized using inert gases (argon, helium, and nitrogen), which were gradually added in the oxidizer stream until extinction occurred. The relative fire suppression efficiency ranking of these three gases was found to be commensurate with that from cup-burner tests. In all the experiments, extinction is defined as the conditions when blow-off occurs (an abrupt transition from a stable enveloped flame to a wake flame). For liquid droplet experiments, water was used as a representative liquid suppressant to evaluate the feasibility of using such a burner for screening liquid agents. Extinction tests were performed by gradually increasing the air flow until blow-off occurred at a fixed water flow. Figure 1 shows the mass fraction of water added as a function of $2V_O/R$ at blow-off, where V_O is the velocity of air and R is the radius of the burner. As shown in the figure, it is easier to blow-off the flame with water droplet addition than without. For low water droplet mass loading, higher air flow is required to cause blow-off. The effect of water became more pronounced when its application rate was increased. Suppression experiments using water with and without nitrogen dilution in the air stream were also performed. The combined effect of nitrogen and water on blow-off is illustrated in Figure 2. With water addition, the blow-off stagnation velocity gradient ($2V_O/R$) is higher than that with air diluted with nitrogen. For a given nitrogen dilution, the blow-off velocity gradient without water application is higher than that with water.

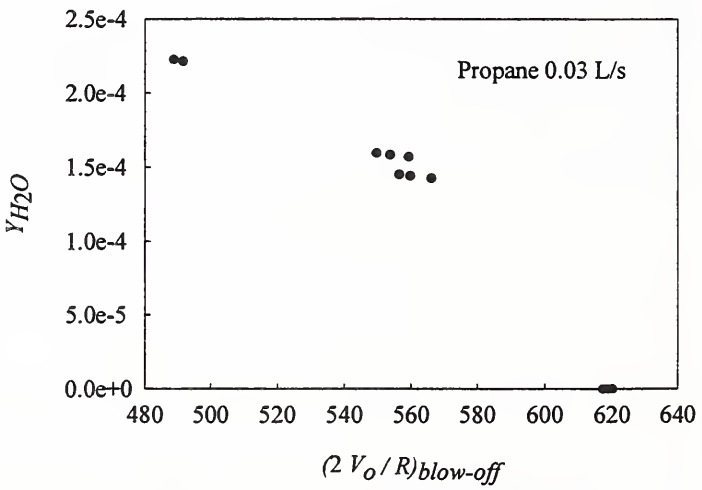

Figure 1. Mass fraction of water added in air as a function of stagnation velocity gradient at blow-off.

Future work will involve the refinement of the methodology. The droplet sizes and number densities at various locations near the burner forward stagnation point are currently being measured by using a Phase Doppler Particle Analyzer (PDPA) in order to assess the uniformity of the droplet size and number density. Such information is needed to better understand the performance of the droplet generator. Potential liquid suppressants that are of interest, including water with additive(s) (*e.g.*, aqueous potassium acetate or lactate solutions), will be evaluated because these fluids have been found in preliminary testing to exhibit better fire suppression effectiveness than pure water.

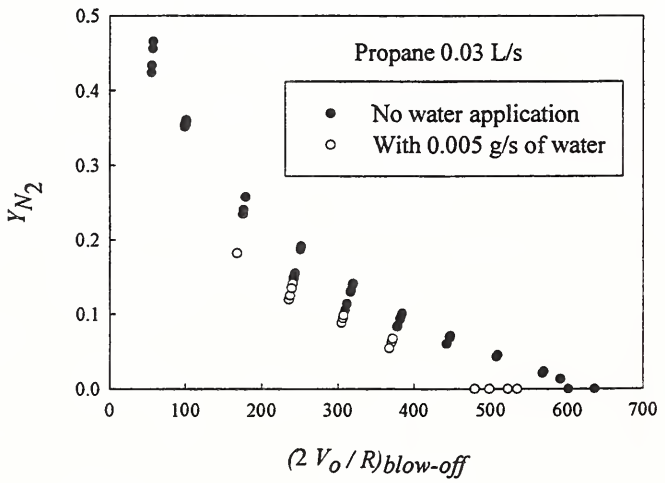

Figure 2. Mass fraction of nitrogen added in air with and without water application as a function of stagnation velocity gradient at blow-off.

TRANSIENT AGENT, RECIRCULATING POOL FIRE (TARPF) SUPPRESSION SCREEN[1]

W.L. Grosshandler, A. Hamins, K. McGrattan and C. Presser

National Institute of Standards and Technology
Gaithersburg, Maryland 20899 U.S.A.

The amount of a gaseous agent required to extinguish fires in full-scale engine nacelle tests varies greatly with the geometry of the fixture and the manner in which the flame is stabilized. It has been observed that if the test is designed to allow fuel to collect behind obstacles in the vicinity of a hot surface, a significantly higher mass of agent is necessary for sustained suppression. The superior performance of chemically acting agents such as CF_3Br and CF_3I relative to a hydrofluorocarbon alternative like HFC-125 is also accentuated in some of these tests. Full-scale testing carried out by the Navy using two different fixtures, each meant to simulate fires in the F/A-18 engine nacelle, has led to different conclusions regarding the amount and relative performance of both HFC-125 and solid propellant gas generator (SPGG) fire suppressants.

The complexity and unpredictability of full-scale tests can be traced to two factors: flame stabilization, and agent mixing. Flame stability is governed by local geometry, surface temperature, and fuel and air flow patterns. Flame extinction will occur if the agent is entrained into the flame zone in sufficient concentration, if the fuel and air flows are disrupted enough by the agent discharge process, or by a combination of the two effects. Entrainment and localized flame stretch are, in turn, controlled by the way the fire suppression system is designed and by the location of the fire relative to the discharge nozzle.

Hirst and Sutton [1] developed a wind tunnel to explore the impact of step height, air flow, and pressure on the blow-out of a jet fuel pool fire stabilized behind a backward facing step. Hirst et al. [2] studied the suppression of these types of fires using various halons, and concluded that a liquid pool burning in a flow behind an obstacle is the most difficult fire to extinguish. This was born out in full-scale tests done later [3]. Experiments by Hamins et al. [4], in cooperation with Walter-Kidde Aerospace, were conducted in a wind tunnel scaled down from the earlier work by Hirst to examine the performance of HFC-125 and HFC-227ea. Research is currently underway at the Air Force Research Laboratory [5] to identify the detailed structure of a flame stabilized by an obstruction in a 0.15 m cross-section laboratory wind tunnel. They are measuring the velocity field and OH levels for a methane pool fire with obstructions of various geometry.

The turbulent spray burner was designed [6] to simulate an engine nacelle spray fire resulting from a ruptured fuel line. This apparatus provides better control of the agent discharge and mixing process than the baffle-stabilized fire test fixtures described above, and can better simulate the discharge of an SPGG with less disruption to the incoming air. The turbulent spray burner can be used with both gaseous and powdered agents. Hamins et al. [4] redesigned the burner to include a heated disk in the center of the flow downstream of the fuel nozzle. They showed that the concentration of nitrogen necessary to extinguish a turbulent propane flame increased substantially with surface temperature. The same trend, but to a lesser degree, was observed with HFCs.

The transient agent, recirculating pool fire (TARPF) suppression screen extends the capabilities of the turbulent spray burner, and combines with it the desirable attributes of the baffle-stabilized pool fire test facility. That is, it reproduces the most difficult fire situation and allows control of critical agent discharge parameters, including discharge rate, duration and air flow. The performance of powders and gases can be examined, and the relation between the suppression duration and the temperature and location of a hot surface can be explored.

The ability to determine the relative effectiveness of alternative agents is key to the development of new fire suppression systems. The Next Generation Program (NGP) has the goal of identifying agents that are as effective as CF_3Br in suppressing fires in spaces currently protected with the halon. The physical and chemical properties, and the manner of storage and release, of these next generation suppression systems may be quite unlike halon, but their effectiveness must be bench-marked against CF_3Br. The TARPF facility will provide the means to screen new concepts in the laboratory for applications in engine nacelles and other spaces involving baffle-stabilized pool fires with adjacent hot surfaces.

---

[1] Supported by Next Generation Program, through SERDP

Schematic diagram of the Transient Agent Recirculating Pool Fire (TARPF) suppression screen

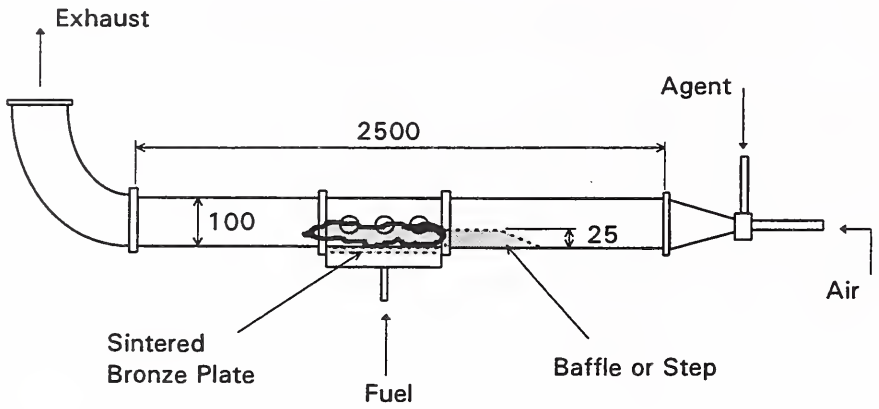

A sketch of the TARPF flow tunnel is shown in the figure. The main portion is about 2.5 m long with a square cross-section 92 mm on a side. Air, supplied by a compressor rated for a maximum flow of about 180 g/s at 1.0 MPa, can be delivered to the tunnel at nominal speeds up to 16 m/s. A heater is available to increase the inlet air temperature to above 200 °C. A porous bronze burner, 92 mm wide by 190 mm long, is located on thefloor of the tunnel test section. Propane is the current fuel, but plans include the capability to burn JP-8. Heat release rates up to about 20 kW are anticipated. A stainless steel baffle, 25 mm high, is located upstream of the burner. A ramp can also be inserted to form a backward-facing step. An electric strip heater about 25 mm by 87 mm is designed to simulate a hot surface reignition point, and should produce average surface temperatures up to 650 °C. It can be placed in the air flow either ahead of or behind the burner, at a position where the JP-8 can be sure to impinge.

The agent is injected downstream of the air metering orifice. Since the flow is choked in the metering orifice plate, the introduction of the agent can be accomplished without altering the total air flow. Mixing of the agent with the air is facilitated by injecting the agent radially from opposite directions into the reduced diameter entrance region. The distance between the injection ports and the pool fire, about one meter, is a compromise between the desire for uniform mixing in the cross-stream direction and plug flow in the stream-wise direction. A pressure vessel is used to store the gaseous agent to be tested. The discharge rate and duration are controlled by the initial agent pressure and an electronically actuated solenoid valve. Powders with physical properties similar to sodium bicarbonate will be injected by pressurizing the vessel with nitrogen and entraining a measured amount of the powder placed in a tee at the entrance to the injection port, as done previously in the turbulent spray burner. The TARPF facility is designed to handle new propellant formulations for SPGG suppressants in quantities of about one gram. It may be possible to evaluate SPGGs of considerably higher mass (if safety can be assured) by designing a pre-discharge chamber to handle the bulk of the effluent, and bleeding a small amount of the combustion products (including particulate) into the tunnel.

[1] Hirst, R. and Sutton, D., *Combust. Flame*, **5**, 319-330 (1961)
[2] Hirst, R., Farenden, P.J., and Simmons, R.F., *Fire Technology 12*, 266 (1976)
[3] Hirst, R., Farenden, P.J., and Simmons, R.F., *Fire Technology 13*, 59 (1977)
[4] Hamins, A., Cleary, T., Borthwick, P., Gorchov, N., McGrattan, K., Forney, G., Grosshandler, W., Presser, C., and Melton, L., "Suppression of Engine Nacelle Fires," chap. 9 in *Fire Suppression System Performance of Alternative Agents in Aircraft Engine and Dry Bay Laboratory Simulations*, NIST SP 890: Vol. II, Gann, R.G. (ed.), U.S. Department of Commerce, Washington, DC, November 1995
[5] Takahashi, F., Schmoll, W.J., and Belovich, V.M., "Extinction of Bluff-body Stabilized Diffusion Flames," Proceedings, 1998 Technical Meeting of the Central States Section of the Combustion Institute.
[6] Hamins, A., Gmurczyk, G., Grosshandler, W., Rehwoldt, R., Vasquez, I., Cleary, T., Presser, C., and Seshadri, K., "Flame Suppression Effectiveness," section 4 in *Evaluation of Alternative In-flight Fire Suppressants for Full-scale Testing in Simulated Aircraft Engine Nacelles and Dry Bays*, NIST SP 861, Grosshandler, W., Gann, R., and Pitts, W. (eds.), U.S. Dept. of Commerce, Washington, DC, April 1994.

AN EXPERIMENTAL AND THEORETICAL INVESTIGATION ON FLAME EXTINCTION BY SODIUM BICARBONATE PARTICLES

H.K. Chelliah, R.H. Krauss, A.M. Lentati and H. Zhou
Department of Mechanical, Aerospace and Nuclear Engineering
University of Virginia, Charlottesville, VA 22903

Introduction

A steady, laminar, nonpremixed flame, established within the mixing layer of a counterflow of methane and air, is used here to quantify the rate-controlling physical, thermal and chemical contributions of sodium bicarbonate particles on flame extinction. The basic understanding obtained from this effort is expected to benefit development of enhanced condensed-phase fire suppressants. A brief description of the present experimental and theoretical/computational efforts and recent results are given below.

Experiments

An enclosed counterflow burner, designed with Pyrex coannular nozzles with nitrogen co-flow on both fuel and air side is used in the present experimental study. The particles are introduced with the air stream. The Pyrex tubes allow for ease of fabrication, and more importantly, for viewing of particle motion through the tubes. The fuel used is methane (99.99% pure, BOC) and air is supplied from an oil free compressor with moisture removed by passing through a drier. Once ignited, very stable diffusion flames with and without particles can be established in the enclosed burner for extended periods of time (Krauss et al. 1998).

Considerable attention has been devoted to the development of a particle seeder that can deliver steady feed rates of particles of various sizes (i.e. from 0 to 100 μm). The design selected is a positive feed auger system consisting of a Teflon screw in a high-precision stainless steel tube where the screw is driven by speed-locked variable speed motor, as illustrated in Fig. 1. The seeder is vibrated by a pneumatic system to assist the particle flow, but the particle feed rate is primarily controlled by the motor rpm. Part of the total air flow is diverted through the particle seeder and is then mixed with the remaining air prior to exiting through the air nozzle. The particle feed rate is continuously monitored using a Mie scattering detection system located at the exit of the seeder air. The actual mass fraction of the particles in the air stream is determined by calibrating the recorded scattering signal by a separate gravimetric analysis, either before or after each experiment.

In counterflow flame experiments, the extinction flow strain rate (which is related to the axial velocity gradient along the axis of symmetry) is typically reported based on the (a) global strain rate formula derived by Seshadri and Williams (1978) under a set of simplifying assumptions or (b) local velocity measurements along the axis of symmetry using LDV. The former requires information regarding the nozzle exit velocities of the fuel and air streams and the nozzle separation distance. In this work, most of the reported extinction strain rates are based on the global formula, but for comparison the locally measured flow strain rate obtained with a LDV system operating forward scattering mode is used.

Numerical Calculations

Based on a hybrid Eulerian-Lagrangian formulation for the gas and the condensed phase, a numerical model was recently developed to describe the interaction of fine-water droplets with counterflow nonpremixed flames (Lentati and Chelliah, 1998). This model is extended here to predict the flame extinction phenomena by sodium bicarbonate particles and the preliminary results with a global particle decomposition model is presented. Such theoretical approaches, once validated, can provide detailed information about the rate controlling physical, thermal and chemical effects of sodium bicarbonate particles.

Results and Discussion

Previous counterflow experiments with fine sodium bicarbonate particles have indicated a nonmonotonic variation in their effectiveness (Hamins et al.1994). The present results, however, do not indicate such

non-intuitive trends as the particle size is decreased. Figure 2 shows a monotonic variation of sodium bicarbonate mass fraction in air plotted as a function of the extinction strain, for three different particle size groups. As the particle size decreases below 20 μm, the particle feed rate becomes rather unsteady and the quantitative values of measured flame extinction strain rate can be unreliable. However, qualitatively, the experimental results for particles below 20 μm indicate a similar monotonic increase in the effectiveness with decreasing particle size, which contradicts the previous data reported by Hamins et al. (1994).

In numerical predictions of flame extinction by sodium bicarbonate particles, a global model for particle decomposition of the form $2NaHCO_3 \rightarrow 2NaOH + 2CO_2$ is employed here, with the associated physical, thermal and chemical effects. Although such a global model can be fine tuned to a very narrow range of conditions, eg. for a narrow particle size range, it should be cautioned that extension of such models to a wider range of conditions may lead to physically unrealistic results. For the homogeneous chemistry associated with NaOH, a detailed reaction model involving 6 species in 20 elementary reactions is used here, in conjunction with the detailed chemistry model for methane oxidation (Lentati and Chelliah, 1998). Figure 3 shows a plot of the predicted variation of peak flame temperature as a function of flow strain rate (up to extinction), for selected particle sizes. The results clearly indicate that as the particle size is decreased, the effect on flame extinction strain rate increases rapidly. These results are qualitatively consistent with experiments, but more comprehensive modelling of the particle heating, heterogeneous and homogeneous decomposition mechanisms must be addressed before any quantitative comparisons are made. Such efforts are currently underway and are expected to provide valuable information in future development of enhanced condensed-phase fire suppressants.

Acknowledgment: This work is supported by National Institute of Standards and Technology, with Dr. W. L. Grosshandler serving as the scientific officer.

[1] Hamins, A., Gmurczyk, G., Grosshandler, W., Presser, C., and Seshadri, K., "Flame Suppression Effectiveness," in NIST SP-861 (1994).
[2] Krauss, R.H., Zhou, H., Fallon, G., and Chelliah, H.K., in preparation.
[3] Lentati, A.M. and Chelliah, H.K., *Combust. and Flame* **115**:158-179 (1998).
[4] Seshadri, K. and Williams, F.A., *Int. J. Heat Mass Transfer* **21**: 251-253 (1978).

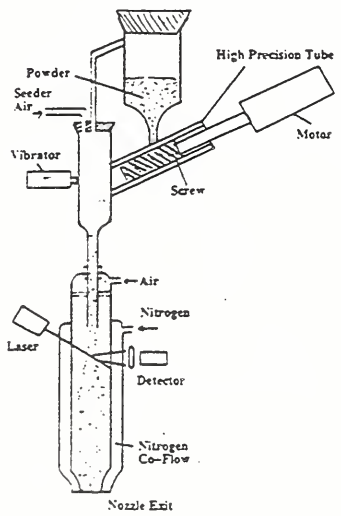

Figure 1: A schematic of the particle seeder.

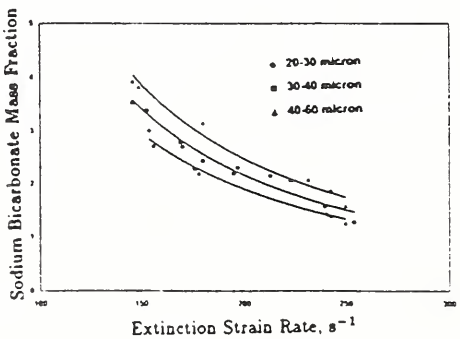

Figure 2: Measured particle mass fraction vs. global extinction strain rate, for three different size groups.

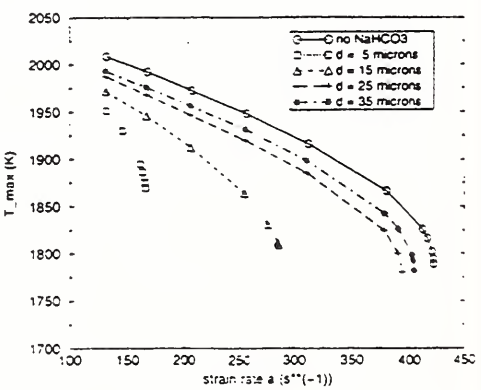

Figure 3: Predicted variation of peak flame temperature as a function of strain rate, for various particle sizes.

Submitted to the Annual Conference on Fire Research, November 2-5, 1998

PARTICLE MEASUREMENTS IN $Fe(CO)_5$-INHIBITED FLAMES

Marc D. Rumminger and Gregory T. Linteris
Fire Science Division
Building and Fire Research Laboratory
National Institute of Standards and Technology, Gaithersburg MD 20899, USA

Introduction

Since iron pentacarbonyl ($Fe(CO)_5$) is among the most efficient flame inhibitors ever identified [1-4], research on flame inhibition by $Fe(CO)_5$ was recently started at NIST with the goal of understanding its mechanism [5]. Obtaining a detailed understanding of this super-effective chemical inhibitor will provide insights and approaches useful for development of the next generation of fire suppressants to replace the ozone-depleting suppressant CF_3Br. Our approach has been to use simple laboratory burners (premixed Bunsen-type flames and counterflow diffusion flames) to obtain global, yet fundamental, information on the action of $Fe(CO)_5$. The burning velocity and extinction strain rate, which provide a measure of the overall reaction rate, are determined with addition of $Fe(CO)_5$, while varying the stoichiometry, oxygen mole fraction, flame temperature, and flame location. Together with numerical modeling and kinetic model development, these data allow interpretation of the detailed chemical mechanism [6].

In previous research, we have shown that in premixed $CH_4/O_2/N_2$ flames, behavior at low and high $Fe(CO)_5$ mole fractions is distinctly different: at low $Fe(CO)_5$ mole fraction the burning velocity is strongly dependent on inhibitor mole fraction, whereas at high $Fe(CO)_5$ mole fraction, the burning velocity is nearly independent of inhibitor mole fraction. The behavior in counterflow diffusion flames is similar in that the inhibition effect becomes weaker as the mole fraction of agent increases (although it does not go to zero as in the premixed flames). A critical part of the research on $Fe(CO)_5$ is to understand iron pentacarbonyl's diminishing effectiveness at high mole fraction in order to avoid similar behavior in future fire suppressants. In recent work [5,6], it has been postulated that the diminished effectiveness of $Fe(CO)_5$ is due to loss of the active gas-phase iron species to the much less active condensed-phase compounds. The present work presents preliminary data on the light scattered by particles in premixed methane-air flames inhibited by iron pentacarbonyl.

Experiment

The premixed burner used for the data presented here has been described previously [7]. The laser scattering and extinction system consists of a laser; three detectors for the reference, extinction, and scattering signals; associated optics and a chopper; and lock-in amplifiers. A 3 W argon-ion laser provides a polarized beam at 488 nm, which is mechanically chopped at 1000 Hz. The burner is located in a chemical fume hood, and a polarization-preserving single-mode optical fiber brings the beam into the hood. After exiting the fiber, the beam is re-collimated to a diameter of approximately 2 mm, and passes through a polarizer to ensure near-complete vertical polarization, and a lens focuses the beam to a waist of approximately 0.1 mm. The transmitted power of the beam traversing the flame is measured using a silicon photodiode with neutral density, opal glass, and laser-line filters placed in front of the detector. The detection system for light scattered normal to the laser beam consists of a circular aperture, collection lens, pinhole aperture, laser-line filter, and 1P28 photomultiplier tube (PMT); the imaged control volume is about 1 mm in length. The reference signal also uses a 1P28 PMT, with a neutral density filter, a laser line filter, and opal glass. The signal from each photomultiplier tube is pre-amplified before entering a lock-in amplifier, which is controlled by a PC. A data acquisition card in the PC records the output from the lock-ins during the experiments. Typically, 500 readings are recorded over a time of about 1 s.

Results

The extinction and scattering signals have been obtained as a function of position above the conical Bunsen-type flame with varying amounts of $Fe(CO)_5$ added to the reactants of a stoichiometric methane-air flame. The attenuation of the laser passing through the flame is small, less than 2% for all beam positions above the flame and inhibitor mole fractions up to 500 ppm. The scattering signal appears to increases rapidly for $Fe(CO)_5$ mole fractions above 100 ppm, indicating that the scattering cross section for 488 nm light increases rapidly under these conditions. This may correspond to the presence of particles, or of new species or clusters with large scattering cross sections, or it may correspond to the growth of existing particles. In future work, we will refine the extinction system to allow measurement of the small attenuation in the flames, so that equivalent spherical diameters and number densities can be obtained, and thermophoretic samples will be obtained.

Acknowledgments

We thank summer intern Nikki Prive for assistance with data acquisition programs.

References

[1] Bonne, U., Jost, W., and Wagner, H.G., *Fire Res. Abstracts Rev.* 4:6 (1962).

[2] Lask, G. and Wagner, H.G., *Eighth Symposium (International) on Combustion*, Williams and Wilkins Co., Baltimore, 1962, pp. 432-438.

[3] Vanpee, M. and Shirodkar, P., *Seventeenth Symposium (International) on Combustion*, The Combustion Institute, Pittsburgh, 1979, pp. 787-795.

[4] Miller, D.R., Evers, R.L., and Skinner, G.B., *Combust. Flame* 7:137 (1963).

[5] Reinelt, D. and Linteris, G.T., *26th Symposium (International) on Combustion*, The Combustion Institute, Pittsburgh, 1996, pp. 1421-1428.

[6] Rumminger, M.D., Reinelt, D., Babushok, V., and Linteris, G.T., *Combust. Flame* 116:207 (1999).

[7] Linteris, G.T. and Truett, L., *Combust. Flame* 106:15 (1996).

COMPUTED FLAMMABILITY LIMITS OF OPPOSED-JET $H_2/O_2/CO_2$ DIFFUSION FLAME AT LOW PRESSURE

Hasan Bedir, Hsin-Yi Shih and James S. T'ien*

Department of Mechanical and Aerospace Engineering
Case Western Reserve University
Cleveland, Ohio 44106, USA
Tel. 216-368-4581
Fax 216-368-6445
Email jst2@po.cwru.edu

Hydrogen and oxygen are gases involved in the proposed in-situ resource utilization (ISRU) scheme in the exploration of Mars. Hydrogen is not only a feedstock of methane production in the proposed Mars mission but also a propellant candidate in many propulsive systems. On the other hand, Carbon dioxide has been used as a fire extinguishment agent and is the main atmospheric component on Mars. Although many of the characteristics of hydrogen premixed or non-premixed flames are well known, their combustion behavior in the unique environments on Mars is beyond the current database. The unusual conditions include reduced gravity, very low pressure (about 0.01 earth atmospheric pressure) and CO_2 atmosphere (95.6%). To be able to determine the flammability of H_2/O_2 flame under this very low pressure condition as a function of the percentage of CO2 dilution has practical implication to fire fighting strategy for Mars operations. One notices that because of the scarcity of water on Mars, depressurization and the use of CO2 as an extinguishment agent are few of the options readily available.

In this work, a detailed numerical calculation of opposed-jet hydrogen and oxygen diffusion flames with varying amounts of CO_2 as diluent is carried out in this work. The numerical analysis utilizes the capability of the OPPDIF program to handle detailed chemical kinetics and transport. A narrow-band radiation model is coupled with this code in order to predict the extinction limits with improved accuracy. The flammability boundary of $H_2/O_2/CO_2$ system at a total pressure of 1.013 kPa is constructed in terms of stretch rate and the percentage of CO_2 dilution. Both the cases with and without the consideration of radiation are presented. Fig. 1 shows that the extinction limits could not be computed accurately without the consideration of radiation. At low stretch rate, the model without radiation actually produces the wrong trend. With radiation two branches of extinction, quenching and blow off, are obtained. At high stretch the flame blows off because of inadequate gas residence time and at low stretch the flame quenches due to the radiative heat loss. The merging point of these two branches defines a fundamental limit on CO2 dilution (64%) above which the system is not flammable at any stretch rate. Besides, the most flammable stretch rate is between 5 – 10 s^{-1}, a rather low value by ordinary standard.

The above calculation shows that at Martian pressure, hydrogen and oxygen can combust as a diffusion flame albeit in a narrower range of stretch rates in comparison with that in normal earth pressure. If such a flame occurs in a confinement, depressurization to Martian atmosphere alone

may not be adequate to extinguish the fire and additional application of carbon dioxide will be required. The computed maximum flame temperature with several levels of CO2 dilution is shown in Fig. 2. As expected, more dilution decreases the flame temperature and the flammable range. It should be pointed out ,however, that the fire suppression function of CO2 comes from the combination of thermal, chemical and radiative effects. With a detailed model such as the one we have, individual contribution can be sorted out. This application to the proposed Martian operation is just an example.

Acknowledgement

This research has been supported by NASA grant NAG3-1046

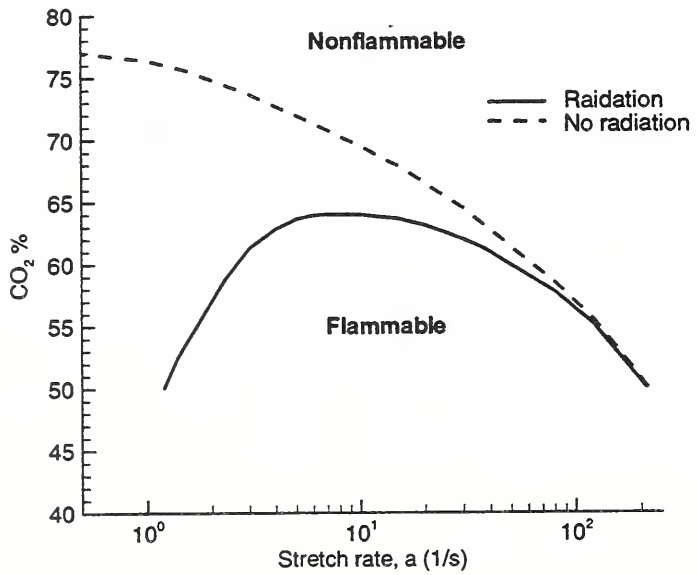

Figure 1. Flammability boundary of $H_2/O_2/CO_2$ opposed-jet diffusion flame with and without consideration of flame radiation. Total pressure, 1.013 kpa , ambient temperature , 300 K.

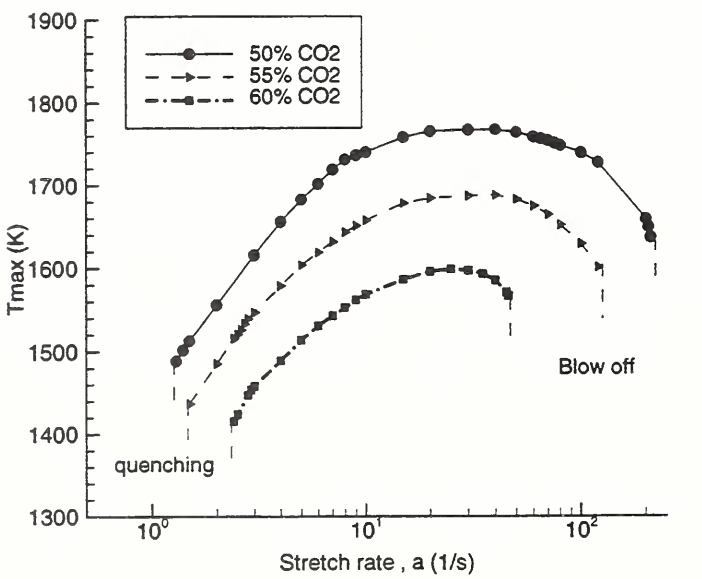

Figure 2. The maximum flame temperature as a function of stretch rate at different CO_2 dilution levels.

Intermediate Species Profiles in Low Pressure Methane/Oxygen Flames Inhibited by 2-H Heptafluoropropane: Comparison of Experimental Data with Kinetic Modeling

Bradley A. Williams, Drew M. L' Esperance*, and James W. Fleming

NAVAL RESEARCH LABORATORY
Navy Technology Center for Safety and Survivability
Combustion Dynamics Section, Code 6185, Washington, DC 20375-5342
(202) 404-6197, FAX (202) 767-1716
E-mail: brad@code6185.nrl.navy.mil; fleming@code6185.nrl.navy.mil

The U.S. Navy has selected 2-H heptafluoropropane (HFP, HFC-227ea) to replace Halon 1301 for some of its near term fire protection needs. HFP has a lower suppression efficiency compared to Halon 1301. It is important to understand the suppression behavior of this compound in order to optimize its performance. Of particular importance is the relative contribution of fluorine chemistry to suppression as opposed to the physical effects of the agent's addition to the flame.

A comprehensive mechanism for C_1 and C_2 fluorohydrocarbon agents has been developed at the U. S. National Institute of Standards and Technology (NIST) [1]. Recently, our laboratory has measured profiles of several intermediate species in premixed low-pressure methane/oxygen flames containing each of the fluoromethanes [2]. The experimental data were compared to predictions of the NIST fluorohydrocarbon mechanism with the C_1 hydrocarbon chemistry modeled using GRI-Mech [3]. Some refinements to the kinetics were suggested by this work on the basis of validation against the low pressure species profile data. Comparison of flame speed predictions of the modified mechanism to atmospheric pressure measurements indicate that the modifications do not substantially alter the mechanism's performance for stoichiometric to slightly fuel rich flames. Here we extend this work to include HFP inhibited flames.

For the present study, the experimental apparatus and procedures were identical to those used in our study on flames containing fluoromethanes [2]. We recorded profiles of H, OH, CH, CF, CF_2 and C.F., derived from LIF intensities, in 10 torr premixed flat flames of methane/oxygen (1:2 molar ratio) inhibited by 4% mole fraction of HFP. The previously reported flames contained the series of fluoromethanes at concentrations corresponding to the same fluorine loading as 4% HFP. All of the data were taken under the same conditions so that direct comparisons can be made on relative mole fractions of intermediate species produced from the different agents. The HFP flame data were not previously reported as a suitable C_3 fluorohydrocarbon kinetic mechanism was not available. Hynes *et al.* [4] have recently published a kinetic mechanism for the initial breakdown of HFP into C_1 and C_2 fragments. When added to the NIST HFC mechanism describing the subsequent chemistry of decomposition products, the HFP sub-mechanism permits kinetic modeling of the HFP-inhibited flame.

We compared the predictions of the HFP kinetic mechanism with our species profile data. The data for CF_2 is presented in Figure 1. Both the location and magnitude of this specie are well predicted by the Hynes et al. mechanism. Similar agreement was observed for the other species studied. We also compared the experimental profiles for the flame inhibited by HFP to data for flames containing CHF_3 and CH_2F_2 under the same conditions of stoichiometry and flux of fluorine atoms. Under these conditions, profiles of temperature and of H and OH mole fraction are identical between the flames containing HFP and CHF_3. The flame inhibited by HFP, however, is much more luminous than the flames containing the C_1 fluorohydrocarbons. The model points out that thermal decomposition, not

---

Supported by the U.S. Naval Sea System Command.

*National Research Council Postdoctoral Associate 1995-97. Present Address: Department of Physical Sciences, New Mexico Highlands University, Las Vegas, NM, 87701-4073

radical attack, dominates HFP destruction. This is in contrast to the conditions of Hynes *et al.* in a low temperature hydrogen/air flame where radical attack predominated.

REFERENCES

[1]. Current NIST HFC mechanism may be downloaded from "http://fluid.nist.gov/ckmech.html".

[2]. "Intermediate Species Profiles in Low Pressure Premixed Flames Inhibited by Fluoromethanes," L'Esperance, D.L., Williams, B.A., and Fleming, J.W., submitted to *Combust. Flame.*

[3]. Bowman, C. T., Hanson, R. K., Gardiner, W. C., Lissianski, V., Frenklach, M., Goldenberg, M., and Smith, G. P., GRI Report GRI-97/0020, 1997, Gas Research Institute, Chicago. http://www.ME.Berkeley.edu/gri_mech/

[4]. Hynes, R.G., Mackie, J.C., and Masri, A.R, *Combust. Flame* 113: 554-565 (1998).

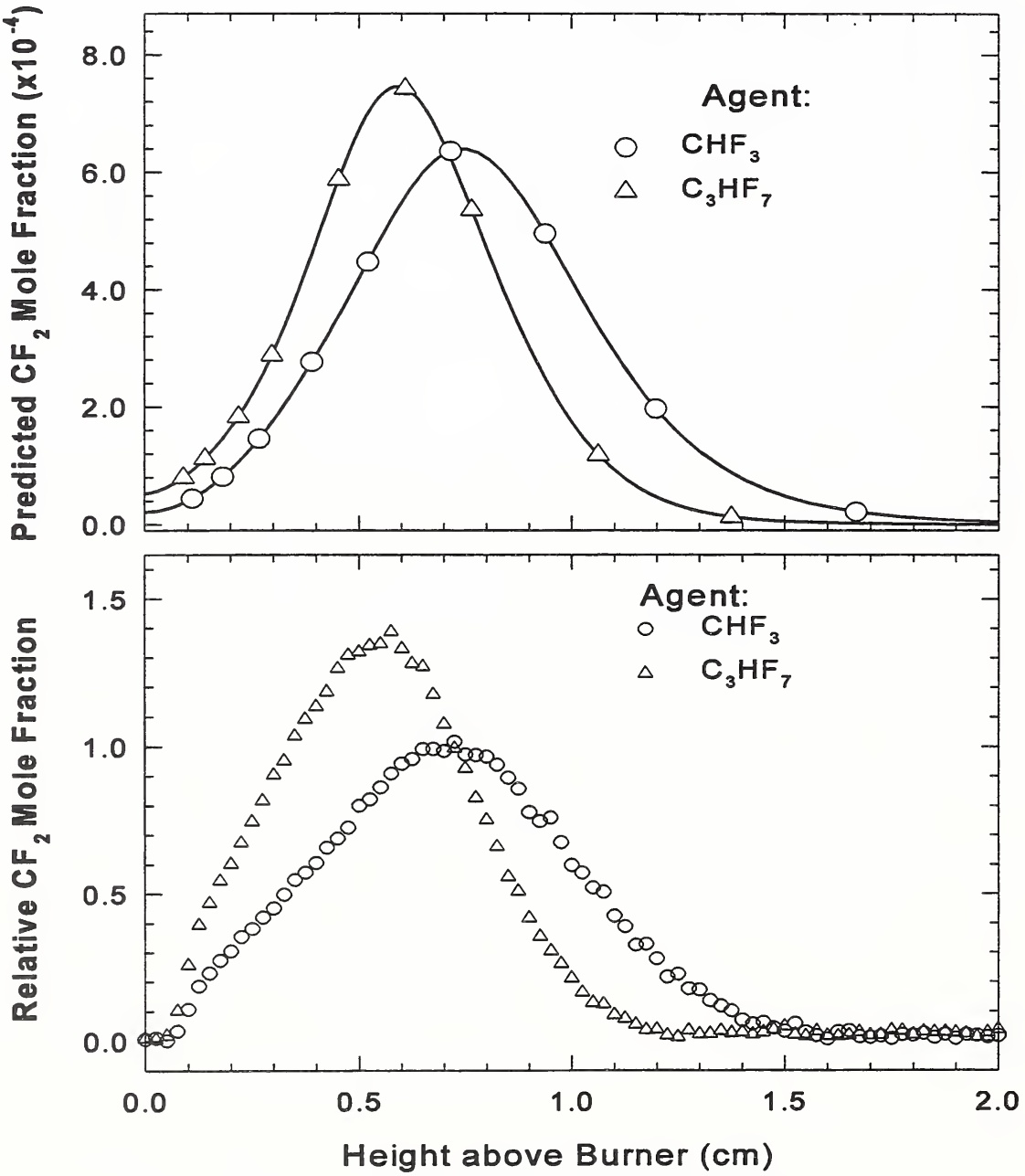

FIGURE 1. Calculated (top) and measured (bottom) profiles of CF_2 in a 10 Torr premixed CH_4/O_2 (1:2 mole ratio) flame containing 4% 2-H heptafluoropropane (triangles) or 8.9% CHF_3 (circles).

INHIBITION OF SILANE IGNITION BY IODINE CONTAINING ADDITIVES

V.Babushok, W.Tsang
National Institute of Standards and Technology
Gaithersburg, MD 20899

Silane is widely used in CVD processing in the semiconductor industry. The highly explosive nature of SiH4-O2 mixtures represents a serious safety problem. In this paper we report the results of numerical studies on the influence of iodine and hydrogen iodide additives on silane self-ignition limits. Previous studies of influence of different additives on silane combustion are summarized.

The kinetic model of silane combustion used in this work is based on previously suggested mechanisms for silane oxidation and pyrolysis. It is adjusted to fit recent experimental and theoretical studies for Si-containing species. The calculations are based on the Chemkin suite of programs.

The results of modeling show that the upper explosion limit of silane is determined by the balance of rates of a chain branching reaction ($SiH_3 + O_2$) and a termination process ($H + O_2 + M = HO_2 + M$). The critical pressure is proportional to the ratio of silane to oxygen concentration. The reactivity of the SiH_4-O_2 mixture increases monotonically with hydride content. Increase of the ratio SiH_4/O_2 at ambient conditions leads to chain ignition of silane mixtures. The experimentally observed violent explosion behavior of silane at ambient conditions is due to the very short ignition delay. In most cases ignition is observed during mixture preparation. With decrease of initial temperature (down to -100C) there might exist conditions for chain ignition for some local volume during mixture preparation. In spite of a very high value of a SiH_4/O_2 critical ratio and, correspondingly, low adiabatic temperature rises it is possible to expect that ignition will be observed for "favorable"(optimum) gradients of concentrations and ignition delay with decrease of initial temperature.

The analysis of the kinetic model demonstrates that the key radical intermediates are the same as those found in any hydrocarbon combustion system. Thus, the usual flame inhibitors should have similar inhibition effects. The consequence is that the hydrogen atoms and OH radicals generated from the chain-branching reaction of SiH_3+O_2 are removed and cannot attack silane. The results for the iodine system can be found in Fig.1. The axes are concentrations of silane and O_2 and we define a boundary between regions where self-ignition exists or fails to occur. The drastic effect of iodine addition is readily seen. The effect of increasing iodine is to continually squeeze the region where ignition can occur. The simulations show the very high sensitivity of the silane ignition limit to iodine additive at the ppm level. At concentrations above 200 ppm iodine and ambient conditions silane is no longer pyrophoric. Increasing initial temperature leads to the increased range of self-ignition and leads to the need to increase the concentration of additive for the same level of inhibition.

The modeling of hydrogen iodide influence shows that much more is needed in order to obtain the same effect as iodine itself. Hydrogen iodide is a less effective inhibitor and concentrations of a factor of 10 higher than those for iodine are required. The effectiveness of iodine in comparison with other inhibitors is associated with the weakness of an iodine bond. Bond energy of I_2 is of the order of 160 kJ/mol. In contrast, the H-I bond strength is of order of 300 kJ/mol while that of the Si-H bond is approximately 390 kJ/mol. The rate constant for $H+I_2$ reaction is very large and is, roughly, an order of magnitude greater than those of H atom reactions with other halogenated and nonhalogenated hydrocarbon additives at room temperature.

The critical conditions for chain ignition can be deduced using an abbreviated kinetic scheme.

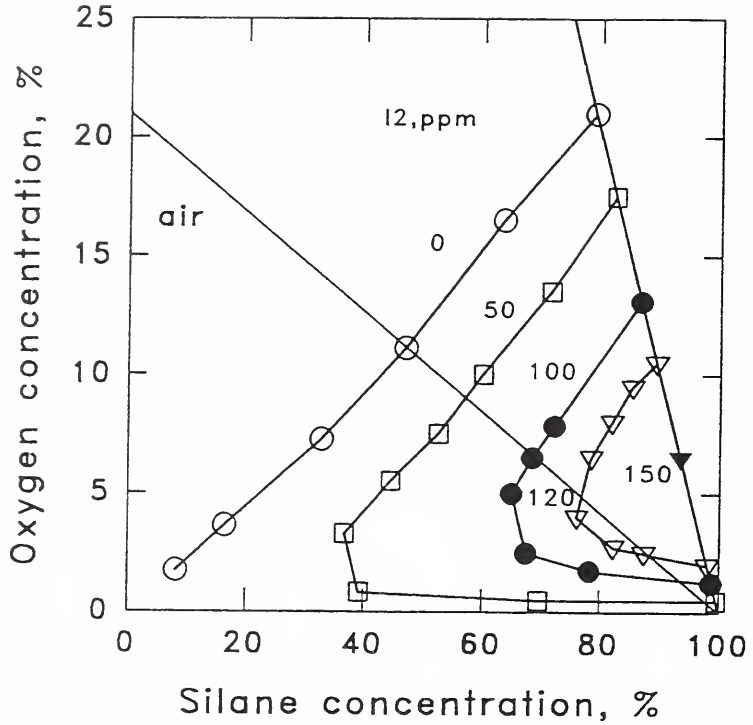

Figure 1. Self-ignition limits for silane/oxygen/nitrogen mixtures for various amounts of added iodine at 1 atm and 300 K.

The simplified mechanism is

$SiH_4 + O_2 = >SiH_3 + HO_2$ (0)
$SiH_3 + O_2 => H + H + SiOOH$ (1)
$SiH_3 + O_2 => SiH_2O + OH$ (2)
$SiH_3 + O_2 => HSiOOH + H$ (3)
$H + O_2 + M => HO_2 + M$ (4)
$SiH_4 + O => SiH_3 + OH$ (5)
$SiH_4 + H => SiH_3 + H_2$ (6)
$SiH_4 + OH => H_2O + SiH_3$ (7)
$SiH_3 + I_2 = SiH_3I + I$ (8)
$H + I_2 = HI + I$ (9)

The following relation for the critical pressure for the uninhibited upper explosion limit as a function of temperature and SiH_4 and O_2 concentrations is obtained

$$M = [K_1K_6/(K_4(K_1+K_3))]*(SiH_4/O_2) .$$

The formula shows that critical pressure depends on the ratio of silane and oxygen concentrations. The critical pressure for the upper explosion limit inhibited by I_2 is the following

$$M = [K_1K_6(SiH_4/O_2) - K_8K_6(I_2/O_2)]/[K_4(K_1 + K_3 + K_8(I_2/SiH_4))] - (K_9/K_4)(I_2/O_2) .$$

The analysis of this formula and simulation results show that there exist two critical values of the ratio of silane concentration to oxygen concentration (Fig.1).

The important result from this work is that pyrophoric properties of silane and inferentially other pyrophoric hydrides can be significantly changed through the use of quite small amounts of additives and this may well lead to reductions in hazards arising from the handling of such substances. This is because in many of these cases the key intermediates are the small inorganic radicals that play a key role in hydrocarbon combustion.

Clean Agent Performance on Fires Exposed to an External Energy Source

K. Steckler and W. Grosshandler
Building and Fire Research Laboratory
National Institute of Standards and Technology
Gaithersburg, MD USA

D. Smith and P. Rivers
3M Chemicals
St. Paul, Minnesota USA

ABSTRACT

Work carried out over the last several years has shown that there can be a significant increase in the amount of agent required to extinguish and to prevent re-ignition of fires that are exposed to a continuous, external, energy source. This has implications regarding the NFPA 2001 Standard on Clean Agent Fire Extinguishing Systems, which currently recommends that in the event of a Class C fire (i.e., fire involving electrical equipment) the power supply should be discontinued before or during agent discharge. In certain critical applications (e.g., remote telecommunications switching stations) disconnecting power, however, is neither an option nor desirable. The current work is aimed at developing a standard test device and method that will provide data necessary to address this situation.

Design concentrations for total flooding agents in NFPA 2001 are based on results from the cup burner testing device [1]. Briefly, a 24 to 29 mm diameter burning liquid pool is located within an 85 ± 2 mm diameter glass tube through which air flows from bottom to top at a rate ranging from 10 to as high as 60 L/min. Agent is added to the airstream in increasing increments until the fire is extinguished, and the agent concentration is calculated from the measured air and agent flow rates.

The approach taken in the current work has been to develop a variant of the cup burner that allows the test to be conducted with the fuel exposed to a source of external energy. In the case of a Class C fire, the Joule heating of the fuel by electrical energy constitutes the external energy source. In our first-generation, modified, cup burner [2], this Joule heating is approximated with radiant heating from an electric heater of the type used in the cone calorimeter. The cone heater was chosen because it is a highly stable, uniform, measurable, and repeatable energy source. A concentric outer glass tube is used to channel a nitrogen flow to protect the cone heater from products of combustion.

Previous work done at NIST with this burner examined the extinguishment of 25 mm diameter polymethylmethacrylate (PMMA) rods at external heat flux exposures of 0 to 40 kW/m^2 in increments of 10 kW/m^2. Six agents were evaluated: N_2; IG-541 (52% N_2, 40% AR, 8% CO_2); FC-3-1-10; FC-2-1-8; HFC-23 and HFC-227ea. At 10 kW/m^2 the average minimum extinguishing concentrations increased by a factor of 2 to 2.5 over that needed at zero radiant flux. As the imposed heat flux level was increased the amount of agent required for extinguishment increased asymptotically (Fig.1 is a typical result). At 40 kW/m^2 re-ignition occurred for all agents, except N_2, when the agent flow was terminated. In each case, however, re-establishing the flow and increasing the agent's concentration eventually produced inertion.

A second burner of the type used in the NIST study was built and was put into operation recently at 3M Company. Experiments to duplicate the PMMA results obtained with the NIST apparatus are underway. Polyethylene (PE) and Polyvinyl chloride (PVC) fuels also will be tested. These results and comparisons will be included in the presentation.

A second-generation, modified, cup burner (Fig. 2) was designed and is being fabricated at NIST. The inner tube has been extended 50 mm above the top face of the specimen to better conform to the original cup burner geometry and improve experimental control. The diameter of the inner tube is 85 mm, which is the diameter of the original cup burner. PE, PVC, and a phenolic laminate will be evaluated in the new unit using N_2, FC-2-1-8, and HFC-227ea. Results will be included in the presentation.

References

[1] ISO/DIS 14520, Part 1, General Requirements, Annex B (normative) - Gaseous Media Fire Extinguishing Systems "Determination of flame extinguishing concentration of gaseous extinguishants by the cupburner method", 30 March 1998.

[2] Smith, D.M., Kelly, A., Rivers, P.E., Braun, E., and Grosshandler, W.L., Energized Fire Performance of Clean Agents: Recent Developments, International Conference on Ozone Protection Technologies, Baltimore MD, November 13, 1997.

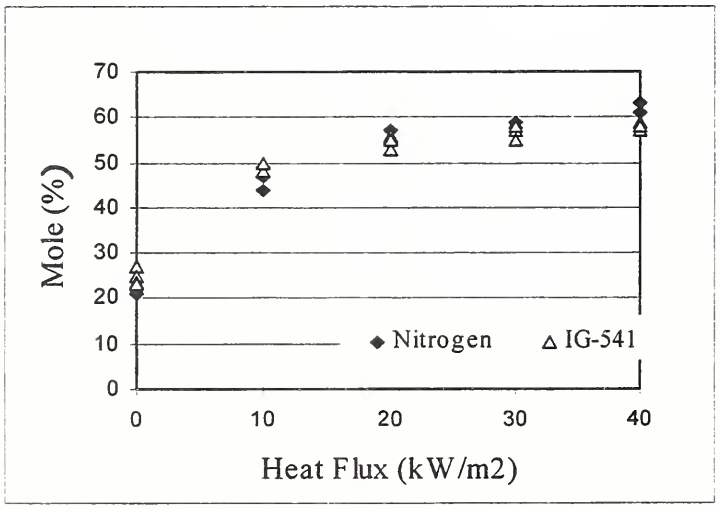

Fig. 1. Extinguishing Concentrations of Nitrogen and IG-541

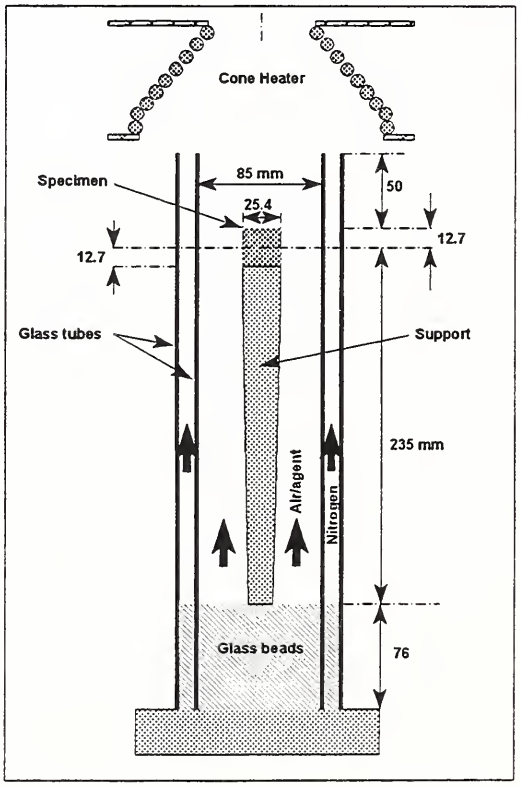

Fig. 2. Sketch of NIST second-generation, modified, cup burner.

Annual Conference on Fire Research
November 2-5, 1998, Gaithersburg, MD

Flammable Liquid Storeroom 1: Halon Alternatives Technology Testing Results

Alexander Maranghides,[a,b] Ronald S. Sheinson[b] and James Cooke III

NAVAL RESEARCH LABORATORY
Navy Technology Center for Safety and Survivability
Combustion Dynamics Section, Code 6185, Washington, DC 20375-5342, USA
(202) 404-6196, Fax (202) 767-1716
E-mail: maranghi@ccfsun.nrl.navy.mil; sheinson@ccfsun.nrl.navy.mil

The Navy Technology Center for Safety and Survivability (NTCSS) has performed extensive intermediate scale and full scale research focusing on the evaluation of Halon replacement agents, i.e., in kind gaseous agents. Test have been conducted in shipboard machinery spaces and Flammable Liquid Storerooms (FLSRs) in which the primary fire threats are pressurized flammable liquids and three dimensional fuel leaks, respectively. This testing included initial candidate agent screening, detailed candidate technology evaluation, and the quantification of the suppression characteristics of HFC-227ea, heptafuoropropane (HFP), the Navy's clean agent halon replacement of choice.[1] The current focus of the Halon Alternatives Program is on the evaluation of self contained Halon Alternative Technologies for future shipboard implementation. These technologies fall into two groups: the first being those technologies which combine powder with HFP, the second being self contained water mist systems (with variations). Currently, testing is ongoing to quantify the performance of those technologies utilizing a blend of HFP and powder. Evaluation of self contained water mist technologies is slated to begin in the near future.

Alternative technology tests are conducted at the Naval Research Laboratory's Chesapeake Bay Detachment (CBD). Testing is currently being conducted in a 28 m^3 (1,000 ft^3) compartment representative of many of the smaller shipboard FLSRs. Tests being conducted simulate both an empty FLSR and an obstructed FLSR filled with mockups of fuel containers (sealed five gallon containers). The fuel used is a mixture of 80% methanol and 20% *n*-heptane. This mixture is designed to both challenge the suppression limits of the technology (i.e., the HFP cup burner value of 6.6% v/v HFP for *n*-heptane, 8.9% v/v HFP for methanol, and 8.3% v/v HFP for the mixture)[1] and to facilitate easy identification of fires through visible and IR cameras.

The primary fire scenario used for alternatives testing simulates a three dimensional, cascading fuel leak forming a pool on the deck of the compartment. This is accomplished through a metered fuel leak above deck level, coupled with a fuel pan near the deck to simulate pooled fuel, resulting in a combined fire size of near 200 kW. Eight small, telltale fires (on the order of one kW)[1] are placed around the compartment to gauge agent distribution within the compartment. The

---

Supported by the U.S. Naval Sea Systems Command.

a. GEO-CENTERS, Inc., Rockville, MD.

b. Authors to whom correspondence should be addressed.

baseline alternative test scenario consists of ventilation for four minutes with small fires burning, then ventilation shutdown in anticipation of fire ignition at twenty seconds before agent discharge, followed by agent discharge at five minutes into the test. After agent discharge, ventilation dampers and fans remain closed for fifteen minutes, and then are activated for a final fifteen minute venting period. Testing utilizes a short, twenty second preburn instead of the longer, two minute preburn utilized in FLSR 1 testing. Although the longer preburn is more representative of an actual shipboard scenario, the shorter preburn is chosen in order to limit oxygen depletion in the compartment and challenge the limits of the alternative technology.[2] Reignition attempts are performed at both the cascading level and at the fire pan during hold time and during the final venting period. These reignition attempts are used both to gauge the effectiveness of the alternative technology in inerting the fire environment and to gain valuable data on compartment reclamation efforts, such as early entry by firefighting personnel.

Fuel leaks, ventilation, and alternative technology activation, are controlled remotely by the Experiment Running Personal Computer (ERPC). Thermocouples, located in trees at two compartment locations as well as placed throughout the compartment shelving, are used to quantify the temperature distribution. Analyzers continuously measure agent, oxygen, combustion products, and halide acid gases produced from interaction of agent and flame. Discrete (in time) gas measurements are taken for later analysis by gas chromatography. Fourier Transform Infrared Spectroscopy (FTIR) is also used to quantify acid gas content and to measure agent and methanol concentrations within the compartment. Suppression and reignition times are determined both through observation on infrared and visible cameras, and through temperature analysis.[1]

The results of alternative technology testing will be compared with results from baseline HFP testing in order to determine the advantage gained or lost through use of each technology. Technologies will be evaluated on the basis of their suppression performance and reignition protection, i.e, suppression and reignition times. The space and weight requirements of candidate technologies will also be weighed against that of an HFP fire suppression system. Compartment tenability concerns, as well as the residue and associated cleanup after discharging nonclean agents (e.g., powders or water) will also be addressed during final evaluation.

Results will be presented from technologies blending HFP and powders, and results from self contained water mist testing will be presented as available.

ACKNOWLEDGEMENTS

Our sincere thanks and appreciation go to the large number of government employees, contractors, interns and summer employees who have participated in Halon Alternatives Technology conception, testing and data analysis.

REFERENCES

1. "Test Plan for Self Contained Total Flooding Halon 1301 Alternative Technologies Evaluation- Test Bed and Scenario Particulars," NRL Ltr Rpt 6180-0331A, July 2, 1998 Maranghides, A. and Sheinson, R.S.

2. Maranghides, A., Sheinson, R.S. and Wentworth, B., "Flammable Liquid Storerooms: Halon Replacement Program," Annual Conference on Fire Research, November 2-5, 1998, Gaithersburg, MD.

Annual Conference on Fire Research
November 2-5, 1998, Gaithersburg, MD

Flammable Liquid Storerooms: Halon 1301 Replacement Program

Alex Maranghides,[a,b] Ronald S. Sheinson[b] and Bryce Wentworth

NAVAL RESEARCH LABORATORY
Navy Technology Center for Safety and Survivability
Combustion Dynamics Section, Code 6185, Washington, D.C. 20375-5342, USA
(202) 404-6196, FAX (202) 767-1716
E-mail: maranghi@ccfsun.nrl.navy.mil; sheinson@ccfsun.nrl.navy.mil

The Naval Research Laboratory's (NRL's) Center for Safety and Survivability has been actively investigating alternative fire suppression agents for Halon total flooding systems. A two phase program has been outlined to characterize the application of alternative gaseous clean agents in shipboard Flammable Liquid Storerooms (FLSRs). Information gathered from this program will be used as guidance in the design of future Navy ships. Two simulated shipboard FLSRs have been constructed at NRL's Chesapeake Bay Detachment (CBD). The compartment used for the first phase, FLSR 1, was designed to simulate a typical small shipboard compartment with dimensions of 3.05 m x 3.05 m x 3.05 m (28 m^3) (1000 ft^3). Phase 1 tests are serving as a learning process for designing and executing the FLSR phase 2 program. The phase 2 Large Scale Test Compartment (LSTC) with dimensions of 10.67 m x 6.10 m x 4.57 m (297.3 m^3) (10,500 ft^3), has been designed to simulate a large shipboard compartment. The compartment is currently being outfitted with the necessary instrumentation and is slated for testing in fiscal year 1999.

The agent evaluated under phase 1 was HFC-227ea, heptafluoropropane (HFP), the Navy's clean agent of choice. Limited Halon 1301 tests were also conducted for baseline comparison. The fire scenario was a cascading fire within the shelving from the upper level and a 0.30 m x 0.30 m deck pan fire, designed to simulate a cascading three-dimensional fuel spill forming a pool at the lower levels of the compartment. The fuel was 80% methanol and 20% *n*-heptane, with a total output of 200 kW. The fires were allowed to burn for a total of two minutes, the last 30 seconds with no ventilation, prior to agent discharge being initiated. After agent discharge, the compartment was kept sealed for a hold time period of fifteen minutes. Reignition of fires was attempted at predetermined times during the hold period and just after ventilation initiation. Continuous measurements of compartment temperatures and concentrations of agent, oxygen, products of combustion, and by-products of suppression were recorded during each test. Discrete (grab sample) measurements of agent, oxygen, carbon monoxide, and carbon dioxide gases were also taken at specific times at six locations.

Supported by the U.S. Naval Sea Systems Command.

a. GEO-CENTERS, Inc., Rockville, MD, USA.

b. Authors to whom correspondence should be addressed.

There is no place for complacency when dealing with energy rich combustion systems. During a baseline fire extinguishment test with HFP, an unexpected explosion occurred that was powerful enough to rupture two protective explosion vents. FLSR 1 is equipped with pressure sensitive relief vents because of the possibility of over pressurization occurring due to the dynamic nature of fires. The relief vents are 61 cm x 61 cm and are rated at a maximum release pressure of 0.14 kg/cm^2 each. The explosion was a result of fuel vapor dispersement caused by flows created at the time of agent discharge. Localized pockets of fuel vapor can be above the upper flammable limit, and will be mixed with air during discharge turbulence.

The phase 1 tests resulted in most fires being suppressed within 2 to 5 seconds from start of agent discharge, aided by a significant amount of oxygen depletion. The concentrations of the suppression by-product hydrofluoric acid (HF) were highest during reignition attempts due to the large flame sheet size and typically reduced agent concentration. Scrubbing of much of the HF was successfully achieved by the application of a Water Spray Cooling System (WSCS).[2]

The second phase of testing will be carried out in the LSTC outfitted to resemble a large shipboard flammable liquid storeroom. The volume of this compartment is significantly larger than FLSR 1, presenting a new set of parameters to evaluate. The larger compartment will use the same fire scenarios (i.e., cascading fire, pan fire, with a combined output up to 1 MW). Total fire suppressions, however, will not be as easily achieved. The fires in the compartment will be much more robust than in FLSR 1, creating different flow patterns within the compartment. The oxygen concentrations within the compartment will not be depleted as dramatically as with FLSR 1. Also, the construction of the shelving and mockups will present more obstructions throughout the compartment, restricting the flow patterns of the agent. The vertical height of the compartment is larger increasing the travel distance of the agent to the fire. The placement of the discharge system nozzles in the compartment will be essential in delivering the agent to the fire in an efficient manner. It is expected that since the fires will be more challenging to suppress, the time period for agent and fire interaction will increase. The concentrations of HF will be higher and will be characterized as to their impact on compartment reclamation procedures.

Evaluations are continuing in FLSR 1 with alternative technologies in addition to HFP studies. The results of testing in FLSR 1 and the LSTC will be used as guidance for designing the new Navy ship fire suppression systems. Critical system design information is needed. The scheduled testing is required to adequately characterize potential fire risks and gain a better understanding of the dynamics of the suppression in FLSRs.

ACKNOWLEDGMENTS

Our sincere thanks and appreciation go to the large number of government employees, contractors, interns and summer employees who have participated in the Halon Replacement Program testing and data analysis.

REFERENCES

1. Maranghides, A., Sheinson, R.S., Cooke III, J., Wellens, J.C., Wentworth, B., Williams, B.A. and Darwin, R., "Flammable Liquid Storeroom 1: Halon 1301 Replacement Testing Results," Proceedings of the Halon Options Technical Working Conference, May 12-14, 1998, Albuquerque, NM.

2. Maranghides, A., Sheinson, R.S. and Cooke III, J., "Flammable Liquid Storeroom 1: Halon Alternatives Technology Testing," Annual Conference on Fire Research, November 2-5, 1998, Gaithersburg, MD.

Fire Tests of a Fixed Gaseous Fire Extinguishing System for Marine Application

Soonil Nam
Factory Mutual Research Corporation
1151 Boston-Providence Turnpike, Norwood, Massachusetts

Richard L. Hansen
U. S. Coast Guard R & D Center
1082 Shennecossett Road, Groton, Connecticut

Six full scale fire tests were conducted to evaluate a gaseous agent fixed fire extinguishing system for marine applications. The tests consisted of the four International Maritime Organization's MSC Circular 776 fire tests (IMO Fire Test # 1, # 2a, # 3, and # 4), a low temperature cylinder discharge test, and a verification test for a side wall discharge nozzle. The gas agent used was FM200®, and the tests were performed inside the IMO Fire Test Compartment located at the United State Coast Guard Fire & Safety Detachment on the test vessel STATE OF MAINE in Mobile, Alabama.

Ninety-five channels of data were recorded measuring temperatures and pressures throughout the gas distribution system; temperatures, pressures and gas concentrations inside the test compartment; and flame temperatures at various fire locations during the tests. The agent discharge times and fire extinguishment times were established based on those measurements and five video cameras installed to watch progress of the tests from a control room.

Figures 1 and 2 show the pressure and temperature measurement at various locations of the gas distribution system during the cold discharge test. The gas agent was discharged from cylinders maintaining –5 °C. The test results verified that the system met the performance requirements in terms of the agent discharge time and the fire extinguishemnt times as specified by IMO Fire Test Protocol[1]. No adverse effects on the system performance due to the cold discharge was observed in the test.

Other test results and issues related to IMO Fire Test Protocol and cold discharge tests will be discussed.

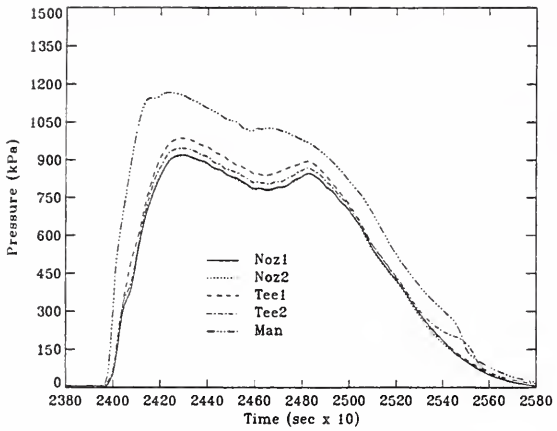

Figure1. Pressure measurement

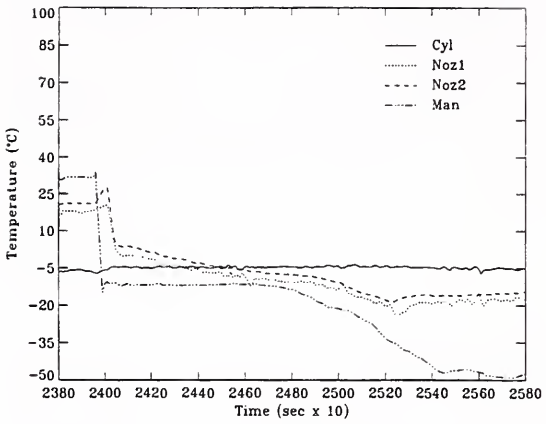

Figure 2. Temperature measurement

REFERENCES

1. "Guidelines for the Approval of Equivalent Fixed Gas Fire-Extinguishing Systems, as Referred to in SOLAS 74, for Machinery Spaces and Cargo Pump-Rooms," MSC/Circ. 776, 12 December 1996, International Maritime Organization, 4 Albert Embankment, London SE1 7SR.

ACKNOWLEDGEMENT

The authors wish to thank Mr. Ernest E. Ellis, Jr. of Metalcraft, Inc. for allowing them to present the test data and for the support provided before and during the tests. Contributions from the dedicated crew members of the U. S. Coast Guard's Fire & Safety Detachment and personnel from Hughes Associates, Inc. during the tests are also gratefully acknowledged.

Comparison of Measured Data with CFAST Predictions for the HDR T51 Wood Crib Test Series

Floyd, J. and Wolf, L.
Dept. of Materials and Nuclear Engineering
A. James Clark School of Engineering
University of Maryland, College Park
College Park, MD 20742

The HDR test facility in Karlstein, Germany, was a decommissioned, research reactor whose containment building was preserved for use as a large scale test facility for a wide variety of nuclear safety studies. One of the test series performed measured the effects of large fires on the containment building using a number of fuel types in different locations inside the building. A subset of the first fire test series, T51, consisted of three wood crib fires located in the bottom third of the HDR facility. While large quantities of cellulose materials are not typically found in reactor containment buildings, the wood crib tests were performed for the benefit of the fire research community which uses wood cribs as a standard fire type.

The wood cribs were burned in a specially prepared compartment inside the containment building. This compartment was lined with firebrick and fireproof insulation to prevent damaging the structural integrity of the HDR facility which, under German law, was still required to meet nuclear safety standards. In addition to the fire compartment, a flow path from it to a vertical shaft rising the length of the building to the upper dome was also constructed using firebrick. A second vertical shaft was present on the opposite side of the building and allowed flow from the dome back down to the level of the fire. The primary purpose of this flowpath was again to protect the facility, in this case the containment building's steel shell pressure boundary. Measured data from the tests consisted of temperatures, flow velocities, gas concentrations, pressure, and extinction coefficients. Data collection took place for ten minutes before ignition of the wood cribs and for at least thirty minutes after the end of significant combustion.

This paper will discuss the efforts required to model the T51 wood crib fires and will compare measured data from two of the three wood crib tests with predictions made by CFAST v3.1.1. The wood crib tests selected include one well ventilated fire and one underventilated fire. The first test modeled, T51.16, combusted five wood cribs and had a maximum power of 1000 kW. This test was well ventilated and little CO or smoke was produced. The second test modeled, T51.18, combusted eleven wood cribs, had a maximum power of 2300 kW, and was underventilated producing significant quantities of CO and smoke.

References

1. Floyd, J. and Wolf. , L. *Evaluation of the HDR Fire Test Data and Accompanying Computational Activities with Conclusions from Present Code Capabilities, **Volume 3**: Test Description and CFAST Validation for T51 Wood Crib Fire Test Series.* Dept. Materials and Nuclear Engineering, University of Maryland. College Park, Maryland. Report NUMAFIRE:03-98. 1998.
2. Portier, R., Reneke, P., Jones, W., and Peacock, R. *User's Guide for CFAST Version 1.6.* Building and Fire Research Laboratory, NIST. Gaithersburg, MD. NISTIR 4985. Dec. 1992.
3. Peacock, R., et al. *CFAST, the Consolidated Model of Fire Growth and Smoke Transport.* Building and Fire Research Laboratory, NIST. Gaithersburg, Maryland. NIST Technical Note 1299. Feb. 1993.

ESTABLISHMENT OF CONE CALORIMETER ACCEPTANCE CRITERIA FOR EVALUATION OF FIRE RESTRICTING MATERIALS FOR HIGH SPEED CRAFT

Marc Janssens, Southwest Research Institute
Andrew Grenier, U.S. Coast Guard
Louis Nash, U.S. Coast Guard

Introduction

On 1 January 1996, the High Speed Craft Code (HSC) entered into force as part of the Safety of Life at Sea (SOLAS) convention. This code deals with all aspects of the construction and operation of high speed craft. The most common type of ships that are regulated by the code are passenger and vehicle ferries that operate within 4 hours from the shore. The code permits that a high speed craft be constructed of combustible materials, provided certain fire performance criteria are met. Materials that meet these criteria are referred to as "fire restricting materials." The determination of fire restricting materials is based primarily on one of two tests. Bulkhead lining, and ceiling materials are tested using the ISO 9705 room corner test. Acceptance criteria for ISO 9705 are published in IMO resolution MSC.40(64) (MSC 64/22/Add.1, Annex 4). Furniture components (other than fabrics, upholstery, or bedding) and other components are tested using the ISO 5660 Cone calorimeter. No acceptance criteria are published for ISO 5660.

Research Program at Southwest Research Institute (SwRI)

This paper summarizes a research program that was conducted at SwRI between August 1997 and July 1998. The program was funded by the U.S. Coast Guard (USCG). The primary objectives of the program were to establish acceptance criteria to qualify materials as fire restricting based on performance in the Cone calorimeter test, and to determine whether the general IMO surface flammability and smoke and toxicity requirements for finish materials are consistent with and perhaps redundant to the requirements for fire restricting materials. Eight composite materials and one textile wallcovering were tested in full-scale in the ISO 9705 room. The same materials were also evaluated in small-scale according to the test procedures of the Cone calorimeter, the IMO surface flammability test (Part 5 of the IMO Fire Test Procedures or FTP Code), and the IMO smoke and toxicity test (Part 2 of the FTP Code). Some of the composite materials were used as framing materials for mock-up chairs and luggage racks. The upholstery of the chairs consisted of a foam/fabric combination that meets the requirements of IMO Resolution A.652(16), "Recommendation on Fire Test Procedures for Upholstered Furniture." Room tests were conducted on these items. The primary objective of the additional full-scale tests was to determine whether the Cone calorimeter acceptance criteria for linings developed in this study, are suitable pass/fail limits for fire restricting materials used as components of contents.

Additional ignition, flame spread, and release rate measurements were made to obtain material properties for modeling. The results of this part of the study are not reported in this paper.

Summary of Standard Test Results

The results of the standard tests are summarized in Table 1. Materials #1 and #6 slightly exceeded the smoke production limits in the ISO 9705 room test. Material #6 is identical to material #5, painted with an intumescent coating. Material #7 did not exceed the ISO 9705 criteria for heat release and smoke production, but failed due to the fact that flaming debris fell to the floor during the test. However, flaming persisted for only a few seconds. Furthermore, this phenomenon occurred only once during the test.

Table 1. Summary of standard test results

Material	#	ISO 9705	FTP Code Part 2	FTP Code Part 5
FR phenolic	1	Fail (no flashover)	Pass	Pass
Fire restricting material	2	Pass	Fail	Pass
FR polyester	3	Fail (flashover @ 6.2 min)	Fail	Fail
FR vinylester	4	Fail (flashover @ 5.3 min)	Fail	Fail
FR epoxy	5	Fail (flashover @ 16.5 min)	Fail	Pass
Coated FR epoxy	6	Fail (no flashover)	Pass	Pass
Textile wallcovering	7	Fail (no flashover)	Fail	Pass
Polyester	8	Fail (flashover @ 1.8 min)	Fail	Fail
FR modified acrylic	9	Fail (flashover @ 11.1 min)	Fail	Fail

Main Conclusions

The proposed Cone calorimeter acceptance criteria for fire restricting materials that resulted from this work are as follows: 1. time to ignition (t_{ig}) greater than 20 sec; 2.maximum 60 sec sliding average heat release rate ($HRR_{60,max}$) less than 60 kW/m^2; 3. total heat release (THR) less than 12 MJ/m^2; 4. maximum 60 sec smoke production rate ($SPR_{60,max}$) less than 0.01 m^2/s; and 5. average smoke production rate (SPR_{avg}) below 0.005 m^2/s. These values are averages from three tests at a heat flux level of 50 kW/m^2, in the horizontal orientation, with the retainer frame. The criteria are similar to those proposed to IMO by Finland in 1996, based on an analysis of data from the EUREFIC program.

There is an inconsistency between the IMO smoke and toxicity test requirements, and the ISO 9705 room test criteria for fire restricting materials. For example, material # 2 performed very well in the room (minimal heat and smoke production), but failed the IMO smoke and toxicity test requirements due to excessive CO generation under non-flaming conditions at a heat flux level of 50 kW/m^2.

The IMO surface flammability test criteria for finish materials appear to be slightly less stringent than the heat release rate criteria for fire restricting lining materials. Only material # 5 met the IMO surface flammabilty criteria, but failed in the room/corner test due to excessive heat release. However, the time to flashover was the longest for this material, so there seems to be some consistency between the two tests.

The room tests on contents confirmed that materials which meet the requirements for fire restricting linings can safely be used as framing materials and components of furniture and contents. The requirements could perhaps be relaxed, but a hazard or risk assessment is needed to develop revised acceptance criteria that do not compromise safety.

Wall and Ceiling Heat Flux Measurements in a Room-Corner Test

S. E. Dillon, J. G. Quintiere
Department of Fire Protection Engineering
University of Maryland
College Park, MD

and

S. Messa and D. Rosa
L. F. S. Laboratories
Montano Lucino, Italy

Measurements were made to determine the incident total radiative and convective heat flux distribution imparted to the wall and ceiling above in the ISO 9705 room-corner test. Measurements were conducted for the 0.17 m square burner diffusion flame located 0.30 m above the floor. The room is 2.4 m high. Data were taken for burner levels ranging from 50 to 300 kW in 50 kW increments, as well as for the standard settings of 100 and 300 kW. These tests were carried out in the LSF facility in Montano Lucino. The method of measurement follows that of Ingason and de Ris [1] which utilizes a thermal steel plate. In this application of their method, a continuous energy balance on the plate, incorporating conduction loss from each thermocouple node to its four neighboring nodes, was used. Hence, as the burner levels were incremented, the data analysis of the thermocouple traces in time could directly used to derive the incident surface heat flux for each node. Complete details are presented in the M. S. Thesis by Dillon [2].

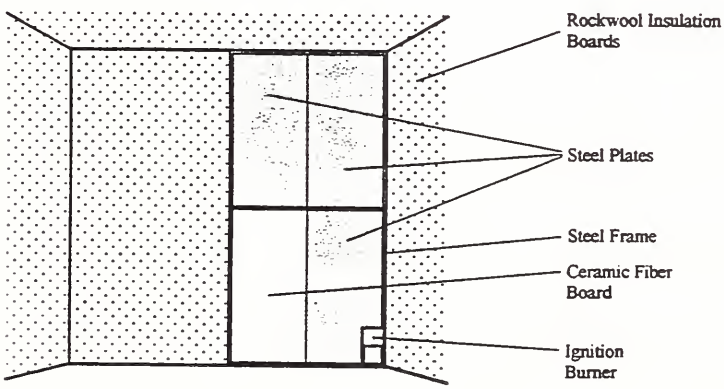

Figure 1. Wall configuration

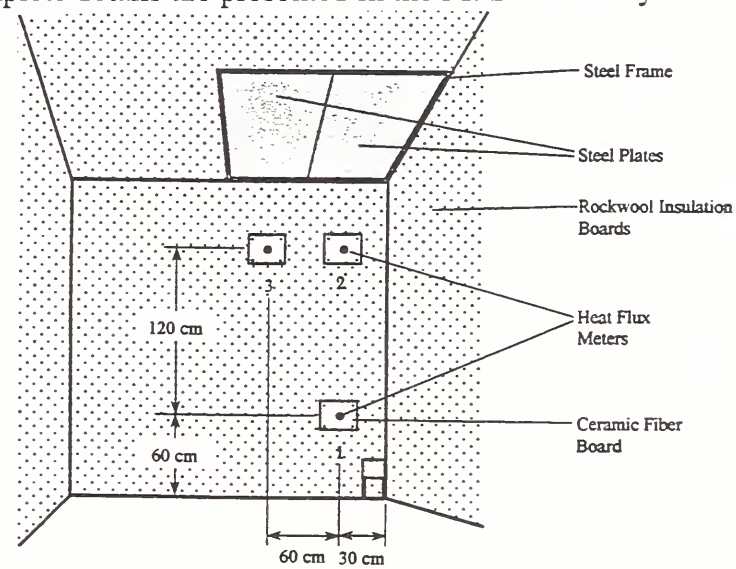

Figure 2. Ceiling configuration

The arrangements of the steel plates used in the room-corner tests are shown in Figures 1 and 2. The plates consisted of 1.2 by 0.6 m C-1018 carbon steel 5 mm thick, and had 32 thermocouples mechanically attached to the back face on 15 mm centers. The back side of the plate was insulated with two layers of 1/2 inch ceramic fiber insulation blanket followed with a rigid ceramic board 1 inch thick. The exposed face of the plate had been sand blasted and coated with high temperature (600 C) black paint.

In order to assess the accuracy of this thermal method, a study was done with a small plate irradiated by a controlled radiant source whose heat flux was simultaneously monitored throughout the heating of the steel plate. A schematic of the steel plate is shown in Figure 3. It was roughened with a glass bead blaster and coated with soot from a gasoline flame. Its back surface was insulated in a similar manner to the LSF tests, and results tend to support a nominal back face heat loss rate of about 5 per cent. Typical results are shown in Figure 4 in which step changes were applied at about 1000 s intervals, and the derived incident radiative heat flux from the energy balance is demonstrated to follow the actual flux. In these validation tests, the convective heat loss from the plate was computed as well.

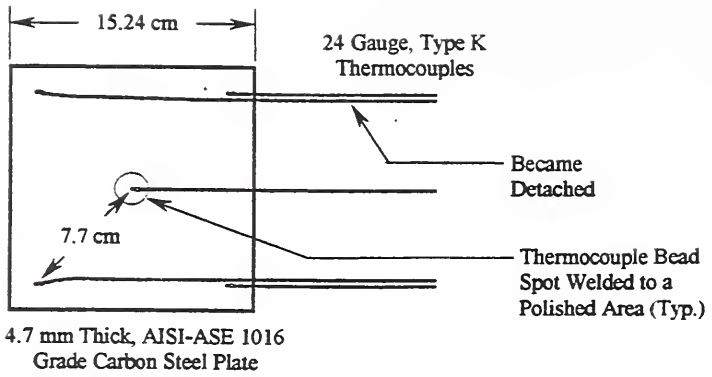

Figure 3. Validation sample

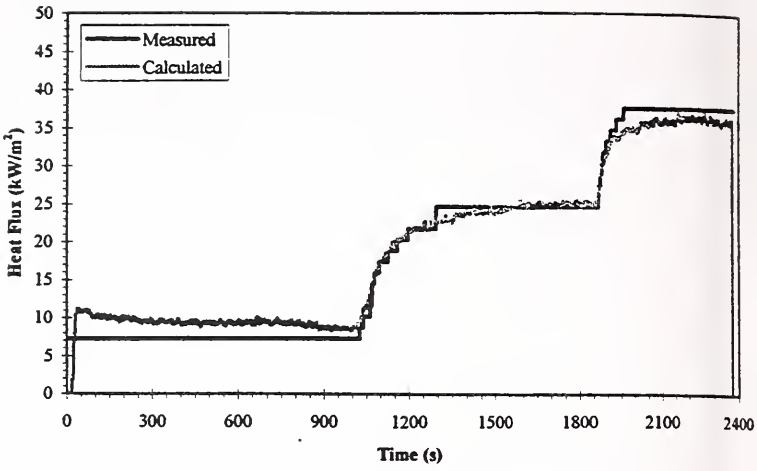

Figure 4. Validation results

Sample incident heat flux distributions for the room-corner test are shown in Figure 5. These room measurements were also compared to imbedded heat flux meters at selected positions. The thermal analysis method compared favorably with the meters measurements, and the previous measurements of Kokkala [3] for an open corner without a ceiling. Plans are underway to more fully analyze the results and explore correlations for their prediction.

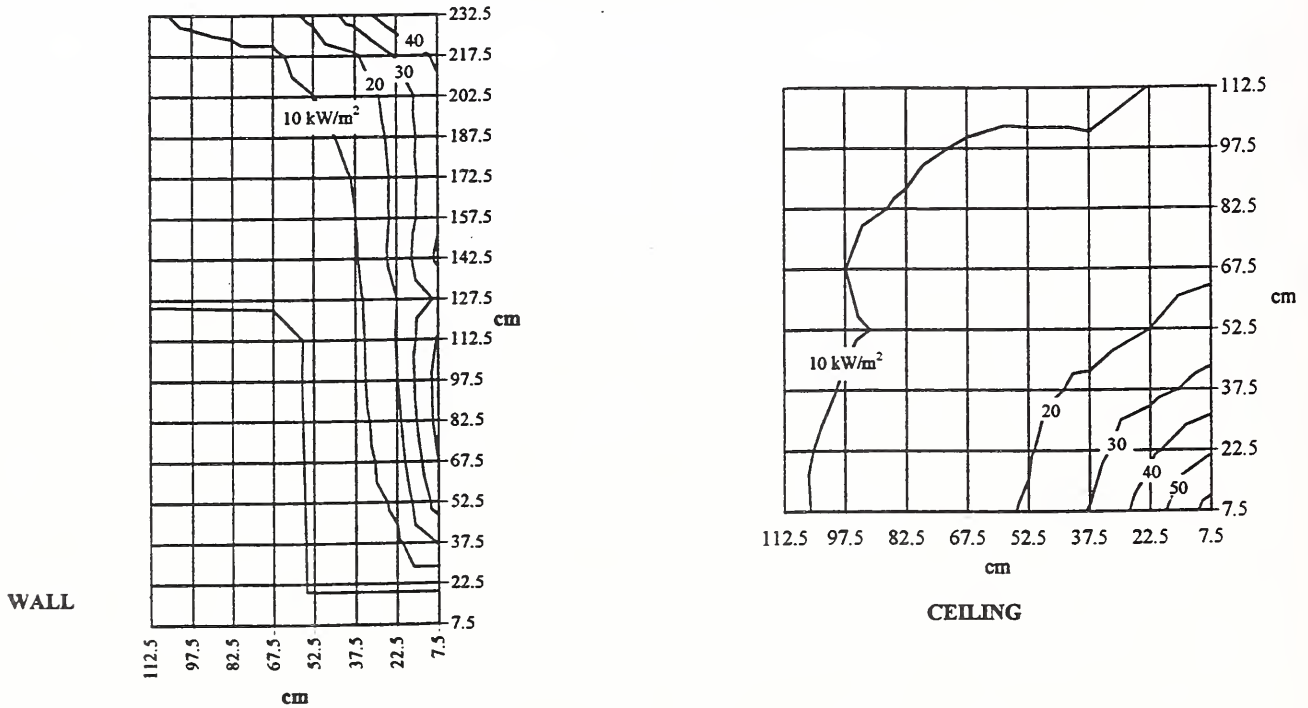

Figure 5. Wall and ceiling heat flux at 100 kW

1. Ingason, H. And de Ris, J., "Flame Heat Transfer in Storage Geometries" in H. Ingason, Dept. of Fire Safety Engineering, Rep. LUTVDG/(TVBB-1013), Lund Univ., Sweden, 1996.
2. Dillon, S. E., M. S. Thesis, Dept. of Fire Prot. Engrg., Univ. of Maryland, College Park, MD, Aug. 1998.
3. Kokkala, M. A., "Characteristics of a Flame in an Open Corner of Walls", Interflam '93, Inter.Sci. Comm. Ltd., London, 1993.

Discussions of a Model and Correlation for the ISO 9705 Room-Corner Test

S. E. Dillon, J. G. Quintiere
Department of Fire Protection Engineering
University of Maryland
College Park, MD

and

Woon. H. Kim
Department of Fire Safety Management
Kyung Min College
Korea

New examinations of a predictive model [1] for the ISO 9705 room-corner test have been made for materials studied by L S Fire Laboratories [2]. The ISO 9705 tests subjects a wall and ceiling mounted material to a corner ignition source of 100 kW for a duration of 10 minutes; if flashover does not occur this is followed by 300 kW for another 10 minutes. Twelve materials studied included many that would melt, drip, or distort during combustion; thus, they would not remain intact as wall and ceiling surfaces. Since the predictive model could not address these effects, they were all represented by an adjustment to the material's total available energy. In effect, the burn time (as a wall or ceiling element) was reduced to account for the material falling to the floor. Subsequent floor combustion was not included.

The materials that did not stay in place during combustion prove to be a challenge in modeling and prediction. For materials that remain in place the simulation model appears to do well in its predictions as illustrated by Figures 1 and 2 for normal and fire retarded plywood, respectively. Properties derived from Cone Calorimeter data for these materials are listed below:

	Ign. Temp.,C	Heat of Comb., kJ/g	Heat of Gasification, kJ/g
Normal Plywood	290	11.9	7.3
Retarded Plywood	480	11.2	9.3

The methodology for deriving these and other properties are described in the M. S. Thesis of Dillon [3].

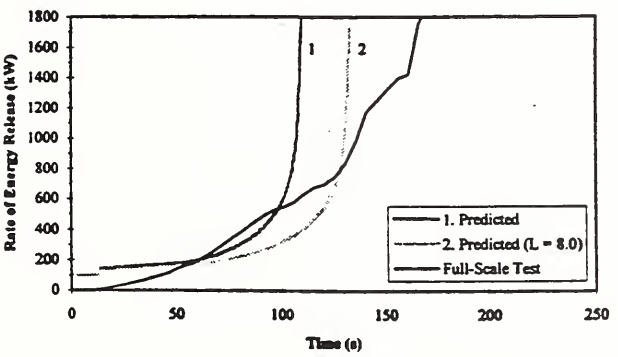

Fig. 1. Normal Plywood

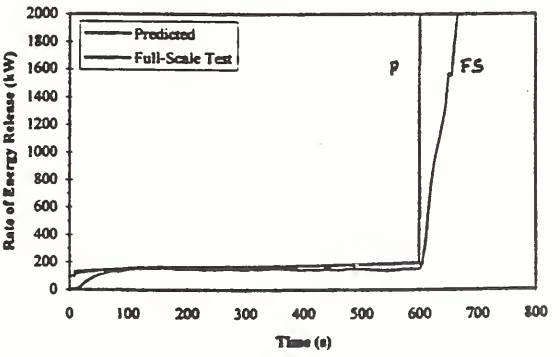

Fig. 2. Retarded Plywood

An example of the simulation prediction for a melting material is shown in Figure 3 for extruded polystyrene board. This is 40 mm thick, 30 kg/m^3. and glued to a non-combustible board in mounting. Its total available energy was measured to be 38.7 MJ/m^2 (Q"), but this had to be reduced to 15 % of its value to account for the melting depletion effect from the walls and ceiling. If we examine the results in Figure 3, we see that the original Q" value achieved the 1000 kW flashover criterion about 30 s before the test result. However, it should be noted that the test measurement of energy release rate by oxygen consumption rate appears to have a lag of about 30 s since the test results do not immediately follow the initial burner setting of 100 kW. Due to melting, the test results lead to a sudden decrease at about 100 s. Observations indicated significant melting and dripping to the floor at 85 s and ignition was observed to

occur at about 20 s. A calculation with the Q" reduced to 15 % of its Cone measured value appears to follow the "second flashover" measured after 600 s. This illustration is indicative of a prediction for a material that does not remain intact, and how it might be accommodated in the model be reducing the Q" value. It suggests a need to characterize the burning time for the material while contiguous with its mounting surface so that appropriate values of Q" can be developed, and to assess the apparent secondary effect of floor burning due to dripping.

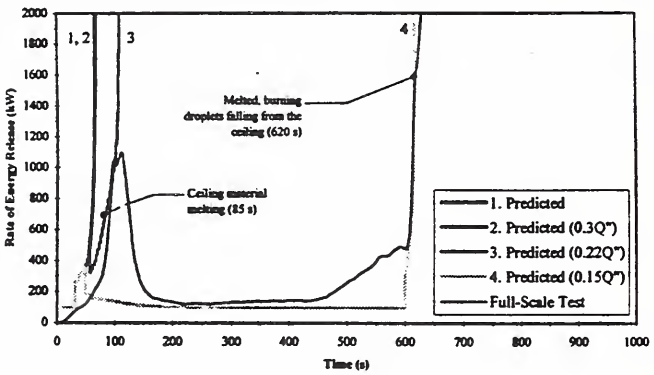

Figure 3. Extruded Polystyrene Board

An empirical correlation based solely on upward spread which appears to dominate the ISO 9705 test, was applied to the LSF data as well as 24 materials previously examined [4]. The correlation explained in Ref. [3],

$\tau_{FO} - 1$ is inversely dependent on a for $\tau_{FO} \le 1 + \tau_b$, and

$\tau_{FO} - 1 - \tau_b$ is inversely dependent on b for $\tau_{FO} \ge 1 + \tau_b$

where $\tau_{FO} = \frac{t_{FO}}{t_{ig}}$ and $\tau_b = \frac{t_b}{t_{ig}}$: t_{FO} is flashover time,

t_{ig} is ignition time computed at 30 kW/m^2,

t_b is burnout time computed at 60 kW/m^2,

$a = 0.01\dot{Q}'' - 1$, $b = a - \frac{1}{\tau_b}$, and $\dot{Q}''$ is the energy release flux (kW/m^2) at 60 kW/m^2.

The results for all materials in our database are shown in Figures 4 and 5 for the two time regimes.

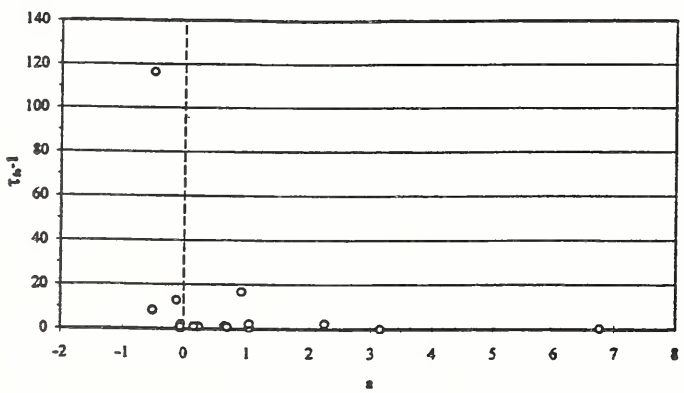

Figure 4. Correlation **a**

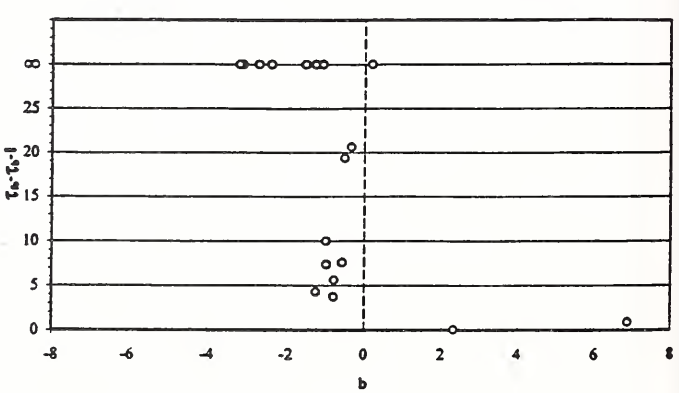

Figure 5. Correlation **b**

1. Quintiere, J. G., Fire Safety Journal, Vol. 20, No. 4, 1993.
2. Thureson, P. "Fire tests of linings according to Room/Corner Test, ISO 9705", Swedish Nat. Test. and Res. Inst. Rept. 95R22049, Jan 1996.
3. Dillon, S. E., M. S Thesis, Dept. of Fire Prot. Engrg., U. Of Maryland, August, 1998.
4. Quintiere, J. G., "Estimating Fire Growth on Compartment Interior Finish Materials", SFPE Engrg Sem., SFPE Meeting, San Francisco, CA, May 16-18, 1994.

STRUCTURE OF SELF-PRESERVING TURBULENT ADIABATIC WALL PLUMES

by

R. Sangras, Z. Dai and G.M. Faeth
Department of Aerospace Engineering
The University of Michigan
Ann Arbor, Michigan 48109-2140

Introduction. Plane turbulent wall plumes, caused by sources of buoyancy along walls, are frequently encountered in unwanted fires within structures. Motivated by this observation, the present investigate extended recent measurements of turbulent round and free line plumes in this laboratory [1-5] to consider plane turbulent wall plumes using similar methods. Only weakly-buoyant turbulent wall plumes along smooth plane vertical surfaces with conserved buoyancy flux were considered; this implies flow along an adiabatic wall for a thermal plume.

The present study emphasized conditions far from the source where source disturbances and momentum have been lost. In this region, self-preserving behavior is approximated with scaling similar to self-preserving free line plumes, except for a narrow wall boundary layer that grows more slowly than the outer plume-like region [6]. While such conditions are rarely encountered in practice, self-preserving behavior is still important because it substantially simplifies reporting measurements and evaluating predictions compared to developing flows [5]. Based on recent study of free line plumes [5], however, it is questionable whether self-preserving behavior was achieved during earlier studies of turbulent adiabatic wall plumes, e.g., Ref. 6 and references cited therein.

Experimental Methods. Experimental methods were similar to Sangras et al. [5]. The plumes were observed in an enclosure with porous side walls and ceiling to control room disturbances while not impeding plume entrainment flows. The source slot (876 mm long and 9.4 mm wide) was mounted flush to a flat floor at the base of a vertical plane wall 2440 mm high. End walls (1120 mm wide and 2440 mm high) helped preserve two-dimensional flow.

Two helium/air source mixtures were studied having initial source/ambient density ratios of 0.750 and 0.500 and source Froude numbers of 3.5 and 3.8. Use of gas mixture sources provided an accurate specification of the plume buoyancy flux that is difficult to achieve for thermal plumes [5].

Mean and fluctuating mixture fractions were measured using laser-induced fluorescence (LIF) similar to Sangras et al. [5]. The source flow was seeded with iodine which fluoreses naturally in an argon-ion laser beam having a wavelength of 514.5 nm. For present conditions, effects of differential diffusion of helium and iodine vapor were negligible. Experimental uncertainties (95% confidence) of the measurements of mean and fluctuating mixture fractions were less than 10%.

Results and Discussion. Present measurements of mean mixture fractions are plotted in terms of self-preserving variables in Fig. 1. Results for $z/Z = 0$ and 1/4 agree with each other, confirming the two-dimensionality of the flow. The present measurements yield universal distributions of normalized mean mixture fractions for distances from the source of 92-155 source diameters (or 12-21 Morton length scales). This corresponds to characteristic Reynolds numbers of 3800-6700 which implies reasonably turbulent flows. Other measurements plotted on the figure include the results for adiabatic wall plumes due to Grella and Faeth [6] and Lai and Faeth [7], results for isothermal wall plumes due to Liburdy and Faeth [8] and results for free line plumes due to Sangras et al. [5]. The measurements of Refs. 6-8 all exhibit streamwise variations in terms of self-preserving variables and are for conditions farthest from the source. The isothermal wall plume is somewhat broader than the rest because the low wall temperature forces the maximum buoyancy condition away from the wall [8]. The other adiabatic wall plumes are broader than present observations because they were not obtained far enough from the source to reach self-preserving behavior. The self-preserving free line plume is much broader than the rest which highlights the stabilizing effect of the wall. A negative aspect of wall stabilization, however, is that the inhibited mixing implies longer flames and hotter plumes for wall plumes than for free plumes at comparable conditions which increases their fire hazard.

Measurements of rms mixture fraction fluctuations are illustrated in Fig. 2, along with measurements from Refs. 5, 7 and 8. Maximum absolute mixture fraction fluctuations are larger in

adiabatic wall plumes than in free line plumes because maximum mean mixture fractions are larger. Maximum mixture fraction fluctuation intensities, however, are actually larger in free line plumes than in adiabatic wall plumes, e.g., 47% as opposed to 39%, which is another effect of wall stabilization. The other measurements differ from present results because self-preserving behavior was not reached and due to the fundamental differences between the structure of adiabatic and isothermal wall plumes [8].

Nomenclature. b = source width, B_o = buoyancy flux, $\bar{f}$ and $\bar{f}'$ = mean and rms fluctuating mixture fractions, g = acceleration of gravity, x and x_o = streamwise distance and location of virtual origin, y = crosstream distance, z= distance along slot from it s center, Z = slot length, ρ_o and ρ_∞ = source and ambient densities.

Acknowledgments. This research was supported by NIST Grant No. 60NANB4D1696 with H. R. Baum of BFRL serving as Scientific Officer.

References

1. Dai, Z., Tseng, L.-K. and Faeth, G.M., J. Heat Trans. 116:409(1994).
2. Dai, Z., Tseng, L.-K. and Faeth, G.M., J. Heat Trans 117:138 (1995).
3. Dai, Z., Tseng, L.-K. and Faeth, G.M., J. Heat Trans 117:918 (1995).
4. Dai, Z. and Faeth, G.M. J. Heat Trans. 118:493 (1996)
5. Sangras, R., Dai, Z. and Faeth, G.M., J. Heat Trans., in press.
6. Grella, J.J. and Faeth, G.M., J. Fluid Mech. 11:701 (1975).
7. Lai, M.C. and Faeth, G.M., J. Heat Trans. 109:663 (1987).
8. Liburdy, J.A. and Faeth, G.M. J. Heat Trans. 100:177 (1978).

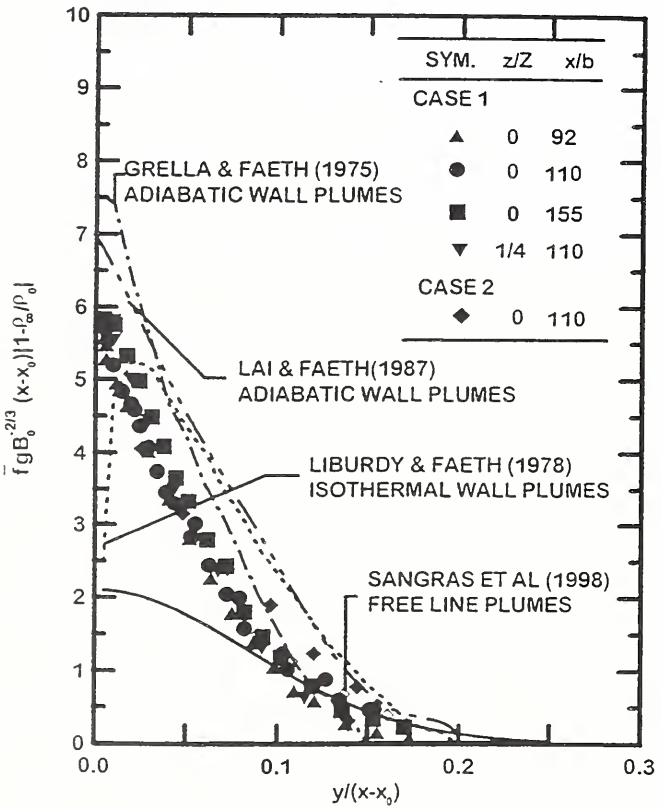

Fig. 1 Mean mixture fraction distributions in plane buoyant turbulent plumes.

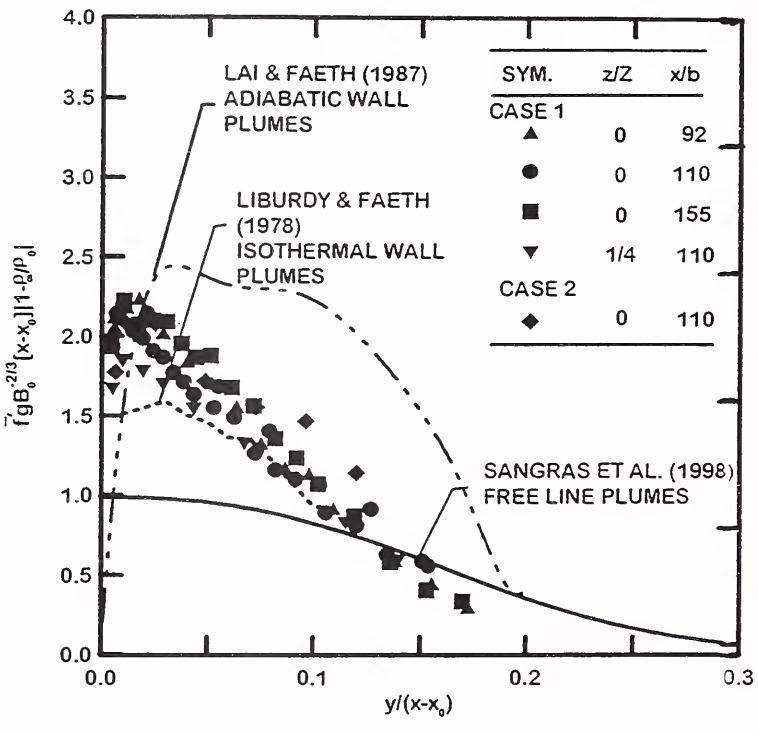

Fig. 2 Fluctuating mixture fraction distributions in plane buoyant turbulent plumes.

Spatial and Temporal Resolution of Buoyant Flows

Sheldon R. Tieszen[1], Timothy J. O'Hern[1], Robert W. Schefer[2], Elizabeth J. Weckman[3]
[1]Sandia National Laboratories, Albuquerque, NM 87185-0836
[2]Sandia National Laboratories, Livermore, CA 94550
[3]University of Waterloo, Waterloo, Ontario, Canada

Progress has been made in diagnostics to simultaneously resolve scalar and momentum fields in two dimensions as a function of time for buoyant flows. The motivation for obtaining such data is the validation of numerical simulation tools. Data has been acquired for a one-meter diameter source for a helium plume, and hydrogen and methane fires. Data processing is currently in progress.

The experiments were conducted in a heavily modified existing facility now called the Fire Laboratory for the Accreditation of Models and Experimentation (FLAME). It is nominally a cube 6 meters on a side with an upward sloping roof leading to a square chimney 2.3 meters on a side. A one-meter diameter plume source was created within the FLAME facility 2.45 meters above the floor. A gas manifold system supplies the plume source with up to about 0.5 m/s of helium, hydrogen, methane, and/or other diluents. Various flow straighteners, the last being 2.5 cm of stainless steel honeycomb with 3 mm cells, are used to create a uniform flow at the plume source.

It was desired to create as close as possible the conditions corresponding to a plume (or fire) source on an infinitely flat plane in an otherwise quiescent atmosphere within the FLAME facility. A numerical simulation tool was used to design the interior so that the lower half of the facility is a cylindrical geometry with an annular air duct near the floor of the facility facing upward with the plume. An annular disk with inner radius of ½ meter and outer radius of 1 meter surrounds the plume source. Calculations show this disk acts as an effective floor plane forcing the annular air flow to cross it radially inward, thereby creating the desired flow pattern.

Diagnostics include flow field measurements above the plume source and boundary condition measurements on the inflow and outflow boundaries. The flow field measurements include particle image velocimetry (PIV) and planar laser induced fluorescence (PLIF). These measurements are taken across a vertical plane that contains the centerline of the plume source. The field of view is approximately 1.5 meters wide by 1 meter high. The vertical measurement plane is created by expanding a 0.3 Joule/pulse, 308 nm, UV excimer laser beam into a light sheet. PIV images are due to laser light scattered off of seed particles in the flow. Various seed particles were used both within the plume and in the surrounding flow. For helium plumes, PLIF images were created by mixing nominally 2% by volume acetone into the plume. No PLIF images were obtained in hydrogen fires. However, in the methane flames, PLIF images corresponding to the flame zones were recorded. It is believe these images are due to the formation of Poly-Aromatic-Hydrocarbons (PAH's) found in such flames.

The pulse rate on the laser is controlled by camera equipment with a maximum pulse rate of 200 pulses per second. Both the PIV and PLIF signatures are imaged with 35 mm Photosonics 4ML movie cameras at up to 200 frames/second. Tmax 400 ASA black and white film is used to record the data. The film is subsequently scanned at nominally a 1200 by 1800 pixel resolution for each frame. Nominally 2500 frames per camera/per test are recorded. To obtain PIV images in the UV, quartz lenses are used on the camera. To obtain PLIF it was found necessary to use an image intensifier to amplify the signal for the helium tests. Boundary condition diagnostics include flow velocity, temperature, and humidity for the

air flow, mass flow rate, temperature and species concentration for the plume source, and momentum and temperature for the exit plane. Temperature measurements were also made on the facility walls.

Data for three test conditions have been acquired. The first is a methane fire with a mass flow rate per unit area of nominally 0.065 kg/m2-sec, which corresponds to that for a large JP-8 pool fire. The second is for a hydrogen fire with the same nominal heat release as the methane flame, about 2 MW. The third is for a helium plume with the same nominal cold inlet Richardson number as the methane fire, about 700.

Raw data will be shown for each of these tests. The nominal puffing frequency for these tests is 1.5 puffs/sec. The fire data was recorded at 200 frames/sec and the helium at nominally 120 frames per sec. Hence, the dynamics of the formation and advection of vortical structures is readily viewable in the films. The buildup of large coherent structures within the first diameter of the plume/fire results in very strong radial indraw of air. This radial indraw results in a deflection of the surface of the plume/fire near the toe of the plume/fire toward the centerline. In this position, the baroclinic generation of vorticity is less than when the plume/fire surface is oriented more vertically. As the large vortex is advected away from the surface, the plume/fire surface moves more into the vertical and baroclinic generation is strong. The mixing layer thickens and the structures amalgamate to become a coherent vortex. The process then repeats itself.

The data is currently being processed for the purpose of creating validation data sets for numerical simulation tools. The data has advantages over previous studies that employ laser doppler velocimetry (LDV) to obtain the velocity field. LDV has been the standard for use in developing/validating Reynolds-Averaged Navier Stokes (RANS) turbulence models which rely on single-point closure assumptions. LDV data is time-resolved only in a point-wise sense. The current data is temporally resolved simultaneously at all points in the two-dimensional plane of the laser sheet. Therefore, the data can be used for the validation of Large Eddy Simulation (LES) approaches and develop multipoint closure models, as well as, be processed for validation of conventional RANS and Unsteady-RANS approaches.

RADIATIVE HEAT TRANSFER IN FIRE MODELING

E. P. Keramida, A. N. Karayannis, A. G. Boudouvis and N. C. Markatos
Department of Chemical Engineering
National Technical University of Athens
Zografou Campus, Athens 157 80, Greece

ABSTRACT

The computational analysis of thermal radiation transfer is essential in many engineering calculations, such as those in fire modeling. Predicting possible secondary ignition due to thermal radiation is particularly important in fire safety engineering, because it enables protection of adjacent material from igniting. This paper describes the application of two widely used radiation models on a CFD product for the simulation of thermal radiation transfer in fire induced flows, in domestic sized rooms.

The case simulated is an experiment conducted by Steckler *et al.* [1] to investigate fire induced flows in a compartment measuring 2.8 m x 2.8 m in plane and 2.18 m in height, containing a fire of 62.9 KW. This particular experiment has been simulated before by Kerrison *et al.* [2], but radiative heat transfer mechanisms were neglected.

The present work proves that neglecting this important mode of heat transfer in fire modeling, leads to under-prediction of the temperature field. It also shows that theory and measurements compare well when radiation is accounted for. The results indicate that a significant percentage of the heat released by the fire, approximately 25%, is transferred via electromagnetic waves towards the bounding surfaces of the system, where it is either absorbed or reflected. Also notable is the difference between the enthalpy flow through the openings of the room with and without radiation; in the former case the energy content of the air is 34% lower than the latter case. This explains the decrease in temperature when radiation is included (see Figure 1).

Two radiation models, namely the 'discrete transfer' [3] and the 'six-flux' [4], are used to study radiative transfer in the case of a fire contained in a three-dimensional enclosure. Both models are well suited for engineering computations [5]. However, they differ in terms of accuracy of predictions and computational efficiency. In the present study the two models are compared and evaluated.

With the discrete transfer method, the total radiative flux is calculated by integrating the contributions along rays emanating from the radiative source and pointing to any selected direction. The six-flux method accounts for contributions to the radiative flux coming from only six directions, parallel to the coordinate directions. The six-flux is a differential model – a significant convenience for the discretisation of the transport equations – and offers computational efficiency. The discrete transfer model has the ability to return any desired degree of precision by increasing the number of rays projected from each physical surface and the number of zones that the domain is divided into, but it may require carefully shaped control volumes and positioning of the rays to achieve the required solution; this increases the accuracy of the solutions but adds considerably to the computational cost.

Computations were carried out with both models in Steckler's room, based on the assumption that the containing medium (a mixture of combustion gases) has uniform absorbing/emitting properties. The models were incorporated on a widely used CFD product, namely the CFX® AEA, Harwell, UK. The comparison between the flow and temperature fields of the two models, has produced reasonable agreement. The predictions of the discrete transfer model proved to be sensitive to changes in the zoning configuration and to changes in the number of rays emanating from the wall. Overall, the six-flux model proved to be superior to the discrete transfer model and, therefore, it is recommended for three-dimensional radiation computations in the cases of fire in rectangular enclosures.

Some temperature profiles of both the discrete transfer and the six-flux results are presented below.

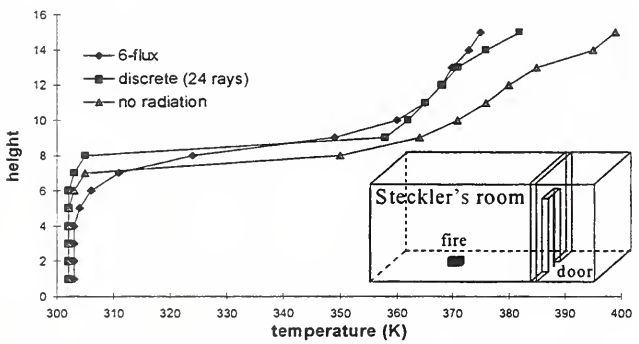

Figure 1. Door centre temperature vertical profile

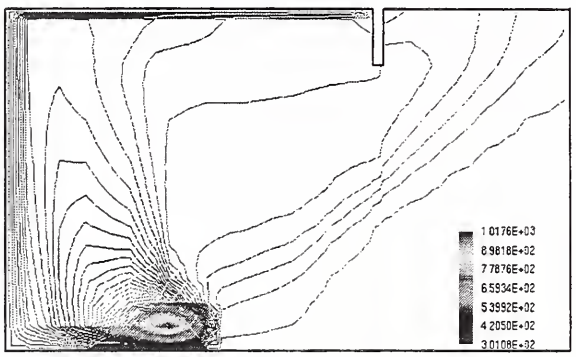

Figure 2. Mid-plane temperature contour

REFERENCES

[1] Steckler K D, Quintiere J G, Rinkinen W J, Flow induced by fire in a compartment, U. S. Dept. of Commerce, NBSIR 82-2520 (1982).

[2] Kerrison L, Galea E R, Hoffmann N, Patel M K, A comparison of a FLOW3D based fire field model with experimental room fire data, *Fire Safety J.*, **23**, 387 (1994).

[3] Lockwood F C, Shah N G, A new radiation solution method for incorporation in general combustion prediction procedures, *Eighteenth Symposium (International) on Combustion,* London, 1405 (1989).

[4] Hoffmann N, Markatos N C, Thermal radiation effects on fire enclosures, *Applied Mathematical Modeling* **12**, 129 (1988).

[5] Howell J R, Thermal radiation in participating media: The past, the present, and some possible futures, *ASME J.Heat Transfer* **110**, 1220 (1988).

Using Bench Scale Fire Measurements in Large Scale Simulations

Kevin McGrattan, Anthony Hamins and Linda Blevins
National Institute for Standards and Technology
Gaithersburg, Maryland, USA

A program is underway at NIST to develop a numerical field model, referred to as the Industrial Fire Simulator (IFS), to simulate large scale fire phenomena. Because the model is intended to simulate fire flows within buildings whose volumes are on the order of tens of thousands of cubic meters, it is not practical to implement detailed submodels of phenomena occurring at length scales less than a few tens of centimeters, including combustion, boundary layer effects, convective heat transfer, and fire suppression. Instead, bench scale measurement techniques are being developed that will provide the necessary information that will represent these phenomena in the simulations.

This type of effort has been undertaken before to provide zone models with empirical characterizations of various fire-related devices, such as sprinklers. Although much of this work is still applicable in field model calculations, the extra level of detail afforded by the increased spatial resolution requires additional measurements. For example, the total heat release rate as a function of time for a fire consuming a given fuel array would be sufficient information for a zone model to make a predication of an average upper layer temperature. However, if one is attempting to predict the growth of the fire from a point ignition source, more information is required, such as the thermal properties of the fuel and its heat release rate per unit volume.

The part of the model requiring the least amount of empirical information is the hydrodynamic calculation. It is based on large eddy simulation (LES) techniques to solve the differential equations that govern the transport of smoke and hot gases from a fire [1, 2]. Although transport is a very important part of the model, most of the uncertainty in its predictions and the need for empirical information is due to the calculation of the growth and suppression of the fire. In the model, the fire is represented by Lagrangian particles, referred to as thermal elements, that release heat as they are transported by the thermally-induced motion. Since the fluid motion determines where the heat is actually released, and the heat release determines the motion, the large scale features of the coupling between the fire and the smoke transport are retained. The heat release rate per unit mass of burning fuel is determined from experiment. The spread of the fire through the fuel array is predicted by the model based on measurements of the thermal properties of the objects and the thermal radiation from the fire. Smoke transport is simulated by tracking the thermal elements after the fuel burnout is completed. A specified percentage of the fuel consumed is assumed to be converted to smoke particulate. Thus, a knowledge of the spatial distribution of the thermal elements is equivalent to a specification of the smoke particulate density at any instant of time.

Computing the effects of a sprinkler spray requires measurements of both the thermal response of the device itself, plus the size and initial trajectory of the water droplets. The temperature of the sensing element of an automatic sprinkler is estimated in the IFS model using the analysis of Heskestad and Bill [3]. The activation of a sprinkler is governed by two parameters, one of which is a measure of the sprinkler link's sensitivity to heat, the second a measure of the conductive losses away from the link. A small wind tunnel, or plunge oven, is used to determine both of these parameters. Once a sprinkler has activated, the sizes, temperatures and trajectories of a representative sample of the water droplets are computed. The sampling of droplets has been referred to as the "superdrop" concept [4]. In the IFS calculations that will be presented, typically five to ten thousand droplets from each active sprinkler interact with the gas at any given time. This number of droplets ensures that a sufficient distribution of the water is obtained. The NIST experimental effort is being directed

towards characterizing the initial conditions for the droplet spray based on measurements of droplet sizes and density patterns of sprays not subjected to a fire plume. Ultimately, a database will be assembled containing the necessary information to compute the effect of the sprinkler spray on a fire. These measurements are not easy to make because of the large amount of water flowing from a typical industrial scale sprinkler.

Extinguishment of the fire is the single most difficult component of the numerical model. To date, most of the work in this area has been performed at Factory Mutual. An important paper on the subject is by Yu *et al.* [5]. Their analysis yields an expression for the total heat release rate from a rack storage fire after sprinkler activation. Unfortunately, this analysis is based on global water fluxes and burning rates. The IFS model requires more detail about the burning rate as a function of the local water flux. Until better models can be developed, the present extinguishment model consists of an empirical rule that decreases the local heat release rate as more water is applied. This estimate of the fire suppression depends strongly on the make up of the commodity. Much of the NIST bench scale experimental effort is presently being directed towards improving this part of the model.

References

[1] H.R. Baum, K.B. McGrattan, and R.G. Rehm. Three dimensional simulations of fire plume dynamics. *Journal of the Heat Transfer Society of Japan*, 35:45–52, 1997.

[2] K.B. McGrattan, H.R. Baum, and R.G. Rehm. Large eddy simulations of smoke movement. *Fire Safety Journal*, 30:161–178, 1998.

[3] G. Heskestad and R.G. Bill. Quantification of thermal responsiveness of automatic sprinklers including conduction effects. *Fire Safety Journal*, 14:113–125, 1988.

[4] S. Kumar, G.M. Heywood, S.K. Liew, and W.S. Atkins. Jasmine sprinkler model - some validation studies. In *Proceedings of the First European Symposium on Fire Safety Science*, 1995. ETH, Zurich.

[5] H.Z. Yu, J.L. Lee, and H.C. Kung. Suppression of rack-storage fires by water. In *Fire Safety Science – Proceedings of the Fourth International Symposium, International Association For Fire Safety Science*, pages 901–912, 1994.

Reliability of Structural Fire Protection

G Ramachandran
Consultant, Risk Evaluation & Insurance
Visiting Professor, University of Hertfordshire

Fire resistant compartmentation has long been the core of fire safety measures. If a building is provided with such compartments, any fire occurring in the building is expected to be confined to the compartment of origin and not to spread to other parts of the building. If the structural boundaries of a compartment, walls, floor and ceiling, are of sufficient fire resistance, it is argued, the compartment will not "fail" for a specified length of time defined as the fire resistant period. Compartment failure and violation of performance criteria relating to load bearing capacity, integrity or thermal insulation can occur if and when a fire grows to a fully developed (flash-over) stage and produces intense heat which can cause a progressive deterioration of the structural boundaries.

For assessing the likelihood of failure of a structural element, analytical (deterministic) models have been developed in fire science literature to provide an estimate of the maximum heat or fire severity expected to be attained in a real fire in the compartment. These models are based on scientific theories supported by experimental data and do not take sufficient account of the uncertainties caused by several factors. The spread of fire is a stochastic phenomenon [1] and the maximum severity likely to be produced can only be predicted in probabilistic terms. Several factors also cause uncertainties in the estimates of fire resistance of structural elements provided by standard fire tests. Fire resistance is also affected by weakness caused by penetrations, doors or other openings in the structural barriers of a compartment. Accepting that, both the fire severity, S, and resistance, R, are random variables, probabilistic models [2] have been developed in recent years for evaluating the probability of failure of a structural element.

Depending on data available for analysis, an appropriate probabilistic model may be applied to any type of compartment for determining the fire resistance required for a structural element for any acceptable level for the probability of failure. However, the fire resistance of an element as judged in standard fire tests, is usually known since it should satisfy a minimum level specified in fire safety regulations and codes. The problem, however, is to evaluate the reliability of the element in performing satisfactorily in a real fire for the resistance period, t, for which it has been designed. This performance depends on several factors affecting severity and resistance [3]. Reliability is defined as the probability of success and is a function, R(t), of the time t. Its counterpart unreliability is the probability of failure and is given by [1 - R(t)].

Estimates of reliability for individual structural elements such as walls, floor and ceiling can provide an estimate of the reliability of the compartment which may be regarded as a "system" in reliability terminology. A compartment would "fail" if any of the structural elements "fail". Hence, it would be appropriate to regard the structural elements as constituting a "series" system [4]. The reliability of the compartment in satisfying a specified fire resistant period is, therefore, the product of the reliabilities of the four walls, floor and ceiling. This fundamental theorem in reliability theory indicates that the reliability of a compartment can be lower than that of any structural element. For example, for a specified fire resistance period t, the reliability of the comportment is 0.78 if the reliability of each of the four walls is 0.95 and the reliability of the ceiling or floor is 0.98. A compartment is unlikely to have 60 minutes fire resistance if the structural elements have 60 minutes fire resistance.

The fundamental result mentioned above is only valid if the failure of a structural element in a fire does not affect the performance of any other structural element, i.e. the structural elements are independent in regard to their fire performance. This may not be true since progressive deterioration of a wall under severe heat might, in some buildings, affect the performance of the floor or ceiling of a compartment. Likewise, a fire-resisting wall may be affected by the deflection of a beam in a fire - see Fig.1. Joints and other constructional features are likely to cause such a dependency. There is a need to carry out an investigation to identify and quantify the interactions between structural elements such as columns and beams which may exercise critical effects on the probability of compartment success or failure in a fire.

REFERENCES

1. Ramachandran, G (1995) Stochastic models of fire growth. SFPE Handbook of Fire Protection Engineering, Second Edition, National Fire Protection Association, Quincy, MA, USA Section 3, Chapter 15, 296-311

2. Ramachandran, G (1998) Probabilistic evaluation of structural fire protection - a simplified guide. Fire Note 8, to Building Research Establishment, Fire Research Station, UK.

3. CIB W14 (1986) Design Guide - structural fire safety. Fire Safety Journal, 10, 2, 77-154.

4. Ramachandran, G (1998) Reliability of fire protection systems. Advances in Reliability Technology Symposium, Manchester, April 1998.

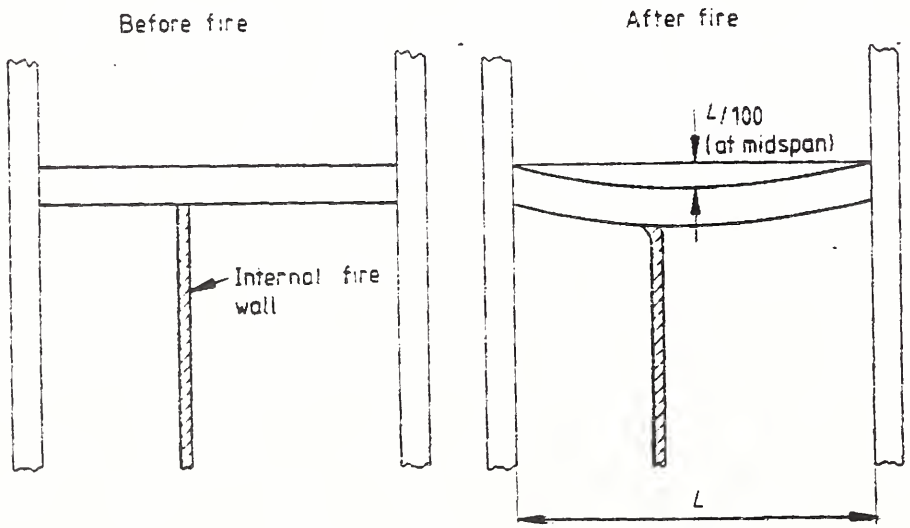

Figure 1 Effect of beam deflection on a fire-resisting wall.
Source: British Standard BS 5950: Part 8, 1990, Section four, page 15.

NIST-114
(REV. 11-94)
ADMAN 4.09

U.S. DEPARTMENT OF COMMERCE
NATIONAL INSTITUTE OF STANDARDS AND TECHNOLOGY

(ERB USE ONLY)
ERB CONTROL NUMBER | DIVISION
PUBLICATION REPORT NUMBER | CATEGORY CODE
PUBLICATION DATE | NUMBER PRINTED PAGES

MANUSCRIPT REVIEW AND APPROVAL

INSTRUCTIONS: ATTACH ORIGINAL OF THIS FORM TO ONE (1) COPY OF MANUSCRIPT AND SEND TO THE SECRETARY, APPROPRIATE EDITORIAL REVIEW BOARD.

TITLE AND SUBTITLE (CITE IN FULL)

Annual Conference on Fire Research, Book of Abstracts, November 2-5, 1998

CONTRACT OR GRANT NUMBER

TYPE OF REPORT AND/OR PERIOD COVERED

AUTHOR(S) (LAST NAME, FIRST INITIAL, SECOND INITIAL)

EDITOR: Kellie Ann Beall

PERFORMING ORGANIZATION (CHECK (X) ONE BLOCK)

- [x] NIST/GAITHERSBURG
- [ ] NIST/BOULDER
- [ ] JILA/BOULDER

LABORATORY AND DIVISION NAMES (FIRST NIST AUTHOR ONLY)

Building and Fire Research, Fire Science Division (865)

SPONSORING ORGANIZATION NAME AND COMPLETE ADDRESS (STREET, CITY, STATE, ZIP)

PROPOSED FOR NIST PUBLICATION

- [ ] JOURNAL OF RESEARCH (NIST JRES)
- [ ] J. PHYS. & CHEM. REF. DATA (JPCRD)
- [ ] HANDBOOK (NIST HB)
- [ ] SPECIAL PUBLICATION (NIST SP)
- [ ] TECHNICAL NOTE (NIST TN)
- [ ] MONOGRAPH (NIST MN)
- [ ] NATL. STD. REF. DATA SERIES (NIST NSRDS)
- [ ] FEDERAL INF. PROCESS. STDS. (NIST FIPS)
- [ ] LIST OF PUBLICATIONS (NIST LP)
- [x] NIST INTERAGENCY/INTERNAL REPORT (NISTIR)
- [ ] LETTER CIRCULAR
- [ ] BUILDING SCIENCE SERIES
- [ ] PRODUCT STANDARDS
- [ ] OTHER

PROPOSED FOR NON-NIST PUBLICATION (CITE FULLY) [ ] U.S. [ ] FOREIGN

PUBLISHING MEDIUM

- [x] PAPER
- [ ] CD-ROM
- [ ] DISKETTE (SPECIFY)
- [ ] OTHER (SPECIFY)

SUPPLEMENTARY NOTES

ABSTRACT (A 2000-CHARACTER OR LESS FACTUAL SUMMARY OF MOST SIGNIFICANT INFORMATION. IF DOCUMENT INCLUDES A SIGNIFICANT BIBLIOGRAPHY OR LITERATURE SURVEY, CITE IT HERE. SPELL OUT ACRONYMS ON FIRST REFERENCE.) (CONTINUE ON SEPARATE PAGE, IF NECESSARY.)

The NIST Annual Conference on Fire Research has long been the prime forum for the presentation and discussion of the latest advances in the science of fire and the engineering of fire safety. This booklet contains the abstracts of the 75 papers and posters focussing on the phenomenology of fire: fire sensing, fire measurement, fire-safe materials, fire suppression, flame structure, pool fires, fire-induced flows, fire plumes, combustion product generation and measurement, compartment fires, and outdoor fires.

KEY WORDS (MAXIMUM OF 9; 28 CHARACTERS AND SPACES EACH; SEPARATE WITH SEMICOLONS; ALPHABETIC ORDER; CAPITALIZE ONLY PROPER NAMES)

fire; fire science; fire sensing; fire measurement; fire-safe materials;fire modeling; fire suppression

AVAILABILITY

- [x] UNLIMITED
- [ ] FOR OFFICIAL DISTRIBUTION - DO NOT RELEASE TO NTIS
- [ ] ORDER FROM SUPERINTENDENT OF DOCUMENTS, U.S. GPO, WASHINGTON, DC 20402
- [ ] ORDER FROM NTIS, SPRINGFIELD, VA 22161

NOTE TO AUTHOR(S): IF YOU DO NOT WISH THIS MANUSCRIPT ANNOUNCED BEFORE PUBLICATION, PLEASE CHECK HERE. [ ]

ELECTRONIC INFORMS